R-06-49

Analysis of meteorological, hydrological and hydrogeological monitoring data

Forsmark – stage 2.1

John Juston, DBE Sweden

Per-Olof Johansson, Artesia Grundvattenkonsult AB

Jakob Levén, Geosigma AB

Mats Tröjbom, Mopelikan

Sven Follin, SF GeoLogic AB

September 2007

Svensk Kärnbränslehantering AB
Swedish Nuclear Fuel
and Waste Management Co
Box 5864
SE-102 40 Stockholm Sweden
Tel 08-459 84 00
+46 8 459 84 00
Fax 08-661 57 19
+46 8 661 57 19

ISSN 1402-3091
SKB Rapport R-06-49

Analysis of meteorological, hydrological and hydrogeological monitoring data

Forsmark – stage 2.1

John Juston, DBE Sweden

Per-Olof Johansson, Artesia Grundvattenkonsult AB

Jakob Levén, Geosigma AB

Mats Tröjbom, Mopelikan

Sven Follin, SF GeoLogic AB

September 2007

This report concerns a study which was conducted for SKB. The conclusions and viewpoints presented in the report are those of the authors and do not necessarily coincide with those of the client.

A pdf version of this document can be downloaded from www.skb.se.

Summary

In the present report, meteorological, hydrological and hydrogeological time series data from SKB's site investigation in Forsmark available up to July 31 2005 (data freeze 2.1), were analysed.

Two meteorological stations were established in the site investigation area in May 2003. The corrected mean annual precipitation of these two stations was 674 and 521 mm for the periods August 2003–July 2004 and August 2004–July 2005, respectively. Data indicated that of the nearby SMHI stations, the station at Östhammar has precipitation values most similar to those of the two SKB stations. Based on data from nearby SMHI stations, SMHI has calculated a 30-year average annual corrected precipitation of 559 mm at Forsmark. There is a strong precipitation gradient from east to west, with an annual corrected precipitation at Örskär that is approximately 150 mm lower than at Lövsta. For the two annual periods August 2003–July 2004 and August 2004–July 2005, the potential evapotranspiration at Forsmark was 497 and 507 mm, respectively.

Surface water levels were recorded in six lakes and at two locations in the Baltic Sea. The highest recorded daily average sea water level was +0.75 and the lowest –0.50 m RHB 70. The single highest 30-minutes value was +0.94 m RHB 70. At high sea water levels, saline water intruded Norra Bassängen, Bolundsfjärden and Lillfjärden, and during the extreme event in January 2005 also Fiskarfjärden.

Groundwater levels were recorded in 38 wells in Quaternary deposits in the site investigation area. 30 of these wells were located on land, while 8 were placed in till below the bottom of lakes and the Baltic Sea. The measured groundwater levels in Quaternary deposits were actually density-dependent point water heads, but due to short water columns and mostly low salinity, corrections to fresh water heads or environmental water heads would be negligible and were not considered. Groundwater levels in Quaternary deposits were in general very shallow. 80% of all recorded groundwater levels in the 30 wells on land were between 0.0 and 1.6 m below ground surface. Groundwater levels in Quaternary deposits were strongly coupled to the ground elevation. In indivual wells the temporal variation in groundwater level was less than 1.5 m in almost all wells and less than 1 m in approximately 50% of the wells. The shallow groundwater implied a strong interaction with root water uptake illustrated by diurnal groundwater variations during dry summer periods. Root water uptake also gave rise to groundwater levels well below lake water levels in the riparian zones of the lakes during such periods, changing the lakes from groundwater discharge areas to groundwater recharge areas.

Point water heads (density-dependent groundwater levels) were analyzed from 22 percussion-drilled boreholes in the site investigation area. No general transformation was made in the report of the actually measured point water heads to fresh water heads or environmental water heads to include the influence water density effects on horizontal and vertical flow gradients, respectively. However, some preliminary calculations were made to see if changes in flow directions would appear if density effects were considered. Due to all ongoing activities in the site investigation area, mainly drilling and pumping, it was difficult to find long enough periods with undisturbed point water heads in the percussion-drilled boreholes for analysis of natural conditions. In contrary to the wells in Quaternary deposits there was no evident correlation to the elevation of the local ground surface except for wells with very low transmissivity. Most bedrock wells within the tectonic lens, constituting the candidate area, had mean natural point water heads between 0.2 and 1.1 m RHB 70. Only two well sections had point water heads outside this range. These two sections had very low transmissivities. The small natural gradients within the tectonic lens indicated high transmissivities in the horizontal and sub-horizontal fracture zones known to exist in the uppermost c. 200 m of the lens. The analysis of responses in other bedrock wells on distinct single disturbances of groundwater levels in three bedrock wells

indicated good hydraulic contacts over large distances within the tectonic lens. The responses confirmed the high transmissivities indicated by the small natural gradients.

The variations in groundwater levels in Quaternary deposits and point water heads in bedrock were strongly coupled to variations in rainfall/snow melt and evapotranspiration while sea water levels had no or little influence. Even for the variations in bedrock point water heads, the rainfall/snow melt and evapotranspiration variations could explain about 80% of the annual variations. However, for point water heads in some percussion-drilled boreholes a probable sea water level influence could be identified.

Where groundwater levels in Quaternary deposits and point water heads in bedrock were observed in wells in close proximity within the candidate area, mostly at drill sites, the groundwater levels in Quaternary deposits were 1–2 m higher than in the bedrock. Preliminary calculations indicated that the difference in groundwater levels and point water heads could not be explained by water density differences but indicated a downward flow gradient from the Quaternary deposits to the bedrock. However, the large difference in level and the lack in response in groundwater levels in Quaternary deposits to pumpings in nearby bedrock wells indicated a limited hydraulic contact at most locations. A probable explanation is that high horizontal transmissivity of the uppermost part of the bedrock means that the limited quantity of groundwater recharge reaching the bedrock can be conducted at very low gradients. There were no data supporting a discharge of deep groundwater to the surface within the candidate area.

Surface discharge was measured at four automatic gauging stations. The upstream catchment areas varied in size from 2.3 to 5.6 km^2. The station for the largest catchment area has been in operation since April 2004 and the other three since December the same year. The time series were too short to draw any strong conclusions on specific discharge and its spatial and temporal variation. However, well-defined relationships were found between time series of surface water discharge and averaged groundwater levels of upstream catchments, with some displacement in time during the rising phase. Furthermore, a conceptual hydrological model was developed. The available time series were too short to allow for both calibration and validation. However, the preliminary results indicated that the model could simulate the measured discharge with good to acceptable accuracy. For the largest catchment, which had the longest available time series, the R^2 according to Nash-Sutcliffe was 0.9 and the error in total discharge 3% over the whole period of available measurements. For the one-year period of July 2004–June 2005, the corrected precipitation input to the model was 548 mm, the calculated evapotranspiration 374 mm, the surface discharge 152 mm, and the increase in unsaturated and saturated storage 22 mm.

The installation of the monitoring equipment had been an on-going process from the first installations were made late in 2002. This meant that the lengths of the times series varied for the observation points, and many of the data series were too short to provide a basis for decisive conclusions. The varying lengths of the time series also made comparison between observation points in terms of means and variances more difficult. However, the uncertainty varied between the different data sets as discussed in more detail below:

- A little more than two years of meteorological data were available for the analysis. These time series were too short to establish strong relationships with nearby SMHI stations with much longer time series which is desirable for long-term analysis and modelling.
- The sea and lake level time series are considered to give a good indication of the variations to be expected. Longer time series are not believed to result in changes in the conceptual model but will be important for further analysis of the connections between surface water and groundwater.
- The groundwater level time series from Quaternary deposits are considered to give a good indication of the variations to be expected. However, some additional observations wells are desirable in wetlands, but also in close proximity to bedrock boreholes, to study vertical groundwater flow gradients.

- Due to the extensive drilling and pumping activities in the site investigation area, the available time series of undisturbed point water heads in bedrock were short and meant that the analysis of natural conditions in surface-near bedrock was complicated. Therefore, the conclusions involving bedrock point water heads should be considered as preliminary. Especially, for studies of correlation to sea water level and vertical flow gradients longer time series from existing wells as well as additional time series from new wells are considered to be crucial. For studies of correlations between sea water levels and point water heads the principal component and independent component analyses, as well as the partial least squares modelling, proved to be powerful tools and should be repeated when extended time series are available. For the recommended studies of vertical groundwater gradients it is important to perform systematic calculations of environmental water heads based on quality assured water density data from the near-surface bedrock well sections.
- The available time series of surface discharge were too short to draw any firm conclusions on specific discharge and its spatial and temporal variation. Discharge data are considered very important for the calculation of the water balance of the area and to constrain the terms of the water balance equation in calibrations of the quantitative hydro(geo)logical models. At the last data freeze, March 31, 2007, another 1.5 years of data will be available and new analysis and modelling should be performed.

Sammanfattning

I föreliggande rapport presenteras analyser av meteorologiska, hydrologiska och hydrogeologiska tidsserier av data från SKB: platsundersökning i Forsmark fram till och med 2005-07-31 (SKB:s datafrys 2.1).

Två meteorologiska mätstationer etablerades i platsundersökningsområdet i maj 2003. Medelvärdet för den korrigerade nederbörden för dessa båda stationer var 674 och 521 mm för de två perioderna augusti 2003–juli 2004 respektive augusti 2004–juli 2005. Data indikerade att av de närbelägna SMHI-stationerna var det stationen i Östhammar som hade en nederbörd som mest liknade den i platsundersökningsområdet. Från de närbelägna SMHI-stationerna har SMHI beräknat den korrigerade årliga normalnederbörden, baserad på 30 års data, till 559 mm. Där är en stark nedebördsgradient från öster mot väster med en ca 150 mm lägre korrigerad nederbörd på Örskär jämfört med i Lövsta. Baserat på platsundersökningsdata beräknades den potentiella evapotranspirationen till 497 och 507 mm för perioderna augusti 2003–juli 2004 respektive augusti 2004–juli 2005.

Ytvattennivåer mättes i sex sjöar inom kandidatområdet och på två platser i havet. Det högsta noterade dygnsmedelvärdet för havsnivån var +0,75 och det lägsta –0,50 m RHB 70. Det högsta registrerade halvtimmesvärdet var +0,94 m RHB 70. Vid höga havsnivåer trängde havsvatten in i Norra Bassängen, Bolundsfjärden och Lillfjärden, och under de extrema förhållandena i januari 2005 också i Fiskarfjärden.

Grundvattennivåer registrerades i 38 grundvattenrör i jord. Av dessa var 30 belägna på land och 8 satta i morän under sjöar och hav. De mätta grundvattennivåerna var egentligen densitetsberoende men eftersom vattenpelarna är korta och salthalterna oftast låga blev inverkan försumbar och inga kompensationer för varierande densiteter gjordes. Grundvattennivåerna i jord var generellt mycket ytnära. 80 % av alla registrerade mätvärden låg mellan 0 och 1,6 m under markytan. Grundvattennivåerna i jord följde markytan väl. De tidsmässiga nivåvariationerna var mindre än 1,5 m i nästan alla rör och mindre än 1 m i ca hälften av rören. Det ytnära jordgrundvattnet i jordlagren innebar också att nivåerna påverkades av växtlighetens vattenupptag vilket illustrerades av tydliga dygnsvariationer under torra sommarförhållanden. Rötternas vattenupptag gav också upphov till lägre grundvattennivåer i sjönära områden än ytvattennivåer i de intilliggande sjöarna under sådana perioder. Detta innebar att sjöarna förvandlades från utströmningsområden till potentiella inströmningsområden för det ytnära jordgrundvattnet.

S k ”point water heads” (grundvattennivåer som inte kompenserats för skilda vattendensiteter till följd av skillnader i salthalt med djupet) från 22 hammarborrhål analyserades. Vissa preliminära beräkningar av s k ”fresh water heads” och ”environmental water heads” gjordes dock för att kunna förstå om densitetseffekterna kunde innebära ändrad riktning på grundvattenflödet i horisontal- respektive vertikalled. Pågående borrnings- och pumpningsaktiviteter i området medförde att det var svårt att hitta tillräckligt långa perioder med ostörda berggrundvattennivåer för att analysera naturliga (opåverkade) förhållanden. I motsats till grundvattennivåerna i jord fanns inget tydligt samband mellan berggrundvattnets nivå och markytans nivå utom för borrhål med låg transmissivitet i berget. Med endast två undantag låg medelgrundvattennivån i alla hammarborrhål inom den tektoniska linsen, vilken sammanfaller med kandidatområdet, mellan 0,2 och 1,1 m RHB 70. De två borrhålssektionerna som hade nivåer utanför detta intervall hade mycket låg transmissivitet. De små naturliga gradienterna inom den tektoniska linsen indikerade höga transmissiviteter i de horisontella och subhorisontella sprickzoner som finns i de övre ca 200 m av berget. Studier av responser i ikringlinggande borrhål vid tre enskilda distinkta pumpningar i bergborrhål tydde på god hydraulisk kontakt över långa distanser inom linsen. Detta styrker den förekomst av höga transmissiviteter som indikerades av de små naturliga gradienterna.

Nivåvariationerna, både i jord- och berggrundvattnet, var starkt kopplade till variationerna i nederbörd/snömältning och evapotranspiration medan förändringar i havsnivån hade ingen eller ringa inverkan. Även för berggrundvattnet kunde 80 % av de årliga variationerna förklaras av variationerna i nederbörd/snömältning och evapotranspiration. I några av hammarborrhålen, som penetrerade utgående flacka sprickzoner, kunde emellertid en trolig inverkan av havsnivåvariationer identifieras.

Där grundvattennivåerna i jord och berg mättes i närbelägna hål inom den tektoniska linsen var grundvattennivån i jord 1–2 m högre än i berg. Dessa skillnader kunde inte förklaras av skillnader i vattnets densitet utan var indikationer på ett nedåtriktat flöde från jord till berg. Den relativt stora skillnaden i nivå, liksom avsaknaden av responser i jordrören på pumpning i berghålen i de flesta fall, tyder dock på en begränsad hydraulisk kontakt. En trolig förklaring till nivåskillnaderna är att den jämförelsevis höga transmissiviteten i den övre delen av berggrunden inom linsen medför att den begränsade del av grundvattenbildningen som når berget kan ledas bort redan vid mycket små gradienter. Det fanns inga data som visar på någon utströmning av djupare grundvatten ända upp till ytan inom den tektoniska linsen (kandidatområdet).

Avrinningen mättes i fyra stationer med automatisk registrering. De uppströms liggande avrinningsområdena varierade i storlek mellan 2,3 och 5,6 km^2. Stationen som mätte avrinningen från det största området hade varit i drift sedan april 2004 medan mätningarna i de tre andra startade i december samma år. Detta betydde att de tillgängliga tidsserierna var för korta för att dra några bestämda slutsatser angående den specifika avrinningens storlek och variationer i tid och rum. Emellertid kunde väldefinierade samband mellan variationer i avrinningen och medelgrundvattennivån i uppströms belägna grundvattenrör i jord identifieras, dock med viss tidförskjutning i flödets stigande fas. En konceptuell hydrologisk modell utvecklades. Tidsserierna var för korta för att tillåta både kalibrering och validering, men preliminära modelleringar tydde på att det uppmätta flödet kunde simuleras med tillfredsställande noggrannhet. För det största området, som hade den längsta uppmätta tidsserien, erhölls ett R^2-värde (enligt Nash-Sutcliffe) av 0,9 och felet i vattenbalansen över hela mätperioden var 3 %. För perioden juli 2004–juni 2005, var den korrigerade nederbörden som input till modellen 548 mm och den beräknade evapotranspirationen 374 mm och avrinningen 152 mm. Under perioden så ökade det simulerade vatteninnehållet i omättad och mättad zon med 22 mm.

Installationen av mätutrustning hade varit en pågående process sedan slutet av 2002. Detta betydde att de olika tidsseriernas längd varierade och att många tidsserier var alltför korta för att några bestämda slutsatser skulle kunna dras. Den varierande längden på tidsserierna försvårade också jämförelsen av deras medelvärden och varians. Osäkerheten i de erhållna resultaten varierade dock mellan tidsserierna, vilket diskuteras nedan:

- Något mer än två års meteorologiska data från platsundersökningen var tillgängliga. Dessa tidserier var för korta för att några säkra samband skulle kunna etableras med omkringliggande SMHI-stationer vilket är önskvärt för mer långsiktiga analyser och modelleringar.
- Havs- och sjönivåmätningarna bedöms ge en god indikation över de variationer som kan förväntas. Längre mätserier bedöms inte medföra några ändringar i den konceptuella modellen men blir viktiga för ytterligare analyser av sambandet mellan yt- och grundvatten.
- Tidsserierna för grundvattennivåer i jordlagren bedöms ge en god indikation av de variationer som kan förväntas. Några ytterligare observationsrör på olika nivåer i våtmarker och i direkt anslutning till hammarborrhål vore dock önskvärda för att studera vertikala flödesgradienter.
- På grund av de intensiva borrnings- och pumpningsaktiviteterna i området, var de tillgängliga ostörda tidsserierna för berggrundvattnets nivåer korta vilket försvårade analyserna gällande naturliga förhållanden. Slutsatser gällande dessa bör därför betraktas som preliminära. Särskilt för studier av sambandet med havets nivå och av vertikala gradienter för grundvattnet flödet bedöms längre ostörda tidsserier som mycket viktiga. För studier av sambandet med havsnivån visade sig principal och oberoende komponent analyserna, liksom den partiella minsta kvadrat modelleringen, vara kraftfulla verktyg och dessa analyser

bör upprepas när längre tidsserier finns tillgängliga. För de rekommenderade fördjupade studierna av de vertikala flödesgradienterna är det viktigt att systematiska beräkningar görs av ”environmental heads” baserade på kvalitetssäkrade mätningar av vattendensiteterna i alla de moniterade sektionerna i bergborrhålen.

- De tillgängliga tidsserierna för avrinningen var för korta för att några bestämda slutsatser skulle kunna dras gällande den specifika avrinningens storlek och variation i tid och rum. Avrinningsdata bedöms som mycket viktiga för beräkningar av områdets vattenbalans och för kalibreringen av de hydro(geo)logiska modellerna. Vid sista datafrysen i Forsmark, den 31 mars 2007, kommer ytterligare drygt ett och ett halvt års data att finnas tillgängligt för nya analyser och modelleringar.

Contents

1 Introduction

1.1 Background

The Swedish Nuclear Fuel and Waste Management Company (SKB) is conducting site investigations at two different locations, the Forsmark and Simpevarp areas, with the objective of siting a geological repository for spent nuclear fuel. The investigations are divided into an initial site investigation phase and a complete site investigation phase /SKB 2001/. The results from the investigations at the sites are used as a basic input to the site descriptive modelling. A Site Descriptive Model (SDM) is an integrated description of the site and its regional setting, covering the current state of the geosphere and the biosphere as well as ongoing natural processes of importance for long-term safety. The SDM shall summarise the current state of knowledge of the site, and provide parameters and models to be used in further analyses within Safety Assessment, Repository Design and Environmental Impact Assessment.

The first steps of the site descriptive modelling for the Forsmark area, included in the initial site investigation phase, have been taken with versions 1.1 and 1.2 of the model /SKB 2004, 2005/. Models are developed on a regional scale (hundreds of square kilometres) and on a local scale (tens of square kilometres). These model areas include the candidate area, within which most of the deep rock boreholes are located. The surface areas covered by the regional model and the candidate area are shown in Figure 1-1.

1.2 Scope and objective

The present report is produced as a background report for the version 2.1 model of the Forsmark area, constituting the first modelling step in the complete site investigation phase, and includes a presentation and an integrated analysis of meteorological, hydrological and hydrogeological monitoring data. Compared with the report on climate, surface hydrology, and near-surface hydrogeology produced for the 1.2 modelling /Johansson et al. 2005/ the present report is restricted to time series data, but besides extended time series also includes data from percussion-drilled boreholes in the bedrock. Hydro(geo)chemical data are not included in the report.

The objectives of this document are to:

- present and analyse meteorological, surface hydrology and hydrogeological data available in the Forsmark 2.1 datasets,
- perform integrated analysis and present relationships between the different datasets,
- discuss implications of the results of the data analysis for the conceptual hydrogeological model of the Forsmark area.

All data used in the report were extracted from the SKB SICADA-database. Most of the data analysed herein have been described in the SKB P-report series. These reports contain comprehensive data presentations and references are made to them in connection to the analysis of the different datasets.

1.3 Site description

In north-eastern Uppland, the highest precipitation occurs some distance inland from the coast. For example, the mean annual precipitation in Lövsta, approximately 10 km inland, is 718 mm, which can be compared with the corresponding value of 564 mm at Örskär (values corrected for wind losses etc by 9% and 16% for Lövsta and Örskär, respectively /Wern and Jones 2006/),

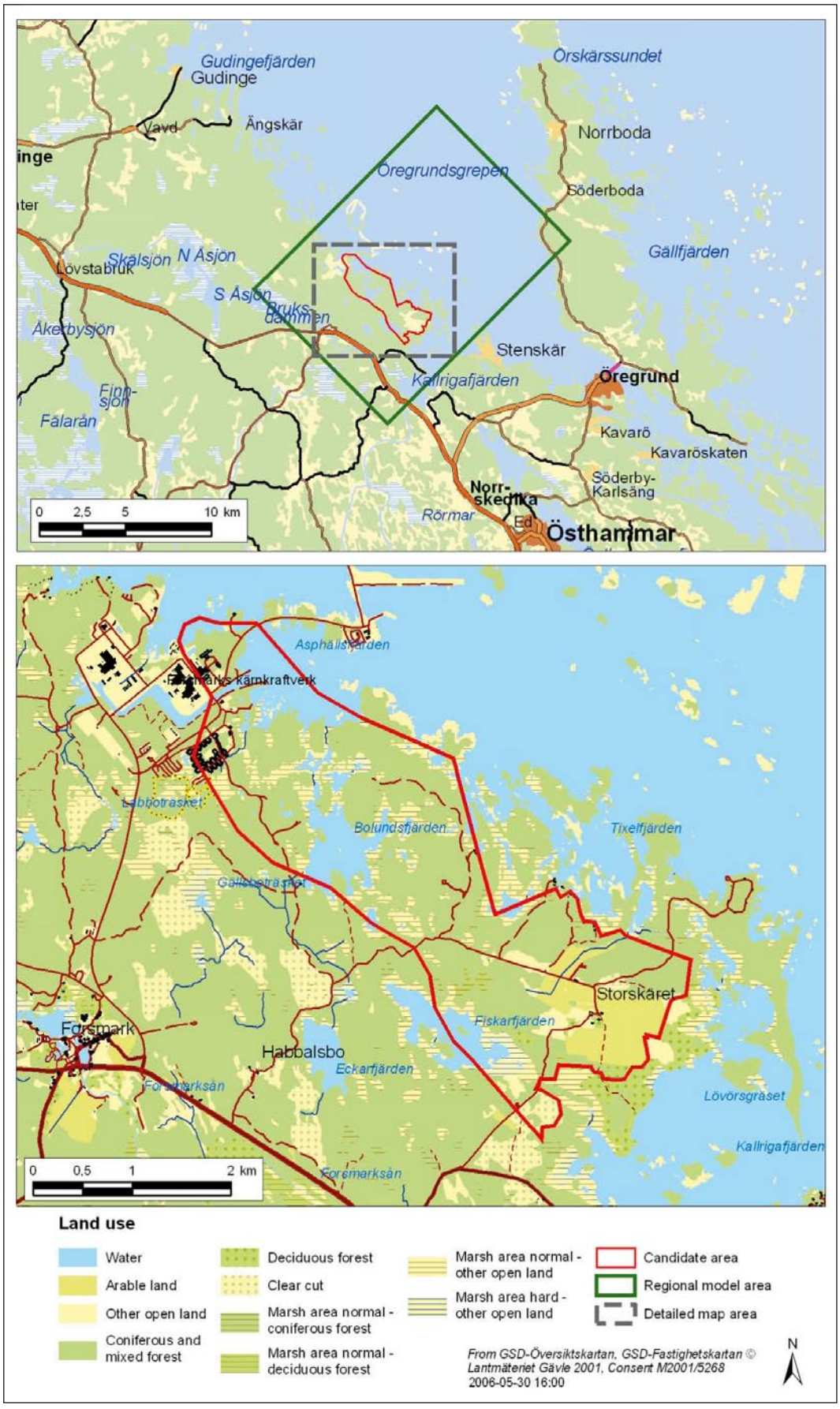

Figure 1-1. *Overview of the Forsmark area and identification of the regional model area and the candidate area.*

see Figure 2-1 for the location of the meteorological stations. From regional data the long-term mean annual precipitation in the Forsmark area has been estimated to 559 mm by the Swedish Meteorological and Hydrological Institute (SMHI) /SMHI 2005/. Some 25–30% of the annual precipitation falls in the form of snow. The average monthly mean temperature varies between –4°C in January–February and +15°C in July. The winters are slightly milder at the coast than inland, and the mean annual temperature at Örskär is 5.5°C compared to 5.0°C at the more inland stations at Risinge and Films kyrkby. The vegetative period, defined as the period with daily mean temperatures exceeding 5°C, is about 180 days. Based on the synoptic observations at Örskär, the mean annual global radiation was calculated to 930 kWh/m^2, with the mean monthly values varying from 4 kWh/m^2 in December to more than 170 kWh/m^2 in June.

The regional meteorological data will constitute an important basis for extrapolating the relatively short time series measured at the local stations (up to 4–5 years during the site investigations) to time series statistics for longer periods. For a more detailed description of the regional meteorological conditions in the Forsmark area, see /Lindell et al. 2000/ and /Larsson-McCann et al. 2002/.

The site invesigation area is characterized by a low relief with a small-scale topography. The study area is almost entirely below 20 metres above sea level, as shown in Figure 1-2.

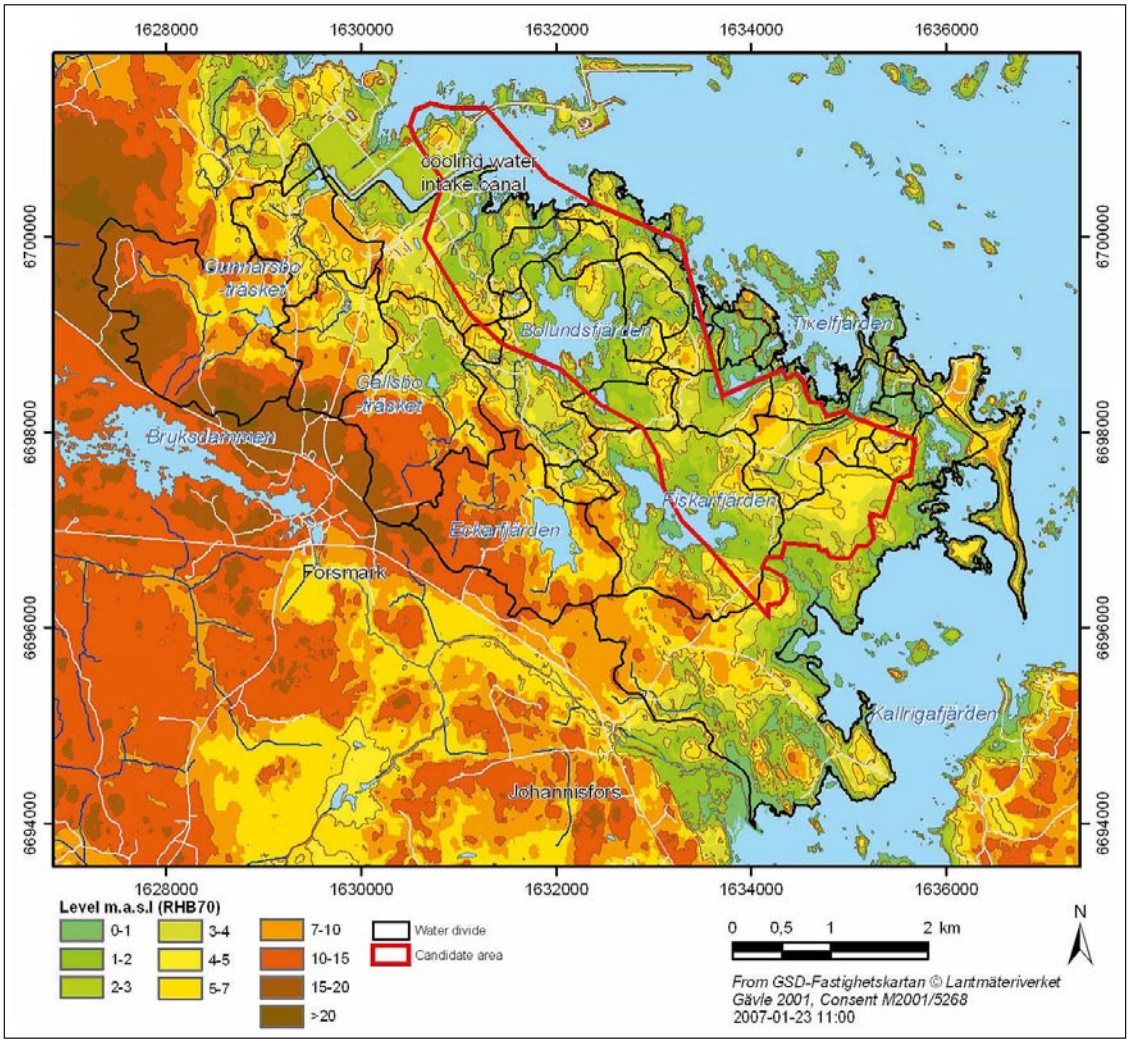

Figure 1-2. *Topographical map of the candidate area and its surroundings with surface water divides indicated.*

As described by /Brunberg et al. 2004/, 25 “lake-centered” catchments and sub-catchments have been delineated, ranging in size from 0.03 km^2 to 8.67 km^2. Forest is dominating and covers approximately 70% of the total catchment areas. Only in the south-east, at Storskäret, is agricultural land an important landuse, see Figure 1-1. The main lakes are Fiskarfjärden (0.752 km^2), Bolundsfjärden (0.609 km^2), Eckarfjärden (0.282 km^2) and Gällsboträsket (0.185 km^2). The lakes are shallow with mean depths and maximum depths ranging from approximately 0.1 to 1 m and 0.4 to 2 m, respectively /Brunberg et al. 2004/.

No major water courses flow through the catchment areas delineated in Figure 1-2. The brooks downstream Lake Gunnarsboträsket, Eckarfjärden and Gällsboträsket carry water most of the year, but can still be dry for long time periods during dry years such as 2003. Many brooks in the area have been deepened for considerable distances for draining purposes. However, the riparian zones are still wide at many locations and relatively large areas are inundated during periods of high water levels.

Wetlands are frequent and cover more than 25% in some sub-catchments /Johansson and Juston 2005/. Bogs are found in the most elevated parts of the area only. These bogs are small and the peat cover is not very thick (< 3 m) /Fredriksson 2004/. Fens and marshes are frequent in the more low-lying parts of the area. The peat in the wetlands can rest directly on till, or be underlain by gyttja and/or sand and clay above the till. This means that the hydraulic contact with the surrounding groundwater system varies among the wetlands in the area.

A map of the Quaternary deposits is shown in Figure 1-3. From this map, it is obvious that till is the dominating Quaternary deposit, covering approximately 75% of the mapped area. Bedrock outcrops are frequent, but constitute only approximately 5% of the area. Wave-washed sand and gravel, clay, gyttja clay and peat cover 3–4% each. The only glaciofluvial deposit, the Börstilåsen esker, runs in a north-south direction along the coast (cf. the “green belt” on the map). The Quaternary deposits are shallow, usually less than 5 m deep /Sohlenius et al. 2004/. The greatest depth to bedrock, recorded in a drilling south-east of Fiskarfjärden, is 16 m.

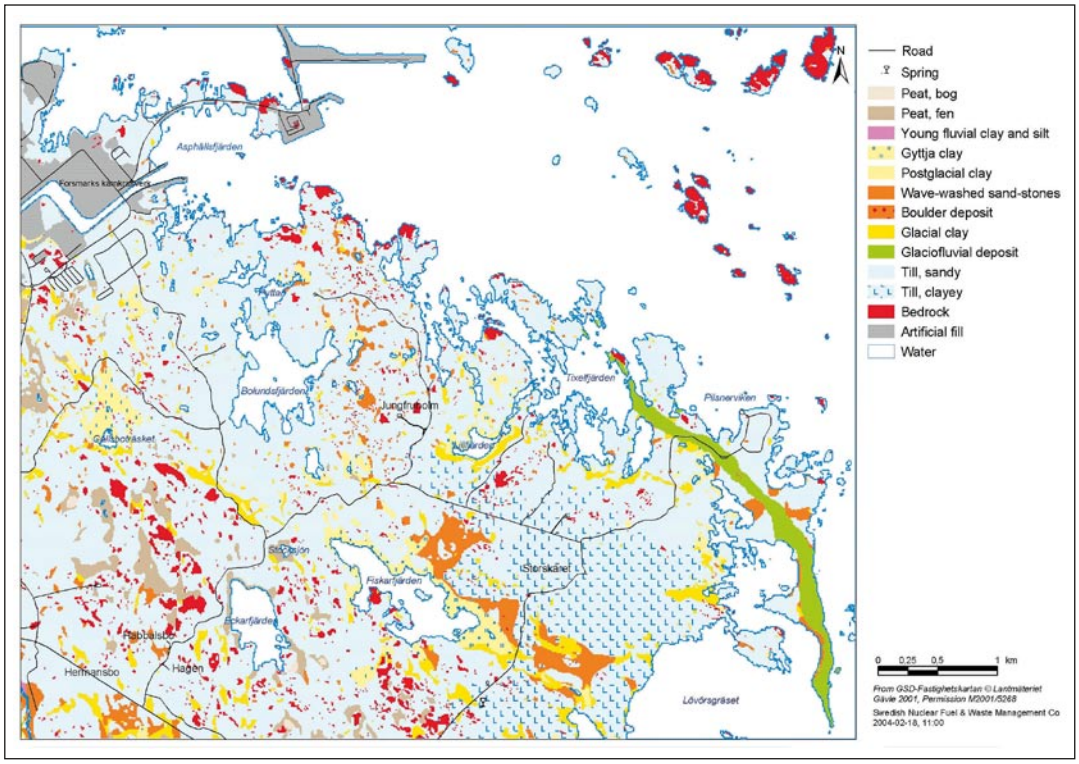

Figure 1-3. *Detailed map of Quaternary deposits /Sohlenius et al. 2004/.*

The hydraulic properties of the till are mainly determined by the grain size distribution, the compactness, and structures as lenses of sorted material. From generic and site-specific data it is known that in the uppermost part of the till, the hydraulic conductivity and specific yield are much higher than further down the profile /Lind and Lundin 1990, Lundin et al. 2005/. This is mainly due to soil forming processes, probably with ground frost as the single most important process, resulting in higher porosity and formation of macro-pores. However, wave washing also implies that the till at exposed locations is coarser at the ground surface, and at some locations coarse out-washed material has been deposited. Based on generic and site specific data, the saturated hydraulic conductivity in the uppermost part or the till can be estimated to 10^{-5}–10^{-4} m/s and the specific yield to between 10% and 20%, with the higher values close to the surface. The total porosity can typically be estimated to 30–40% mainly depending on depth. Below the depth interval strongly influenced by the soil forming processes, the hydraulic conductivity and the porosity of the till are considerably lower. The results from the slug tests indicate a higher hydraulic conductivity in the Quaternary deposit/bedrock contact zone than in the till itself, with geometric mean values of $1.3 \cdot 10^{-5}$ m/s and $1.2 \cdot 10^{-6}$ m/s (not including wells installed below open water), respectively /Johansson and Juston 2005/. From generic and site specific data, the total porosity and specific yield of the till below the upper c. 0.5 metre can be estimated to 20–30% and 2–5%, respectively.

For the only glaciofluvial deposit in the area, the Börstilåsen esker, the obtained hydraulic conductivity of $2 \cdot 10^{-4}$ m/s is relatively low, and the storativity of $2 \cdot 10^{-3}$ indicates mainly confined conditions. No site-specific hydraulic data exist for clay, gyttja or peat in the 2.1 dataset. The existence and the hydraulic conductivities of clay and gyttja below wetlands and lakes are important factors for the surface water-groundwater interaction. Supplementary investigations will be conducted of the stratigraphy and hydraulic properties of the wetlands during the 2.2 stage of the site investigation.

The stratigraphy of bottom sediments in lakes has been investigated, and typical profiles have been identified for some of the lakes /Hedenström 2003, 2004, Vikström 2005/. Typically, the sediment stratigraphy from down and up is glacial and/or postglacial clay, sand and gravel, and nested layers of gyttja in different fractions. The clay layer is missing in major parts of the area below Bolundsfjärden. However, a pumping test in the vicinity of this lake still indicated a very limited hydraulic contact between the lake and groundwater in till below the lake /Werner and Lundholm 2004/.

The bedrock hydrogeological conditions in Forsmark reveal a significant hydraulic anisotropy within the tectonic lens, which covers the body of the candidate area. The upper c. 200 m of bedrock contains high-transmissive horizontal fractures/sheet joints. These fractures/sheet joints occur at different elevations in the percussion drilled boreholes, but are found to interconnect hydraulically across large distances (1–2 km) /Gokall-Norman et al. 2005/. The horizontal fractures/sheet joints have transmissivities in the range c. $1 \cdot 10^{-6}$–$1 \cdot 10^{-3}$ m^2/s (hydraulic conductivity c. $1 \cdot 10^{-6}$–$1 \cdot 10^{-3}$ m/s). The bedrock in between the horizontal fractures/sheet joints, however, is considerably less conductive (hydraulic conductivity c. $1 \cdot 10^{-11}$–$1 \cdot 10^{-8}$ m/s) except where it is intersected by transmissive steeply-dipping or gently-dipping deformation zones. Below the uppermost c. 200 m of bedrock the occurrence of high-transmissive horizontal fractures/sheet joints vanish totally and the conductive fracture frequency becomes very sparse and fairly low-transmissive (fracture transmissivity c. $1 \cdot 10^{-10}$–$1 \cdot 10^{-7}$ m^2/s). In some of the 1,000 m deep cored boreholes there are almost no flowing fractures observed below c. 200 m depth, which is exceptional in a national perspective.

Figure 1-4 shows a section illustrating the conceptual hydrogeological model of the site investigation area as presented in the SDM 1.2.

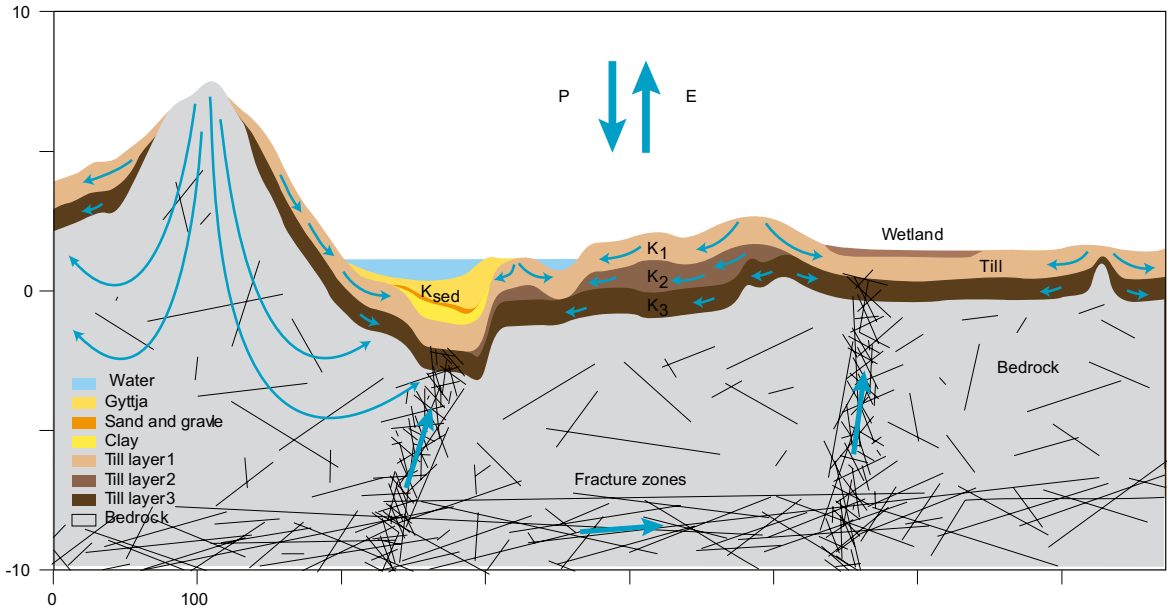

Figure 1-4. *Section illustrating the conceptual hydrogeological model of the site investigation area as presented in the site descriptive model 1.2 /Johansson et al. 2005/.*

2 Presentation of time series data

2.1 Introduction to the hydrological time series data

There are five principal hydrological datasets reviewed in this document. Those are time series of meteorological data, surface water levels, surface water discharge, and groundwater levels in the Quaternary deposits and in the bedrock. The installation of instrumentation to measure these time series is an ongoing process in the Forsmark site investigation area. Figure 2-1 gives an historical overview of the number of available data records for each dataset from January 2003 through the July 2005 data freeze 2.1. The short-term variations in the number of available data are due to malfunction of equipments and specific tests in some wells.

All data used in the present report are derived from SKB's SIDACA and GIS databases. Table 2-1 summarises SKB P-reports up to data freeze 2.1 for the drilling and monitoring of wells, and monitoring of meteorological data, surface water and groundwater levels and surface discharge.

The meteorological data of most concern in this study were precipitation (P) and potential evapotranspiration (PET) time series. P was measured and PET was calculated at two stations in the study area from May 2003, but with some intervals of missing data. This study also utilized longer P and PET time series data from close-by SMHI stations for comparison.

Surface water levels were measured in the sea at two locations and in six of the larger lakes in the study site (Bolundsfjärden, Eckarfjärden, Fiskarfjärden, Norra Bassängen, Gällsboträsket, and Lillfjärden). Surface water discharges in streams were measured at four flume gauging stations /Johansson 2005/. The first station became operational in April 2004 and the other three followed eight months later in December 2004.

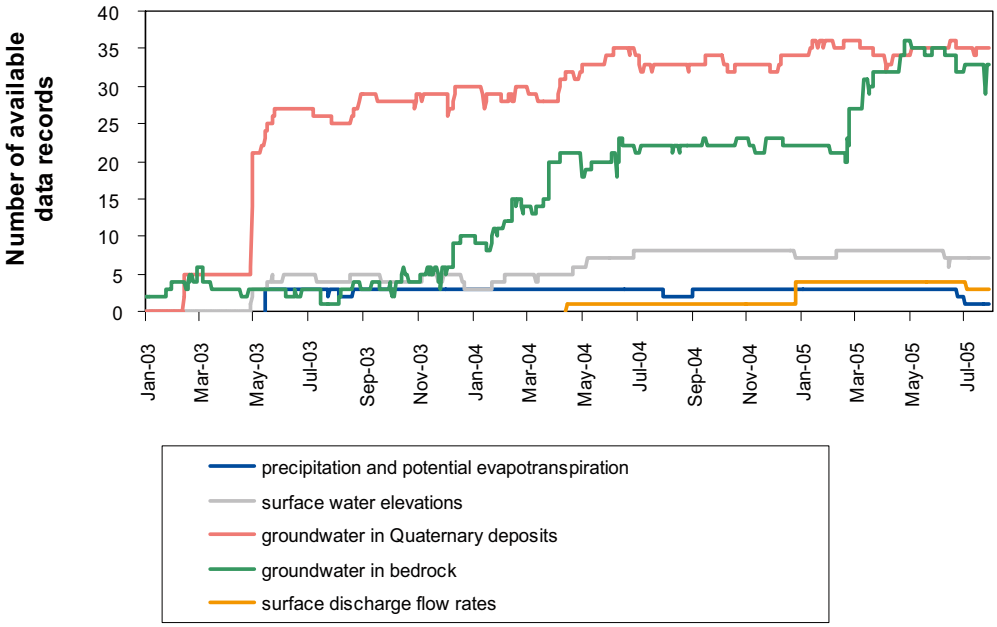

Figure 2-1. *Overview of the availability of data from time series of meteorological data, surface water levels, surface discharge, and groundwater levels in the Quaternary deposits and in the bedrock.*

Table 2-1. Reports in the SKB P-series on drilling of wells in Qaternary deposits and percussion-drilled boreholse in bedrock, and monitoring of meteorological data, surface water and groundwater levels and surface discharge. (Reports can be downloaded from www.skb.se.)

P-03-30	**Claesson L-Å, Nilsson G.** Drilling of a flushing water well, HFM01, and two groundwater monitoring wells, HFM02 and HFM03 at drillsite DS1.
P-03-51	**Claesson L-Å, Nilsson G.** Drilling of a flushing water well, HFM05, and a groundwater monitoring well, HFM04 at drillsite DS 2.
P-03-58	**Claesson L-Å, Nilsson, G.** Drilling of a flushing water well, HFM06, and two groundwater monitoring wells, HFM07 and HFM08 at drillsite DS3.
P-03-64	**Johansson P-O.** Drilling and sampling in soil. Installation of groundwater monitoring wells and surface level gauges.
P-03-117	**Aquilonius K, Karlsson S.** Snow depth, frost in ground and ice-cover during the winter 2002/2003.
P-04-76	**Claesson L-Å, Nilsson, G.** Drilling of a flushing water well, HFM10, a groundwater monitoring well, HFM09 and a groundwater monitoring well in soil SFM0057, at drillsite DS4.
P-04-85	**Claesson L-Å, Nilsson, G.** Drilling of a flushing water well, HFM13, two groundwater monitoring wells in solid bedrock, HFM14–15, and one groundwater monitoring well in soil, SFM0058, at and close to drilling site DS5.
P-04-94	**Claesson L-Å, Nilsson, G.** Drilling of a monitoring well, HFM16, at drilling site DS6.
P-04-106	**Claesson L-Å, Nilsson, G.** Drilling of five percussion boreholes, HFM11-12 and HFM 17–19, on different lineaments.
P-04-137	**Heneryd N.** Snow depth, ground frost and ice cover during the winter 2003/2004.
P-04-138	**Werner K, Lundholm L, Johansson P-O.** Drilling and pumping test of wells at Börstilåsen.
P-04-139	**Werner K, Lundholm L.** Supplementary drilling and soil sampling, installation of groundwater monitoring wells, a pumping well and surface water level gauges.
P-04-245	**Claesson L-Å, Nilsson, G.** Drilling of two flushing water wells, HFM21 and HFM22, one groundwater monitoring well in solid bedrock, HFM20, and one groundwater monitoring well in soil, SFM0076.
P-04-313	**Nyberg G, Wass E, Askling P, Johansson P-O.** Hydromonitoring program. Report for June 2002–July 2004.
P-05-134	**Heneryd N.** Snow depth, ground frost and ice cover during the winter 2004/2005.
P-05-154	**Johansson P-O.** Installation of brook discharge gauging stations.
P-05-221	**Wern L, Jones J.** Meteorological monitoring at Forsmark, June 2003 until July 2005.
P-05-245	**Nyberg G, Wass E.** Hydromonitoring program. Report for Augusti 2004–July 2005.

As of July 2005, there were 36 monitoring wells in the Quaternary deposits with automatic data registration that produced groundwater level time series. These include seven boreholes that were situated directly under surface waters. Measurement in many of these wells started in May 2003 and that, therefore, is generally taken as the start month of time series analysis in this report. Most groundwater time series from these wells were interrupted for one or more intervals of various lengths after they came online, hence the number of available data records is not constant through the study period.

The number of percussion-drilled boreholes in the bedrock producing point water head data increased steadily during the study period. As of July 2005, there were 22 separate percussion-drilled well locations, and 11 of those wells were sectioned with between 1–3 packers. Thus, there were a total of 40 time series that were potentially available from these wells in July 2005.

It should be noted that, due to considerable differences in groundwater salinity with depth, and thereby in density, measured groundwater levels in percussion-drilled boreholes in the bedrock should be regarded as point water heads. For some of the wells, these heads need to be transformed to so-called environmental water heads in order to interpret vertical groundwater flow components (for a discussion of groundwater levels, point water heads and environmental water heads, see Appendix 1).

2.2 Meteorological data

Figure 2-2 and Figure 2-3 show locations for Högmasten and Storskäret meteorological stations in the Forsmark site investigation area, as well as for several nearby SMHI stations. All precipitation data presented in this report is corrected for losses according to /Alexandersson 2003/. The corrections largely compensate for wind losses.

Figure 2-4 shows an 11-year history of annual total precipitation from three nearby precipitation stations maintained by SMHI at Lövsta, Östhammar, and Örskär. Figure 2-5 shows these same data represented as a range and mean at each station, using an August to July data year, with the two most recent data years specifically indicated for reference. (August to July data years are used to correspond to SKB's 1.2 and 2.1 data freezes for Forsmark). Combined, these figures suggest that precipitation in the region for the August 2003 to July 2004 and August 2004 to July 2005 data years was fairly typical compared to longer term time series, with the first of the two years a little bit wetter than normal and the second year somewhat drier.

Figure 2-6 shows daily corrected precipitation measured by SKB at Högmasten and Storskäret stations within the Forsmark site investigation area from May 14, 2003 through July 31, 2005. Högmasten was missing a total of 31 days of data, all in July 2005, while Storskäret was missing 56 days, most of which were from late June through July 2005. Figure 2-7 shows that the available daily data at these stations was well-correlated, particularly during non-summer months. The difference in correlation between daily precipitation during summer (defined here as June, July and August) and non-summer periods can be explained by localized convective storms that are typical during summer months.

Figure 2-2. *SKB's two meteorological stations, Högmasten and Storskäret, within the Forsmark site investigation area and nearby SMHI stations.*

Figure 2-3. *Detailed map of the locations of the meteorological stations, Högmasten and Storskäret, within the Forsmark site investigation area.*

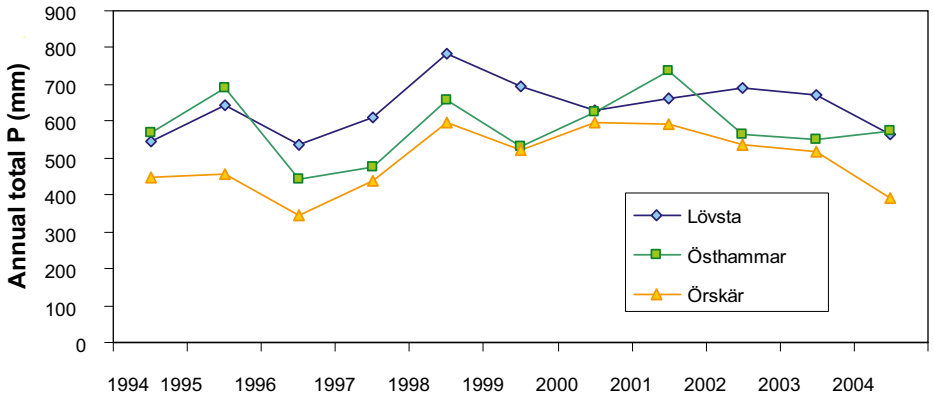

Figure 2-4. *11-year history of annual* corrected *precipitation* (P) *at three regional SMHI stations (data were missing at Örskär for November 1995).*

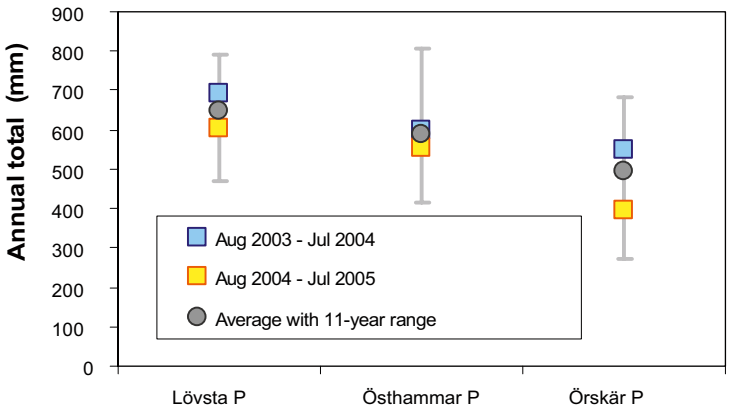

Figure 2-5. *Comparison of annual corrected precipitation (P) from the two most recent data years (using August to July annual intervals) at three regional SMHI stations to the means and ranges from the previous 11-years.*

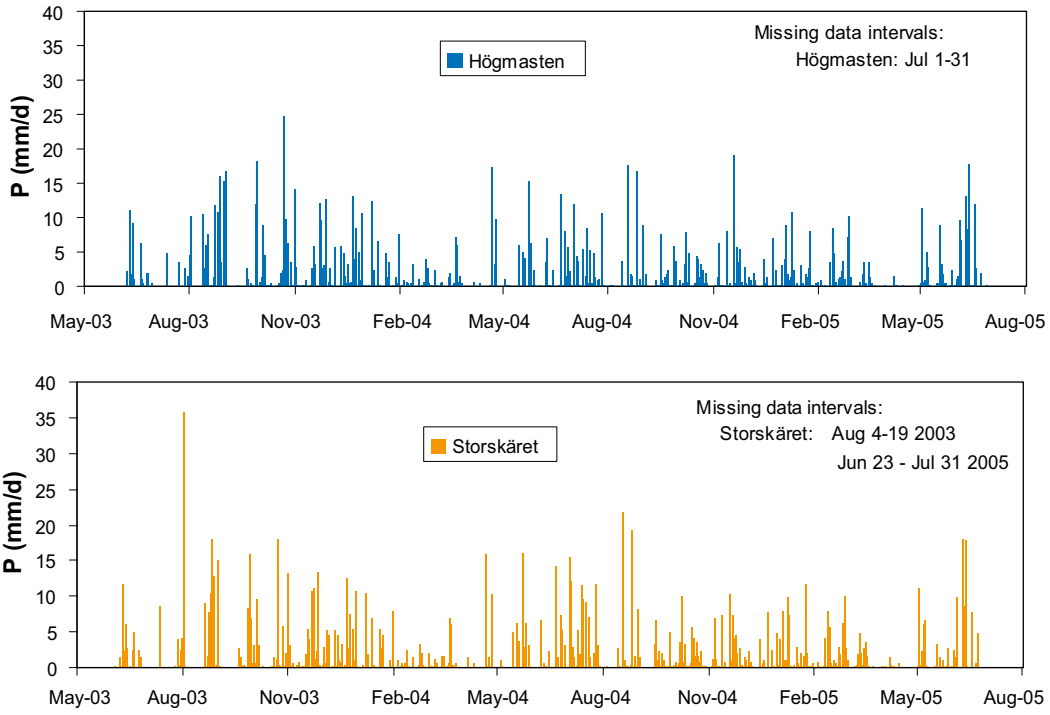

Figure 2-6. *Daily corrected precipitation (P) measured at Högmasten (PFM010700) and Storskäret (PFM010701). (Tick marks on the X-axis indictate the first date of the labeled months.)*

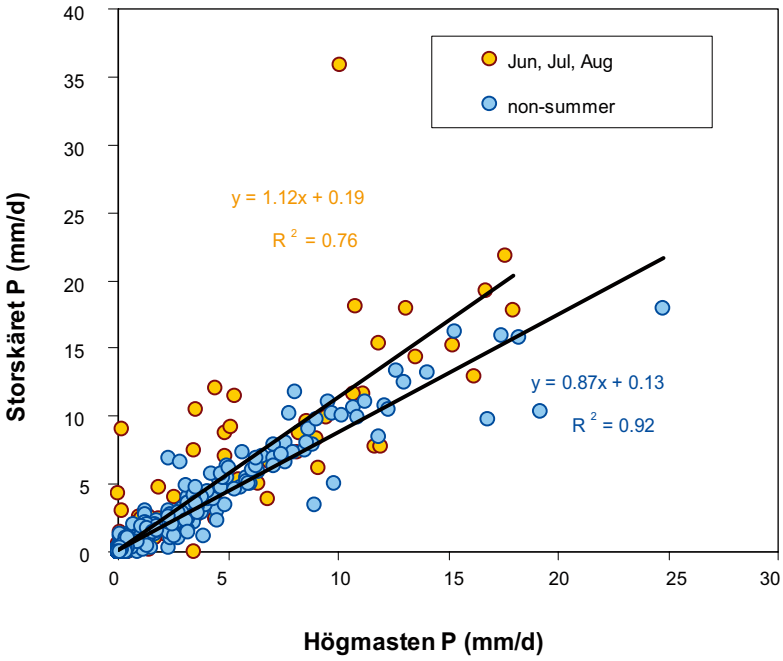

Figure 2-7. *Correlation of daily measured precipitation (P) at Högmasten (PFM010700) and Storskäret (PFM010701), shown separately for summer months and the remainder of the year.*

Figure 2-8 presents monthly total precipitation for the two SKB stations and the three SMHI stations, Lövsta, Östhammar and Örskär. Similar seasonal patterns are observable at these five stations, with Örskär typically reporting the lowest rainfall on a month-to-month basis. Figure 2-9 shows annual totals of these same data based on August to July intervals. To facilitate comparison between stations, the second "year" of data in Figure 2-9 is only a 10-month total (August 2004 through May 2005) due to missing data in the Högmasten and Storskäret time series. However, it is evident that the precipitation at Högmasten and Storskäret is closer on an annual basis to Lövsta and Östhammar than to Örskär.

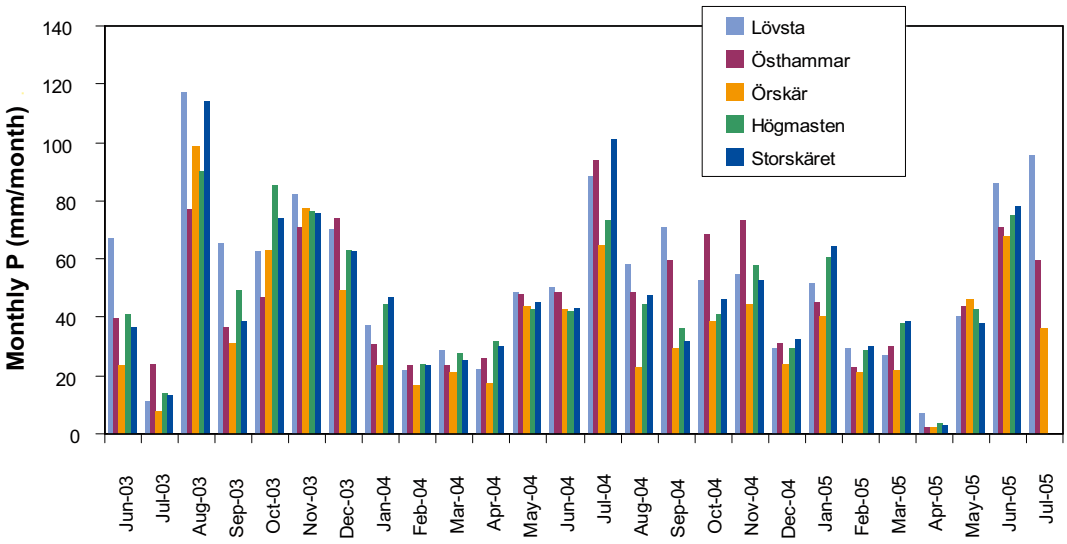

Figure 2-8. *Monthly total precipitation (P) time series measured at two SKB stations (Högmasten and Storskäret) and three nearby SMHI stations (Lövsta, Östhammar, and Örskär).*

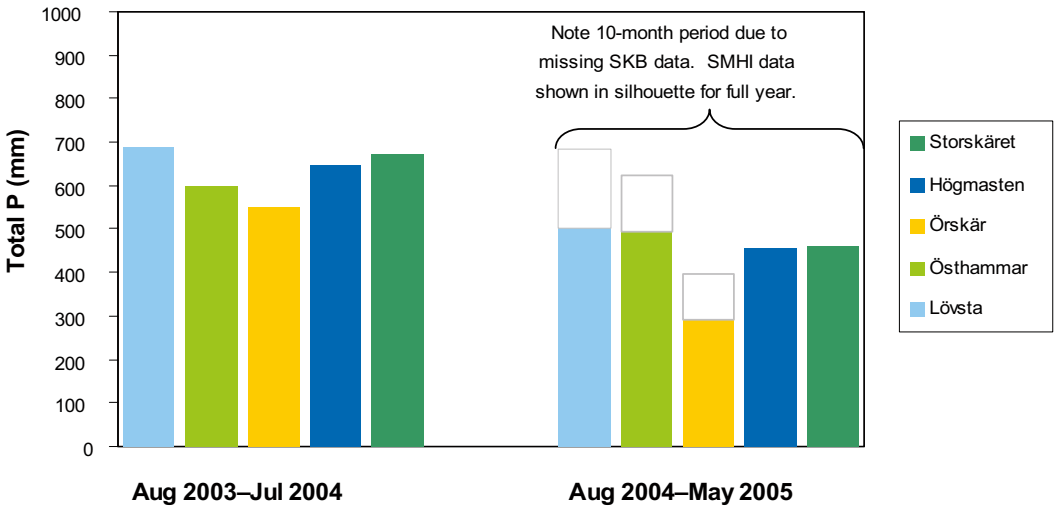

Figure 2-9. *Annual total measured precipitation (P) at both SKB stations and three nearby SMHI stations. Note that totals for the second period represent 10 months and not a year due to missing SKB data in June and July 2005.*

The annual total corrected precipitation measured at Högmasten and Storskäret between August 2003 and July 2004 was 649 and 672 mm, respectively. Note that the real difference between the stations is most probably somewhat higher since 27 mm of precipitation were measured at Högmasten during the 16-day interval in August 2003 when Storskäret was offline. The annual totals at the same two stations for the interval of January–December 2004 were 488 and 519 mm, respectively. There were no missing data during this interval. For reference, SMHI reports, based on calculations from surrounding SMHI stations, a 30-year average annual precipitation at Högmasten and Storskäret of 568 and 549 mm, respectively, with corresponding standard deviations of 108 and 104 mm /SMHI 2005/.

Figure 2-10 shows the daily potential evapotranspiration (PET) time series calculated from measured data at Högmasten. The PET was calculated based on the Penman equation applied according to /Eriksson 1981/. The annual total PET from August 2003 through July 2004 was 497 mm, and from August 2004 through July 2005 was 507 mm. Figure 2-10 also shows a rolling annual total PET, calculated from May 14, 2004 forward. The average annual PET at Högmasten from the 444 days of calculated annual totals was 497 mm with a standard deviation of 10 mm.

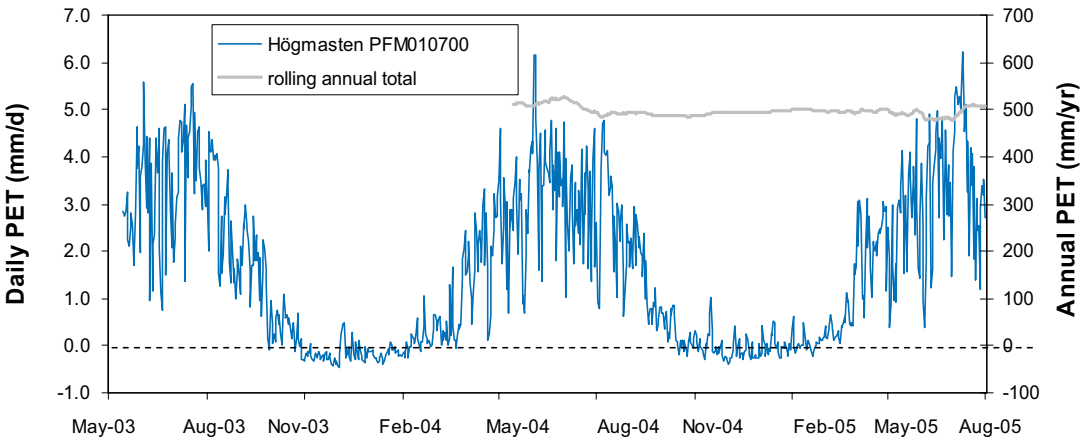

Figure 2-10. *Daily potential evapotranspiration (PET) time series estimated from measured meteorological data at Högmasten, and the rolling annual total PET calculated from the daily time series. Tick marks on the X-axis indictate the first date of labeled months.*

Figure 2-11 shows monthly total precipitation and potential evapotranspiration data measured in the site investigation area. Monthly values for total precipitation in June and July 2005 were estimated data to fill in the data gaps, see Figure 2-6. Missing data were estimated because complete continuous time series were useful for assessing influences on meteorological inputs to the hydrological responses in the site investigation area. The missing precipitation data in Högmasten and Storskäret time series were estimated with separate regression equations that were calibrated to the regional SMHI stations at Lövsta, Östhammar, and Örskär. The calibration used only overlapping summer months in these datasets (June, July and August; five months total). The predictive relationship was based on monthly totals because regressions to daily data were poor ($R^2 < 0.5$), whereas correlations were high to monthly totals in both cases ($R^2 > 0.98$). The equations derived from monthly data were used to estimate missing daily data during June and July 2005.

The average of mean daily air temperatures from Högmasten and Storskäret is shown in Figure 2-12. The two temperature time series measured at these stations were virtually identical and highly correlated ($R^2 = 0.99$).

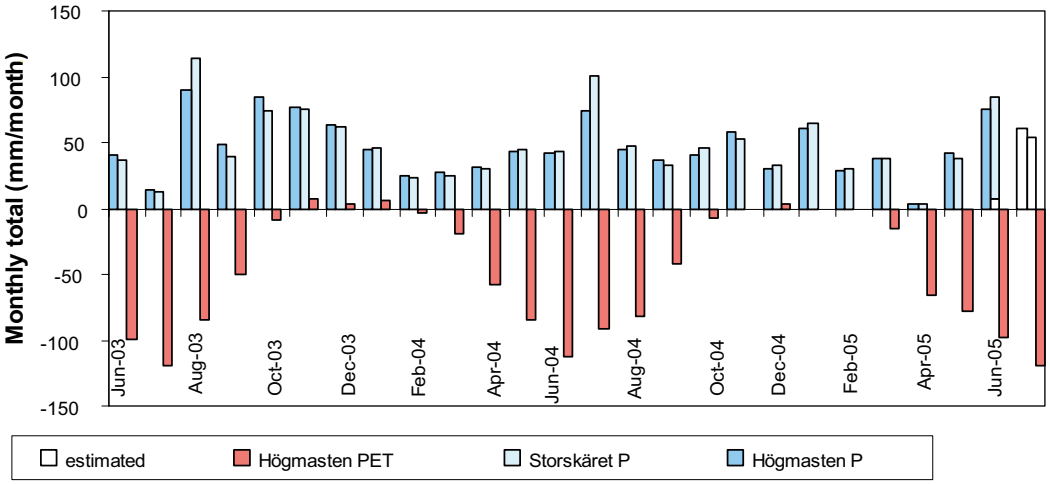

Figure 2-11. *Monthly total corrected precipitation (P) and potential evapotranspiration (PET) data measured on the Forsmark study site, showing estimated monthly totals for missing data. (Tick marks on X-axis separate monthly data.)*

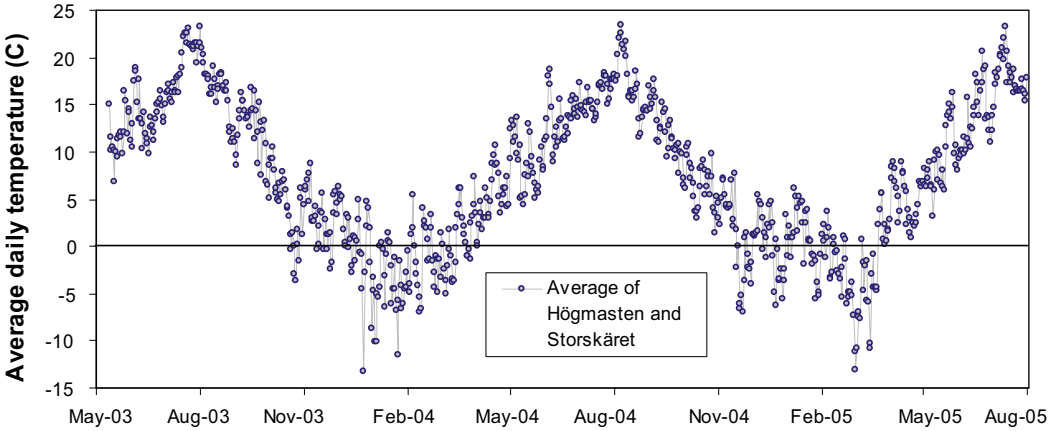

Figure 2-12. *Daily average air temperature from measurements at Högmasten and Storskäret. (Tick marks on the X-axis indictate the first date of the labeled months.)*

Snow depth and snow water content are measured at three locations within the site investigation area, see Figure 2-13. Figure 2-14 shows the water content in snow accumulations measured at these stations. Air temperature and snow water content data were used in this study primarily to calibrate a snowmelt model, which in turn was used to estimate a site average "surface inflow" time series with separately identified snowmelt and rainfall events. These results are described in Section 3.1.

Figure 2-13. *Locations of the three snow depth and snow water content monitoring sites.*

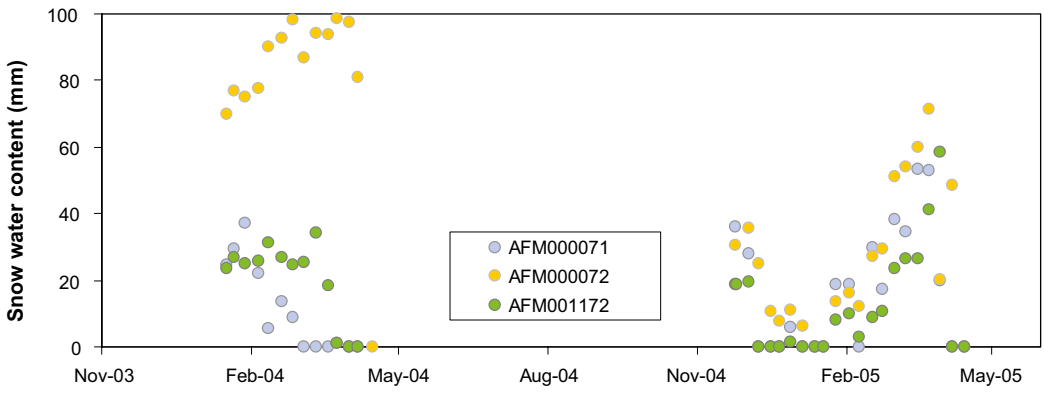

Figure 2-14. *Average water content in accumulated snow at three locations sites across the study area.*

2.3 Surface water levels

As shown in Figure 2-15, surface water level gauges have been installed in six lakes (SFM0039–42, SFM0064 and SFM0066) and at two locations in the Baltic sea, one at Forsmark harbour (PFM010038, previously SFM0038) and the other at Kallrigafjärden (SFM0043). Additionally, SMHI also has a sea level gauge at Forsmark harbour.

A comparison of SMHI's and SKB's sea level measurements is shown in Figure 2-16. The two SKB time series show similarities, but the reported levels at Kallrigafjärden average about 12 cm less than at the Forsmark harbour. Towards the end of April 2005 the reported levels at Kallrigafjärden drift even lower and the station is taken out of the monitoring system. Most likely the station has been lifted by the ice. On the other hand, the available SKB and SMHI data at Forsmark harbour show excellent agreement in both amplitude and trend ($R^2 = 0.95$). Because of missing data and suspected periods of uncertainty in data from the Kallrigafjärden station, only the sea level data measured at Forsmark harbour (PFM010038) will be used throughout the remainder of this report.

The daily average time series from lake surface water level gauges are presented in Figure 2-17. Figure 2-17a shows all six water level measurements and Figure 2-17b shows a close-up of the four lakes with the lowest water levels together with the sea level. The time series for Lillfjärden (SFM0066) indicates that the lake level is mainly determined by the sea level. The lake levels of Norra Bassängen (SFM0039) and Bolundsfjärden (SFM0040) are also quite low, but these levels seem to be determined mainly by the lake thresholds and the surface water and groundwater inflow from the inland. However, during specific intervals, the sea level rises high enough for direct sea water intrusion to the lower elevation lakes in the site investigation area. During one such episode in October 2004, sea levels were in excess of water levels in Norra Bassängen and Bolundsfjärden, but not in Fiskarfjärden. However in January 2005, sea levels rose above water levels in all four of these lower lying lakes, as shown in Figure 2-17b.

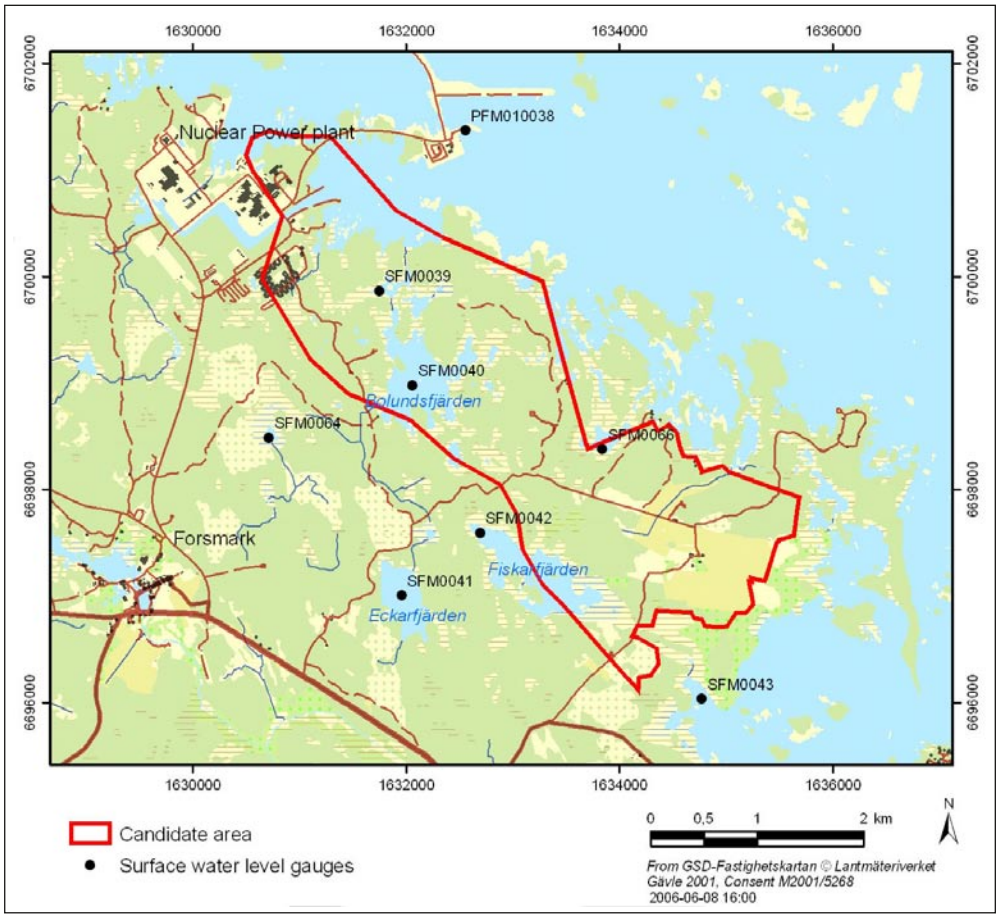

Figure 2-15. *Locations of the surface water level gauges.*

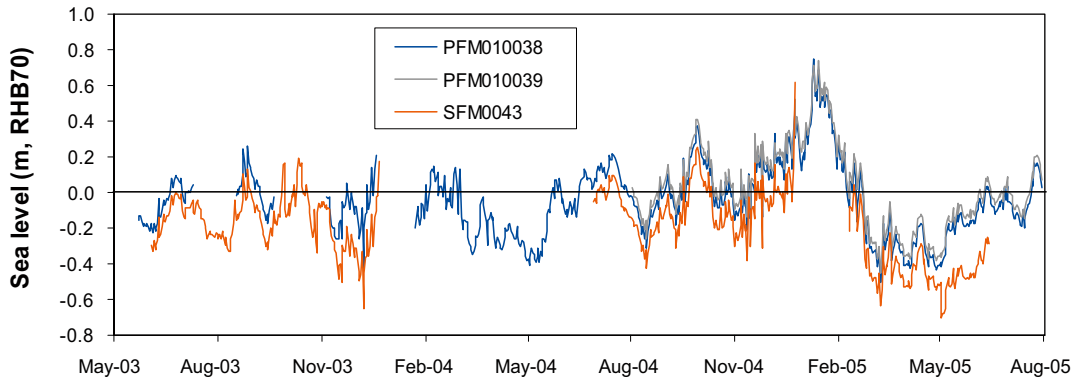

Figure 2-16. *Daily average sea level measured at the SMHI station at Forsmark harbour(PFM010039) and the SKB's stations at Forsmark harbour and Kallrigafjärden, PFM010038 and SFM0043, respectively.*

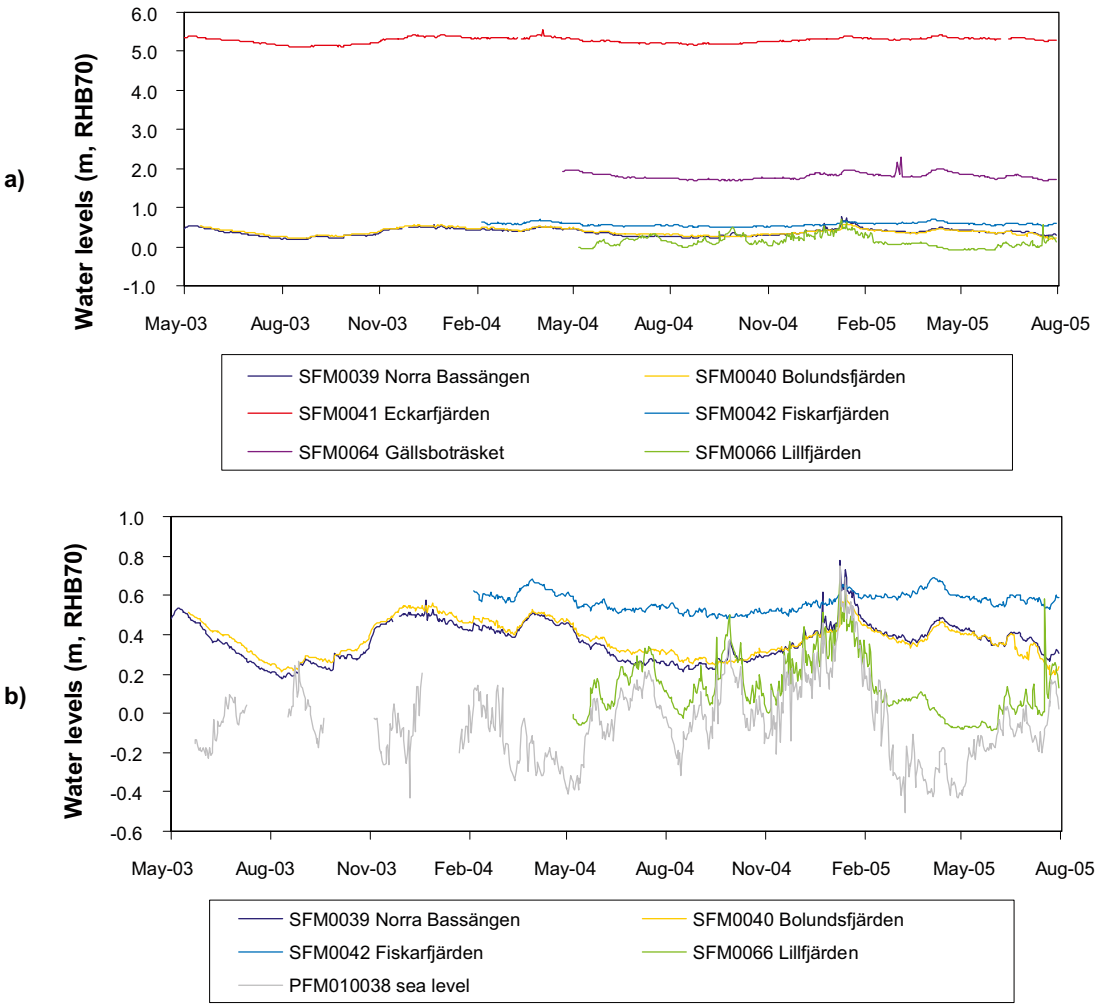

Figure 2-17. *Daily average surface water levels in the Baltic Sea and the larger lakes in the study area shown for all in a) and in close-up for the four lakes with the lowest levels in b). (Tick marks on the x-axis indicate the first date of labelled months.)*

2.4 Groundwater levels in the Quaternary deposits

Groundwater levels in Quaternary deposits were measured in 38 instrumented groundwater monitoring wells. Figure 2-18 shows a map of the locations of these wells.

Figure 2-19 presents daily average groundwater levels expressed as a) elevations (RHB70) and b) depth below surface for the 30 well situated on land. Measured groundwater elevations in Quaternary deposits range from about –1 m (SFM0030) to +13m (SFM0010) (Figure 2-19a). However, there is only about a 5.5 m range in groundwater levels when represented as depths below surface (Figure 2-19b). The majority of wells form a tight-packed cluster with reported groundwater levels in the range of approximately +0.25 to –1.5 m relative to the surface. These wells typically show a strong uniformity in response to drier summer conditions in July and August. Similarly, these wells also display uniformity in response to recharge events following major precipitation and snowmelt events. SFM0026, which is located in a confined till aquifer at the outlet of Fiskarfjärden, reveals clear artesian conditions with a groundwater level up to approximately one metres above ground. The deepest observed groundwater levels are from two wells situated in Börstilåsen (SFM0059 and SFM0061), a glaciofluvial deposit. The wells SFM0006, SFM0008 and SFM0058, which also have relatively depp groundwater levels, are located in till in locally elevated areas, i.e. in typical groundwater recharge areas. The low groundwater level in SFM0030 during the dry summer of 2003 is believed to be caused by root water uptake indirectly and directly from the groundwater zone.

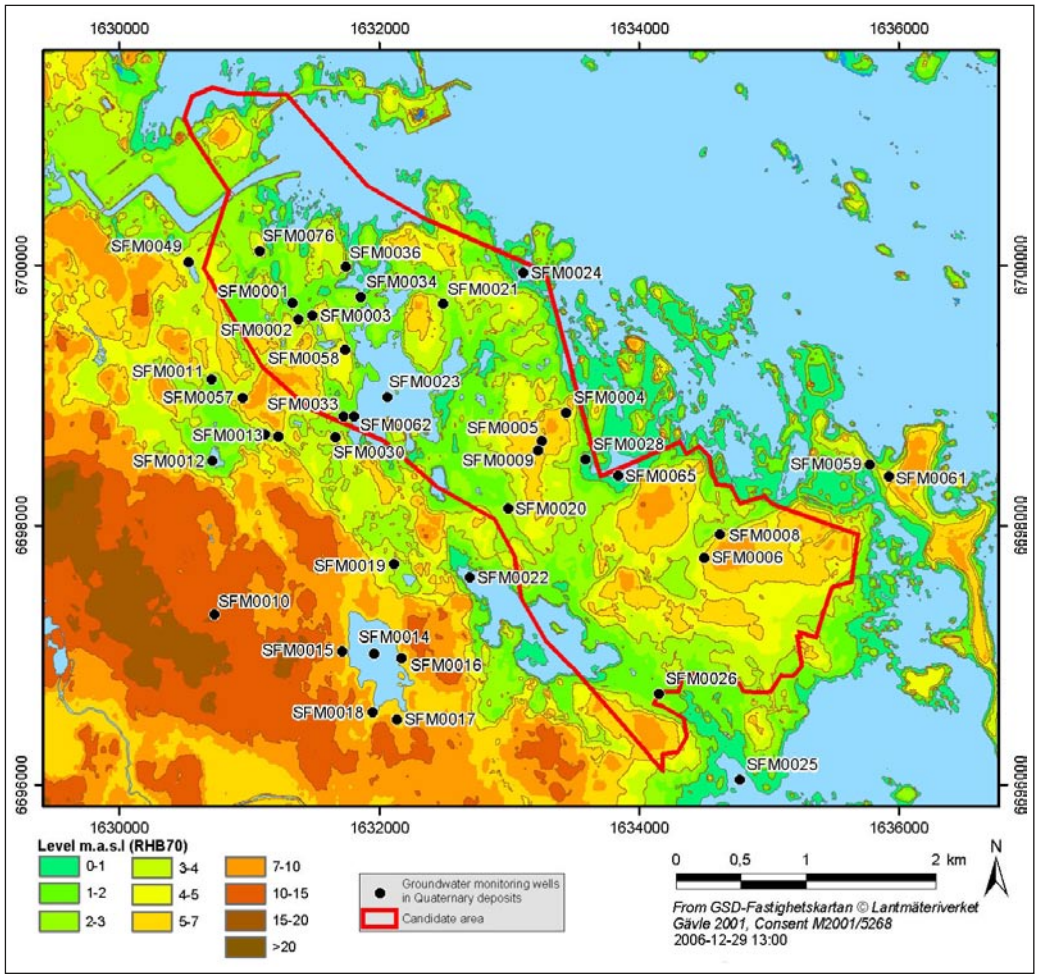

Figure 2-18. *Locations of groundwater monitoring wells in Quaternary deposits with automatic registration of groundwater levels.*

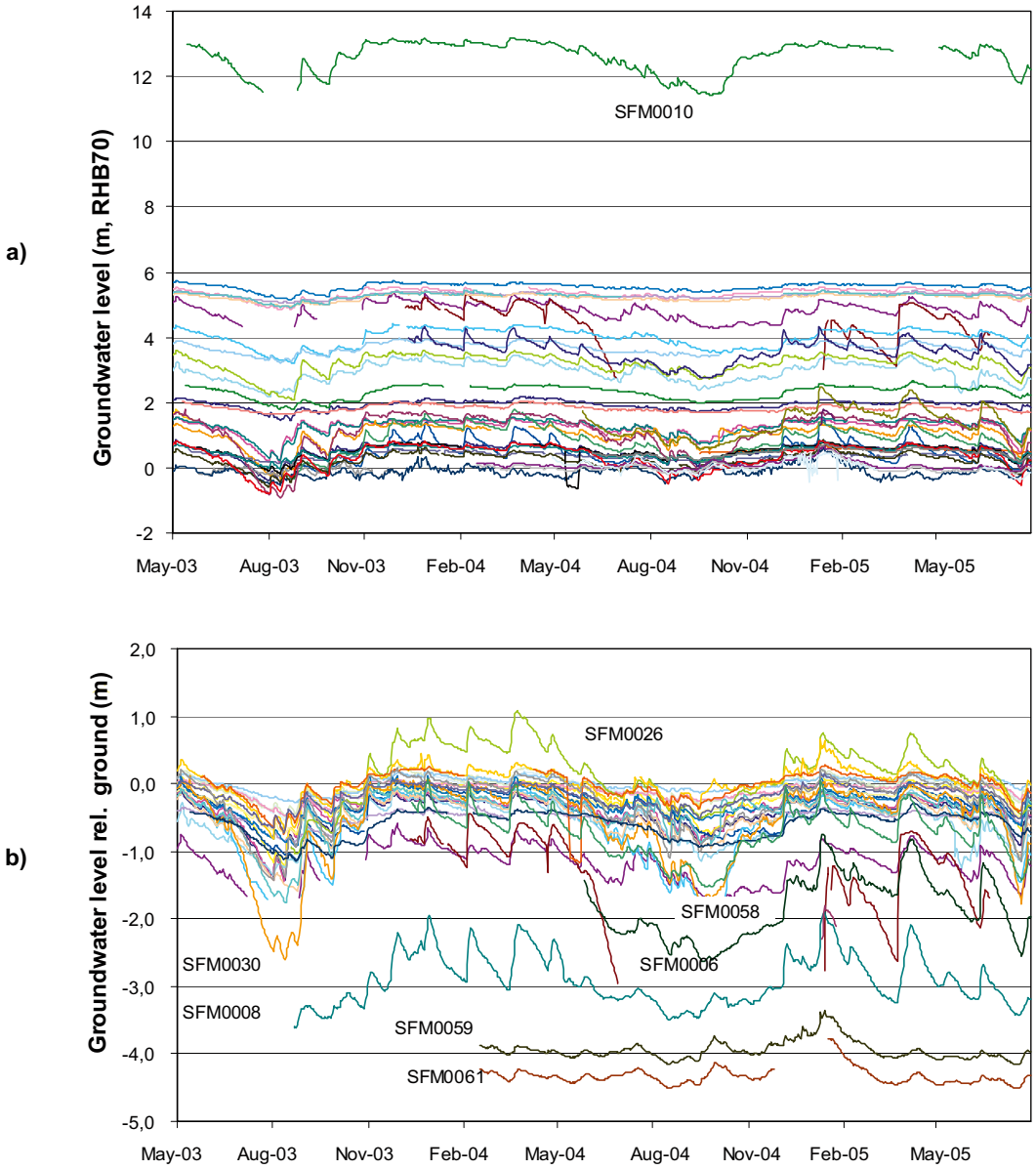

Figure 2-19. *Daily average groundwater levels expressed as a) elevations (RHB70) and b) relative to ground surface for 30 monitoring wells in Quaternary deposits on land.*

Figure 2-20 shows plots of cumulative frequency distributions of the data presented in Figure 2-19b. Two different methodologies for calculating distributions yield two different curves, but they both have similar interpretation. If a daily average groundwater level in Quaternary deposits relative to ground surface is first calculated from the 30 well time series, the cumulative distribution of that average time series indicated that 80% (between the 10th to 90th percentiles) of the site average groundwater levels were between 0.25 and 1.00 m below ground surface. If instead the cumulative distribution is based on pooled analysis of the 30 individual well time series, then 80% of measured groundwater levels were between 0 and 1.6 m below ground surface. In either case, it can be concluded that groundwater in Quaternary deposits is shallow in 30 observation wells across the site investigation area.

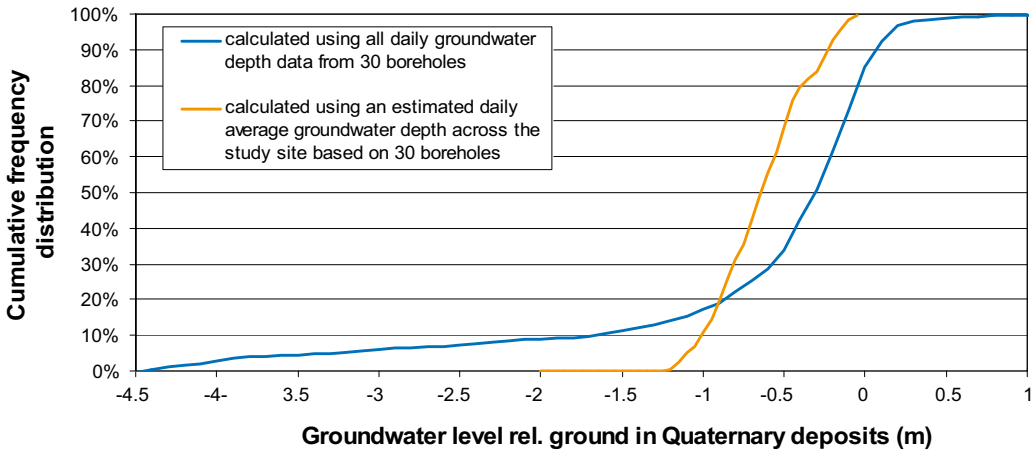

Figure 2-20. *Cumulative frequency distribution of groundwater depth in Quaternary deposits from 30 monitoring wells in the Forsmark site investigation area.*

To facilitate comparisons between well locations, Figure 2-21 shows summaries of the groundwater level in Quaternary deposits time series in terms of means and observed ranges. Figure 2-21a shows the mean and range of groundwater depths in the Quaternary deposits, co-plotted with bedrock depth at each site, and shown ranked according to increasing groundwater depths. In Figure 2-21b the same data are presented ranked according to bedrock depth. Finally, Figure 2-21c shows the mean and range of groundwater elevations, co-plotted with bedrock and ground surface elevations at each site, and shown ranked according to bedrock elevations. All wells exhibited mean groundwater elevations above 0.0 m RHB70. Eleven of the 30 wells exhibited minimum groundwater elevations less than 0 m, with the lowest reported level of –0.95 m in SFM0030.

Figure 2-22 and Figure 2-23 summarise the strong correlation that was observed between mean observed groundwater and ground surface elevations in the Quaternary deposits. With a few exceptions, it can be stated that the average position of groundwater in the Quaternary deposits appears to be largely determined by local ground surface elevation. In other words, the three-dimensional shape of the groundwater surface in Quaternary deposits appears to generally follow that of the ground surface. There are some outliers indicated by name in Figure 2-22. SFM0008 and SFM0058 are located in till in locally elevated areas, while SFM0059 and SFM0061 are located below the ridge of the glaciofluvial deposit Börstilåsen.

The strong correlation between the mean groundwater elevations observed in the till and ground elevation data shown in Figure 2-22 means that the mean vertical hydraulic flux at some point below the surface is considerable less than the net infiltration into the saturated zone of the till. From a hydrogeological point of view a contrast in the vertical hydraulic conductivity between the till and the bedrock seems quite plausible, but there could also be a contribution from anisotropy in the hydraulic conductivity in the till as such.

In Figure 2-24 and Figure 2-25 mean groundwater depths are plotted against a field classification of local geomorphology and groundwater recharge-discharge conditions /Werner et al. 2007/. Figure 2-24 shows that groundwater depth below ground is more variable and generally larger in locally elevated areas, while no clear coupling can be seen between absolute groundwater elevation and local geomorphology. From Figure 2-25 it is obvious that depth to groundwater varies considerably within typical recharge areas while the variations are small and the groundwater level close to the ground in discharge areas. No coupling can be seen between groundwater elevation and the classification in recharge-discharge areas. The two figures indicate that groundwater flow in the Quaternary deposits is mainly governed by local topography and forms small local flow systems.

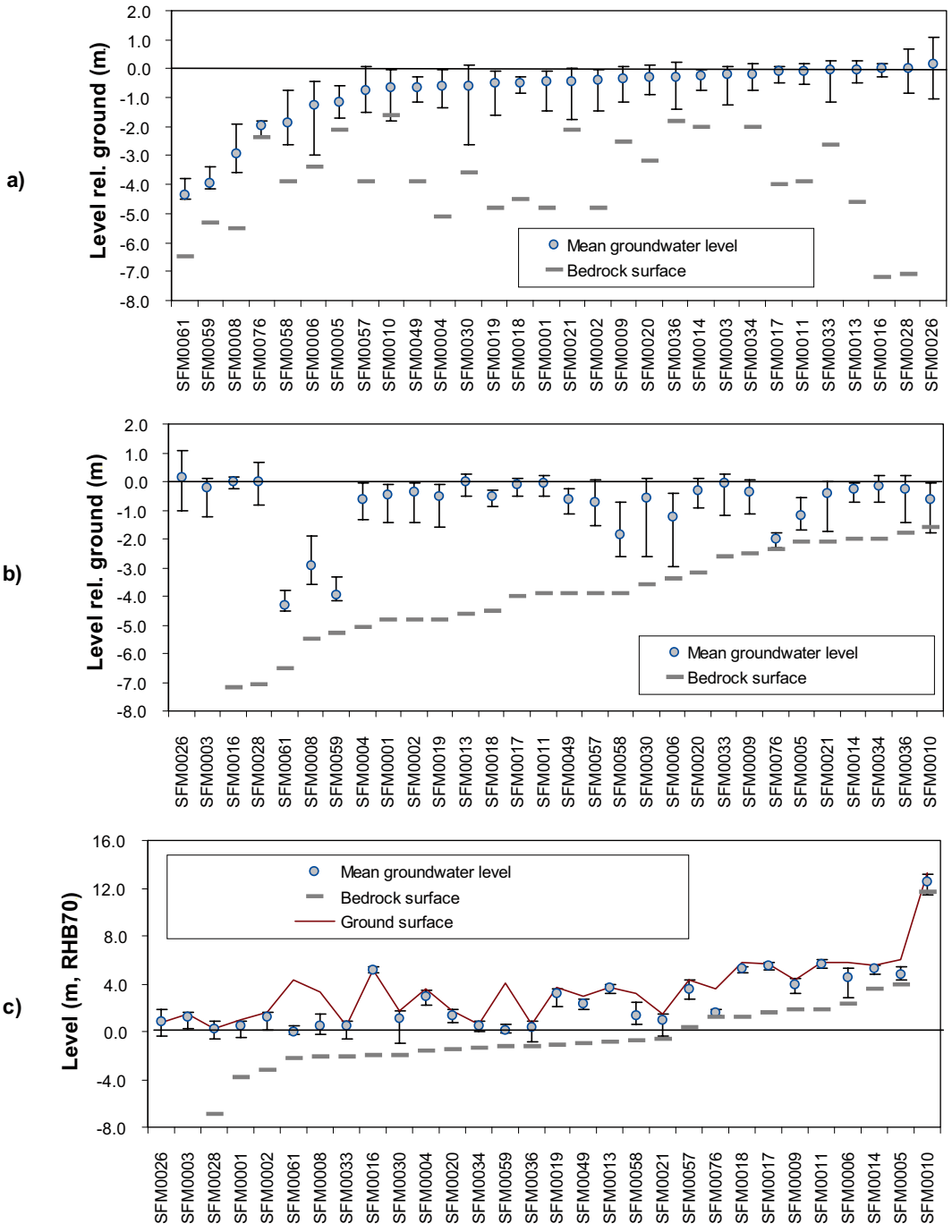

Figure 2-21. *Summary of mean and range of groundwater levels in the Quaternary deposits shown as a) level relative to ground surface ranked accordingly, b) level relative to ground surface ranked by depth to bedrock and c) levels RHB70 ranked by bedrock elevation. In all figures, bedrock surface levels at SFM0026 (–15.4 m RHB70 and 16.1 m below surface) and SFM0003 (–8.7 m RHB70 and 10.2 m below surface) are not shown to increase resolution on the remaining data.*

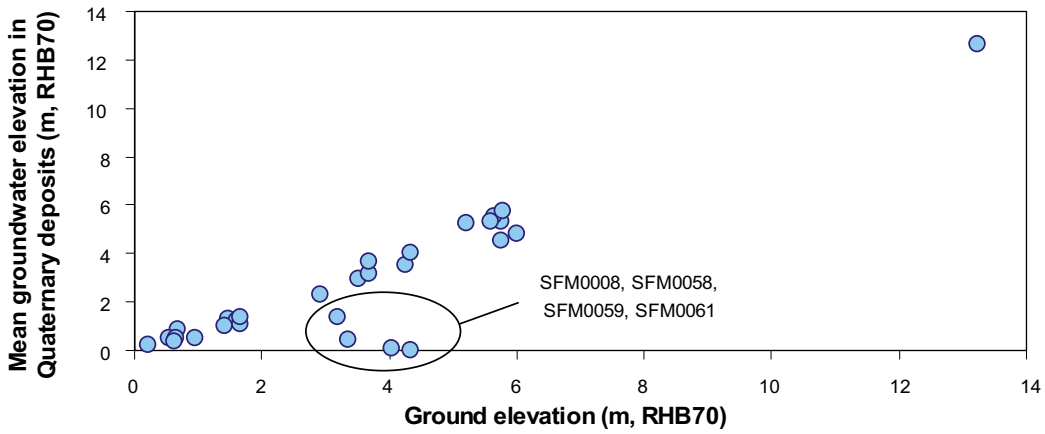

Figure 2-22. *Cross-plot of average groundwater level elevations in Quaternary deposits versus ground elevations.*

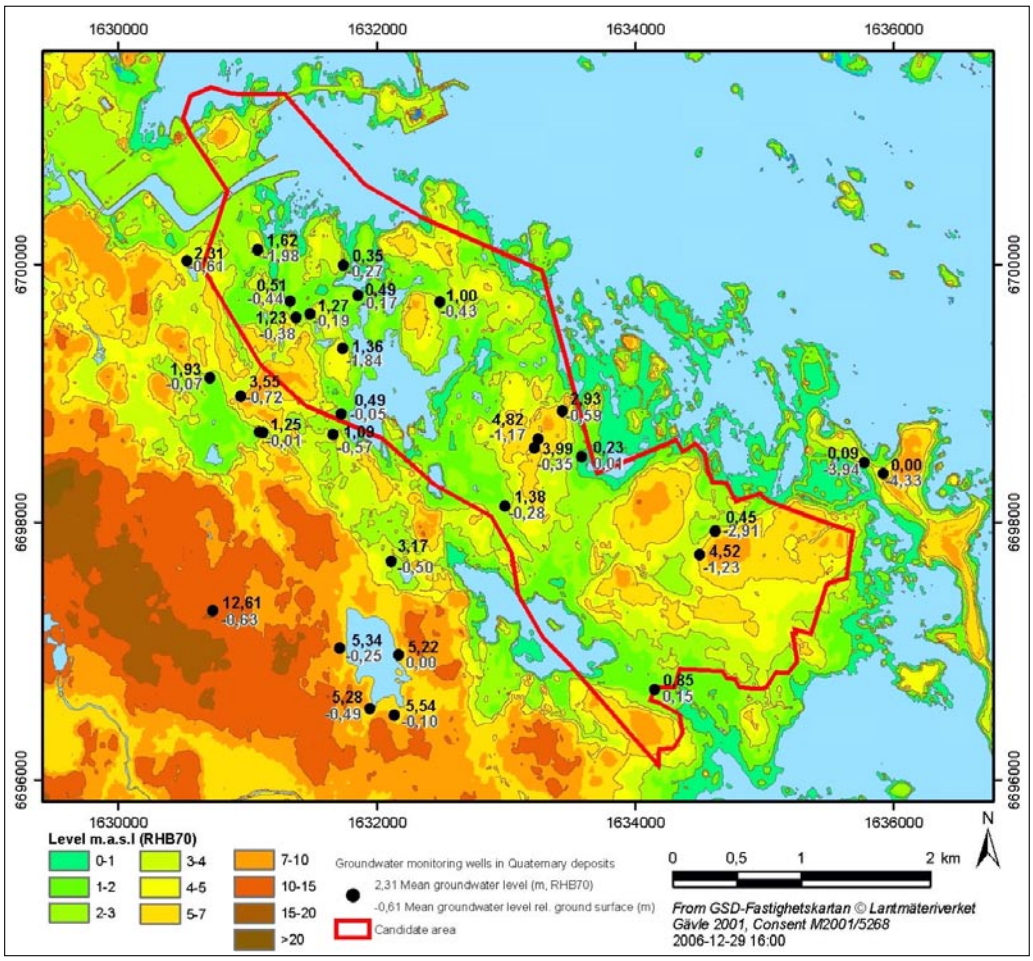

Figure 2-23. *Mean groundwater level elevations and depths below ground in monitoring wells in Quaternary deposits.*

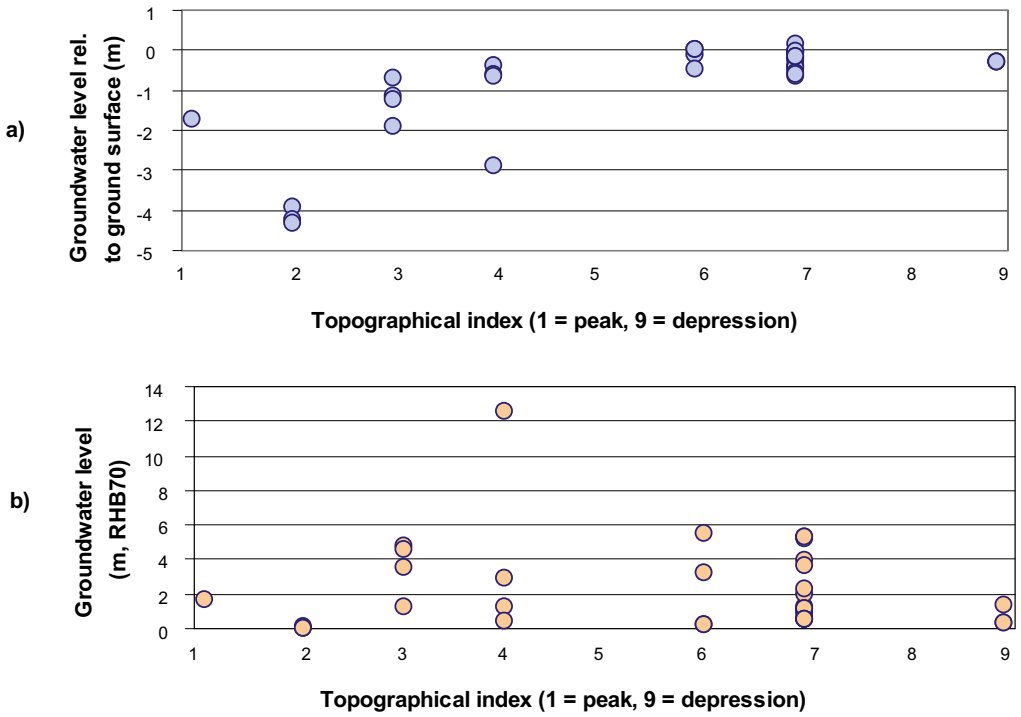

Figure 2-24. *Mean a) groundwater depths and b) elevations as a function of topographic index based on in-field assessments. Numeric categories were defined as follows: 1 = peak, 2 = ridge, 3 = upper slope, 4 = mid slope, 5 = pass, 6 = lower slope, 7 = flat, 8 = channel, 9 = regional depression.*

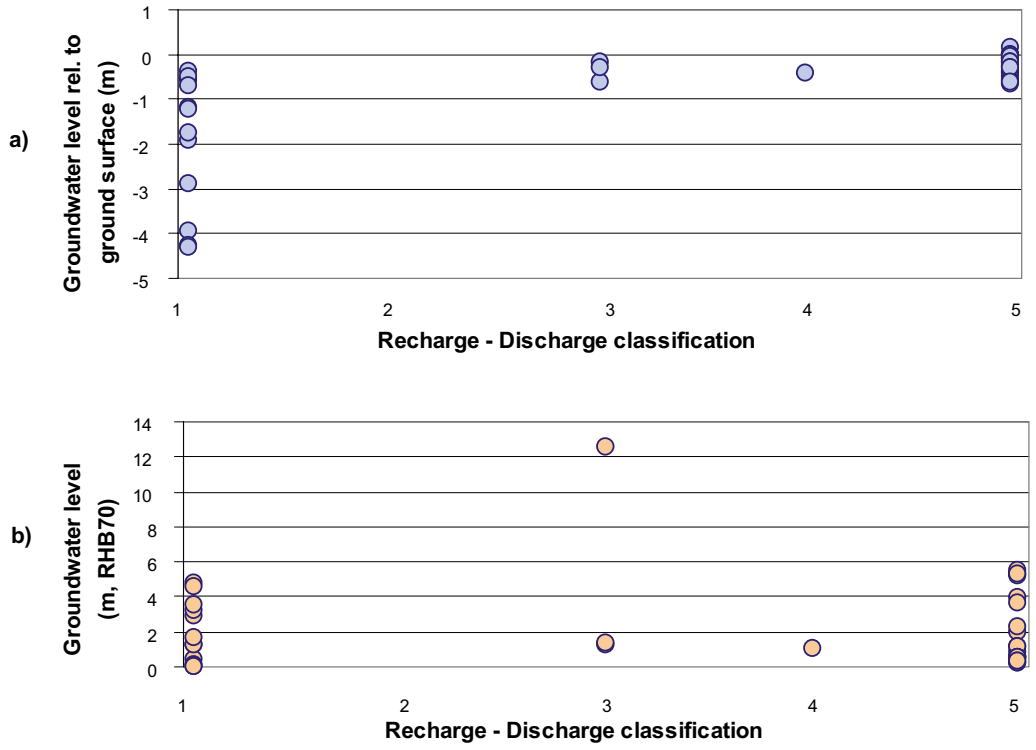

Figure 2-25. *Mean a) groundwater depths and b) elevations as a function of recharge-discharge classification based on in-field assessments (Werner et al. 2007). Numeric categories were defined as follows: 1 = recharge area, 2 = probable recharge area, 3 = varying, 4 = probable discharge area, 5 = discharge area.*

Numerous combinations of wells in the Quaternary deposits indicated similar time series responses. The time series from groundwater wells in Quaternary deposits were analysed to identify wells with high covariance ($R^2 > 0.9$) and similar range of variation (± 10%). Result tables presenting the matrices of results are shown in Appendix 2. Figure 2-26 shows three sets of wells that demonstrated near-identical groundwater level pattern. Figure 2-26a shows closely coupled time series at SFM0001, SFM0002, and SFM0003, which are all located in close proximity at Drill site 1. Similarly, Figure 2-26b shows SFM0016, SFM0017 and SFM0018, which are closely situated around the shore of Eckarfjärden. On the other hand, Figure 2-26c shows nearly identical time series from SFM0010 and SFM0030, in spite of these wells being located almost two km apart.

2.5 Groundwater levels in the bedrock

Groundwater levels in the bedrock were measured in 22 percussion-drilled boreholes in the site investigation area. Figure 2-27 shows a map indicating the positions of these boreholes. It is noted that, due to considerable differences in groundwater salinity with depth, and thereby in density, measured groundwater levels in percussion-drilled boreholes in the bedrock should be regarded as point water heads.

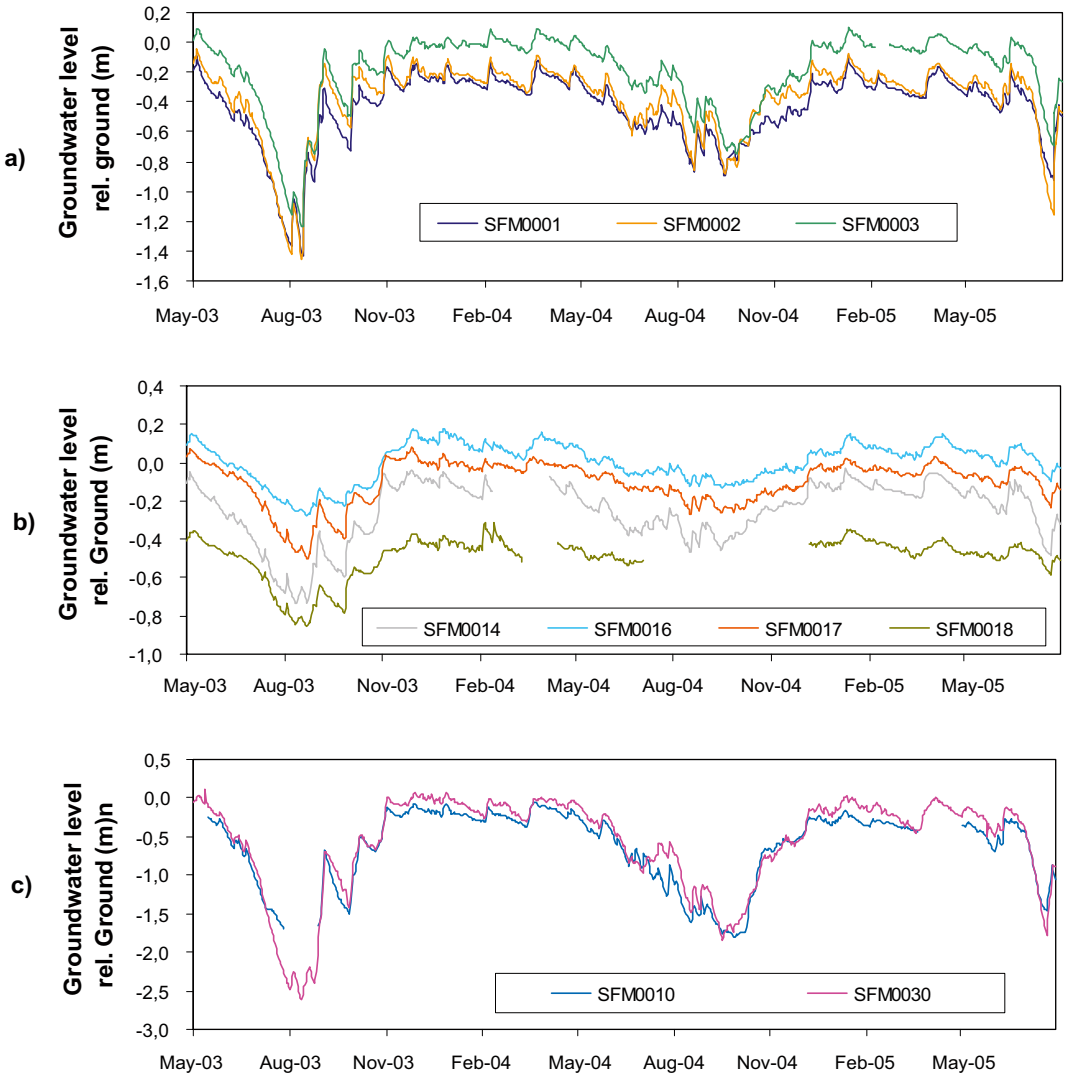

Figure 2-26. *Strong correlations exist between some groundwater level time series in wells close to one another (a and b) and also in wells distant apart (c).*

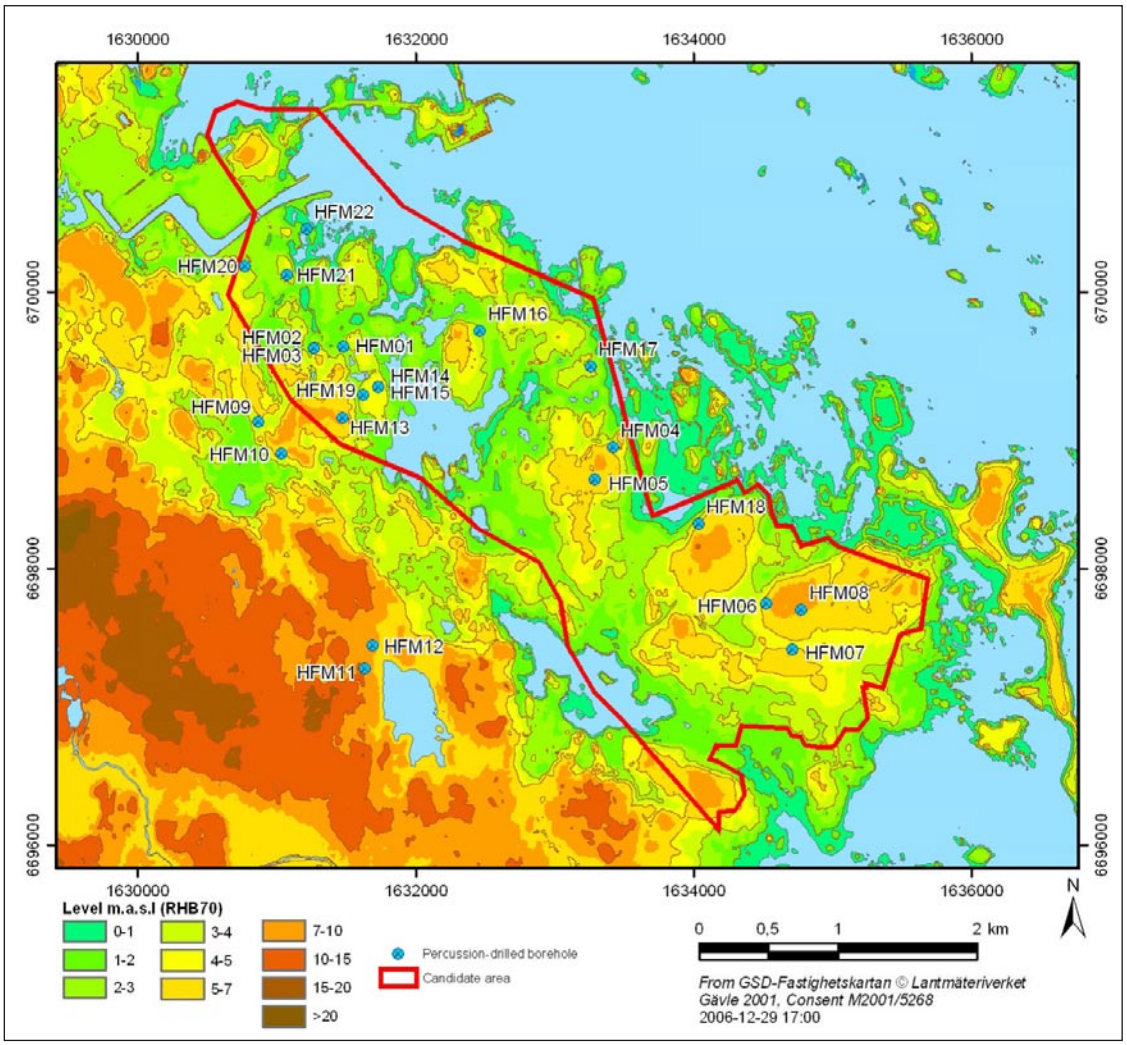

Figure 2-27. *Locations of the percussion-drilled boreholes HFM01-HFM22.*

Figure 2-28a shows all available daily average point water head data. The raw data shows several intervals of high amplitude disturbances that were related to core drilling activities and other pumping. The network of groundwater wells in the bedrock responded differently to activities at different locations, thus suggesting that these disturbance intervals contain valuable information on interconnectivity in the bedrock. Accordingly, these intervals were analysed to identify which wells responded and to what extent for different source disturbances. These results are presented in Section 3.8.

The disturbances were oscillatory and with high amplitude and tended to obscure more subtle groundwater level changes in response to infiltration and sea level changes. Therefore, a thorough data screening was performed to produce a second "clean" data set with no visible artefacts from disturbance activities.

Figure 2-28b contains a horizontal bar graph showing raw data that were available (grey lines) and data that were subsequently screened to remove artefacts from disturbances (red circles) for each well. The data represent a composite of available data from all sections in wells that have packers. Figure 2-28c shows the resulting "undisturbed" time series. Groundwater point water heads varied between –0.2 to +6.6 m in undisturbed data.

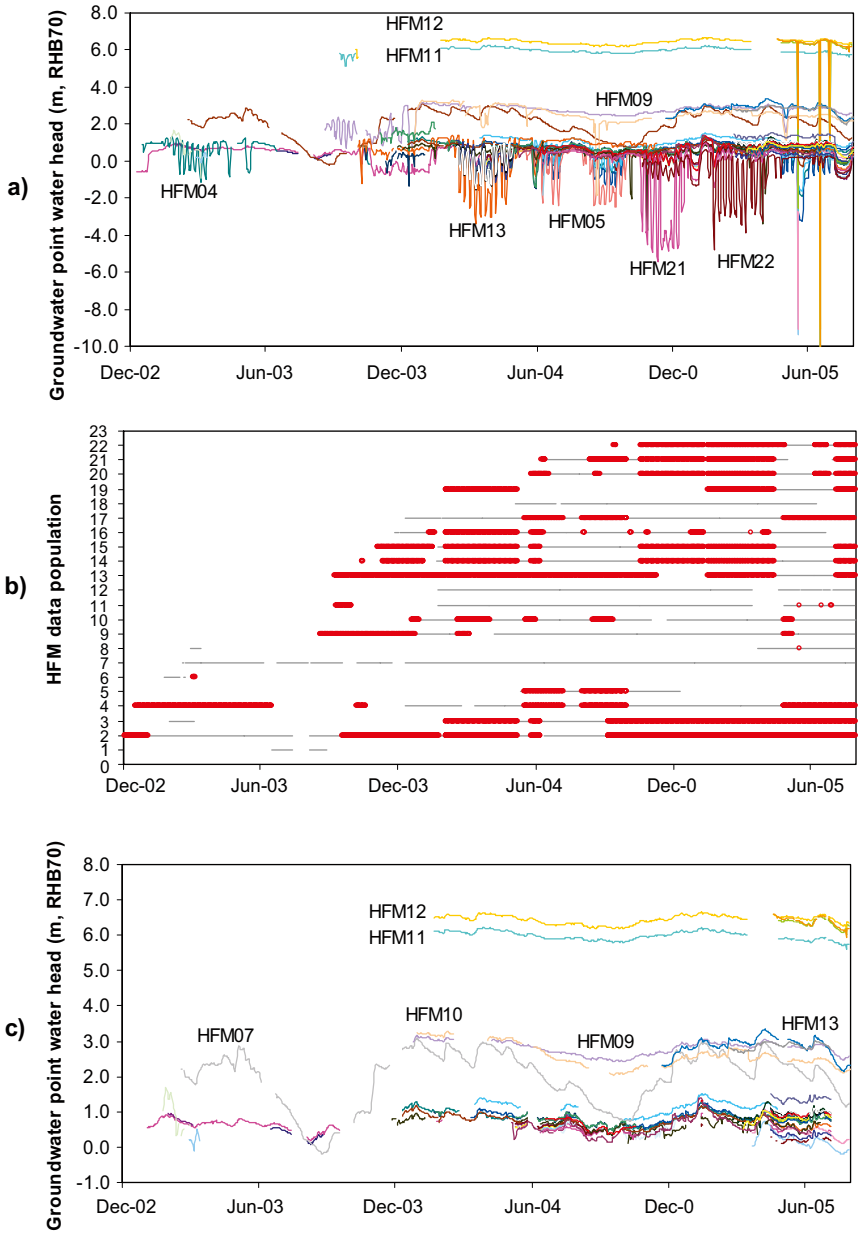

Figure 2-28. *Daily average groundwater point water heads measured in the bedrock at 22 locations in the study area. Raw data are shown in a) and includes numerous disturbance intervals due mostly to drilling related activities. Data populations are shown in b) with grey lines indicating available data and red circles indicating data that were screened to remove disturbances. "Clean" data, with disturbance intervals removed, are shown in c).*

Figure 2-29 shows summaries of undisturbed groundwater levels in the bedrock in terms of means and observed ranges. Note that it is difficult to establish meaningful comparisons of time series summary statistics when the time series themselves are so unevenly populated (Figure 2-28b). For this reason, the summary values shown in Figure 2-29 should be considered "best available". The means and ranges shown in the figure are based on August 2004 through July 2005 data to the extent possible, but required data from 2003 for two wells (HFM01 and HFM06) that had no available data during that interval. Even so, the range of available data between August 2004 and July 2005 was wide between well locations. For instance, HFM02.3 and HFM03.2 had only 35 available data points for calculating means and ranges, while HFM07 had 364 data points. The data points in Figure 2-29 are colour-coded to indicate the variable populations used in the mean and range calculations. (In the notations used for the percussion-drilled boreholes, HFMXX.Y, XX is the borehole number and Y is the borehole section counted from the bottom of the borehole.)

Figure 2-29a shows the mean and range of groundwater point water heads in the bedrock, co-plotted with bedrock and ground surface elevations at each site, and shown ranked according to increasing bedrock elevations. As with the groundwater wells in Quaternary deposits (Figure 2-21b), all wells in the bedrock exhibited mean groundwater point water heads above 0.0 m RHB70. Only HFM05 and HFM22 exhibited minimum ranges that extended below 0.0 m. It is interesting to note that many well locations demonstrated point water heads above local bedrock levels. As was evident in the undisturbed time series (Figure 2-28c), most wells had mean point water heads within a close range (between 0.2 and 1.1 m RHB70). The six wells with means outside this range were HFM07, HFM09, HFM10.2, HFM11.2, HFM12.2, and HFM13.3. It is important to note that most of these wells (HFM09–HFM12) are located east of the candidate area, outside the geologic tectonic lens constituting the candidate area. HFM07 and HFM13:3 are located inside the lens but are situated above the A2 deformation zone. Other studies have shown that these borehole sections have very low transmissivity and do not appear to be affected by any of the highly transmissive sub-horizontal fracture zones.

Figure 2-29b shows these same data plotted as point water head depths below ground surface, co-plotted with bedrock depth below ground surface, and ranked according to decreasing depth to bedrock. Note that the different ranking criteria in Figure 2-29a and b resulted in different order for the well data presentation.

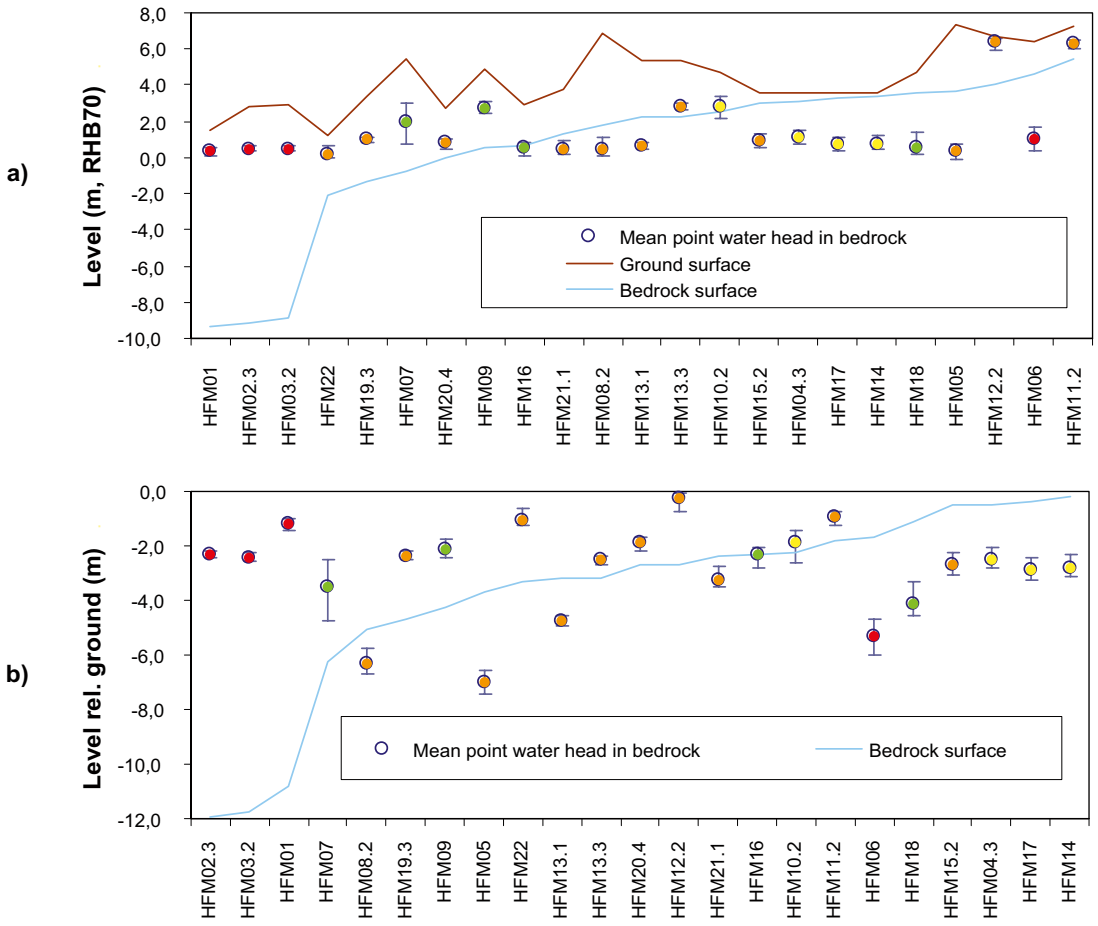

Figure 2-29. *Mean groundwater point water heads in bedrock with observed ranges based on available "clean" data from August 2004 through July 2005 plotted as a) groundwater level elevations ranked according to bedrock elevations, and b) groundwater relative to ground surface ranked by depth to bedrock. Note that the ranked order of wells is different in a) and b). Data are from the topmost section in wells with packers or open boreholes for wells with no packers. Red dots indicate means based on less than 50 days of available data during this one-year interval, orange indicates a range of 50–150 days of available data, yellow 150–250, and green > 250. Note also that HFM01 and HFM06 had no available data during this one year data interval, therefore values in the chart are based on the only available data which was from the first half of 2003.*

Figure 2-30 shows a cross plot of best available mean point water heads versus ground surface elevations at the well locations. As opposed to groundwater depths in Quaternary deposits (Figure 2-22), the relationship between these variables was not strong.

Figure 2-31 shows a map of the study area and the spatial distribution of measured point water heads and corresponding depths below surface. Point water heads in bedrock do not follow the ground surface to the same extent as the groundwater levels in the Quaternary deposits.

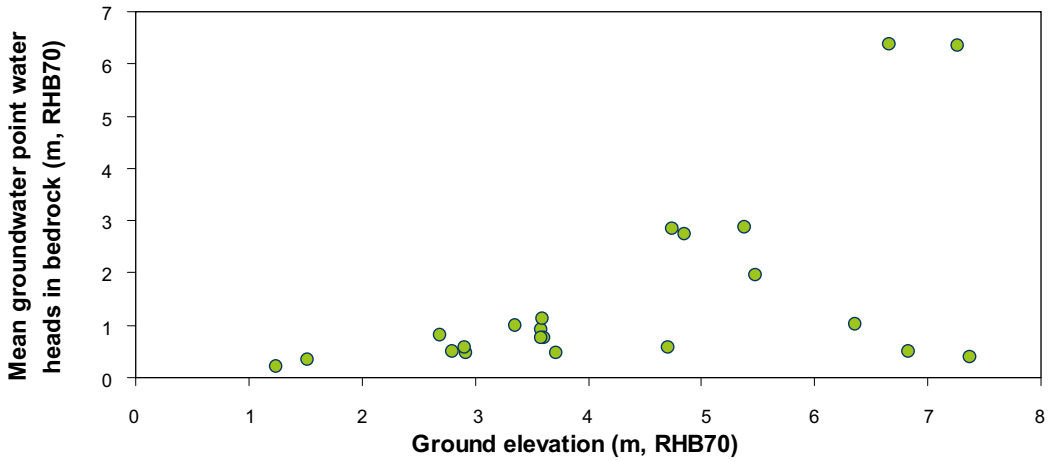

Figure 2-30. *Cross-plot of average groundwater point water heads in bedrock versus ground surface elevations.*

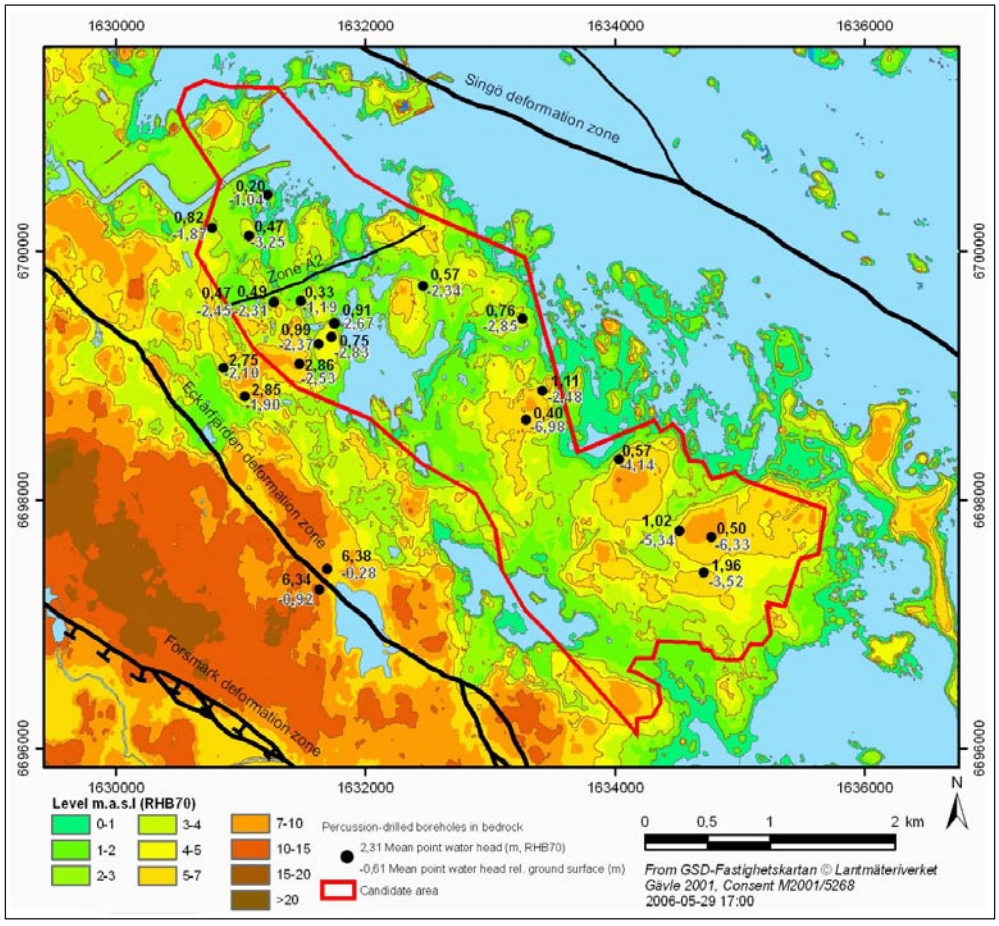

Figure 2-31. *Map indicating the mean point water heads in bedrock (RHB70) and the depth below ground surface of the heads.*

Figure 2-32 shows multiple point water head time series measured in HFM04 at sections separated by packer installations. These data suggest downward vertical gradients in point water heads in the bedrock penetrated by HFM04, but must be interpreted with care since they indeed represent point water heads and not environmental heads (see Appendix 1). However, according to existing data the difference in salinity between the uppermost section and the one directly below is not big enough to change the indicated downward direction of the vertical component of the total gradient between these sections. It should be noted that this transformation of point water heads to environmental heads assumes that the density profile along the vertical is continuous, i.e. that the bedrock can be treated as a porous medium (see Appendix 1).

Figure 2-33 shows average point water head differentials for the boreholes that have multiple sections (packers). Downward gradients are most prevalent. However, as mentioned above these data must be interpreted with care since they represent point water heads. Additional water sampling in all borehole sections is under way to enable an interpretation in terms of vertical groundwater flow gradients.

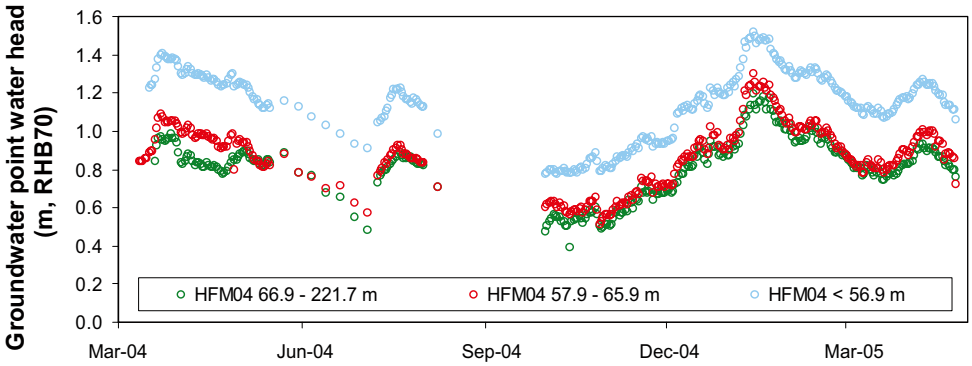

Figure 2-32. *An example of vertical groundwater point water head differentials measured in three sections at HFM04.*

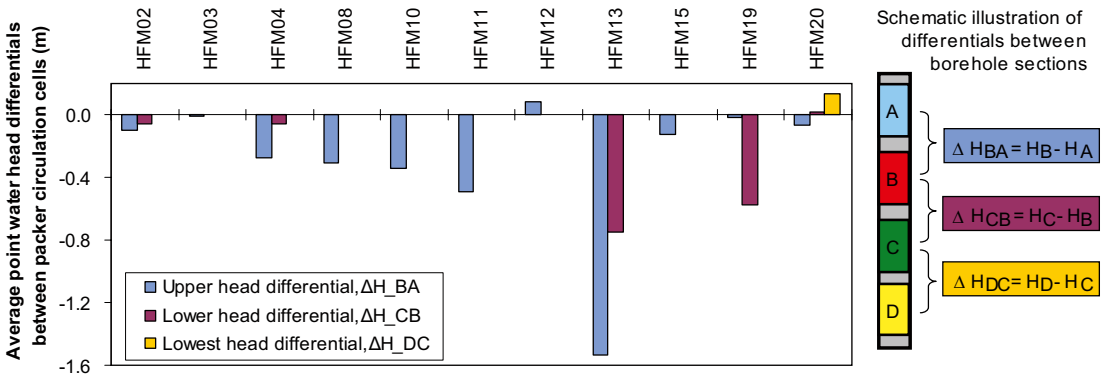

Figure 2-33. *Summary of average point water head differentials in the 11 percussion-drilled boreholes with packers installed.*

2.6 Surface discharge

Surface discharge flow rates in brooks were measured at four gauging stations, see /Johansson 2005/ and /Johansson and Juston 2007/. The first station (PFM005764) became operational in April 2004 and the other three (PFM002667, PFM002668, and PFM002669) followed eight months later in December 2004. Figure 2-34 shows the locations of the gauging stations and their associated catchment areas. Table 2-2 shows the surface area and official nomenclature for these four catchment areas. Note that for simplicity, catchment areas will be referred to by the gauge station name throughout the reminder of this report, rather than the using the catchment nomenclature. Note also that some of the catchment areas are sub-catchments of others. For instance, the catchment area for PFM002668 is a sub-catchment of PFM002667, which in turn is a sub-catchment of PFM005764.

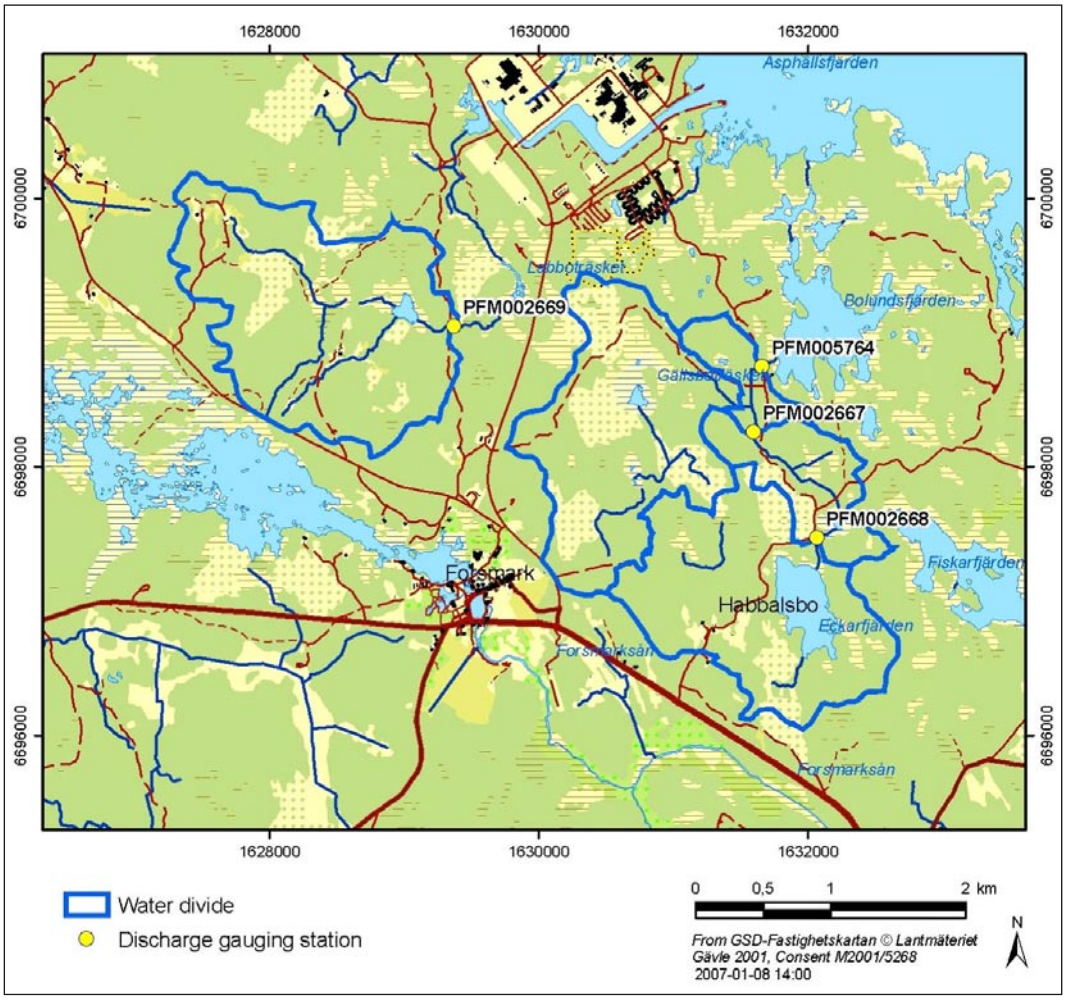

Figure 2-34. *Map showing locations of the four surface water discharge gauging stations and their associated catchment areas.*

Table 2-2. Summary of catchment areas associated with surface water discharge gauging stations.

Gauging station	Catchment area (km^2)	Catchment nomenclature	Notes
PFM005764	5.59	AFM001267	Measurement contains nested response of PFM002667
PFM002667	3.01	AFM001268	Measurement contains nested response of PFM002668
PFM002668	2.28	AFM001269	Autonomous measurement
PFM002669	2.83	AFM001270	Autonomous measurement
PFM005764-PFM002667	2.58	none	Calculated difference of sub-catchment response
PFM002667-PFM002668	0.73	none	Calculated difference of sub-catchment response

Figure 2-35 shows the daily average surface discharge measured at the four gauging stations. Similarities in response are evident amongst the four datasets, with larger flows measured at stations with larger associated catchment areas. The highest measured daily average flow was 83 L/s at PFM005764 in January 2005. Figure 2-36 shows these same responses represented as daily specific discharges (flows normalized to catchment surface areas) for the two autonomous catchment areas and the two autonomous sub-areas that were calculated by difference. Similar trends in dynamic response are again evident, however there are important differences in response between basins also. Peak specific discharge responses differed by approximately a factor of 1.5 between sub-catchments. Furthermore, the daily specific discharge for the PFM002667-PFM002268 sub-catchment demonstrated a notably more jagged response and also had a short interval of negative discharge.

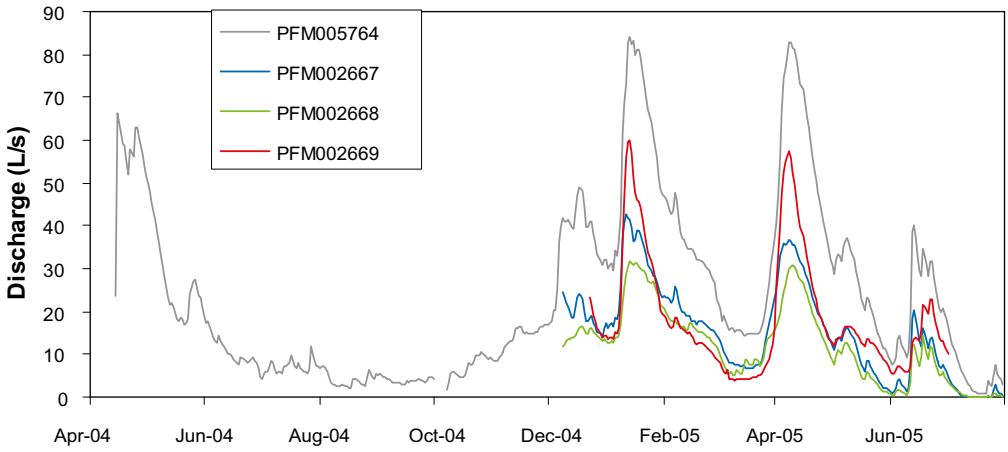

Figure 2-35. *Daily average surface discharge measured at four discharge flume locations in the study area.*

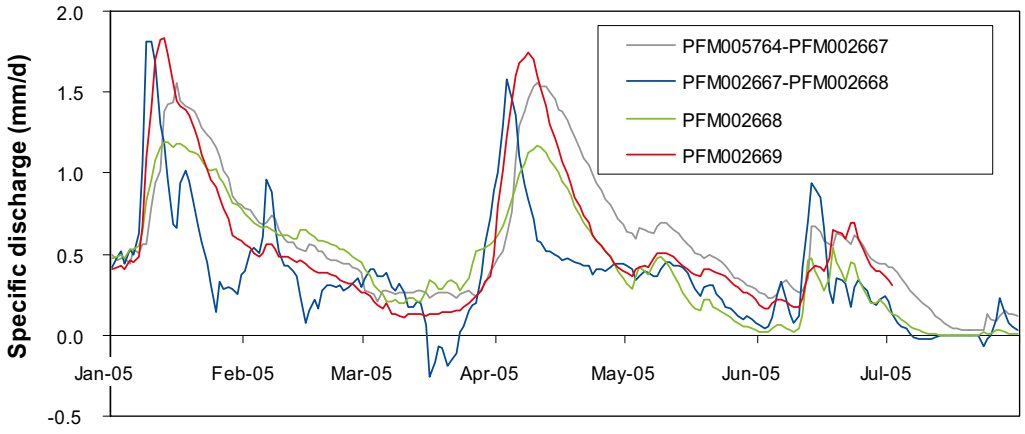

Figure 2-36. *Daily average specific discharge from four catchment areas defined by the gauge station locations.*

Figure 2-37 shows total annual specific discharges for the four discharge stations and for two sub-basins calculated by difference for the period of August 2004 through July 2005. The discharge at PFM005764 was the only station with complete data for this annual interval. The annual specific discharge measured at PFM005764 was 136 mm. Annual values for specific discharge were estimated at the other stations by scaling their available data to the PFM005764 data. The lowest estimated annual discharge was in PFM002667-PFM002668 and was 102 mm/year, while the highest estimated discharge occurred in PFM005764-PFM002667 and was 158 mm/year. The average annual estimated specific discharge from the four directly measured stations was 128 mm/yr (range: 118–136 mm/yr). The average annual estimated specific discharge from the four separate sub-basins was 129 mm/yr (range: 102–158 mm/yr).

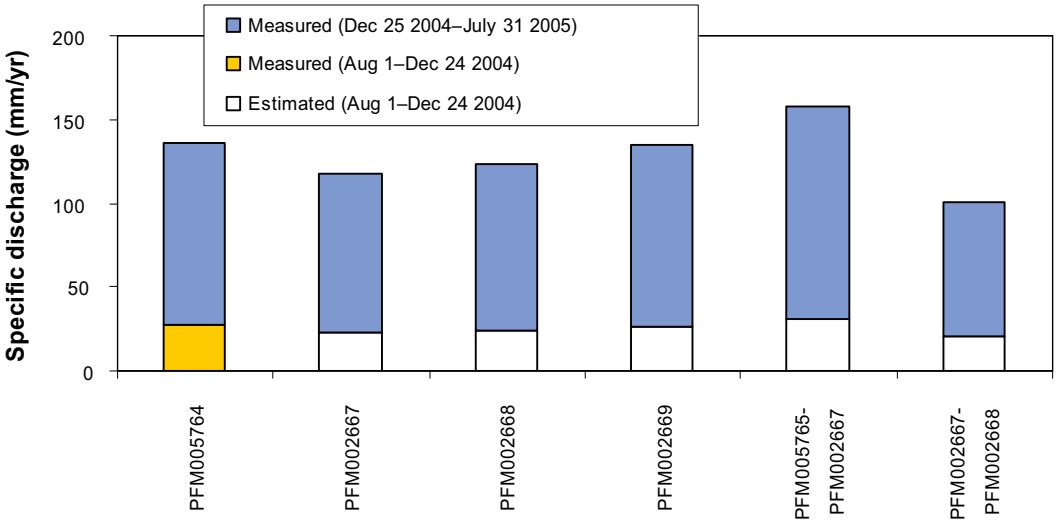

Figure 2-37. *Total specific discharges represented as annual or total available values, depending on data availability. Only one station had a complete year of data (PFM005764). Annual specific discharges at the other locations were estimated by scaling the available data intervals to PFM005764 data. A breakpoint date of December 24 was used, as this was the first day that data were available from all discharge stations.*

3 Hydrological relationships between datasets

3.1 Site average rainfall/snowmelt time series and monthly precipitation – potential evapotranspiration budget

A simple snow accumulation and melt model was used to derive a rainfall/snowmelt time series from the precipitation time series. The model assumptions were:

- Precipitation that occurred on days with mean daily air temperatures above 0.0°C was rainfall that infiltrated the ground surface.
- Snow accumulated at the ground surface from precipitation occurring on days with mean daily air temperatures equal and below 0.0°C.
- The accumulated water content in the frozen above-ground storage melted on days when the mean daily air temperature was above 0.0°C. The melt rate was estimated using a standard degree-day formulation and a calibrated rate constant of K = 1.23 mm/degree above 0°C.

The input to the model was the daily average precipitation time series from Högmasten and Storskäret (Figure 2-6) and the daily average air temperature from the same stations (Figure 2-12). Calibration was based on the average of measured snow water content at three sites across the study area (Figures 2-13 and 2-14). The output from the model was a simulated time series for water storage in snow and a site-average rainfall/snowmelt time series.

Figure 3-1 shows the simulated time series for water content in snow storage compared to the observed site average data. The snow routine model appeared to adequately captured the site-average dynamics for water storage in snow ($R^2 = 0.79$).

Figure 3-2 shows the resulting time series for site-average rainfall/snowmelt (R/S). Rainfall and estimated snowmelt events are shown separately, as are estimated daily data for July 2005. This time series are used in subsequent sections to develop hydrological relationships in groundwater level and surface discharge time series.

It will also be useful to consider a monthly rainfall/snowmelt minus potential evapotranspiration differential in subsequent evaluations of time series. Figure 3-3 shows monthly rainfall/snow-melt and potential evapotranspiration time series based on monthly totals from the rainfall/ snowmelt (Figure 3-2) and potential evapotranspiration time series (Figure 2-10).

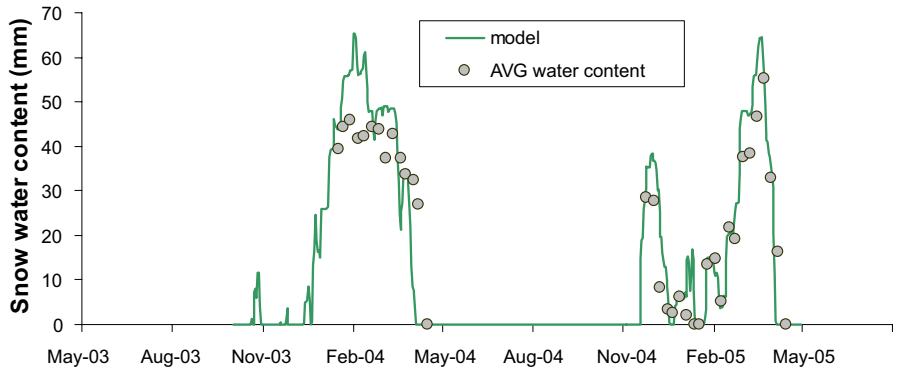

Figure 3-1. *Comparison of measured and simulated site-average snow water content based on a simple degree-day snowmelt model.*

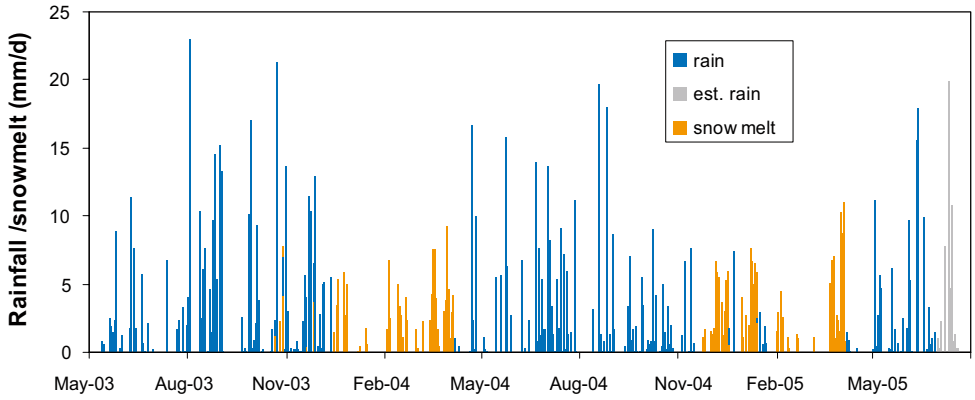

Figure 3-2. *The site-average rainfall/snowmelt record.*

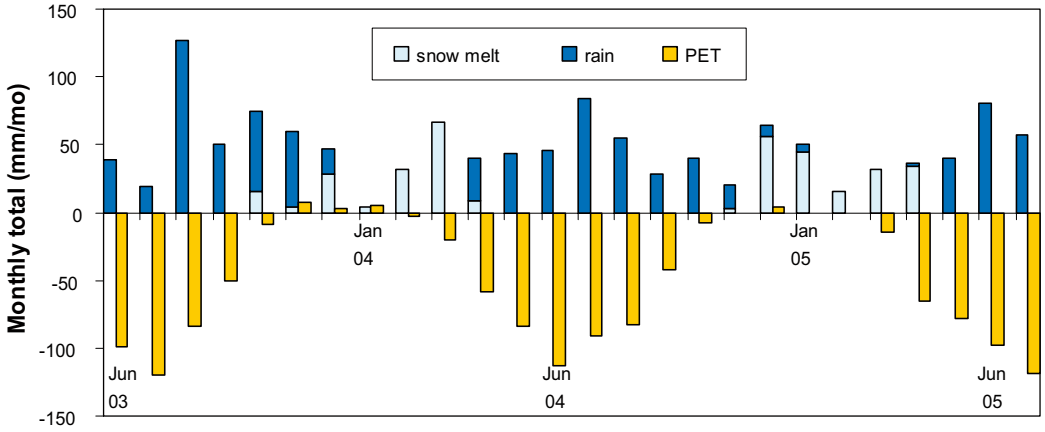

Figure 3-3. *Monthly total R/S (rainfall/snowmelt) and PET (potential evapotranspiration).*

Figure 3-4 shows the rolling annual sum of R/S-PET from the site data. On an annual basis, the sum of rainfall/snowmelt is consistently greater than the rolling PET sum. However, the difference is quite variable (between 11 and 183 mm/yr). The positive differences in R/S-PET represent the minimum water available (due to differences between potential and actual evapotranspiration) for contributions to surface water discharges, storage changes in surface waters, unsaturated and saturated zones of the ground, and groundwater flow out of the area.

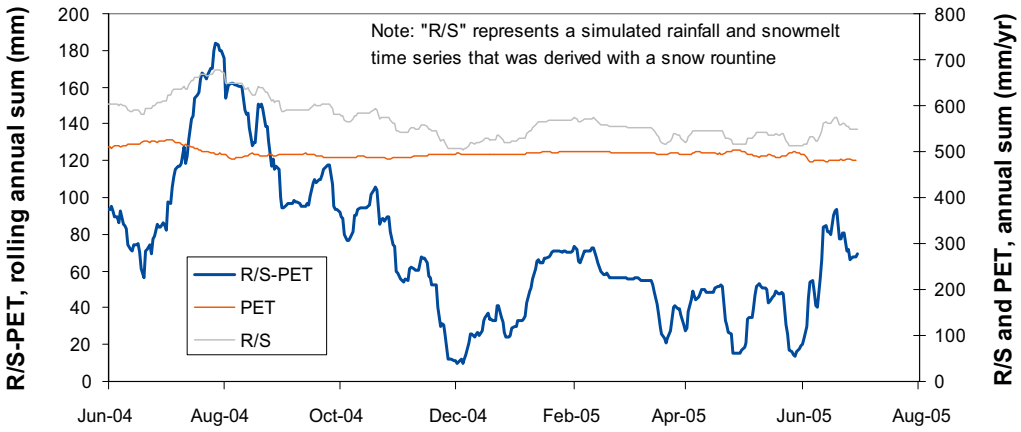

Figure 3-4. *Rolling annual sum of rainfall/snowmelt minus potential evapotranspiration (R/S-PET) for the site, using site average precipitation, adjusted for snowmelt and accumulation. July 2005 is not calculated due to missing P data for that month.*

3.2 Water balance estimates for the PFM005764 basin

An annual water balance was estimated for the upstream catchment area of the PFM005764 surface discharge station (see Figure 2-34 for location of the station). The purpose of this estimation is to provide a general feeling for the relative importance of hydrological fluxes in the site investigation area and to emphasize fundamental limitations in the available data. This water balance was also useful for evaluating simulation results from a near-surface hydrological model in Section 3.10. The PFM005764 catchment area was the only catchment within the site investigation area that had at least one full year of surface discharge data. A water balance equation for the catchment area can be written as:

$$\Sigma \text{ rainfall/snowmelt} + \Sigma \text{ surface water inflows} + \Sigma \text{ groundwater inflows} = \Sigma \text{ evapotranspiration} + \Sigma \text{ surface water outflows} + \Sigma \text{ groundwater outflows} \pm \Delta \text{ surface water storage} \pm \Delta \text{ unsaturated zone storage} \pm \Delta \text{ groundwater storage} \pm \Delta \text{ snow storage.}$$

The water balance interval began and ended after seasonal snowmelts and was from April 22, 2004 to April 21, 2005. Although this may seem like an odd annual interval, it was chosen since the average groundwater depth in the catchment on the beginning and end dates were identical and quite shallow, which would assist in minimizing uncertainties associated with underground water storages.

Figure 3-5 shows locations of 10 groundwater wells in Quaternary deposits within the PFM005764 catchment, and Figure 3-6 shows the time series for groundwater depth below surface for these wells. A “catchment-average” groundwater response for this sub-basin was estimated by averaging eight of these ten time series. Two of the wells fringing Eckarfjärden (SFM0016 and SFM0018) were excluded from the averaged response because they were in close proximity to other wells around Eckarfjärden and had correlated time series responses (see Figure 2-26). However, inclusion of those wells would not have significantly altered this analysis. Catchment-average groundwater depths at the beginning and end of the one-year analysis period were both 178 mm below ground.

The annual total precipitation for the analysis interval was 547 mm and the annual total surface outflow was 136 mm. Surface and groundwater inflows were assumed zero. The change in saturated storage was assumed to be zero, since begin and end dates had equivalent catchment-average groundwater depths. The change in unsaturated storage was also assumed to be zero. As follows from the assumption of the zero change in saturated storage, the catchment-average depth of the unsaturated zone was equivalent at the begin and end dates, and it seemed likely that begin and end storages would both be at or very close to field capacity. The change in lake storage (Eckarfjärden and Gällsboträsket), normalized to the entire catchment area, was very small at +1 mm. By difference, the sum of annual ET and groundwater outflow calculated as 410 mm. For reference, the annual total PET over this same interval was 497 mm.

3.3 Relationships with precipitation, snowmelt events and evapotranspiration

The influence of rainfall, snowmelt, and evapotranspiration are clearly evident in groundwater level and surface discharge time series, in terms of both long-term cycles and short-term event-driven responses. Figure 3-7 shows co-plots of time series for rainfall/snowmelt minus potential evapotranspiration, groundwater levels relative to ground surface in Quaternary deposits, point water head elevations in bedrock, and surface water discharge. The rainfall/snowmelt minus potential evapotranspiration data are shown with monthly totals (Figure 3-7a) to emphasize the overall trends. There is a strong seasonal cycle in rainfall/snowmelt minus potential evapotranspiration that is reflected in the overall shape of many of the groundwater responses in both the Quaternary deposits and in the bedrock.

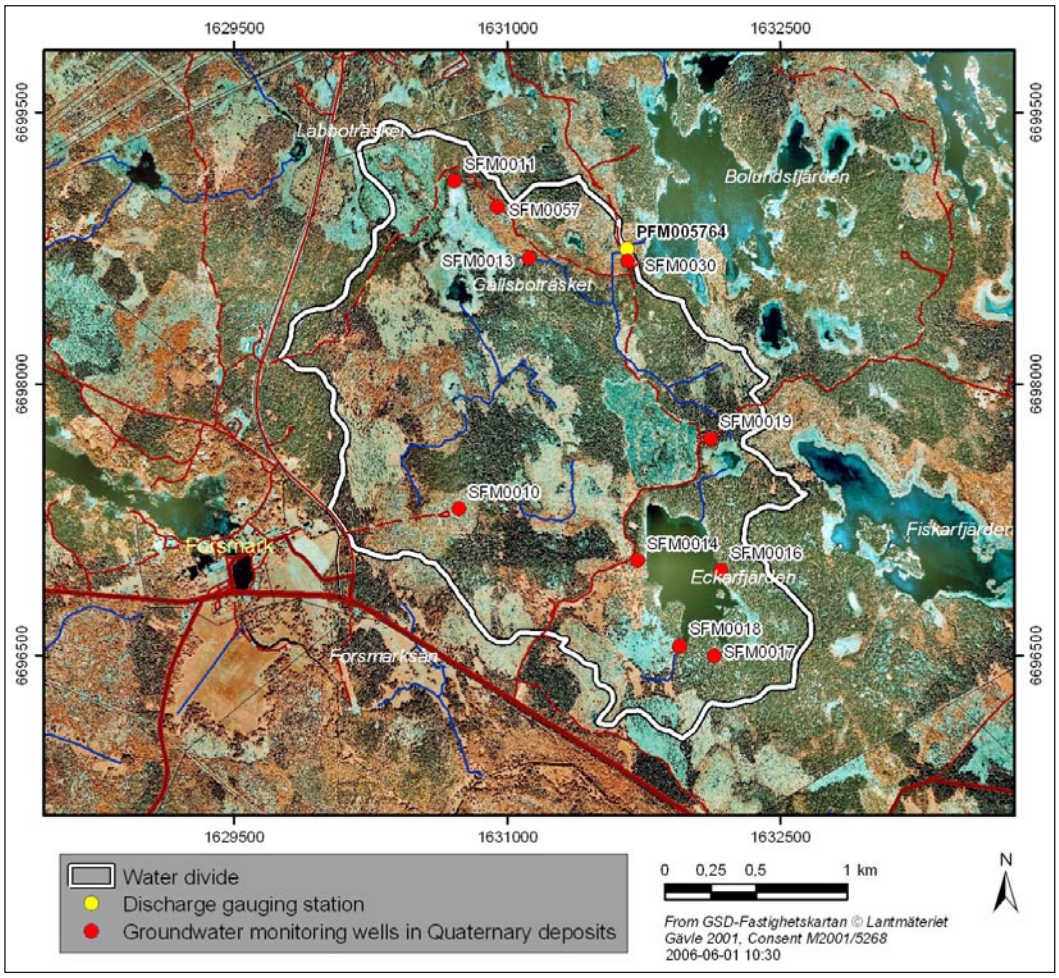

Figure 3-5. *Location of the 10 groundwater monitoring wells in Quaternary deposits contained within the catchment area of PFM005764. Of the four wells surrounding Eckarfjärden, only two (SFM0014 and SFM0017) were used in calculating a catchment average response, so as to not over-represent this region.*

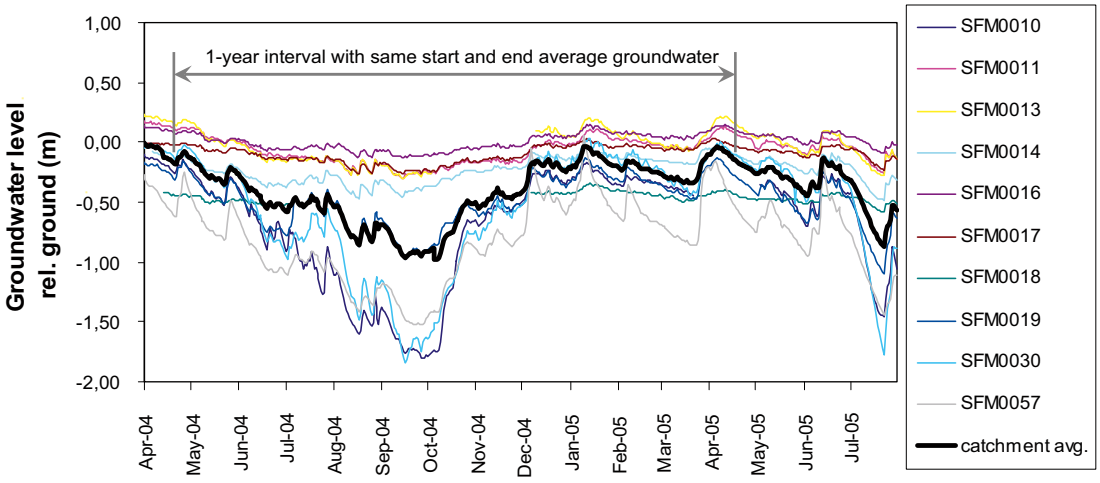

Figure 3-6. *The catchment average time series for groundwater levels in Quaternary deposits relative to ground surface for the PFM005764 catchment area, shown with the ten individual well time series. Data from SFM00016 and SFM00018 were omitted in calculating the catchment-average groundwater response. The interval indicates the period for the annual water balance estimate.*

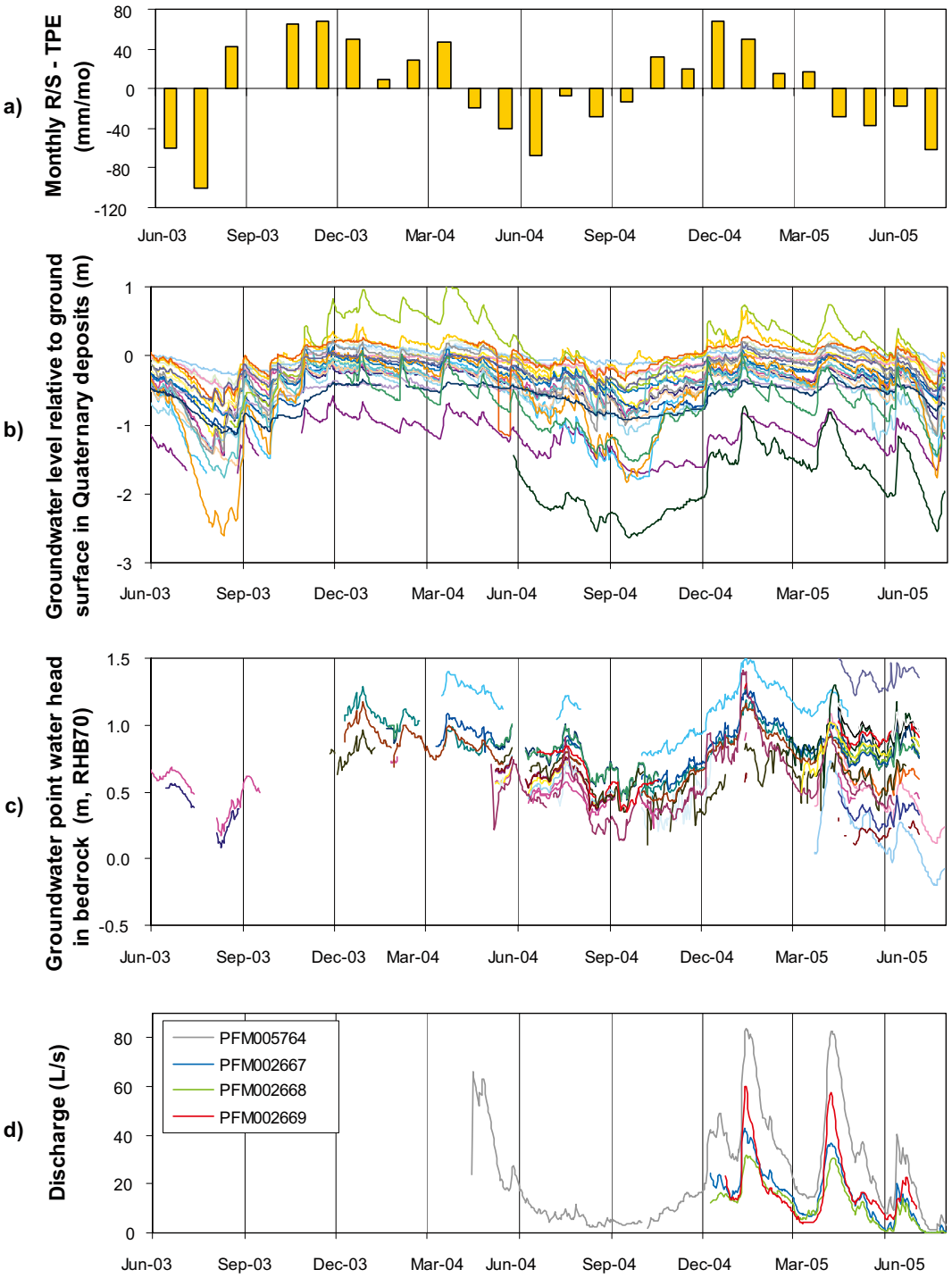

Figure 3-7. *Time series comparisons for monthly rainfall/snowmelt minus potential evapotranspiration (a), daily groundwater levels in Quaternary deposits relative to ground surface (b), daily groundwater point water head elevations in the bedrock (c), and daily surface water discharge (d). Not all wells are shown in b) and c) in order to provide better resolution on the overall trends.*

Figure 3-8 shows coefficients of determination (R^2) for groundwater wells in Quaternary deposits (excluding wells below lakes) compared to the rainfall/snowmelt minus potential evapotranspiration time series. The correlations were estimated using monthly average data to help eliminate the influence of short-term dynamics. Month-to-month correlations were typically low in most wells (< R^2 = 0.30), with the exception of SFM0059 and SFM0061. However, correlations of monthly groundwater levels to the average of the antecedent two months rainfall/snowmelt minus potential evapotranspiration deficit was substantially higher in almost all wells (R^2 = 0.60–0.70), with the exceptions of SFM0005, SFM0006, SFM0009, SFM0049, SFM0058, SFM0059, and SFM0061. SFM0006 was the only well that showed poor correlation to both month-to-month and antecedent R/S-PET. The two wells in glaciofluvial deposits (SFM0059 and SFM0061) were the only wells with higher correlations to month-to-month R/S-PET values compared to the antecedent average. However, in general these results suggest that rainfall/snowmelt minus potential evapotranspiration cycles to a great extent explain the monthly average variations in groundwater levels in most wells.

The time series for point water heads in the bedrock show similar trends as the groundwater levels in the Quaternary deposits (Figure 3-7c), however correlations to rainfall/snowmelt minus potential evapotranspiration were not as high as with groundwater in Quaternary deposits. Figure 3-9 and Figure 3-10 show coefficients of determination for monthly average groundwater point water heads in bedrock compared to monthly rainfall/snowmelt minus potential evapotranspiration. Coefficients of determination are shown for all packer sections, as correlations varied in different sections of the same well. Note that the correlations between monthly average point water heads and monthly average R/S-PET (Figure 3-9a) were mostly negative when they existed at all. On the other hand, correlations were mostly positive to the two-month prior average of R/S-PET. Correlations were not calculated for 24 of the 40 well sections (9 of the 22 wells) because there were less than 6-months of available data from these wells.

In general, correlations between point water heads and rainfall/snowmelt minus potential evapotranspiration were weak and inconsistent in the bedrock. The highest observed positive correlation to the monthly average data was at HFM11.1 and was only R^2 = 0.01. HFM11.1 also had the highest correlation to the two-month prior average of R/S-PET and that value was R^2 = 0.55. HFM04, HFM07, HFM09, HFM10, HFM12, HFM17, and HFM18 also exhibited correlations to antecedent R/S-PET in the range of R^2 = 0.07–0.35. Results from a principal component analysis (PCA) is presented in Section 3.5 that further investigate relationships between groundwater point water heads in bedrock and meteorological variables (R/S-PET), as well as with the sea level time series.

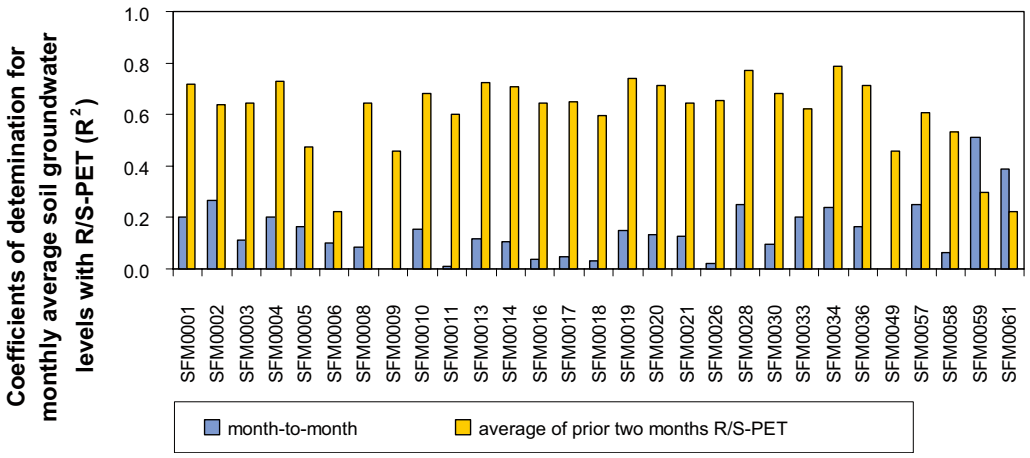

Figure 3-8. *Correlation of monthly average groundwater levels in Quaternary deposits with monthly and bi-monthly rainfall/snowmelt-potential evapotranspiration differentials (R/S-PET).*

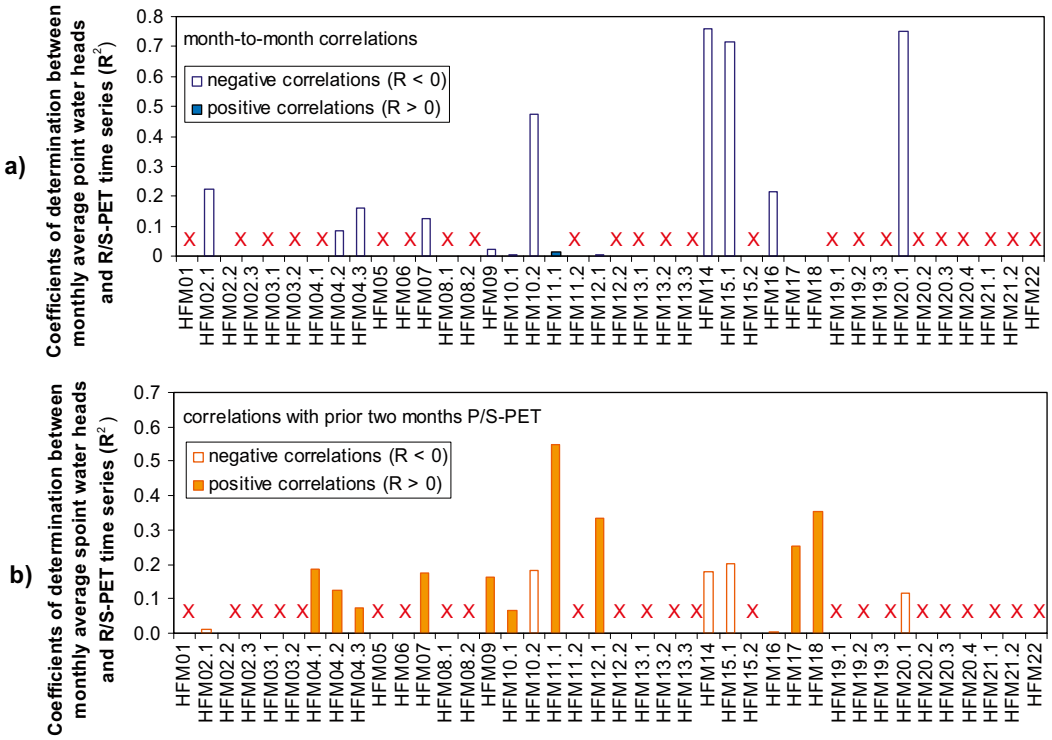

Figure 3-9. *Correlations for monthly average groundwater point water heads in bedrock to a) monthly average and b) average of prior two-months rainfall//snowmelt minus potential evapotranspiration (R/S-PET) time series. X's indicated wells that had less than 6-months months of available data with at least 15 days of data in each month. See Figure 2-27 for the locations of the wells.*

For closer examination of short-term dynamics (as opposed to monthly averages), Figure 3-10 shows a close-up of daily snowmelt and rainfall values during the spring of 2005. This period is particularly illustrative, as the large snowmelt event beginning in late March was preceded and followed by approximately one-month of very low rainfall/snowmelt, thus providing isolation of events to examine them in detail.

In this case, rainfall data and snowmelt estimates are represented with daily values (Figure 3-10a) to emphasize their influence on event-driven hydrological responses. The large snowmelt event beginning in late March (65 mm total over 15 days) produced well-defined hydrologic responses in several of the groundwater wells in Quaternary deposits (Figure 3-10b) and in the bedrock (Figure 3-10c), as well as well-defined increased surface water discharges (Figure 3-10d). Additionally, a decrease in electric conductivity in surface discharge waters was observed (Figure 3-10e), which suggests the addition of "new" fresh water (lower salinity) to stream flows. The 6-day period of rain in early April was smaller in magnitude (25 mm total) than the late March snowmelt, and produced correspondingly smaller hydrologic responses. Interestingly, the 3-day rain period in mid-June (42 mm total) was about 2/3 as large as the snowmelt event, and produced more uniform responses in groundwater (particularly in Quaternary deposits), a proportionally smaller response in surface water discharge, and virtually no response in discharge conductivity.

Diurnal fluctuations driven by evapotranspiration cycles were evident in the data from many of the groundwater wells in Quaternary deposits. Figure 3-11 shows two examples of diurnal ET-driven cycles for shallow groundwater (SFM0034) and deeper groundwater (SFM0030) wells, respectively, with one-hour resolution data for an 8-day period in August 2003. As would be expected, the location with shallower groundwater depth exhibited a stronger diurnal response (~6 cm) compared to the location with deeper groundwater (~0.5 cm). Additionally, the shallow system exhibited a sharper and higher amplitude response to precipitation beginning on August 12.

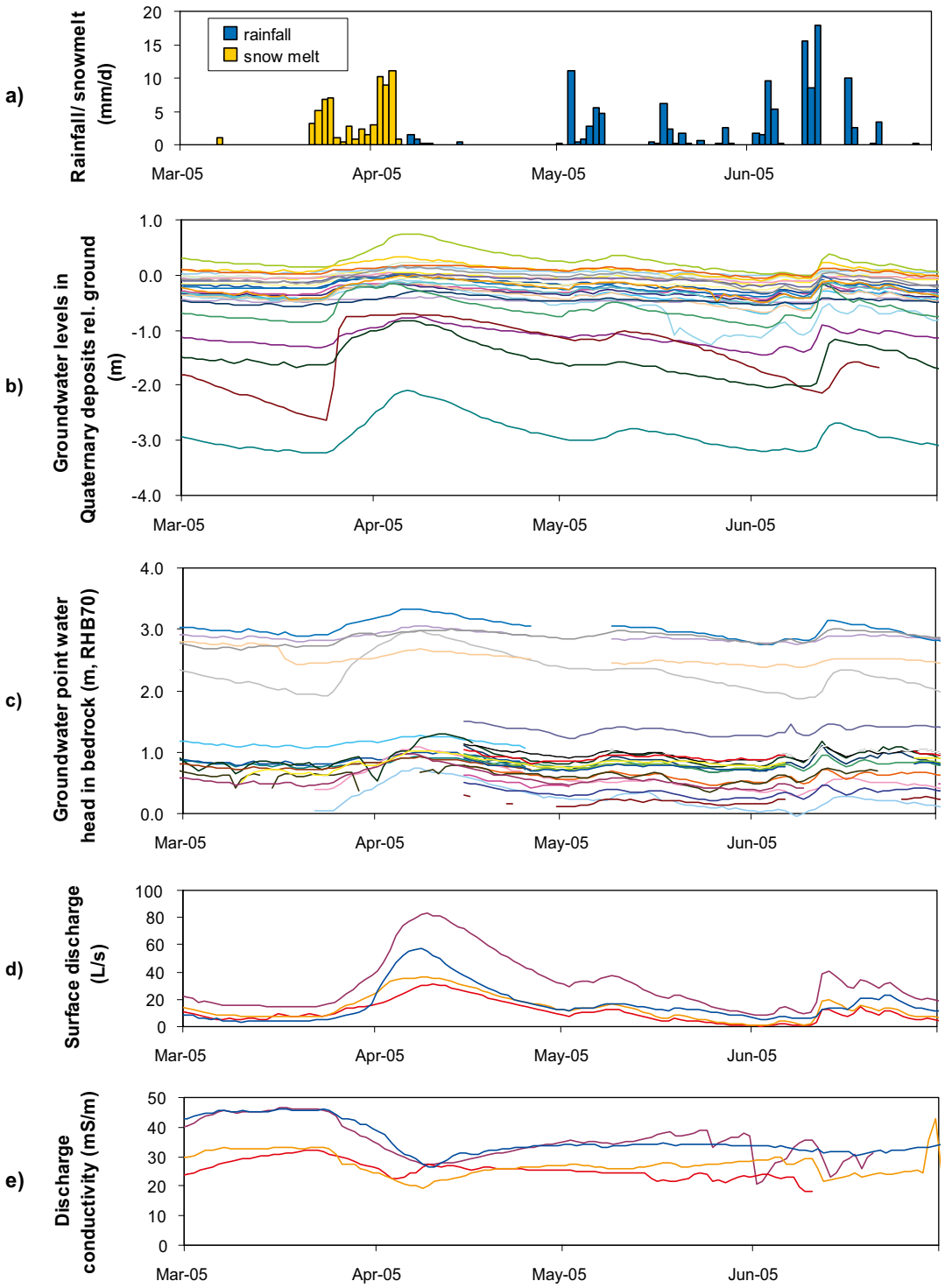

Figure 3-10. *Close-up comparison of responses to isolated snowmelt and rainfall events a), in groundwater levels in Quaternary deposits b), point water heads in bedrock c), surface discharge d), and electric conductivity in surface discharge waters e).*

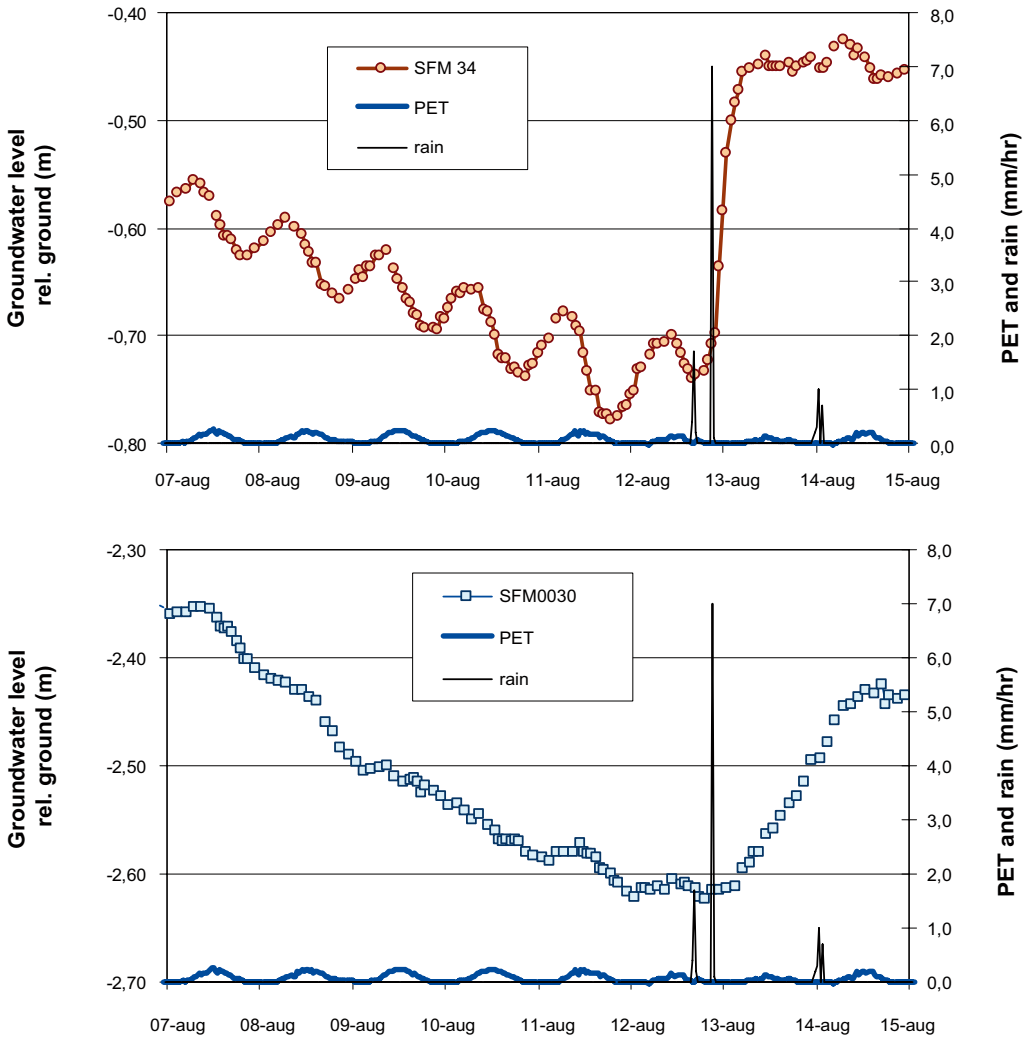

Figure 3-11. *Influence of evapotranspiration and rainfall on groundwater levels in Quaternary deposits with a shallow (SFM0034) and a deeper (SFM0030) groundwater level relative to ground surface in August, 2003 after /Juston and Johansson 2005/.*

3.4 Relationships with the sea level

Figure 3-12 shows comparison of sea level time series to groundwater levels in Quaternary deposits and point water heads in bedrock. In general, groundwater levels in Quaternary deposits across the site investigation area showed no or little response to sea level changes. Coefficients of correlation between daily average time series for sea level and groundwater wells in Quaternary deposits were typically very low at all locations ($< R^2 = 0.1$), with the exception of SFM0059 and SFM0061, which were both located in glaciofluvial material within 100 m of the sea. The "undisturbed" time series from wells in bedrock also had typically low correlations to sea level. In wells with more than one-half year of available data (n = 13), correlations were very low ($< R^2 = 0.1$) in all but one well, and the correlation in that well (HFM18) was still poor ($R^2 = 0.2$).

Figure 3-13 shows coefficients of determination for monthly average groundwater levels in Quaternary deposits and sea level. Only two wells showed moderate correlations (SFM0059 and SFM0061), and both of these were located in a glaciofluvial deposit close to the sea. As opposed to correlations with rainfall/snowmelt minus potential evapotranspiration time series, there was no benefit in looking at the influence of antecedent sea levels on average groundwater levels.

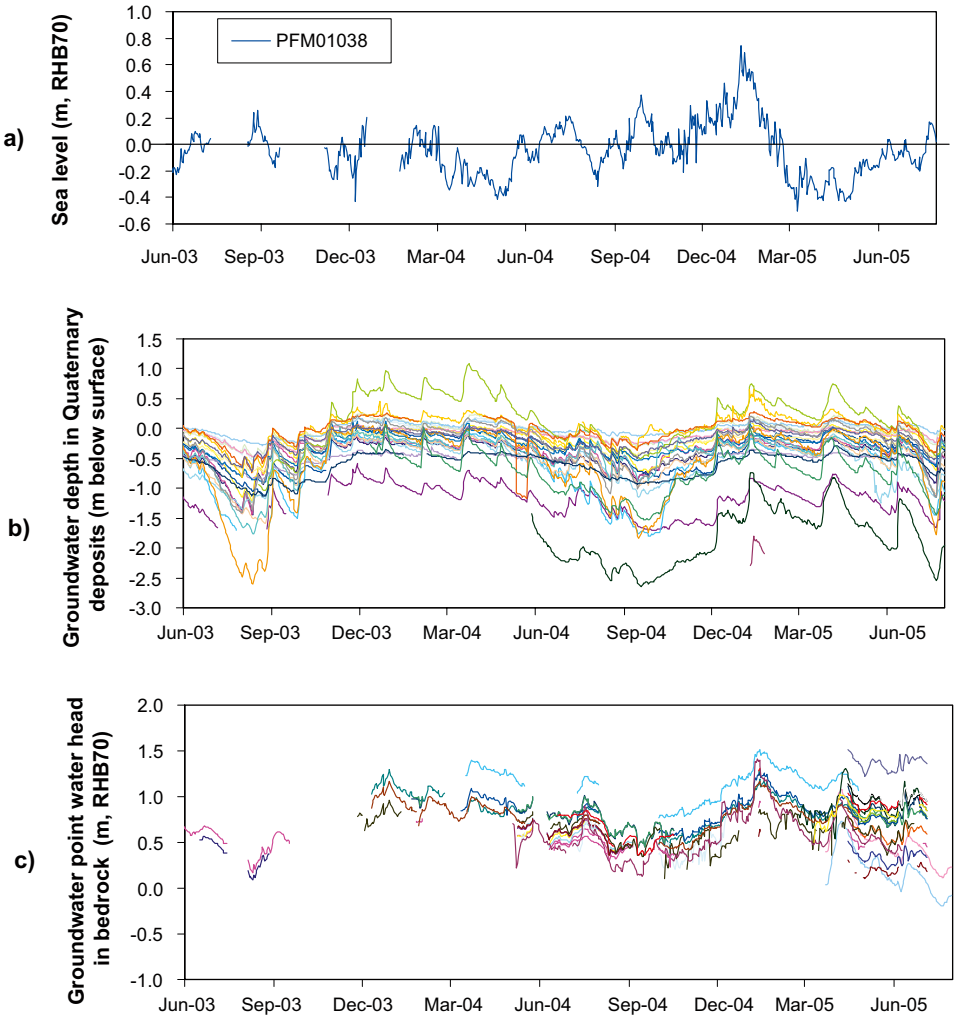

Figure 3-12. *Comparison of sea water levels a), to groundwater depths in Quaternary deposits b), and point water heads in the bedrock c).*

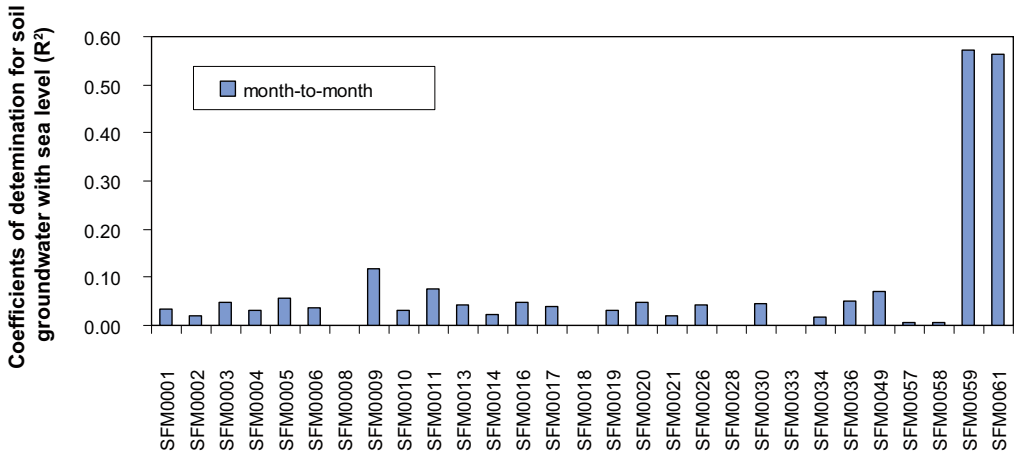

Figure 3-13. *Correlations of monthly average groundwater levels in Quaternary deposits with monthly average sea levels.*

Figure 3-14a shows coefficients of determination for monthly average point water heads in bedrock with sea levels. As with the correlations to rainfall/snowmelt minus potential evapotranspiration, only 13 of the 22 wells had adequate data to make preliminary comparisons. The strongest correlation was observed at HFM18, which is adjacent to the sea, but this was still a weak relationship ($R^2 = 0.21$). While these results are preliminary and often based on sparse data sets, the overall influence of sea level on monthly trends in bedrock groundwater appears small. Figure 3-14b shows R^2 values for day-to-day relationships between sea level and point water heads. HFM18 was the only well that demonstrated any appreciable correlation. Correlations between point water heads with one, three, and five day lags relative to daily sea level values were also investigated. In all cases, results were virtually identical to those in Figure 3-14b, supporting the assessment that sea levels have exerted only minor influence on sub-annual trends in bedrock groundwater. Results from a principal component analysis (PCA) are presented in Section 3.5 that further evaluates relationships between groundwater point water heads in bedrock and sea level time series, as well as meteorological variables.

Over shorter intervals than the complete time series analysis in Figure 3-14, some evidence of sea level influence has been observed. For example, Figure 3-15 shows a close-up of a six-month period from the time series in Figure 3-12 centered on the peak daily average sea level of +0.75 m observed in January 2005. Many of the wells that are shown in Figure 3-15b are in close proximity to the sea (HFM04, 16, 17, 18, 20, 21). Unfortunately, a direct assessment of the influence of this sea level peak on point water heads is clouded by coinciding snowmelt events. Groundwater levels in Quaternary deposits are also shown (Figure 3-15a) to help separate these combined influences on groundwater levels. For reference, Figure 3-16 from /Juston and Johansson 2005/ shows data from a different period that helps to support the notion that groundwater levels in Quaternary deposits do not respond to sea level events. Therefore, it can be inferred that the groundwater level responses shown in Figure 3-15a represent responses to rain and snowmelt inflows. The point water heads in the bedrock (Figure3-15b) show some response

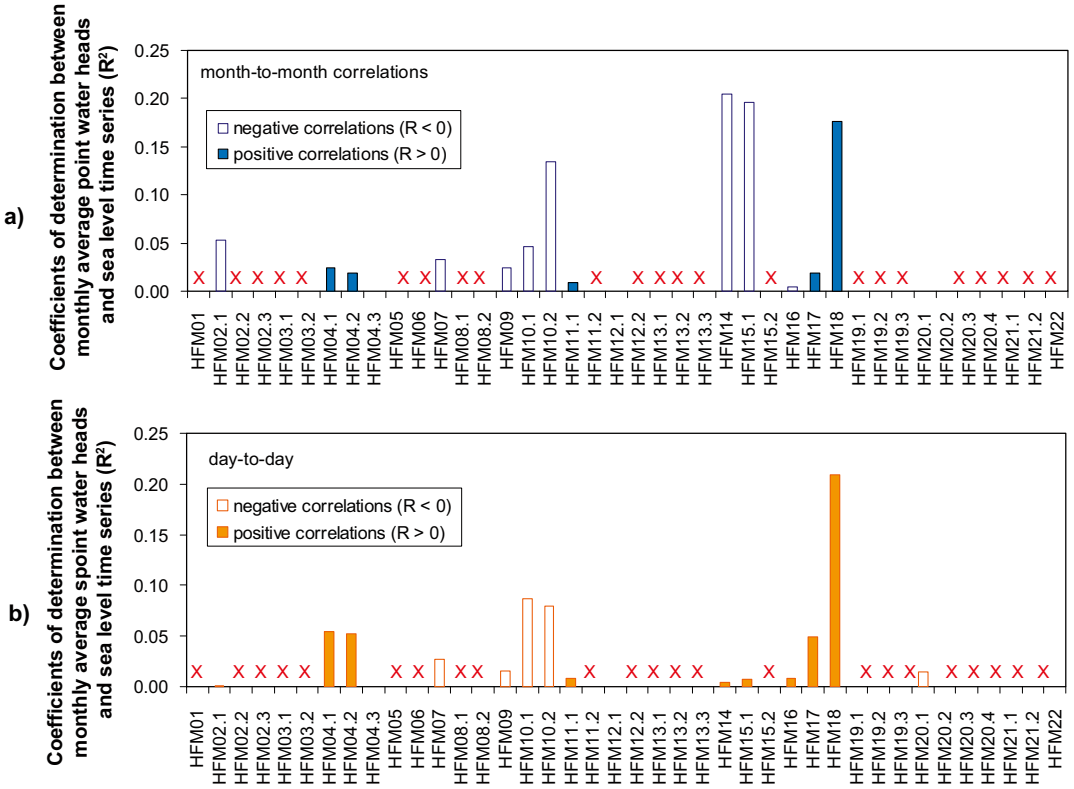

Figure 3-14. *Correlations of monthly average groundwater point water heads with sea level on an a) month-to-month basis, and b) day-to-day. Red X's signify well sections for which correlations were not calculated due to less than six months of available data.*

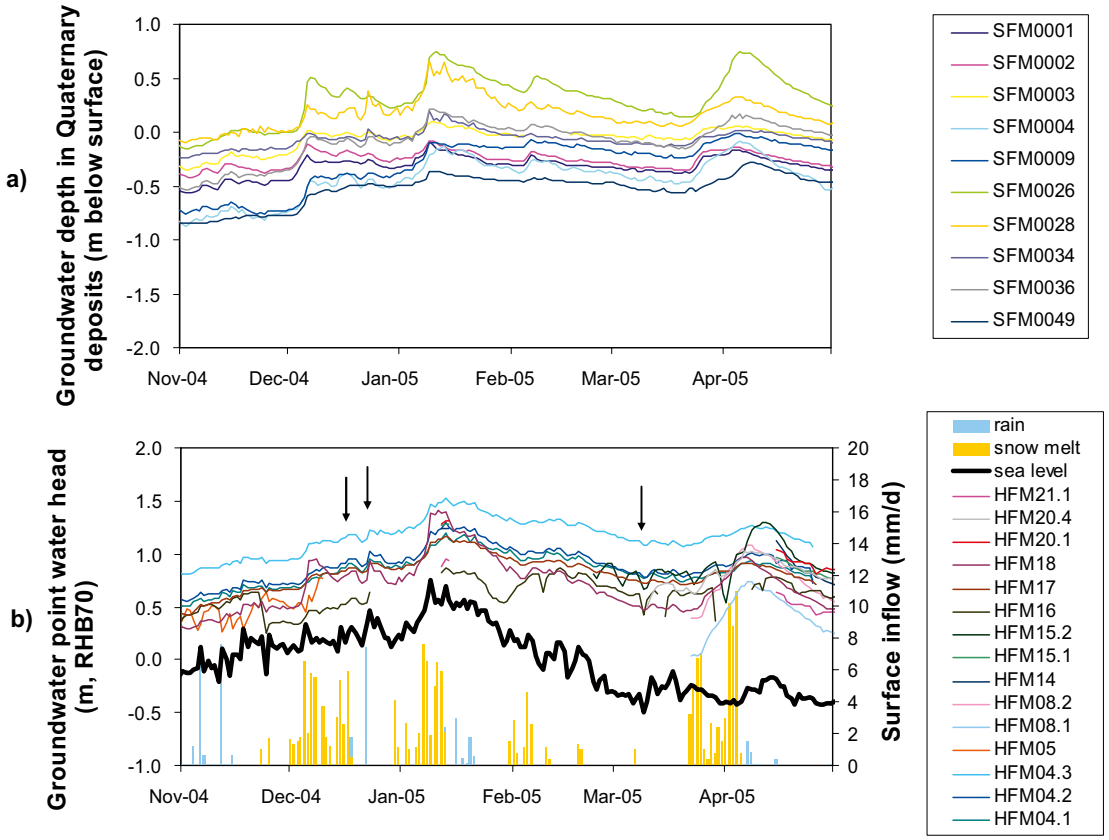

Figure 3-15. *Close-up response of a) groundwater levels in Quaternary deposits, and b) point water heads in bedrock to a combination of a 1-m change in sea water level and infiltration from rain and snowmelt events.*

to the April 2005 snowmelt, but no strong response to the December 2004 snowmelt. Additionally, there are "mini-events" in sea level change, indicated with the arrows in the figure that clearly have echoes in several of the bedrock groundwater responses. Furthermore, groundwater in the bedrock shows a recession after the peak sea level event that more closely follow the sea level recession than do the groundwater responses in Quaternary deposits. This evidence is not conclusive, but it does suggest some responses to sea level changes during this peak event, in spite of the low correlations observed with the longer duration time series. Overall, seasonal rainfall/snowmelt minus evapotranspiration patterns seem to provide a stronger influence on point water heads in the bedrock. More and longer timer series, particularly during undisturbed periods, are required to solidify this assessment.

As was discussed in Chapter 2, sea water does occasionally directly intrude to low elevation lake waters in the site investigation area. Figure 3-17 shows an 8-day close-up of the sea level peak in early January 2005 plotted with the surface water level in Bolundsfjärden and the electrical conductivity from a station in the (typically) outlet from Bolundsfjärden. Here, the data are plotted with hourly data and hence the peak observed sea level here is higher than shown with the daily average data shown in Figure 3-15 (0.94 m from 30-minutes data versus 0.75 m for daily average). High conductivity waters were observed in the outlet of Bolundsfjärden when sea levels rose above approximately 0.6 m (RHB70), suggesting sea water inflows that in turn resulted in the observed increases in lake surface elevations. Figure 3-18 complements these observations with electrical conductivity profiles from lake water in Bolundsfjärden taken at three occasions during 2005. The first occasion (January 31, 2005) was approximately 3 weeks after the sea water intrusions and shows the settling of saline waters at the lake bottom. Two months later (March 29, 2005), the conductivity profile was virtually identical. At that time the lake was still covered by ice preventing wind-driven water mixing. However, in late summer the profiles indicate well-mixed conditions.

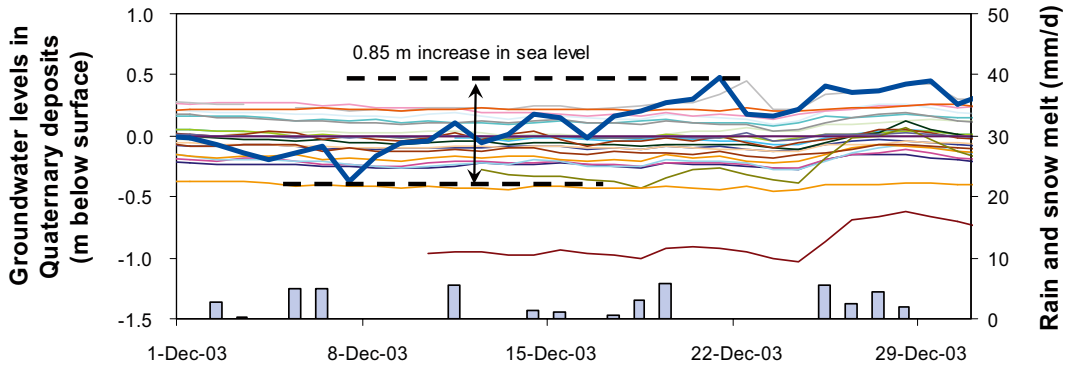

Figure 3-16. *Response in groundwater levels (or lack thereof) in the Quaternary deposits to a 0.85 m rise in sea water level in December 2003 from /Juston and Johansson 2005/.*

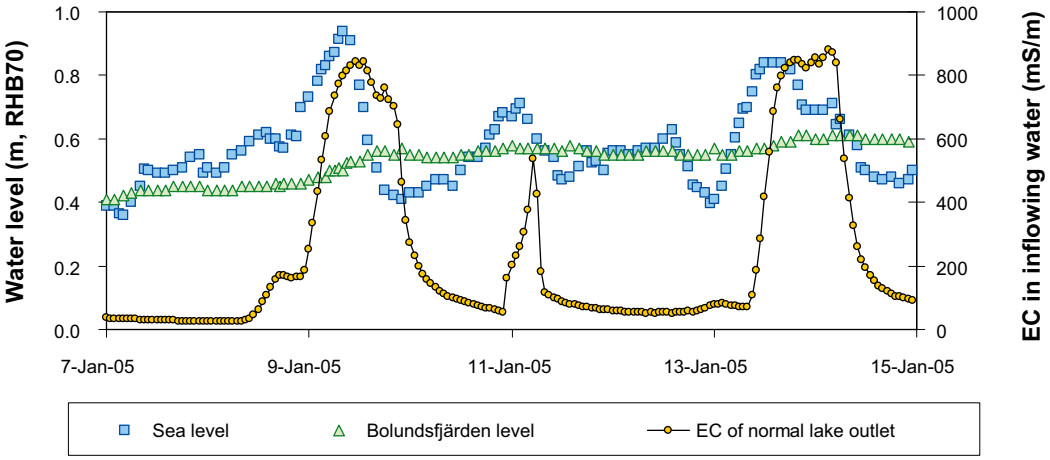

Figure 3-17. *Selected data interval illustrating occasional direct sea water inflows to Bolundsfjärden.*

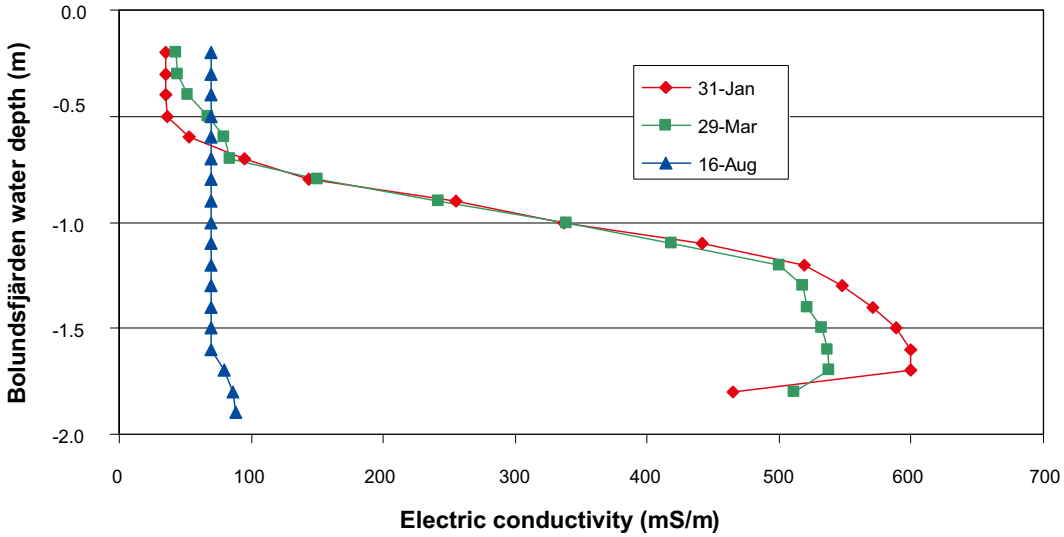

Figure 3-18. *Electrical conductivity profiles in Bolundsfjärden measured during winter, early spring, and summer, 2005.*

3.5 Principal Component Analysis of groundwater point water heads, and meteorological and sea level data

3.5.1 Data sources

This analysis is based on the undisturbed time series of point water heads observed in percussion-drilled boreholes, see Figure 2-28. These series that were cleaned with respect to anthropogenic disturbances due to pumping activities etc reflect as far as possible natural variations coupled to meteorological factors and sea level changes.

Daily time-series of daily precipitation, potential evapotranspiration, air pressure and sea levels were also included in the analysis. The daily infiltration was estimated as the accumulated difference between daily rainfall/snowmelt and potential evapotranspiration, see Figure 3-4.

3.5.2 Preparation of data prior to analysis

In order to maximize both the number of percussion-drilled boreholes and observations included in the analysis, three datasets were selected according to Table 3-1. The main data set A, marked in green, covers few objects but a long time period, including the storm event "Gudrun" that hit Sweden in January 2005. Complementary datasets B and C marked in blue represent shorter time periods but include more boreholes. In tables and figures are throughout this section, individual sections in the percussion boreholes labelled HFM# _section (e.g. is the deepest section of HFM04 labelled HFM04_1).

Table 3-1. Compilation of available number of point water head data from percussion-drilled boreholes. Three datasets denoted A (marked green), B (upper blue), and C (lower blue) was used in three separate analyses. The column of precipitation is also representative for air pressure and evapotranspiration data. Throughout this section individual sections in the percussion boreholes are labelled HFM _section (e.g. is the deepest section of HFM04 labelled HFM4_1).

Year	Month	HFM	1	2	2	2	3	3	4	4	4	5	7	8	8	9	10	10	11	11	12	12	13	13	13	14	15	15	16	17	18	19	19	19	20	20	20	20	21	21	22	Precipitation	PFM01038 Sea level
		Level	1	1	2	3	1	2	1	2	3	1	1	1	2	1	1	2	1	2	1	2	1	2	3		1	2	1	1	1	1	2	3	1	2	3	4	1	2	1		
2003	5			10								10																												10	10
2003	6		15	30								13																												30	30
2003	7		14	14								31																												31	9
2003	8		23	27								29																												31	15
2003	9			17								18																												30	19
2003	10											26																												31	
2003	11											22																	5											30	26
2003	12								22			22				7	2											30	22											31	18
2004	1			7					31			31				31	31		10		10					11	9	12	30											31	10
2004	2			5					23			29				17	16		29		29					5	5	4	29		3	3	3						29	29
2004	3			3	1	1			13	21	16	31							31		31					1	1	4	31		1	1	1						31	31
2004	4			4	4	4	4	4	30	30	30		30			24	29		30		30					4	4	4	30		4	4	4						30	30
2004	5			18	18	18	18	18	18	18	18	7	31			31	17		31		31					18	18	18	18	28										31	31
2004	6			20	20	20	23	23	4	4	4	4	30			30	29		30		30					23	23	19	4	28					12				16		30	30
2004	7			31	31	31	31	31	24	24	24	24	31			31	31		31		31					31	31	31	24	27					31				31		31	31
2004	8			31	31	31	31	31	2	2	2	4	31			31	15		31		31					31	31	28	4	31					22				9		31	31
2004	9			4	4	4	4	4				2	30			30	18		30		30					30	30	30	1	30					30						30	30
2004	10								31	31	31	31	31			31	31		31		31					19	19	24	31	31					19				19	2	31	31
2004	11								30	30	30	30	30			30	11	9	30		30					4	4	30	30	30					2				2	2	30	30
2004	12								31	31	31	10	31			31	31	31	31		31					4	4	23	31	31					4				4	4	31	31
2005	1								31	31	31		31			31	31	31	31		31					6	6	20	31	31					6				5	4	31	31
2005	2								28	28	28		28			28	28	28	28		28		1	1	8	4	1	6	28	28	28	1	1	1	2			3	4	28	28
2005	3								31	31	31		31	10	10	31	31	31	15		15		4	4	31	4	4	31	28	31	31	4	4	4	3	3	3	22	2	4	31	31
2005	4								25	25	25		30	30	30	26	26	26	5	5	11	11	18	18	30	18	18	30	23	26	30	18	18	18	18	18	18	30	18	7	30	30
2005	5												31	30	30	23	23	23	30	30	30	30	31	31	31	31	31	31	31		31	31	31	31	31	31	31	31	2	31	31	31
2005	6												30	30	30	30	30	30	27	27	27	27	30	30	30	30	30	30	21		9	30	30	30	10	10	10	10		12	30	30
2005	7										1		30	30	30	30	31	31	30	30	30	30	5	5	5	5	5	5				5	5	5	5	5	5	5	5	5	31	30

Due to the heterogeneity of the cleaned dataset, with both missing data and different sampling frequencies, the time series were filled by linear interpolation thereby maximizing the matrix available for data analysis. This technique could be questioned as it may introduce errors, but the advantages of extended parallel time series was thought to outweigh the disadvantages. The original and the interpolated time series of dataset A may be compared in Figure 3-19. The complementary datasets B and C are only shown as interpolated series in Figure 3-20 and Figure 3-21.

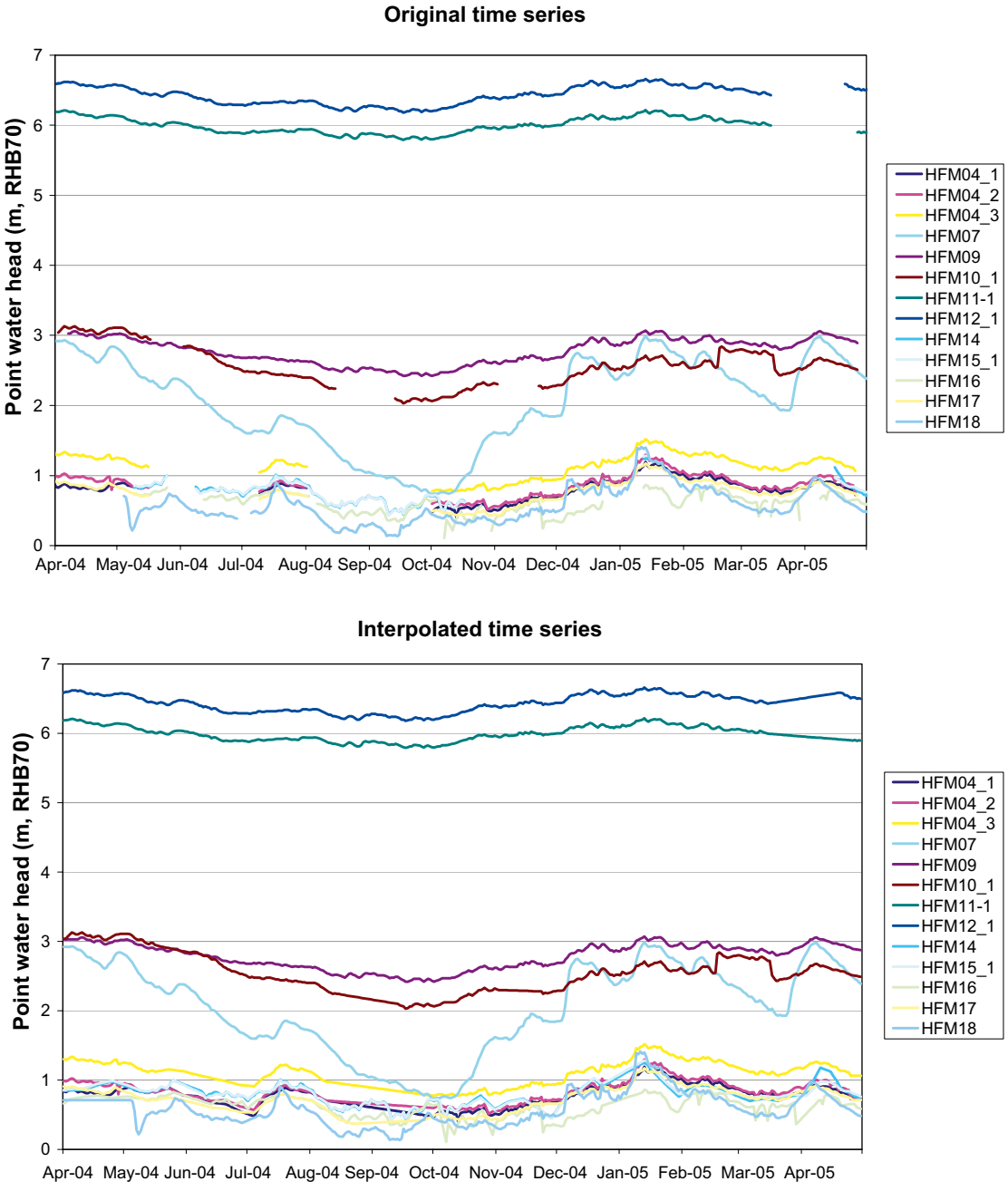

Figure 3-19. *The original time series of point water heads in percussion-drilled boreholes of dataset A (top), and the linearly interpolated time series (bottom).*

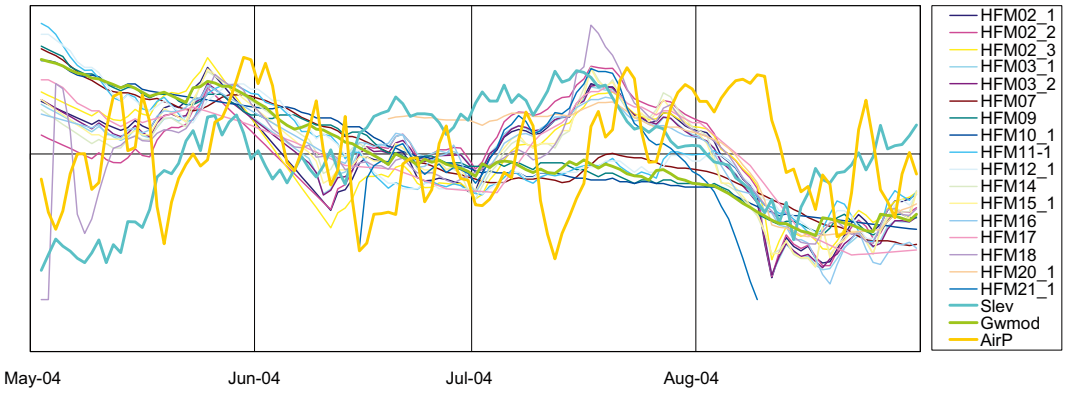

Figure 3-20. *All data from subset B (May 2–August 31, 2004) are included in the plot, together with sea water level (Slev), modelled groundwater level (Gwmod), and air pressure (AirP). All time-series are standardized to zero mean and equal variance.*

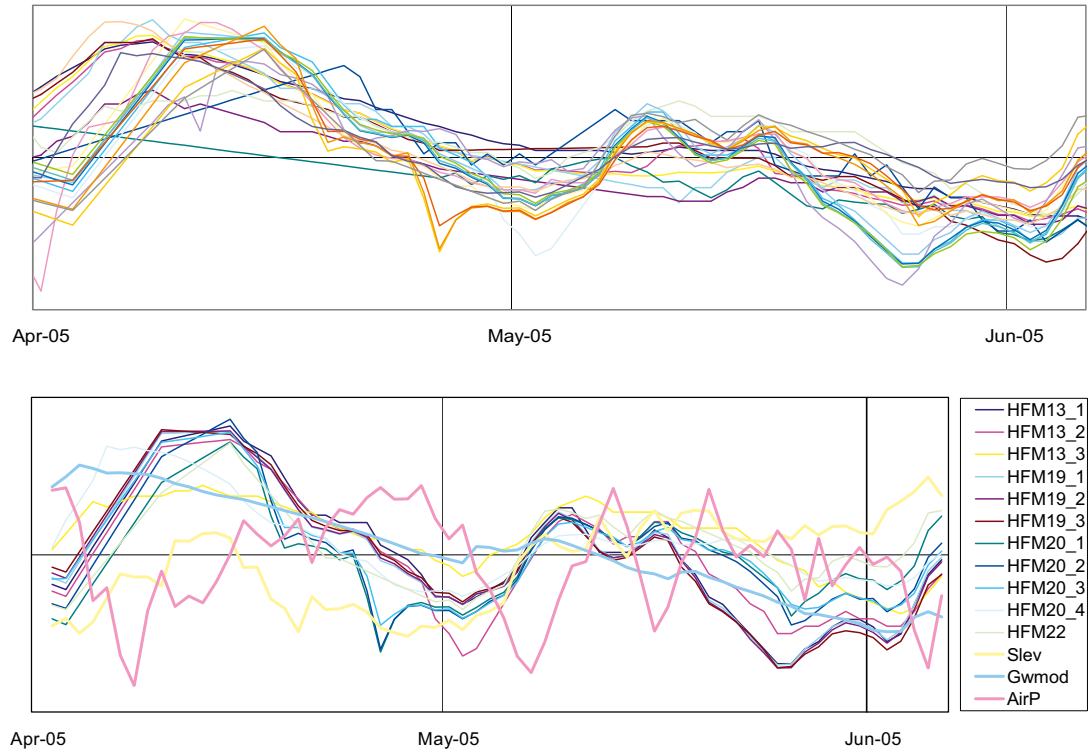

Figure 3-21. *The time series of complementary dataset C (April 1–June 5, 2005). All percussion-drilled boreholes are included in the upper figure. The lower figure contains percussion-drilled boreholes from the northern part of the candidate area together with sea water level (Slev), modelled groundwater level (Gwmod), and air pressure (AirP). All time-series are standardized to zero mean and equal variance.*

3.5.3 Summary of data used for comparison with the point water heads in the bedrock wells

Data used for comparisons with the point water head levels in the percussion-drilled boreholes are summarised in this section.

The three variables precipitation, sea water level and estimated groundwater level show little co-variation according to Figure 3-22. The strongest correlation is displayed by precipitation and sea water level probably due to the common influence from low pressures.

The air pressure, shown in Figure 3-23, show, however, very strong correlation to the sea water level when the inverted 14-day moving average (centred) of the air pressure is compared to the sea water level. This shift may be an effect of the underlying dynamics of the Baltic Sea and the prevailing pattern of low pressures coming from west. The sea water level is normally high at low air pressures.

The variation of the local groundwater level was estimated by a simple tank model. The level in the groundwater storage was assumed to be a function of daily inflow (difference of snow storage corrected precipitation and potential evapotranspiration), and an outflow function proportional to the groundwater level. A constant of the outflow function was calibrated to meet the assumption of zero change of groundwater storage during 2003-05-22 to 2005-05-22.

The total difference between accumulated inflow and potential evapotranspiration during this period is 60 mm/year, indicating that the actual evapotranspiration is overestimated by using the potential evapotranspiration. There is, however, a good match between the modelled ground-water level (blue) and the observed point water head variation in HFM07 (green) according to Figure 3-24. This annual cycle is most controlled by variations in evapotranspiration.

3.5.4 Variance analysis of point water heads in percussion-drilled boreholes

The point water heads in all percussion-drilled boreholes follow a general pattern closely coupled to the annual cycle of infiltration (rainfall/snowmelt minus potential evapotranspiration) as seen in Figure 3-25 and Figure 3-26. The highest levels generally appear during late winter and early spring, and the lowest during late summer and early autumn. The standardized mean of point water heads of all percussion-drilled boreholes and the modelled groundwater level (GWmod) show very good correlation according to Figure 3-26. The main differences during April 2004 to April 2005 are found for two events: the low pressure in July 2004 and the "Gudrun" storm in January.

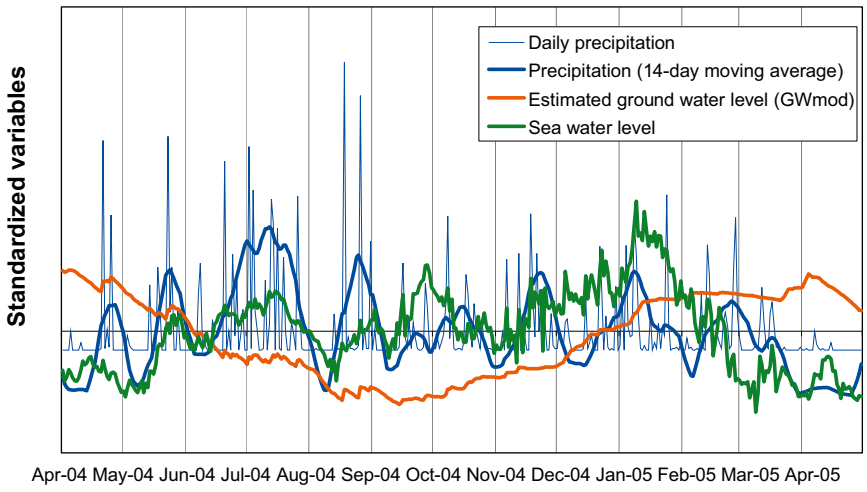

Figure 3-22. *Daily precipitation, 14-day moving average of precipitation, estimated groundwater level (modelled – see text) and sea water level. All time-series are standardized to zero mean and equal variance.*

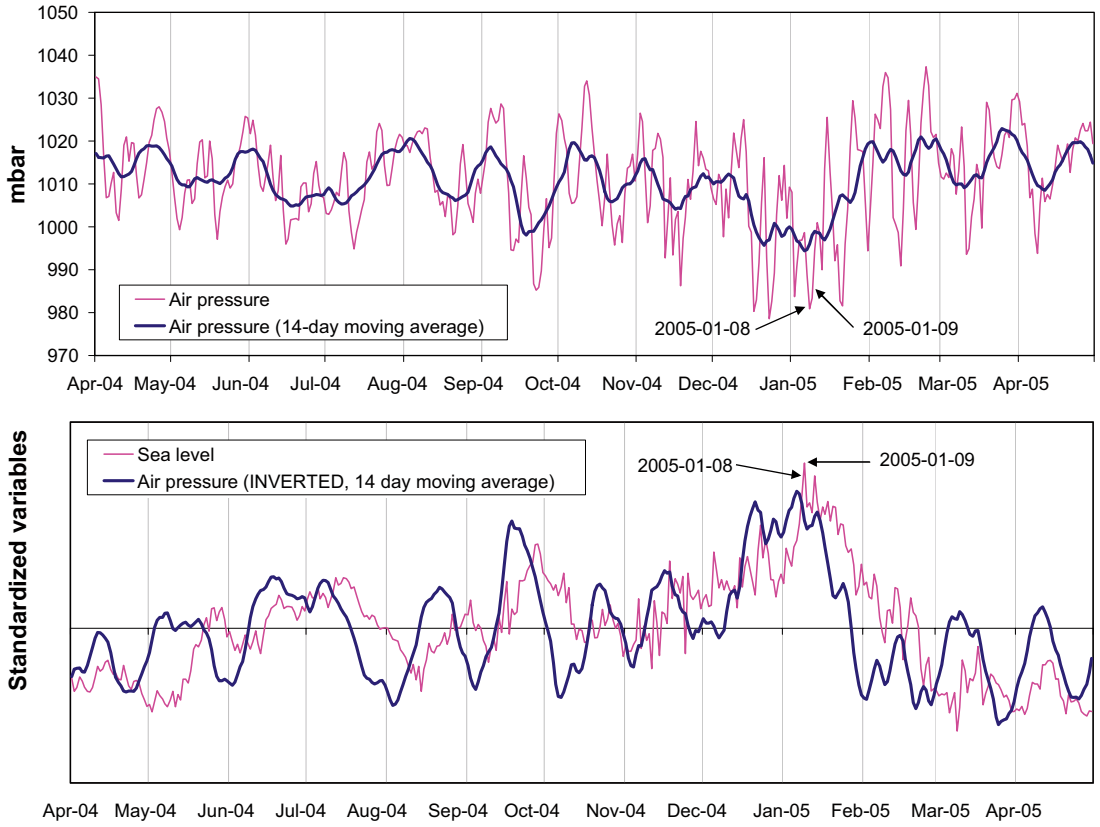

Figure 3-23. *Daily air pressure in the Forsmark area. In the upper figure daily values are compared to the 14-day moving average. In the lower figure the air pressure (14- day moving average) is inverted in order to facilitate comparisons with sea water level. Time-series in the lower panel are standardized to zero mean and equal variance.*

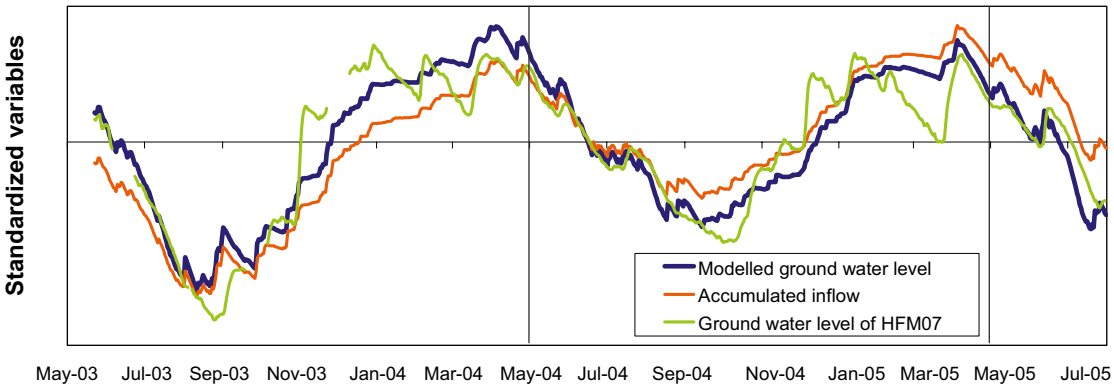

Figure 3-24. *Groundwater level estimated by a simple tank model (blue), compared to the accumulated difference between inflow and potential evapotranspiration (orange) and the observed point water head in HFM07. All time-series are standardized to zero mean and equal variance.*

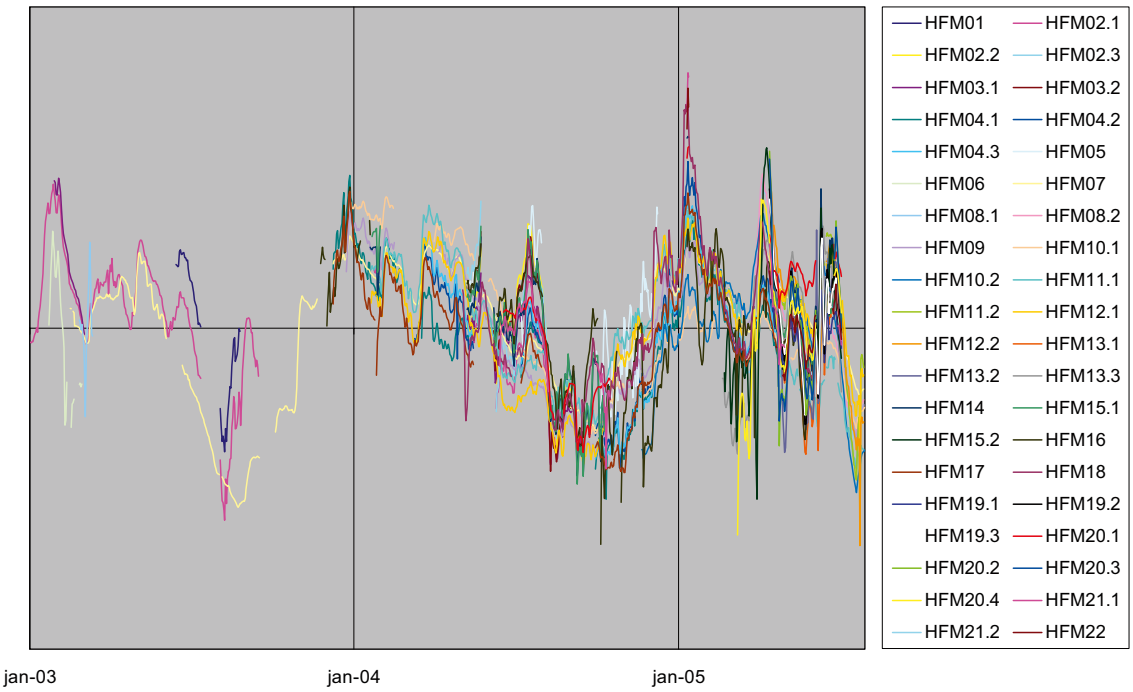

Figure 3-25. *Standardized point water heads in all percussion-drilled boreholes during 2003-2005. All time-series are standardized to zero mean and equal variance. Note that this figure includes more data than the selected time series in Figure 3-19.*

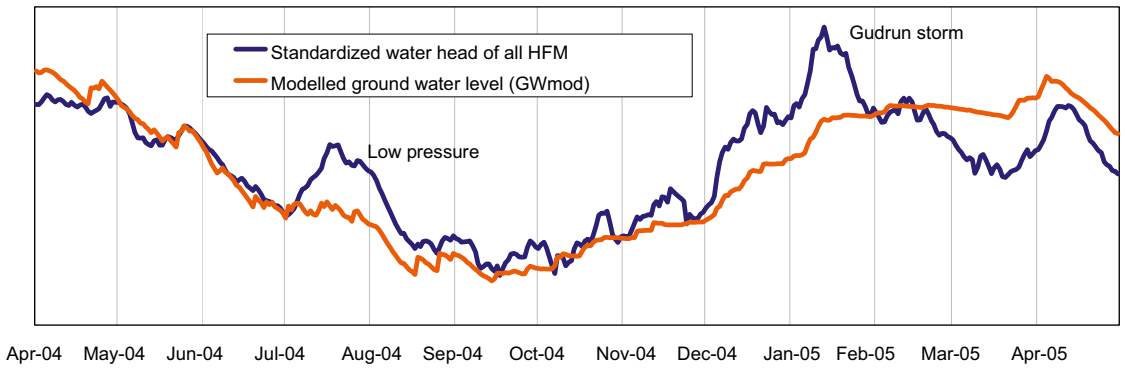

Figure 3-26. *Mean value of standardized (same mean and variance) observed point water heads in the HFM-boreholes compared to modelled groundwater level (based on accumulated difference between precipitation and potential evapotranspiration).*

If a Principal Component Analysis (PCA) is applied on dataset A, three components (factors) comprise about 93% of the total variation observed in the point water heads of the percussion-drilled boreholes. The first component, that describes about 80% of the total variance, captures the seasonal variation in precipitation/evapotranspiration that is the major cause of the overall pattern seen in Figure 3-25 and Figure 3-26.

The two higher components that comprise about 13% of the total variation in point water heads (PC2 7% and PC3 6%) reveals the correlation structure among the percussion-drilled boreholes when the mean annual cycle has been withdrawn.

From the loading plot in Figure 3-27 it can be seen that some boreholes located geographically close to each other show a higher degree of correlation as they are clustered in the plot. Examples are HFM11 and HFM12 near Eckarfjärden, HFM14 and HFM15 near Bolundsfjärden.

In the score-plot in Figure 3-27, the correlation structure among the individual observations in time is shown for the second and third components. The numbers in the plot correspond to the number of the month. In this score plot there is an interesting pattern that exactly coincides with the "Gudrun" storm event, encircled in green. The storm hit southern Sweden with a maximum during January 8–9, and the lowest scores of the vertical component 3 also appear on these dates (encircled in red).

If this pattern, described by component 3, is a measure of the influence of the variations in sea level, HFM18 is most influenced, whereas HFM10_1 is least influenced. The two deepest levels of HFM04 as well as HFM17 also show positive correlation to component 3 indicating a possible influence. These most influenced boreholes are all located near the coast in the Lillfjärden area.

How to interpret a principal component analysis

A Principal Component Analysis (PCA) is based on a standard Pearsson correlation matrix and may be seen as a graphical tool to interpret the correlation structure among both variables (here individual percussion-drilled borehole sections) and observations (different observations in time at each borehole section).

In the loading plot the relationships among the variables are revealed. Variables that plot close to each other are correlated, whereas variables located on opposite sides of the origin are negatively correlated. Variables located near the origin show little correlation to the selected principal components, and therefore little could be said about the correlation structure among these variables. Each variable is projected onto the so called principal components that could be seen as latent factors influencing several variables to a varying degree. If a variable show close connection to a principal component, it is located far from origin in the loading plot in the direction of the current component. The principal components may have a real meaning, for example correspond to a climatic factor, or may just represent a linear combination of unknown factors.

The score plot reveals the relationships among the observations. A score plot is a complement to the loading plot in the sense that observations that are located in a specific region of the score plot show high values for variables located in the corresponding region of the loading plot. In the PCA in Figure 3-27, the observations during the storm Gudrun show especially high values in HFM18, indicating a fast response that is mainly captured by the third vertical principal component.

3.5.5 Independent component analysis of point water heads

By applying an *Independent Component Analysis,* ICA /Hyvärinen et al. 2001 and Hyvärinen 2006/, on the time series of point water head data, hidden "signals" were extracted from the time series of dataset A. This powerful blind source separation technique, which is related to principal component analysis, is suitable for finding common independent signals (e.g. climatic factors) from a set of parallel measurements. The main variation is extracted into three "signals" shown in Figure 3-28.

The first signal in Figure 3-28 describes the general pattern coupled to the annual water balance. It is also very close to the modelled groundwater level (GWmod) and the mean of all standardized groundwater levels shown in Figure 3-26.

The second signal is more difficult to interpret, as it shows no correlation to the climatic variables. There is, however, a connection to the variation pattern in HFM10_1 as seen in Figure 3-28, where patterns encircled in green show high resemblance. These patterns could be coupled to disturbances in, or in the vicinity of the borehole, or less likely, is an effect of a natural influencing factor. This second signal captures one of the most noticeable anomalies found in the cleaned dataset.

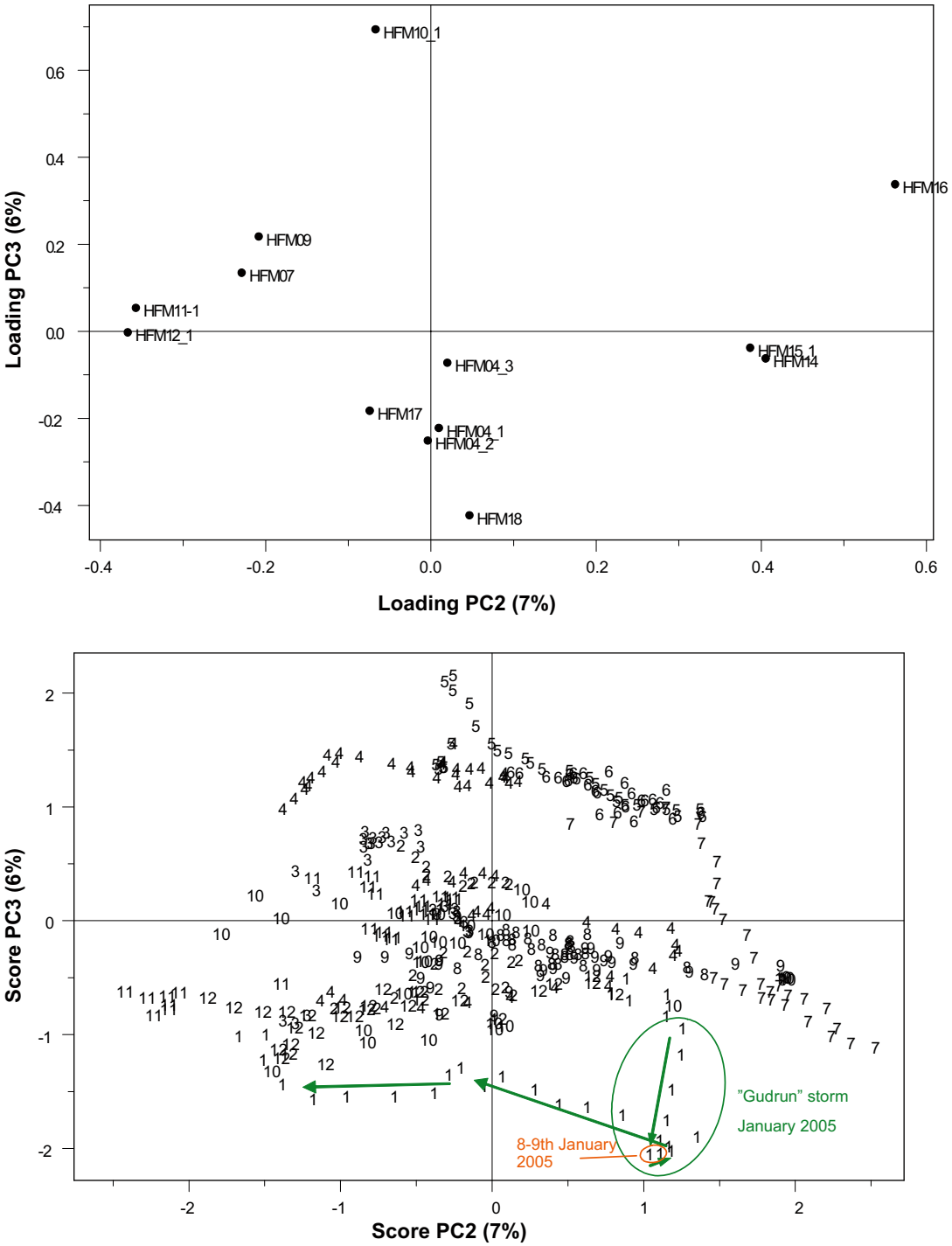

Figure 3-27. *Loading plot (upper), and score plot (lower) of the second and third principal components (PC2 and PC3). See separate box for an explanation of how to interpret a PCA-plot. The first principal component, which is not shown, captures the seasonal variation common to all boreholes according to Figure 3-25 and 3-26.*

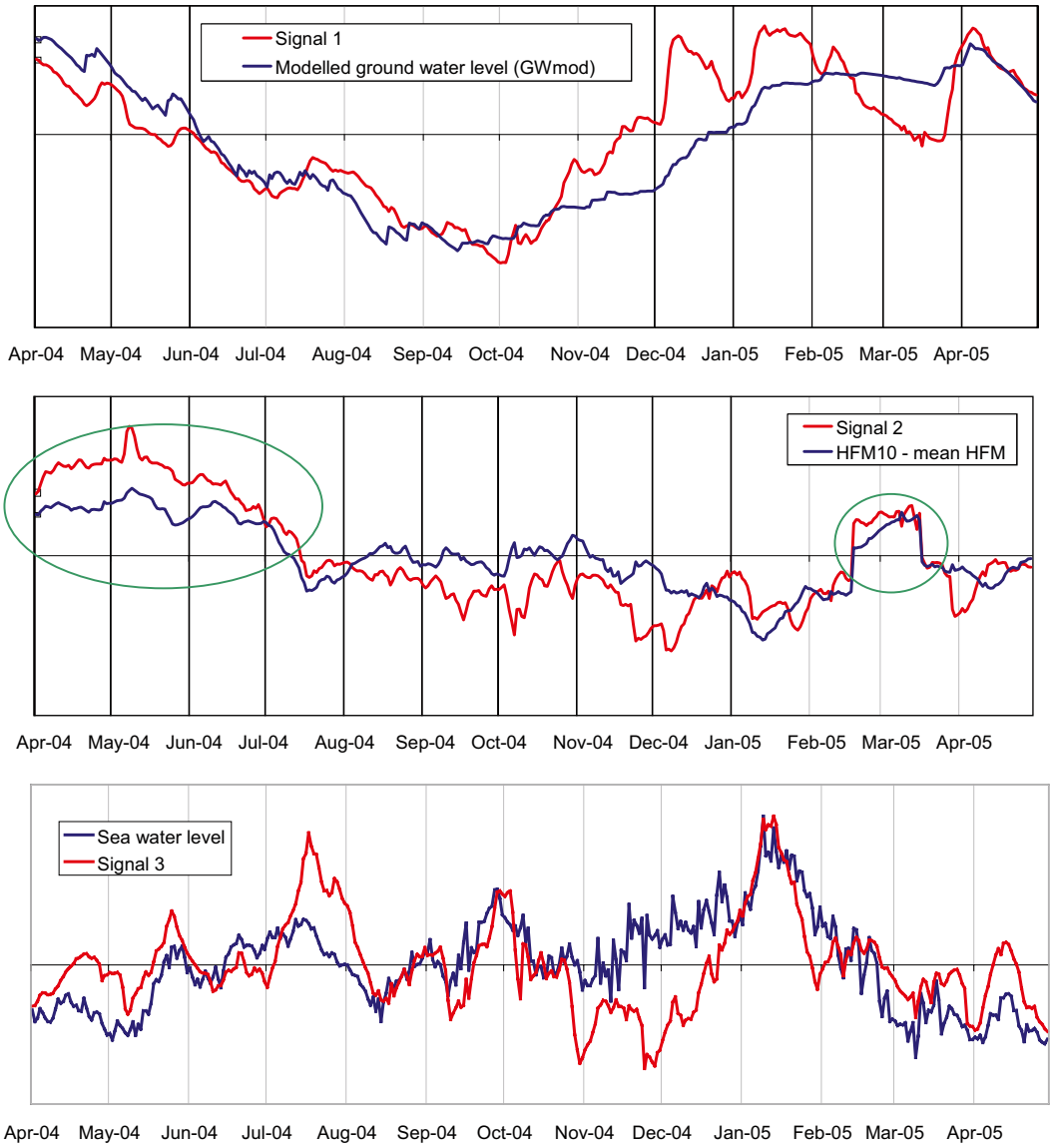

Figure 3-28. *Signals separated from the percussion-drilled borehole point water head data by the Independent Component Analysis technique based on data from subset A. Reference time series is shown besides the extracted signals: modelled groundwater level (upper), the difference between HFM10 and the average point water head of all percussion boreholes (middle) and the observed sea water level (lower).*

The third signal show a close connection to the variation pattern of the sea water level, indicating either indirect influence of low pressures or presence of direct coupling to the sea water level. In Figure 3-29 is signal 3 compared to both sea level and air pressure. The Pearson correlation coefficient is 0.55 when signal 3 is correlated to the sea water level, while 0.25 for air pressure, probably indicating a closer coupling to the sea water level. This signal probably corresponds to the third component in the previous principal component analysis.

3.5.6 Comparisons of observed point water heads and "climate" parameters

As a third step *Partial Least Squares modelling* (PLS) was applied in order to explore the correlation structure between the "HFM groundwater level matrix" and the "climate matrix". This technique is closely related to the principal component analysis, PCA, and the plots may be interpreted in a similar manner. The main difference is that PLS rotates the components in hyperspace in order to maximize the correlation between the two studied matrices.

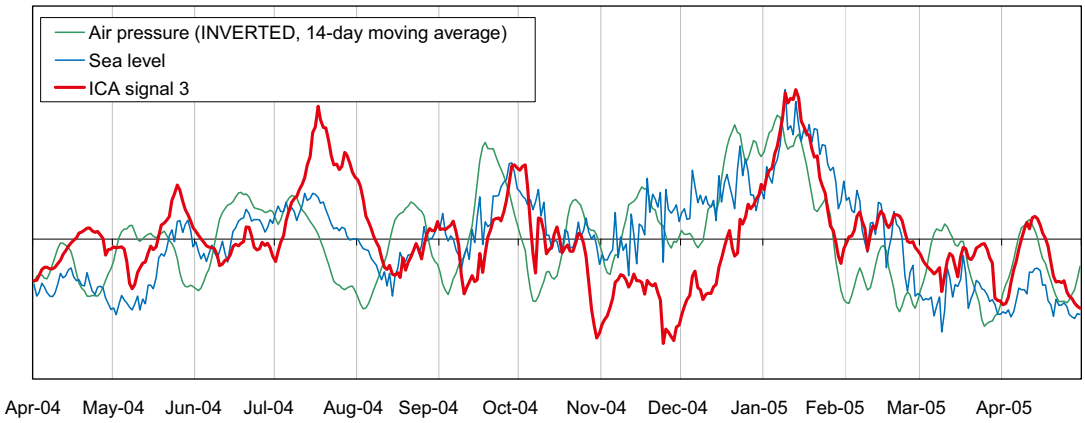

Figure 3-29. *Signal 3, as separated by ICA, compared to time series of sea water level and air pressure. (To facilitate comparisons is the inverted time series smoothened by 14-day moving average shown.)*

Three parallel analyses were conducted on the datasets A, B and C described in Table 3-1. A compilation of the results of these analyses is summarised in Table 3-2. The main analysis is conducted on dataset A (Figure 3-30), whereas the datasets B and C are used to give a complementary picture including more percussion-drilled boreholes (Figure 3-32). The vector score plots shown in Figure 3-31 give an indication on how well the point water heads are modelled during different parts of the year. The main deviation is shown for observations from January to Mars 2005, perhaps indicating that the Gwmod parameter (modelled groundwater level) not satisfactorily model the storage effects of the snow cover this time of the year. However, Figure 3-1 shows a good agreement between measured and modelled snow water content. See more on this issue in Section 3.10.

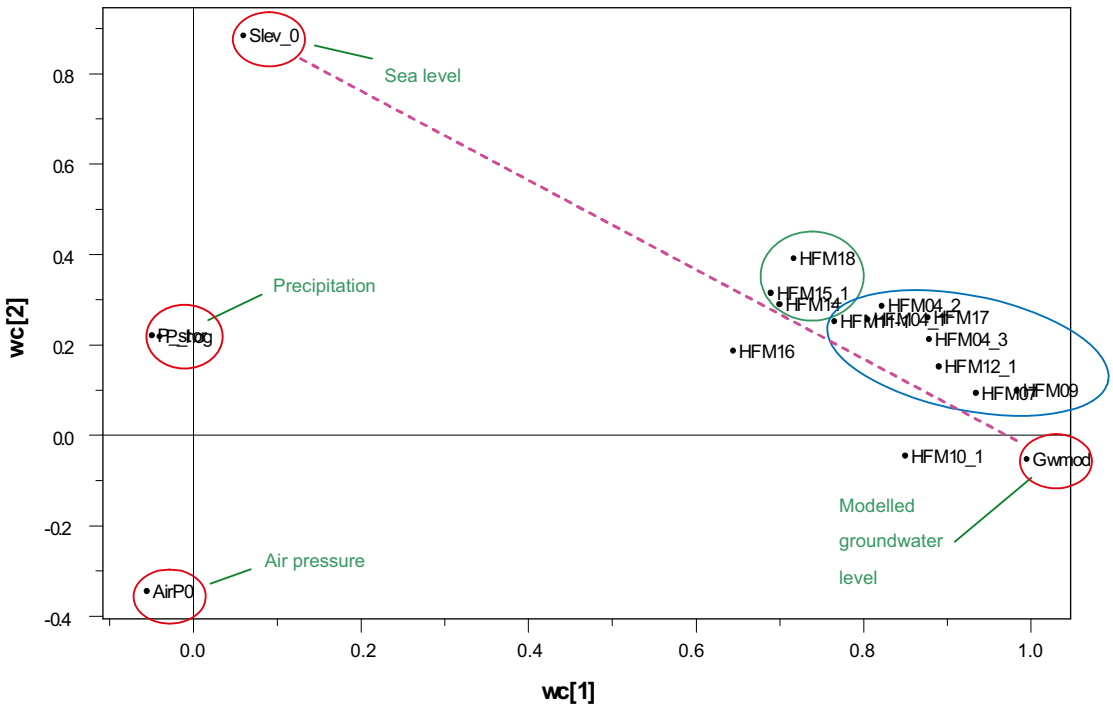

Figure 3-30. *The two components of the PLS-model applied on dataset A. The "climatic" driving variables are encircled in red. Percussion borehole time series that show little correlation to the sea level variation are encircled in blue and possible influence are marked in green. The relative location of the individual percussion boreholes (e.g. HFM18) with respect to the driving variables encircled in red give an indication to what extent different factors influence the point water heads of the boreholes. Variables located close to each other show a higher degree of correlation.*

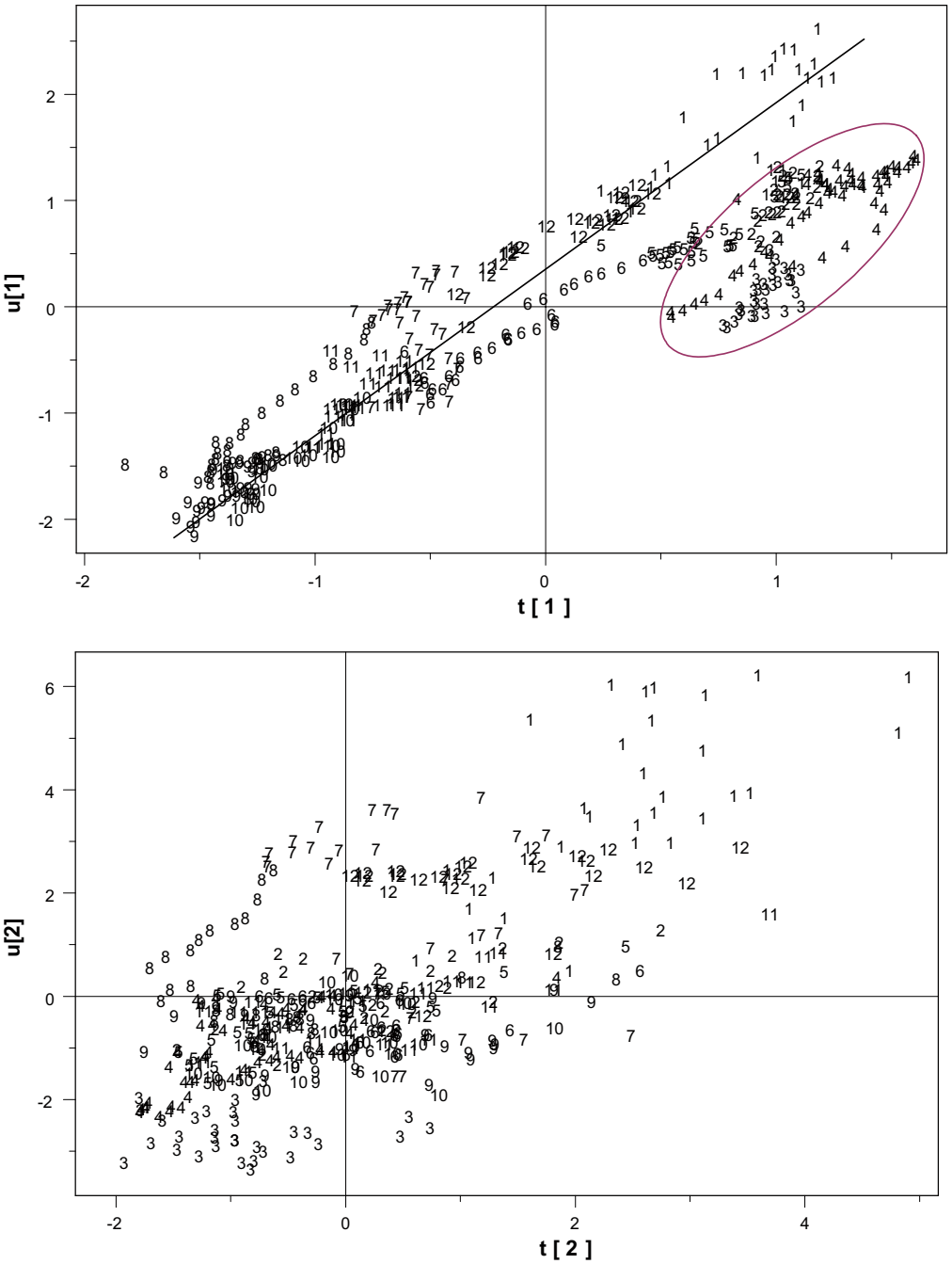

Figure 3-31. *PLS score vector plots of component 1 (top) and component 2 (bottom). In a perfect model the observations (here number of month) show a straight line. The most obvious deviation is shown by a series of observations from February to April 2005 (encircled in the figure). This may be an indication that the GWmod parameter not satisfactorily model the storage effects of the snow cover this time of the year.*

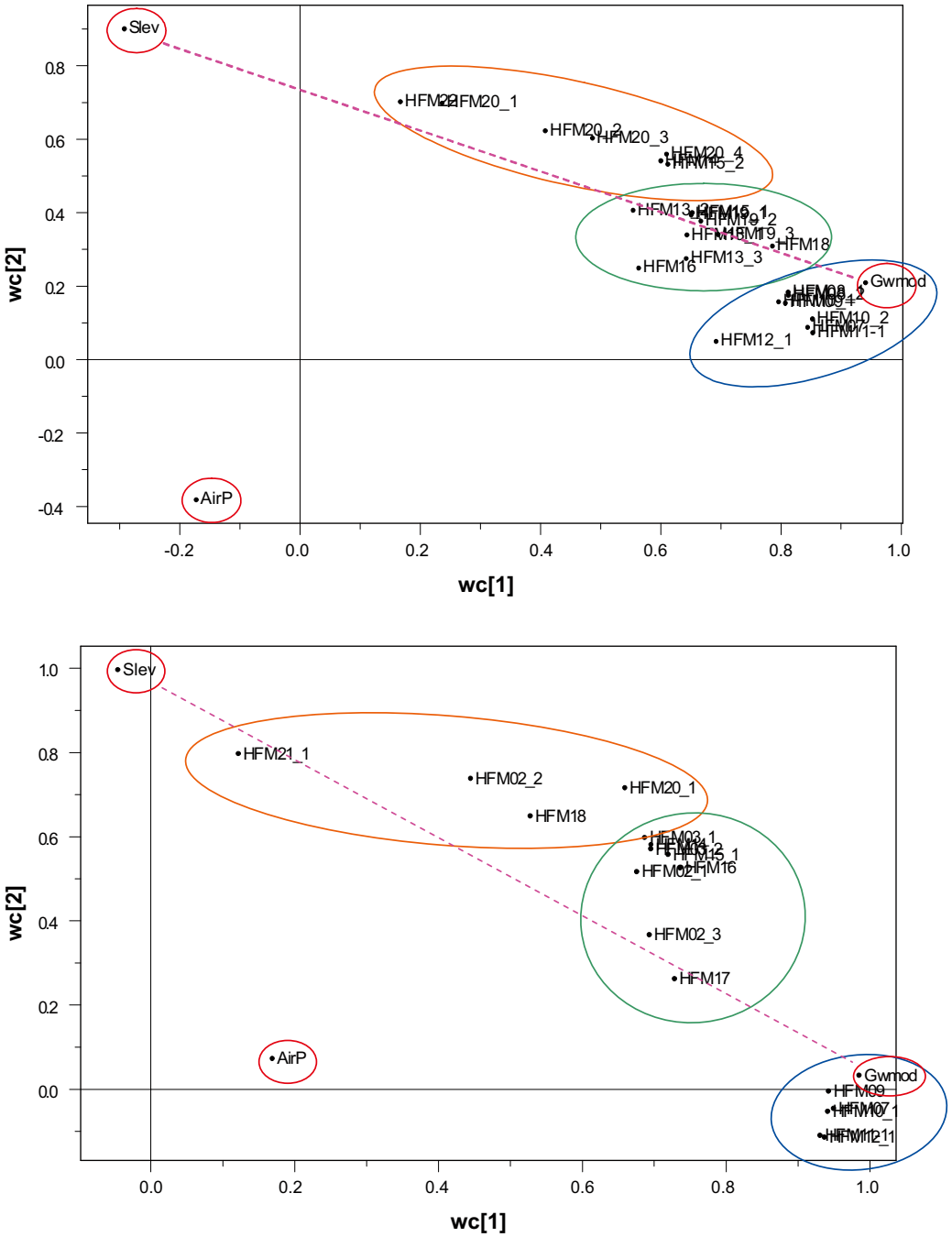

Figure 3-32. *The two components of the PLS-models of data set B (top) and dataset C (bottom), respectively. The "climatic" driving variables are encircled in red. Percussion borehole time series that show little correlation to the sea level variation are encircled in blue, possible influence are marked in green and probable influence are encircled in orange. The relative location of the individual percussion boreholes (e.g. HFM18) with respect to the driving variables encircled in red give an indication to what extent different factors influence the point water heads of the boreholes. Variables located close to each other show a higher degree of correlation.*

When all three datasets are considered, the variation of point water heads in the percussion boreholes is most correlated to the Gwmod parameter. The sea water level (Slev_0) shows the second strongest influence followed by air pressure (AirP0), whereas precipitation (P_hog & P_stor) shows little influence. With a two-component PLS model, 68% of the variation among the percussion borehole point water heads may be modelled by the variables GWmod, Slev_0 and AirP0 (in dataset A).

The PLS-models of dataset B and C show patterns very similar to the main analysis of dataset A, according to Figure 3-32. In order to make a pooled evaluation of the three PLS analyses, the boreholes in the three loading plots are classified according to the relative correlation to parameters Slev0 (sea water level) and GWmod (modelled groundwater level). Three different classes are used: probable influence, possible influence, and no influence. Note that the denomination and boundaries of these classes are rather arbitrarily and should only be seen as a relative indication and not literally seen as a measure of connectivity. The results are summarised in Table 3-2 and in Figure 3-33 is the spatial distribution of these classes shown.

Table 3-2. A compilation of the classification of relative connectivity to the sea water level according to the PLS-models of dataset A-C. 1 denotes “no influence”, 2 “possible influence” and 3 “probable influence”. The table is sorted after the median of the classifications.

Borehole	Dataset			Median
	A	B	C	
HFM04_1	1			1
HFM04_2	1			1
HFM04_3	1			1
HFM07	1	1	1	1
HFM08_1		1		1
HFM08_2		1		1
HFM09	1	1	1	1
HFM10_1	1	1	1	1
HFM10_2		1		1
HFM11_1	1	1	1	1
HFM12_1	1	1	1	1
HFM17	1		2	2
HFM02_1			2	2
HFM02_3			2	2
HFM03_1			2	2
HFM03_2			2	2
HFM13_1		2		2
HFM13_2		2		2
HFM13_3		2		2
HFM15_1	2	2	2	2
HFM16		2	2	2
HFM19_1		2		2
HFM19_2		2		2
HFM19_3		2		2
HFM14	2	3	2	2
HFM18	2	2	3	2
HFM02_2			3	3
HFM15_2		3		3
HFM20_1		3	3	3
HFM20_2		3		3
HFM20_3		3		3
HFM20_4		3		3
HFM21_1			3	3
HFM22		3		3

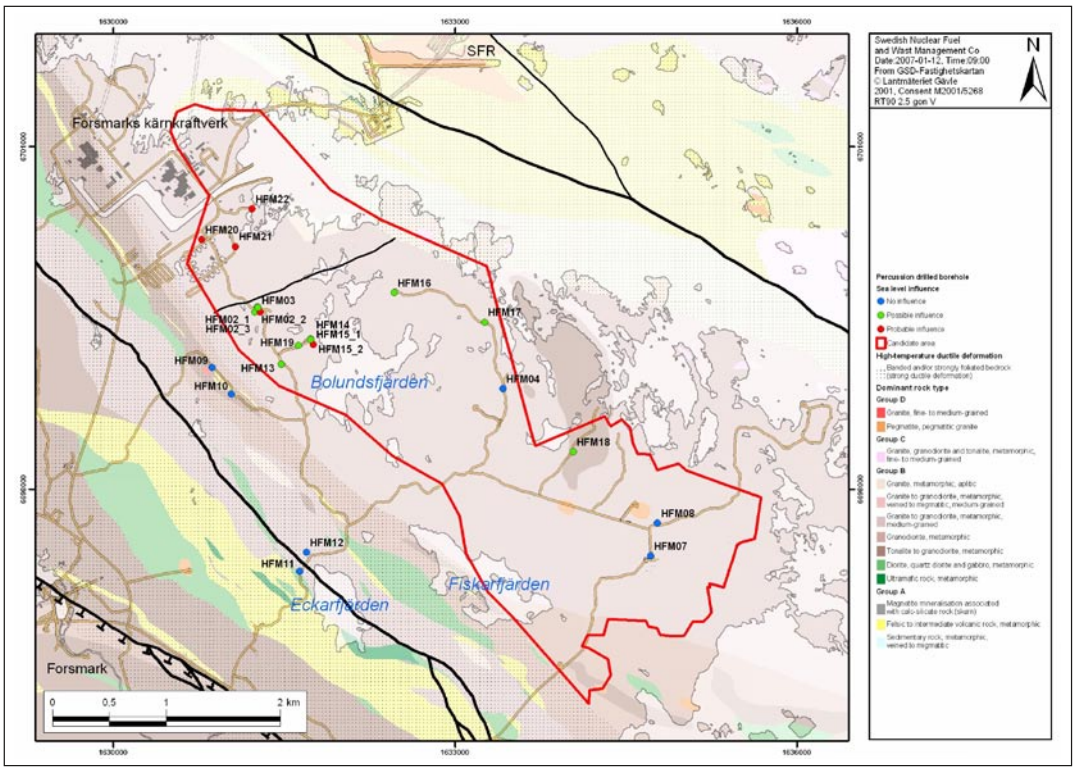

Figure 3-33. *Map showing the classification of the percussion-drilled boreholes according to the estimated degree of influence from variations in sea water level. The bedrock classification is shown as background.*

Boreholes in the last section of Table 3-2 show strongest correlation to the sea water level, e.g. HFM02, HFM15, HFM20, HFM21 and HFM22. Also HFM14 and HFM18 in the middle section of Table 3-2 show a possible connection to the sea water level. There are also examples of individual percussion-drilled boreholes where the different depth sections are classified differently, e.g. HFM02, and HFM15.

The results are in accordance with previous studies in Section 3.5, where the point water head of HFM18 was found most correlated to the variations in sea water level among the selected percussion boreholes in dataset A. The complementary datasets comprising shorter time series pointed out percussion boreholes showing even higher sea water level influence than HFM18.

All of the percussion-drilled boreholes with probable influence from sea water level variations are located in the north-western part of the candidate area. All boreholes located outside the tectonic lens in the south-western part show no influence.

3.5.7 Conclusions

The variations of the point water heads in the percussion-drilled boreholes show a complex pattern mainly connected to the annual water balance due to seasonal variations in rainfall/snowmelt and evapotranspiration. The fact that the sea water level covariates with the occurrence of low pressures with accompanying precipitation makes the correlations difficult to elucidate.

There is, however, point water heads that show a stronger correlation to the variations in sea water level than to variations in air pressure. This is especially evident in HFM02, HFM15, HFM20, HFM21 and HFM22. There is also a large group of boreholes showing intermediate (possible) influence from variations in the sea water level, of which HFM14 and HFM18 show strongest influence.

The spatial distribution of the influence-classification of the percussion-drilled boreholes is shown in Figure 3-33. The northern part of the area is dominated by boreholes with probable high influence from sea water level variations, whereas the inland part shows lower influence.

The very fast response to the storm event "Gudrun", most evident in the principal component analysis, may be an indication of a connection between e.g. HFM18 and the sea water level. Further analysis of similar extreme events could elucidate the status for the other boreholes where a high connectivity is suspected (e.g. HFM02, HFM15, HFM20, HFM21 and HFM22).

When the point water head time-series is separated by a statistical signal processing algorithm into independent "signals" (Independent Component Analysis, ICA), one of the extracted signals is clearly correlated to the sea water level. The correlation coefficient is 0.55 compared to 0.25 when the air pressure is correlated to this extracted signal. Concomitant minor transitions in the time series during the Gudrun storm may be an indication that the sea water level transitions are transferred into the percussion-drilled boreholes by a rather fast mechanism.

HFM_10 located close to KFM04 show to some extent a deviating variation pattern compared to most other percussion-drilled boreholes. This is most probably due to disturbances in, or in the vicinity of the borehole, indicating that this time-series still may contain anomalies from pumping activities.

3.6 Relationships between lake levels and groundwater levels

3.6.1 Vertical gradients between lake levels and wells in till below

Groundwater levels in the till below lake surfaces were measured where surface water levels were measured at Eckarfjärden, Gällsboträsket, Fiskarfjärden, Bolundsfjärden, and Lillfjärden, but not at Norra Bassängen. Elevations for surface water levels and groundwater levels below lakes are shown in Figure 3-34 for Eckarfjärden, Gällsboträsket, Fiskarfjärden, Bolundsfjärden, and Lillfjärden. Figure 3-35 shows the same data represented as level differentials, where positive values indicate upward gradients from groundwater to surface water, and negative values indicate downward gradients from surface water to groundwater. Level gradients were variable and typically small (a few centimetres) and often within uncertainties of the measurements (levelling and level measurements uncertainties), although Lillfjärden often had downward gradients of higher magnitude (10–30 cm), probably due to direct influence of the sea level. All lakes showed both upward and downward gradients. Some single peaks with large downwards gradients are caused by water sampling in the groundwater wells (see for example the time series from Bolundsfjärden), while some others are suspected measurement errors. Differentials in some lakes exhibited higher downward gradients during late summer and early autumn, such as Eckarfärden and Bolundsfjärden during summer 2003 (Figure 3-35a and d).

3.6.2 Gradients between lake levels and local groundwater wells

This section presents time series data for Eckarfjärden, Bolundsfjärden, and Fiskarfjärden, combining lake level data with data from local groundwater wells. There were insufficient data for similar compilations at the other lake locations. See maps in Figure 2-18 and Figure 2-27 for locations of groundwater wells in Quaternary deposits and bedrock, respectively.

Figure 3-36a shows the long-term time histories of wells in and near to Eckarfjärden compared with the lake water level. As would be expected, the lake water level (SFM0041) showed the smallest response amplitude, followed by the below water well (SFM0015). The lake water level appears to provide a buffering effect on groundwater level amplitudes close to the lake. This helps explain why the response amplitudes in SFM0014, 16, 17 and 18 were amongst the lowest reported for groundwater wells in Quaternary deposits (Figure 2-21). The three wells located in closest proximity to the lake shore (HFM0014, 16, and 18) all had periods (mostly in summer) when groundwater levels were below lake water level. These periods typically coincided with intervals when the groundwater level below the lake (SFM0015) was lower than the surface water level, therefore providing complementary evidence of select periods of groundwater recharge from the lake. The groundwater point water heads in the wells in

bedrock closest to the lake (HFM11.1 and HFM12) maintained well above the lake water level at all times, most often in the range of +1 to +1.5 m.

Figure 3-36b shows a close-up of the same Eckarfjärden data for summer 2003. Groundwater levels well below the lake water level are clearly evident at SFM0014, SFM0016, and SFM0018 during most of this interval, while the level in SFM0017 was consistently above the lake water level.

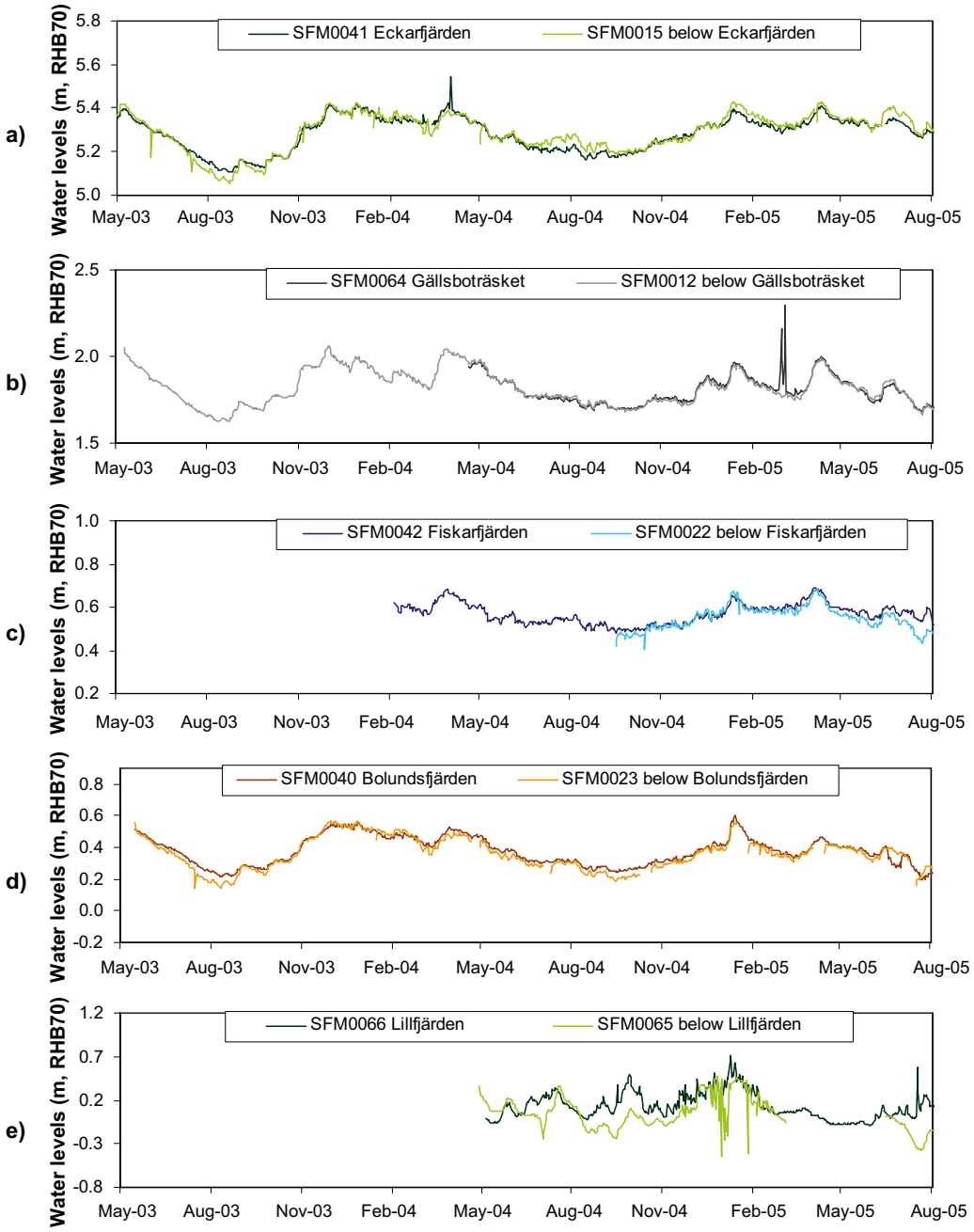

Figure 3-34. *Lake water levels and groundwater levels (m, RHB70) below the lakes for a) Eckarfjärden, b) Gällsboträsket, c) Fiskarfjärden, d) Bolundsfjärden, and e) Lillfjärden.*

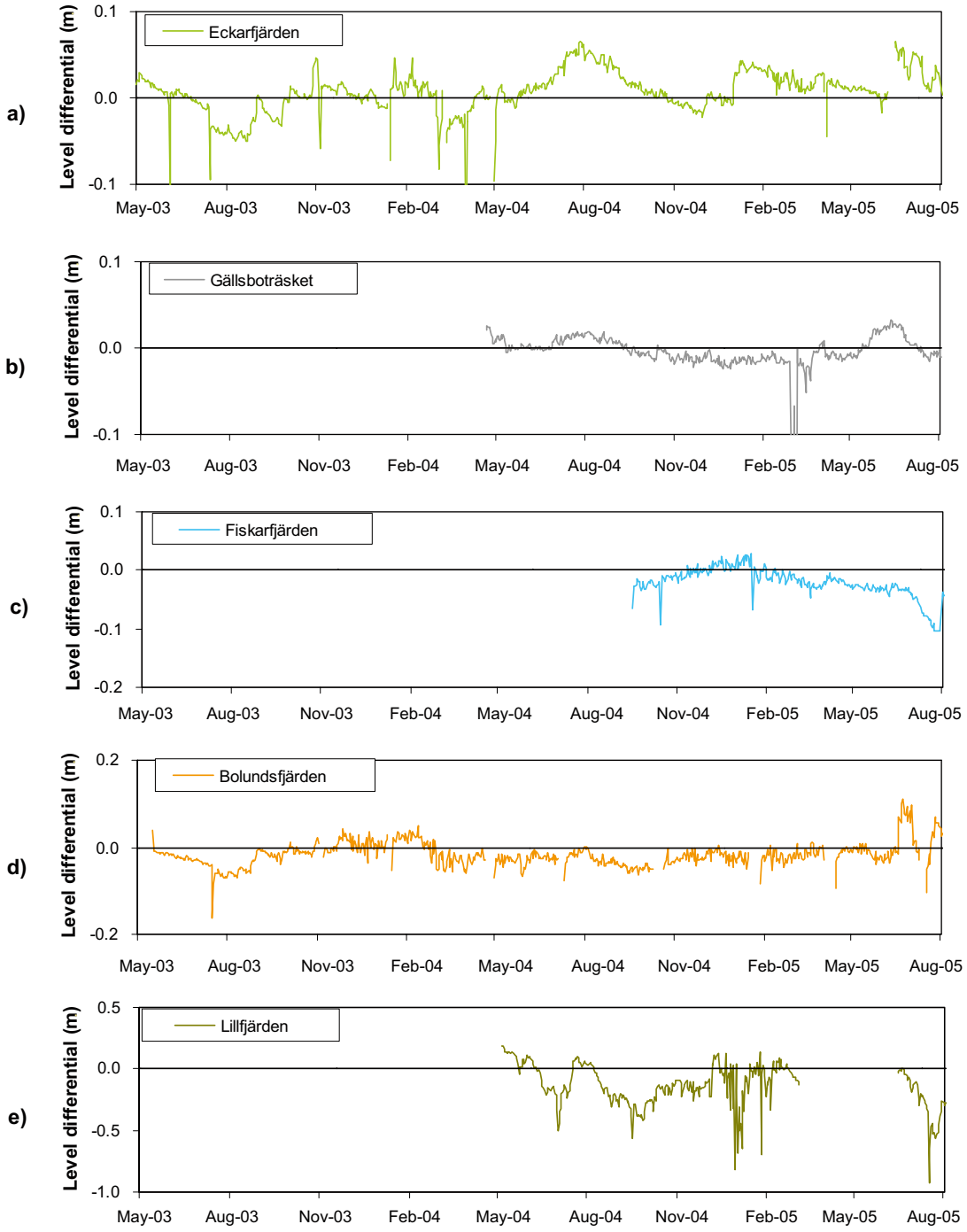

Figure 3-35. *Level differentials between surface water and below bottom wells in five lakes in the site investigation area. Negative differentials indicate downward gradients (groundwater recharge), while positive differentials indicate upward gradients (groundwater discharge).*

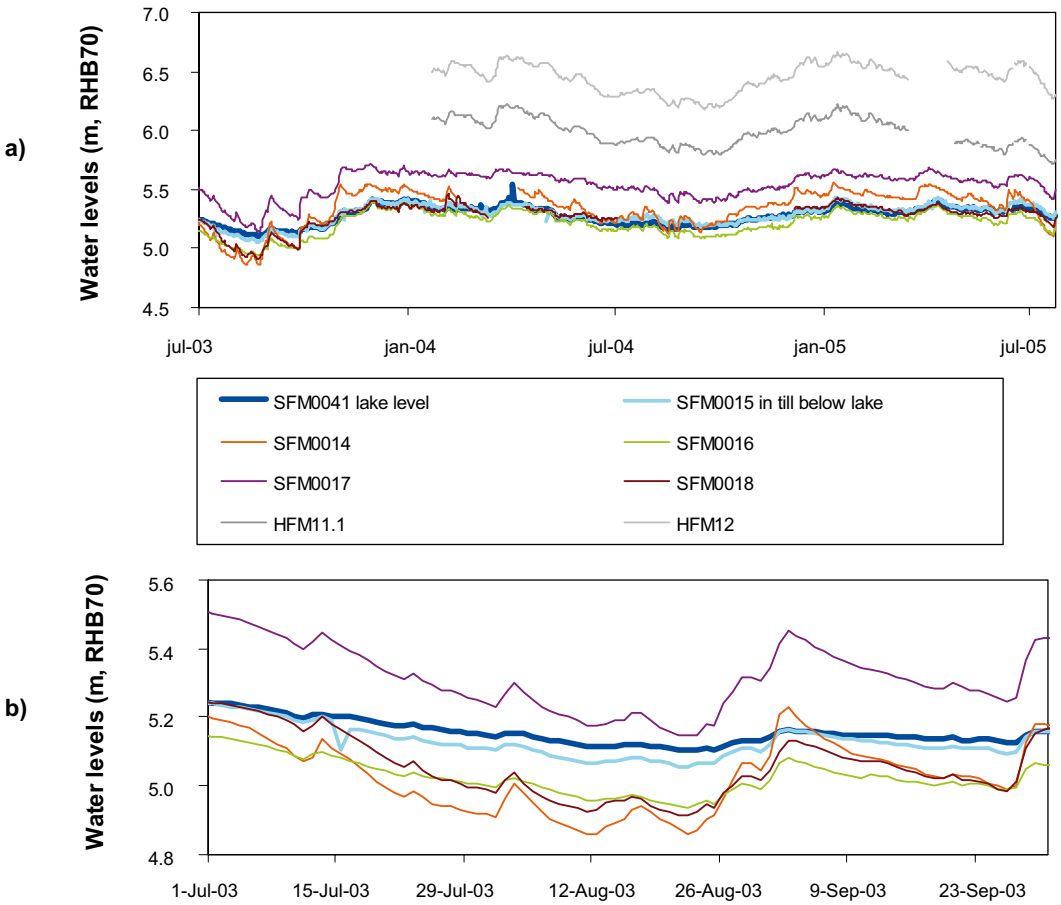

Figure 3-36. *Lake water level, groundwater levels in Quaternary deposits, and groundwater point water heads in bedrock from wells in and close to Eckarfjärden for a) July 2003 through July 2005, and b) close-up of summer 2003. The lake water level is represented by SFM0041, and SFM0015 is the well at the same location but in till below lake sediments. Data for bedrock groundwater were not available for the summer 2003 interval.*

Figure 3-37 shows similar data for wells in the vicinity of Bolundsfjärden. Once again, the higher lake surface elevations compared with local groundwater elevations in Quaternary deposits suggested that the lake acts as a source of groundwater recharge to the local aquifer during those periods. During other periods, the higher groundwater levels suggest the lake acts as a discharge area for the surrounding aquifer. As with the wells close to Eckarfjärden, SFM0033 (excluding the disturbance in May 2004) and SFM0034 had amongst the lowest reported response amplitudes in groundwater wells (Figure 2-21). However, SFM0030 which is located a little more than one hundred metres southwest of the lake had the highest reported amplitude of all wells. The very low groundwater level at this well during the summer 2003 indicated a strong influence on the groundwater level from evapotranspiration. Groundwater point water heads in nearby wells in the bedrock (HFM14 and 15) maintained heads above the lake level for all available data.

The lake water level of Fiskarfjärden (SFM0042) is shown in Figure 3-38 together with the groundwater level in till below the lake (SFM0022), and in a well in till below clay approximately 150 m southeast of the lake along the outlet brook (SFM0026). At SFM0026 the groundwater level is often well above the ground surface at 0.70 m RHB70.

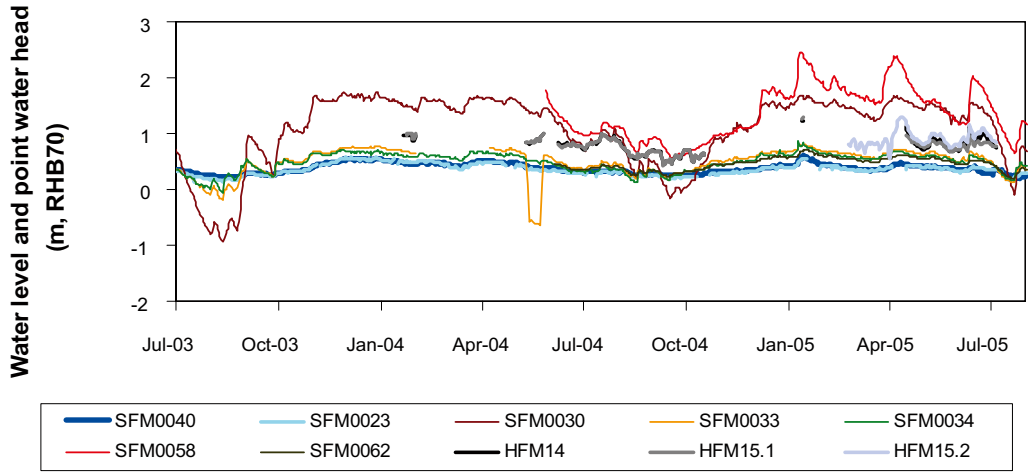

Figure 3-37. *Surface water level, groundwater levels in Quaternary deposits, and groundwater point water heads in bedrock from wells in and close to Bolundsfjärden. SFM0040 shows the lake water level, SFM0023 is the well in till below lake sediments in the middle of the lake, and SFM0062 is a well in till below lake sediments but close to the shore, see Figure 2-18.*

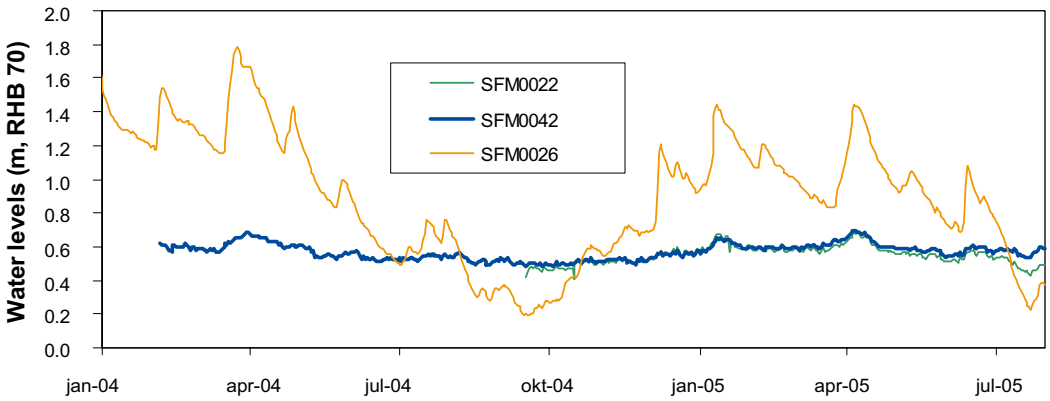

Figure 3-38. *Lake water level and groundwater levels in Quaternary deposits in wells close to Fiskarfjärden. SFM0042 shows the lake level, SFM0022 is the well in till below the lake, and SFM0026 is a well in till 150 m southeast of the lake along the outlet brook.*

3.7 Relationships between groundwater levels in the Quaternary deposits and point water heads in the bedrock

In general, the hydrological connections between groundwater in Quaternary deposits and groundwater in bedrock appear to be in a downward direction, with the influence of seasonal ET cycles and precipitation event responses in the soil producing a mirrored response at depth in the bedrock aquifers. However, there were also isolated observations of activities in the bedrock, such as pumping, producing small responses in the upper soil aquifers. In this section, relationships between soil and bedrock groundwater levels are examined by looking at wells in close proximity to one another at five of the Drill sites. One difficulty with comparisons at the Drill sites is that not all wells may be closely situated (sometimes only within a few hundred metres), and topographical variations of several metres exist between well sites. Therefore, plots are presented of both groundwater elevations and depths below surface for each Drill site and these should be interpreted together to assess vertical groundwater interactions. Another difficulty is the difference in groundwater salinity with depth, and thereby in density, which means that measured groundwater levels in percussion-drilled boreholes in the bedrock should be regarded as point water heads.

3.7.1 Drill site 1

Figure 3-39 shows a map of locations of groundwater wells in Quaternary deposits and bedrock in the vicinity of Drill site 1. The wells are located within 100–220 m of one another. Figure 3-40 shows the time series for groundwater levels and depths below surface for groundwater wells in Quaternary deposits (SFM) and for point water heads and depths below ground surface for the percussion-drilled wells (HFM). As stated above, ideally it would be preferable to have the wells in closer proximity (in the range of 20–30 m rather than 100–220 m) to provide a stronger basis for drawing conclusions about vertical interactions. Over larger distances, the effects of ground surface topography complicate the assessment. For instance, reported groundwater elevations at SFM0001 are indeed less than at HFM02.1 and HFM03.1 (deepest sections of the wells sealed off by packers) for part of the time series. However, the ground elevation at SFM0001 is approximately 2 m less than at either of the percussion well sites and it is situated more than 100 m away.

During undisturbed intervals in the bedrock time series, the time series for groundwater in the bedrock tends to follow the groundwater in the Quaternary deposits. This is particularly evident in comparing responses of HFM03.1 to SFM0001 in Figure 3-40a. However, the high amplitude disturbances in the deep bedrock produced no discernable artifacts in the groundwater in the Quaternary deposits.

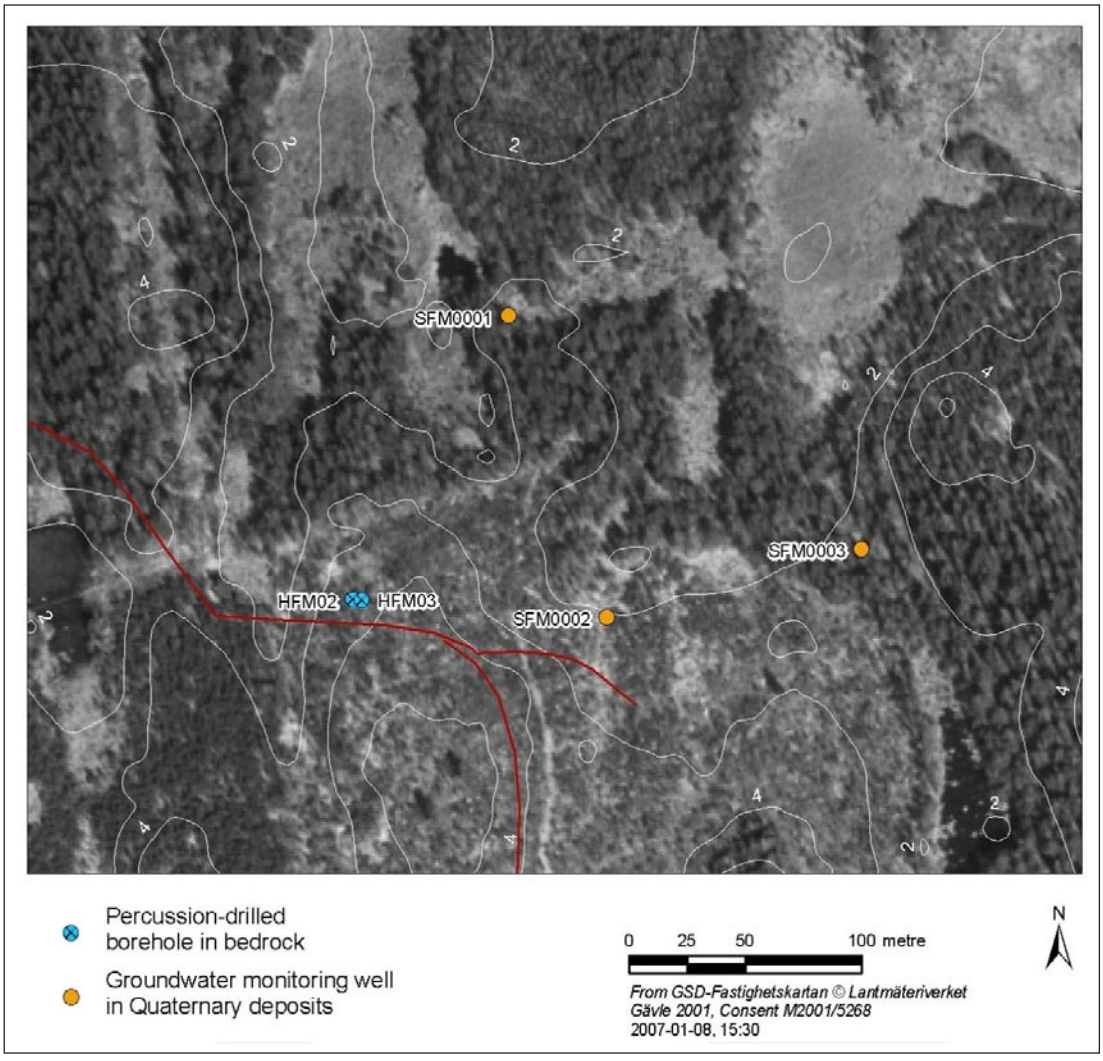

Figure 3-39. *Groundwater monitoring wells in Quaternary deposits (SFM) and percussion-drilled boreholes in bedrock (HFM) at Drill site 1.*

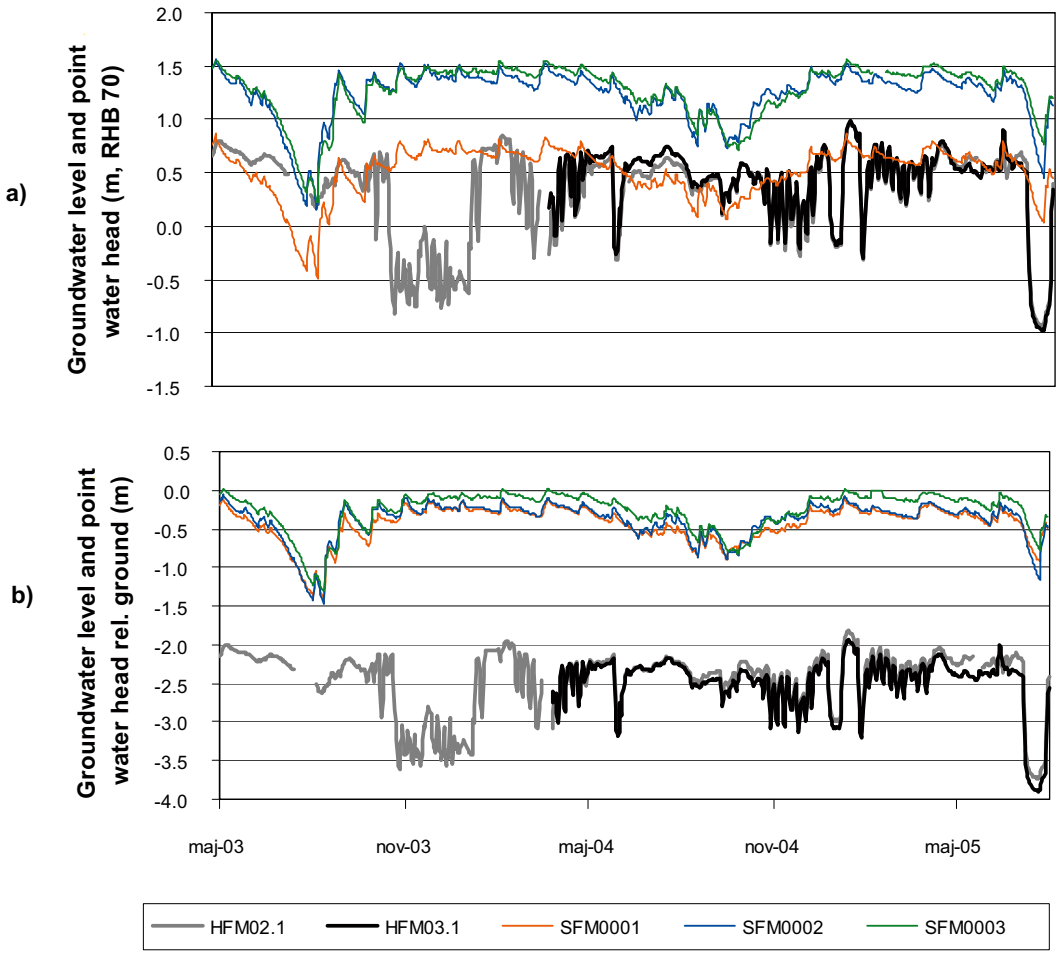

Figure 3-40. *Comparison of groundwater levels in wells in Quaternary deposits (SFM0001–3) and in bedrock (HFM02.1 and HFM03.1) at Drill site 1 in terms of a) metres above sea level and b) depth below ground surface. (Data from the deepest HFM-sections are shown because the deepest HFM2-section is longer in duration than data from the shallower sections. However, the head difference between sections is within a few centimetres.)*

Figure 3-41 shows a close-up of five months of the groundwater data that were plotted in Figure 3-40. In this plot, bedrock well data are plotted on an enlarged scale on the second Y-axis. Clearly, there is good correlation between time series of Quaternary deposit and bedrock wells over this interval, however, the amplitude of the deeper groundwater is diminished (less than half) in comparison to the upper levels. These data further reinforce the notion of a contact between near-surface and deeper groundwater, but perhaps only through low conductivity pathways.

Figure 3-42 shows a close-up of groundwater levels at Drill site 1 during the July 2005 pump test in HFM01. The drawdown response in the bedrock wells is clearly evident, but the response in the Quaternary deposits appears to be more related to dry conditions due to little rainfall during the prior month. When rainfall events occur in mid-July, the groundwater in the Quaternary deposits recovers while the response to the pump test is still evident in the bedrock wells.

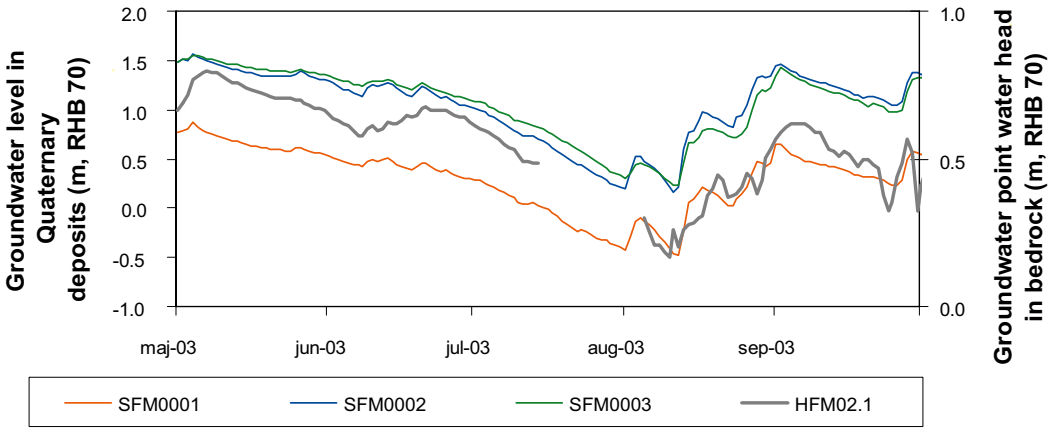

Figure 3-41. *Close-up view of groundwater levels for a five-month period at Drill site 1 with Quaternary deposit (SFM) and bedrock (HFM, deepest section) well data plotted on separate axes for greater resolution.*

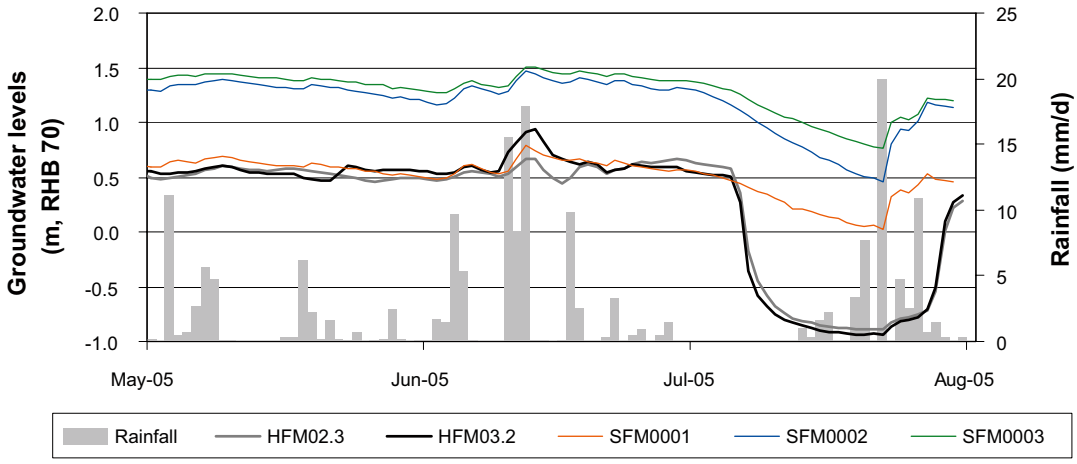

Figure 3-42. *Close-up of groundwater levels for a 3-month period at Drill site 1 during the July 2005 pump test in HFM01.*

3.7.2 Drill site 2

Figure 3-43 shows the locations of groundwater wells in Quaternary deposits and bedrock in the vicinity of Drill site 2. Here, the well in Quaternary deposits, SFM0004, is located close to the bedrock well HFM04 (24.4 m) while SFM0009 is separated by 360 m. Figure 3-44 shows time series for groundwater levels and depths below surface for groundwater wells in Quaternary deposits (SFM) and for point water heads and depths below surface for the percussion-drilled well. The data indicate a consistent downward gradient for groundwater flow in this region. Compared with the ground surface, the groundwater level in Quaternary deposits is about 2 m higher than the level in the bedrock. Furthermore, the groundwater time series in the bedrock were highly correlated to both the SFM0004 and SFM0009 time series (R^2 = 0.87 and 0.77, respectively), excluding the three disturbance intervals.

Interestingly, there was an observable response in the groundwater of the Quaternary deposits at this site during the disturbances intervals in bedrock groundwater. Figure 3-45 shows a close-up of the last disturbance interval in the HFM04 time series. The seven day cycles in groundwater levels oscillations from nearby pumping activities are clearly evident in the HFM04 time series, but they are also evident in SFM0004, the closest well in the Quaternary deposits.

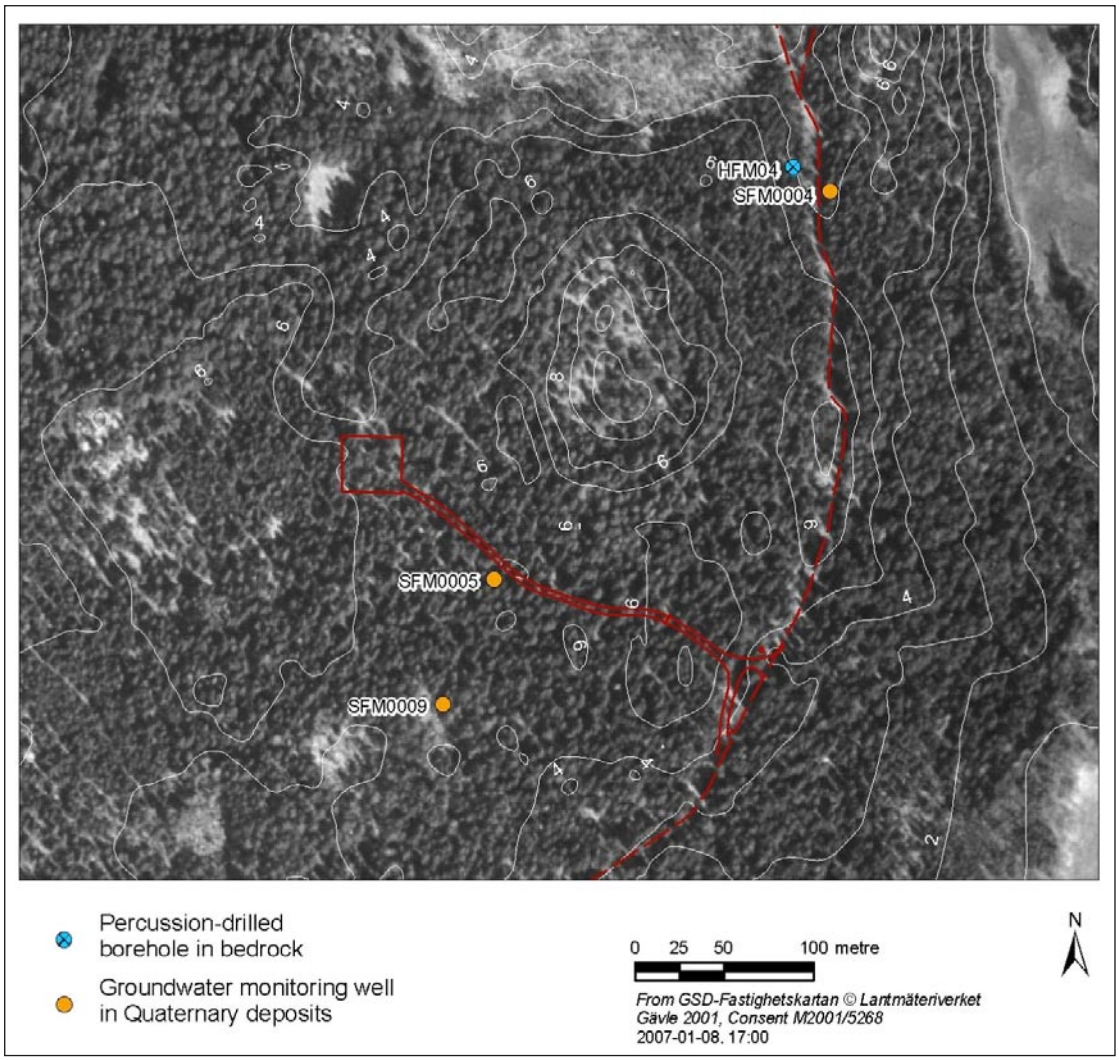

Figure 3-43. *Groundwater monitoring wells in Quaternary deposits (SFM) and percussion-drilled boreholes in bedrock (HFM) at Drill site 2.*

3.7.3 Drill site 3

Figure 3-46 shows the locations of groundwater wells in Quaternary deposits and bedrock in the vicinity of Drill site 3. Here, both SFM0006 and SFM0008 are separated by over 275 m from either bedrock well. Figure 3-47 shows time series for groundwater levels and depths below surface for groundwater wells in Quaternary deposits (SFM) and for point water heads and depths below surface for the percussion-drilled wells (HFM). The HFM07 and SFM0008 time series were well correlated ($R^2 = 0.71$), although the groundwater levels in the Quaternary deposits were approximately 2 m below the distant bedrock observations. Note that both ET-related cycles and precipitation event responses are evident in the groundwater in bedrock time series.

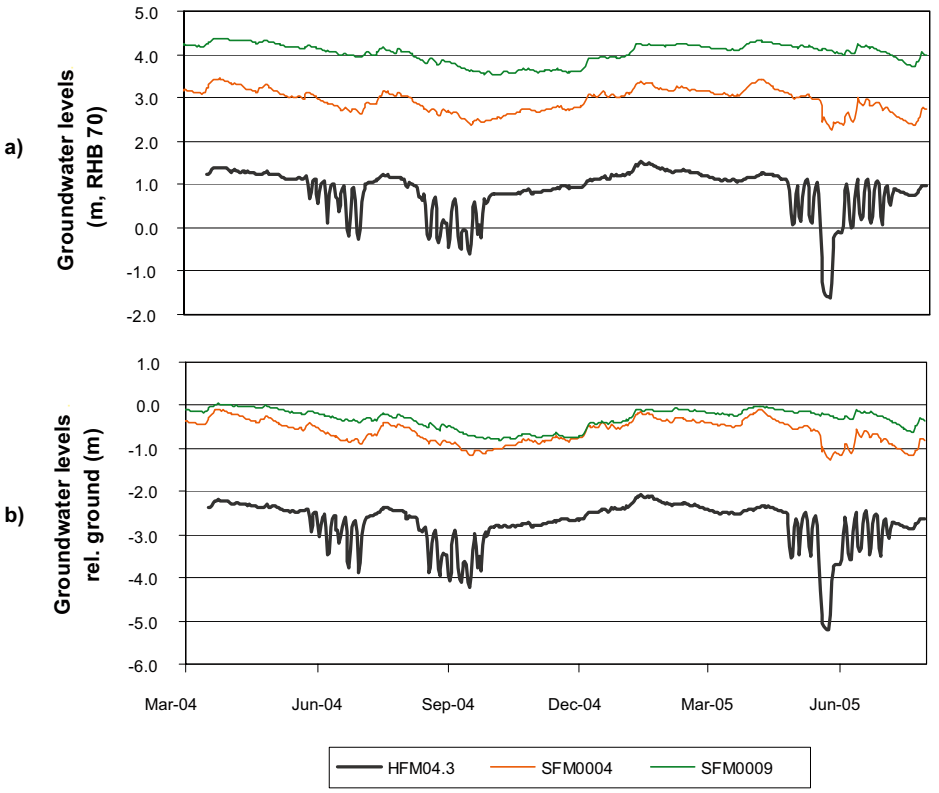

Figure 3-44. *Comparison of groundwater levels in Quaternary deposits (SFM) and point water heads in bedrock (HFM, uppermost section) at Drill site 2 in terms of a) metres above sea level and b) depth below ground surface.*

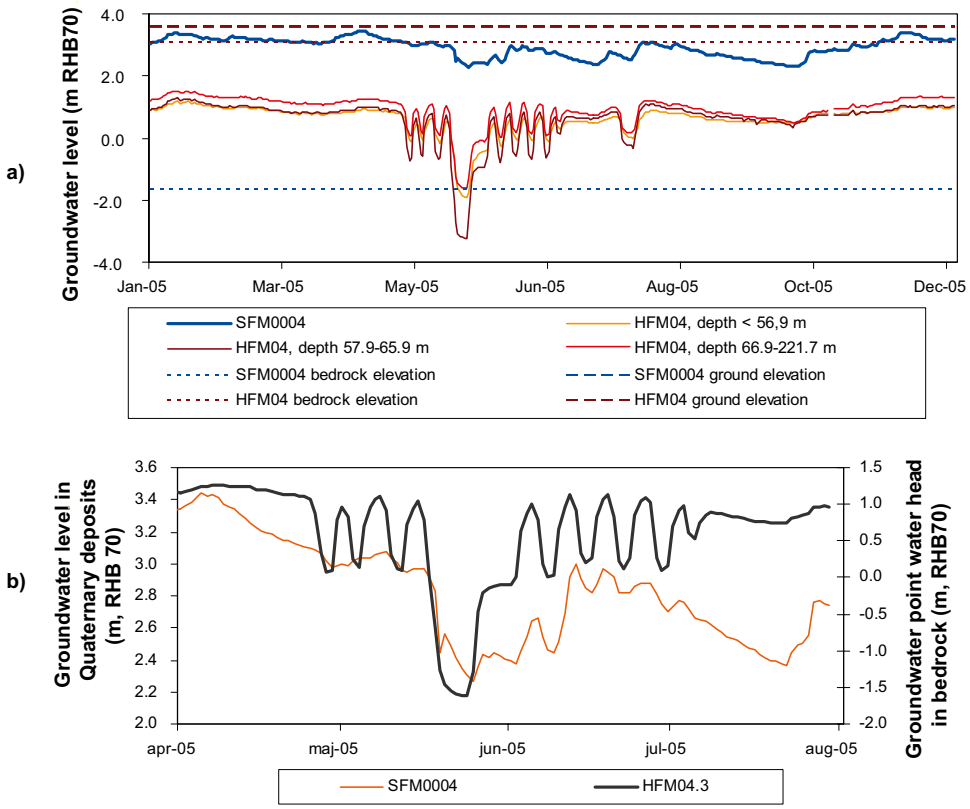

Figure 3-45. *Two close-up views of groundwater elevations for a 3-month period at Drill site 2 with Quaternary deposits (SFM) and bedrock (HFM, shallowest section) well data plotted on separate axes for greater resolution.*

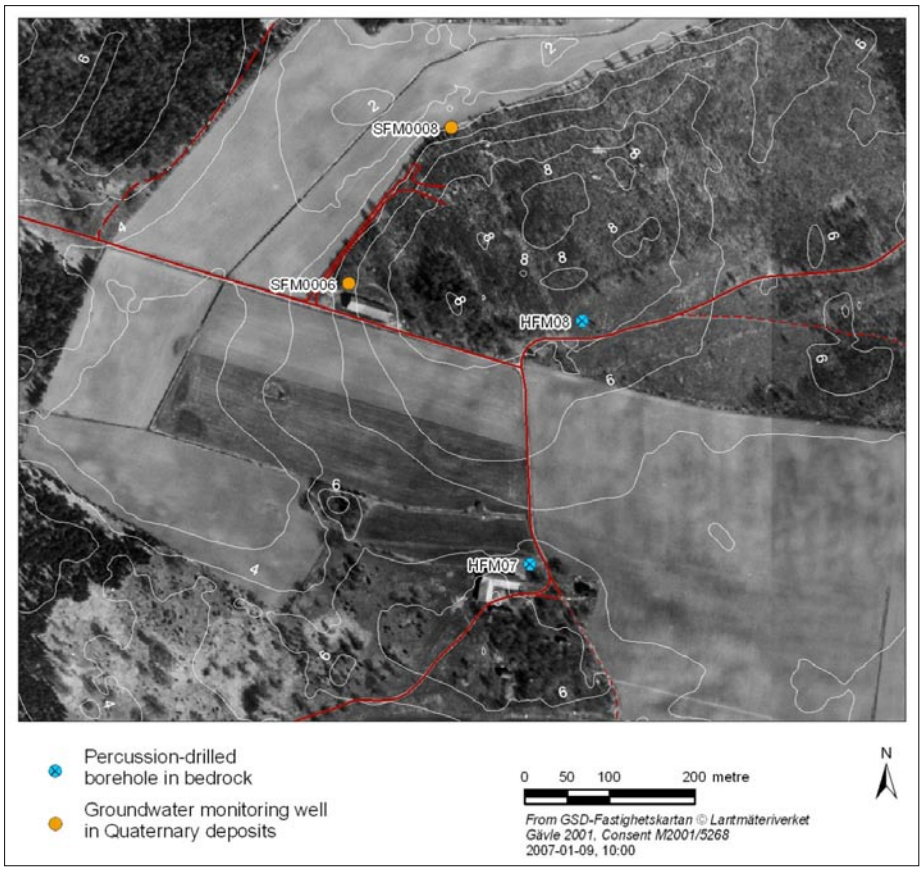

Figure 3-46. *Groundwater monitoring wells in Quaternary deposits (SFM) and percussion-drilled boreholes in bedrock (HFM) at Drill site 3.*

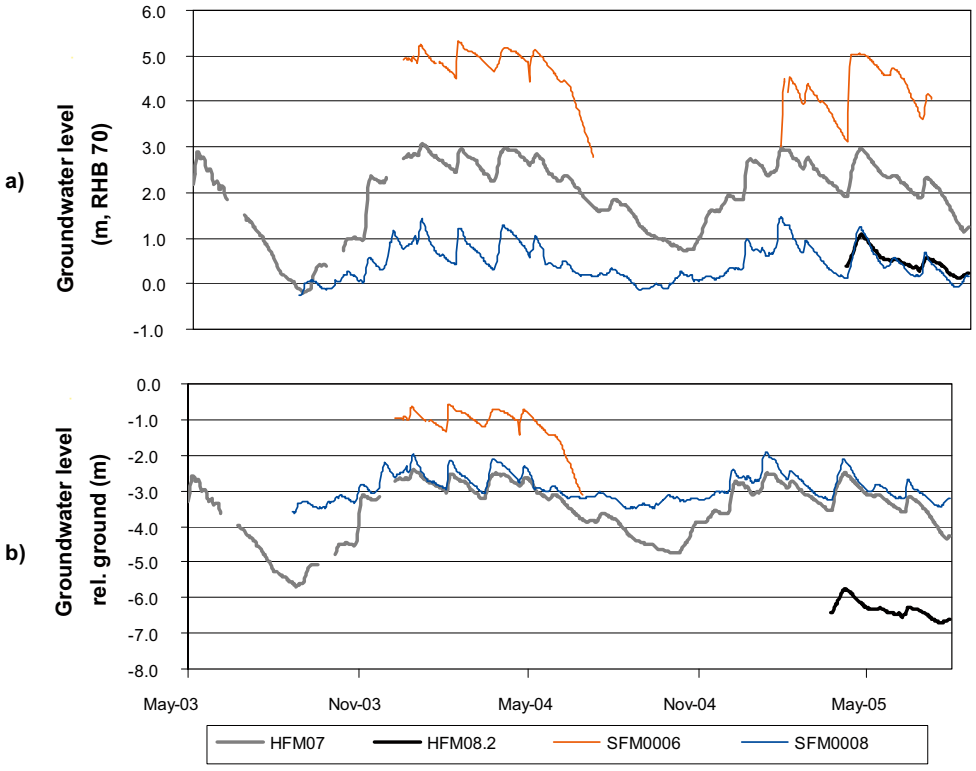

Figure 3-47. *Comparison of Quaternary deposit (SFM) and bedrock (HFM) groundwater level data at Drill site 3 in terms of a) metres above sea level and b) depth below ground.*

3.7.4 Drill site 4

Figure 3-48 shows the locations of groundwater wells in Quaternary deposits and bedrock in the vicinity of Drill site 4. These wells are also physically separated by 117–445 m. Figure 3-49 shows time series for groundwater elevations and depths below ground for groundwater wells in Quaternary deposits (SFM) and for point water heads and depths below ground for the percussion-drilled wells (HFM). Here the groundwater levels in the SFM0011 and SFM0013 are considerably lower than in the bedrock wells. These SFM-wells are situated in the topographical depression hosting Gällsboträsket. On the other hand, in SFM0057 the groundwater level is above the levels in the bedrocks well all the time. Correlations were high between Quaternary deposit and bedrock groundwater time series during undisturbed periods (R^2 = 0.56–0.92). However, this seemed largely due to ET related cycles, as the bedrock well data at Drill site 4 did not exhibit any of the short-term response similarities that were observed at Drill sites 1 and 3 (see Figure 3-40 and Figure 3-47).

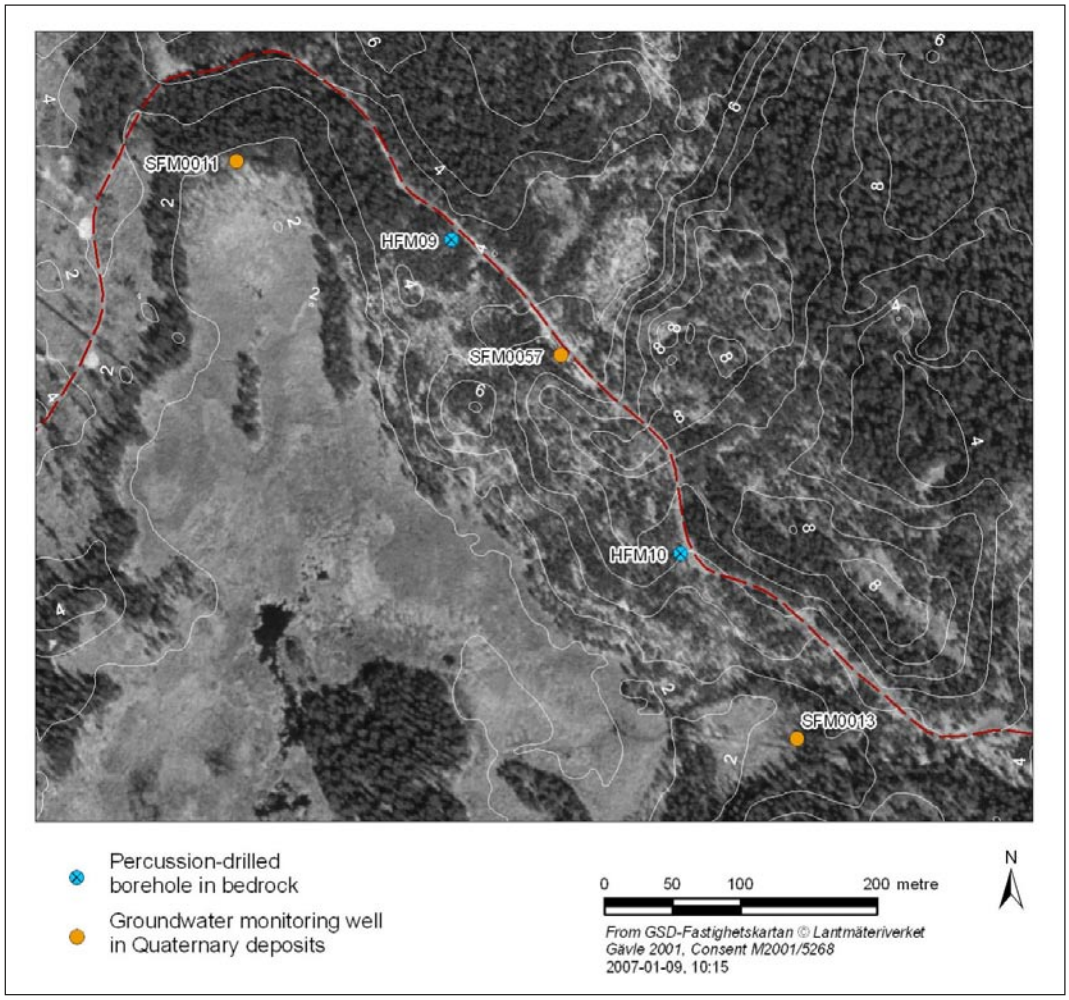

Figure 3-48. *Groundwater monitoring wells in Quaternary deposits (SFM) and percussion-drilled boreholes in bedrock (HFM) at Drill site 4.*

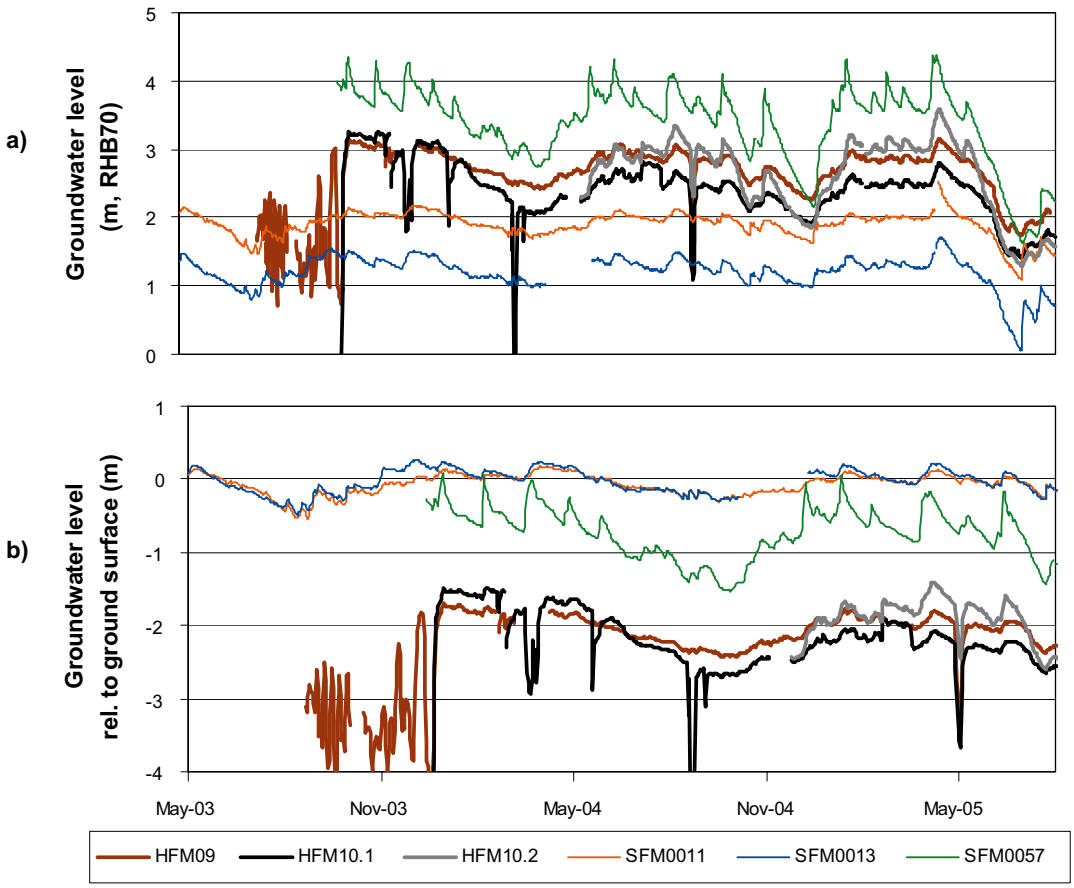

Figure 3-49. *Comparison of Quaternary deposit (SFM) and bedrock (HFM groundwater level data at Drill site 4 in terms of a) metres above sea level and b) depth below ground. Data for the lowermost section in HFM10 are shown because it is longer in duration than the uppermost section.*

3.7.5 Drill site 6

Figure 3-50 shows the locations of groundwater wells in Quaternary deposits and bedrock in the vicinity of Drill site 6. These two wells are located within 31 metres of one another. Figure 3-51 shows time series for groundwater level and depth below ground for the groundwater well in Quaternary deposits (SFM) and for point water head and depth below ground for the percussion-drilled well (HFM). The data indicated a downward direction for groundwater flow in this region. However, there did now appear to be strong evidence of coupling between Quaternary deposit and bedrock groundwater in this region, as the two time series appeared fairly independent.

3.8 Relationships in point water heads in the bedrock during disturbance intervals

The percussion-drilled wells inside the candidate area, denominated HFM01 to HFM22, show a large heterogeneity in terms of water yielding capacity and connectivity. Many of these wells intersect highly transmissive fractures of great aperture and assumed lateral extension but there are also a number of boreholes with little or no transmissivity. To establish the magnitude of connectivity between boreholes, responses to disturbances in the form of pumpings were determined for a few time periods. During the chosen time periods only a single source of disturbance occurred in the area.

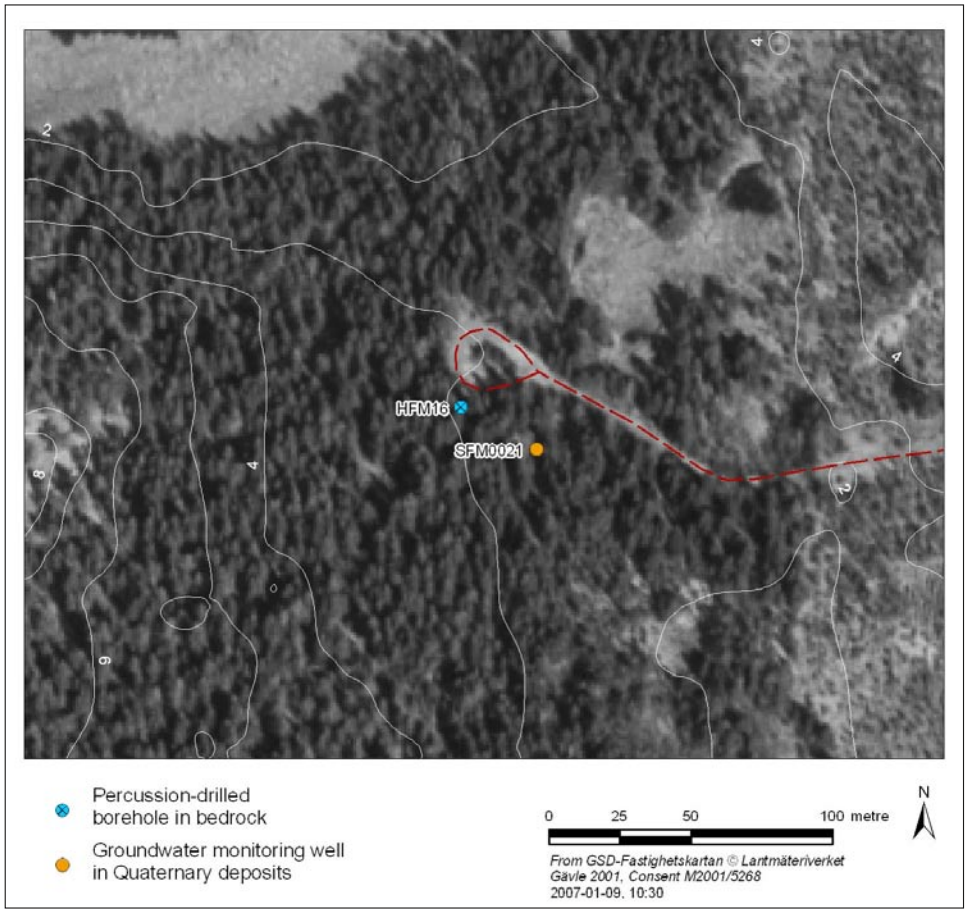

Figure 3-50. *Groundwater monitoring wells in Quaternary deposits (SFM) and percussion-drilled boreholes in bedrock (HFM) at Drill site 6.*

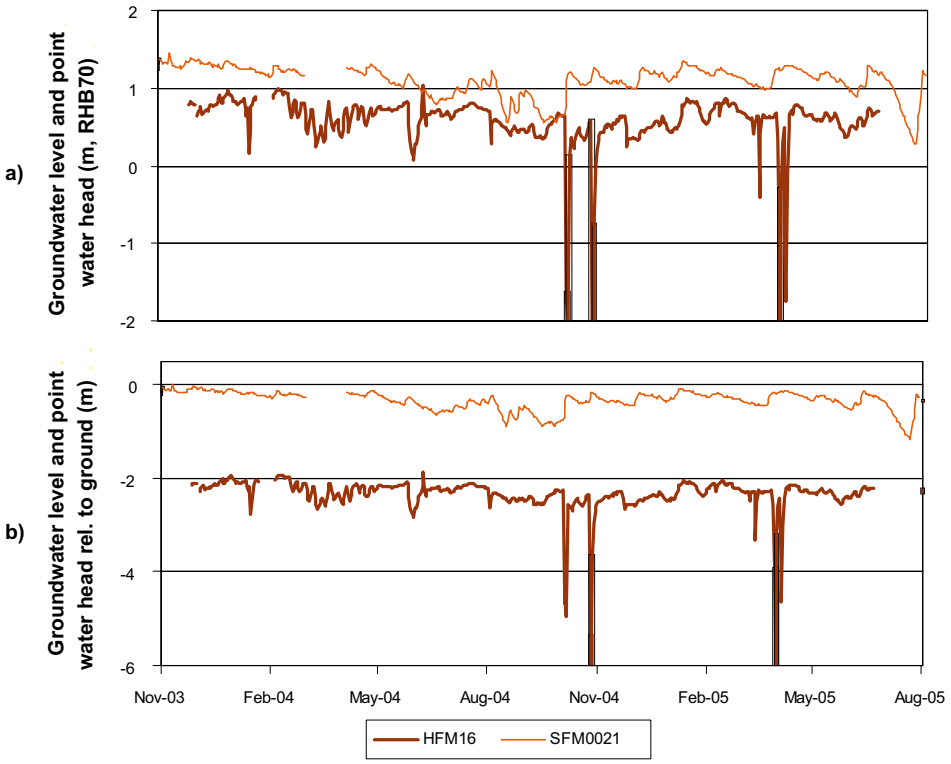

Figure 3-51. *Comparison of Quaternary deposit (SFM) and bedrock (HFM) groundwater level data at Drill site 6 in terms of a) metres above sea level and b) depth below ground.*

The three chosen time periods, spread out over the year, are a pumping period in HFM13 in April 2004, a rinse pumping in KFM07A in December 2004, and a long-term pumping test in HFM01 in July 2005 /Gokall-Norman et al. 2005/.

Simple response ratios, defined as the ratio between the drawdown at the monitoring wells and the pumping well (or a well in the immediate vicinity of the pumping well), are displayed in Figures 3-52, 3-53 and 3-54.

During four days in April 2004 pumping activities occurred in HFM13. The response ratios of the surrounding boreholes are displayed in Figure 3-52. It should be noted that not all drawdown are likely to origin from the disturbance in HFM13. At boreholes far from HFM13 natural trends are the likely cause to small declines in point water heads.

In December 2004 a rinse pumping were performed during one week in the long core- drilled borehole KFM07A. Borehole HFM21 is closely situated and the drawdown in this borehole is used as "source of disturbance" to calculate response rations, see Figure 3-53. It should again be noted that the groundwater level declines in distant wells are likely due to natural trends and not responses from pumping in KFM07A.

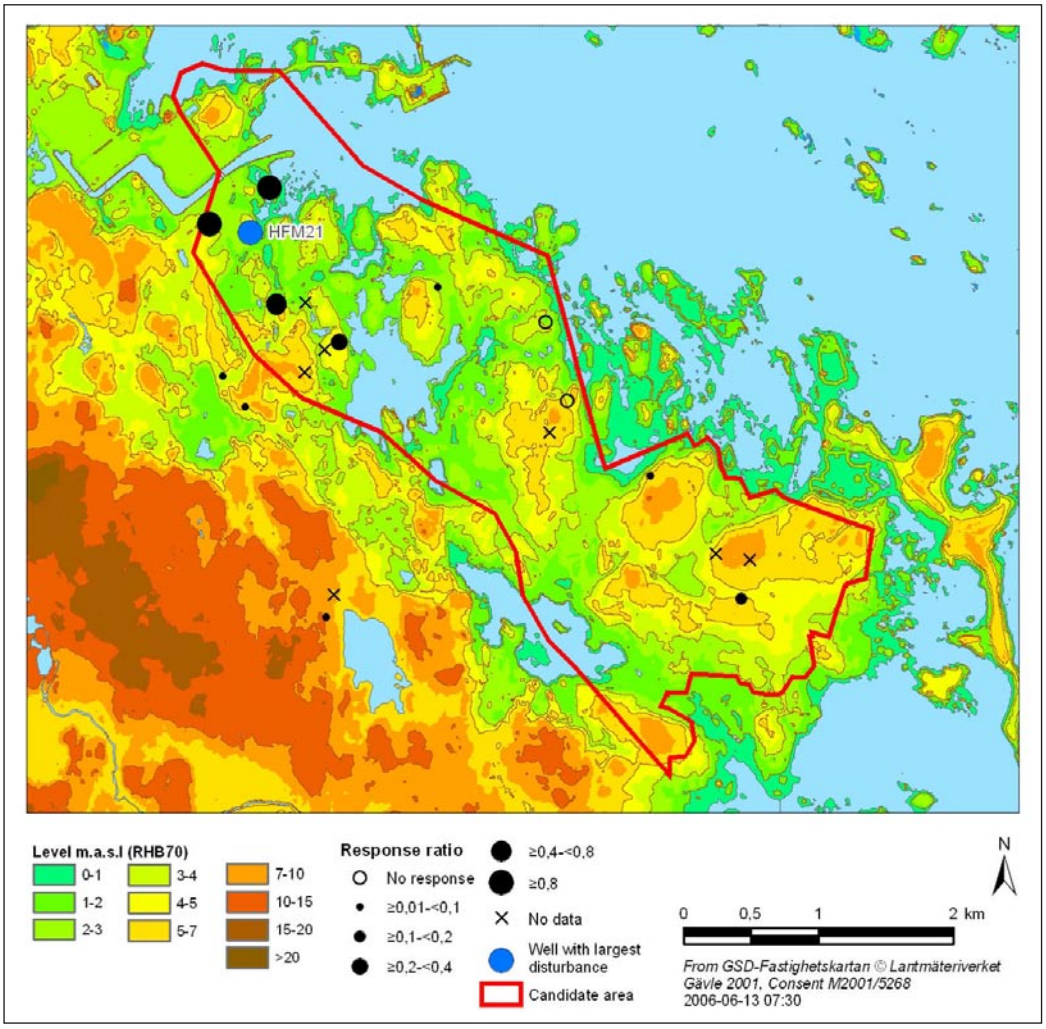

Figure 3-52. *Response ratios during pumping activities in HFM13 in April 2004.*

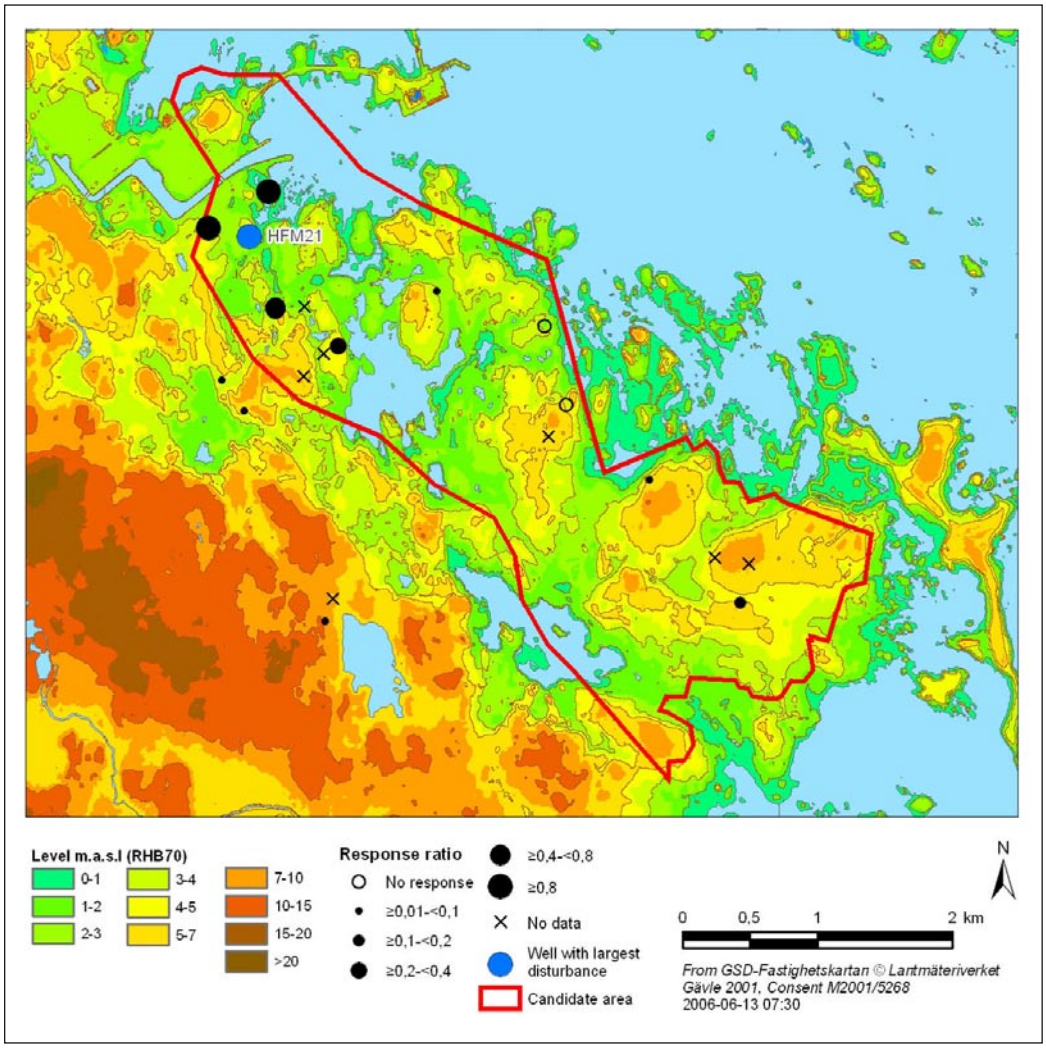

Figure 3-53. *Response ratios during pumping in KFM07A, situated about 40 m from HFM21. The drawdown in HFM21 is used disturbance source in the response ratio calculations.*

During July 2005 an approximately three weeks long pumping test was conducted in HFM01. A drawdown of 25 m was obtained in the borehole. To enable identification of differences in responses, the response ratios of the surrounding boreholes shown in Figure 3-54, are normalized to the drawdown in the closest observation borehole HFM02 where the drawdown was 1.5 m. During the summer strong trends of decreasing point water heads occurred and therefore most monitored wells showed apparent detectable response ratios. However, the drawdowns are larger and clearly coupled to the pumping in the wells in the northwestern part of the candidate area.

The relationship between the disturbance in the bedrock groundwater and the groundwater level in the Quaternary deposits are very weak in this data set. No obvious contacts are identified but during the long pumping test in HFM01 the decreasing level trends in the overlying Quaternary deposits are slightly altering, this is however also the case for a number of observation wells further away from HFM01. To be able to monitor this type of connection it is likely to be of great importance to place the observation wells in the Quaternary deposit close to the appearance of conductive bedrock fractures.

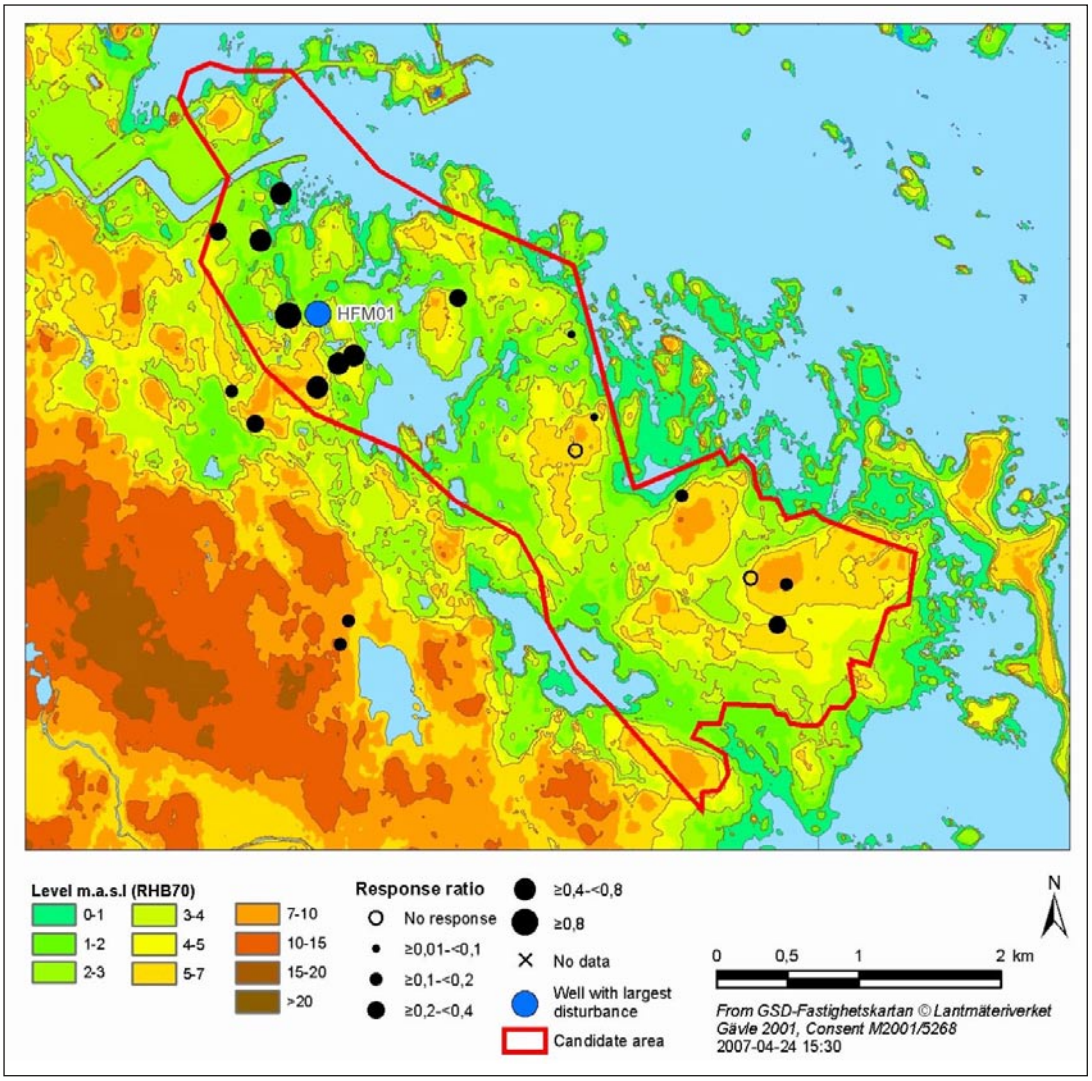

Figure 3-54. *Response ratios during disturbance in HFM01. To enable identification of differences in responses, the drawdown in the closest well (HFM02, 1.5 m) is used as a base for the response ratio calculations.*

3.9 Relationships between surface discharge and groundwater levels in the Quaternary deposits

Well-defined relationships were identified between specific discharge magnitudes and the dynamic groundwater storage in upstream catchment areas. Figure 3-55 shows cross-plots of daily average specific discharge versus daily average groundwater levels in the upstream catchment for four catchment areas in the site investigation area.

Table 3-3 summarises the groundwater wells that were used for estimating "catchment-averaged" groundwater levels. Recall that the catchment area for PFM005764 contains the three other catchments, which are in series from a surface discharge perspective, see Figure 2-34. Recall also that there were approximately 16-months of available data for the PFM005764 catchment area as a whole, compared to only approximately seven months of data for the three contained sub-catchments. The X-axes in Figure 3-55 represent the catchment-averaged groundwater depths in Quaternary deposits, and were estimated as the daily average of the indicated groundwater time series (Table 3-3) within that particular catchment area.

Table 3-3. Summary of wells used for estimating catchment-average groundwater levels.

Catchment area	Groundwater wells contained within catchment area
PFM005764	SFM0010, SFM0011, SFM0013, SFM0014, SFM0017, SFM0019, SFM0030, SFM0057
PFM005764-PFM002667	SFM0010, SFM0011, SFM0013, SFM0030, SFM0057
PFM002667-PFM002668	SFM0019
PFM002668	SFM0014, SFM0017

The four discharge-groundwater level curves in Figure 3-55 exhibited similar overall patterns. In all cases, the shape of the relationships was approximately exponential, high upstream groundwater tended to result in higher catchment discharge, and discharge approached zero below groundwater levels that may be thought of as a "dead zone" in terms of catchment contributions to discharge. The relationships for the catchment areas of PFM005764 and PFM005764-PFM002667 were quite similar, which is sensible since they share the same downstream discharge station. In general, it appeared that the "dead zone" depth decreased in each upstream sub-catchment (PFM005764-PFM002667 was deeper than PFM002667-PFM002668, which was in turn deeper than PFM002668). Responses for PFM005764, PFM005764-PFM002667, and PFM002668 exhibited hysteresis in peak flow values relative to average groundwater levels. Typically, the lower values in the "loops" evident in Figure 3-55a, b, c and d corresponded to the rising limbs of peak events in the response hydrographs, suggesting storage and transport delays in the stream responses relative to groundwater levels.

The averaged data from PFM002668, which contained Eckarfjärden, had the shallowest range of groundwater depths and the steepest slope in the discharge-groundwater relationship (Figure 3-55). These characteristics in the data are due to the close proximity of the wells in this sub-basin to the lake shore (both of the wells used to create the catchment-averaged values were within 10-m of open water). Groundwater levels in these wells closely follow lake levels (Figure 3-36). Therefore, the average of these wells is more representative of local conditions in the vicinity of Eckarfjärden as opposed to a "catchment-average" response. Of course, the other catchment-averaged data may also exhibit regional biases, but this was most evident in the PFM002668 groundwater data.

To further investigate these discharge relationships, a conceptual groundwater storage-discharge model was developed. The model structure and key equations are shown in Figure 3-56. The model used an exponential function to define a soil porosity profile, which was in turn integrated on a daily basis to approximate the volume of saturated groundwater stored above a saturated storage "dead zone". The model hypothesized that daily average specific discharge was a power function of this "active" saturated storage, using a relationship similar to that found in some versions of the SMHI HBV model /Lindström et al. 1997/.

The soil porosity equation was derived from measured field data /Lundin et al. 2005/. Please refer to Appendix 3 for a more detailed discussion of the pertinent data and the porosity profile equation. However, the equation had three variables that defined its shape: the soil porosity at the surface ($\rho_{surface}$), the ratio of the surface porosity to an asymptotic porosity at depth (k_4), and an exponent that defined the shape of the profile between these endpoints (k_3). The available field data provided a basis for assuming that two of these parameters, k_3 and k_4, were constant across the study site, while the third, $\rho_{surface}$, was an important site specific parameter.

In total, there were four calibration parameters: k_1 and k_2 from the discharge equation, $\rho_{surface}$ that defined the porosity profile equation, and the depth of the discharge "dead" zone. However, in practice, it was found that the exponent in the discharge equation (k_2) could be fixed to $k_2 = 3.0$ in all calibrations with no influence on the net quality of calibration. The two other parameters from the porosity profile equation, k_3 and k_4 were calibrated separately to the available soil profile field data (see again Appendix 3). Parameters were estimated with the Solver algorithm in Microsoft Excel to minimize a sum of squared errors criteria.

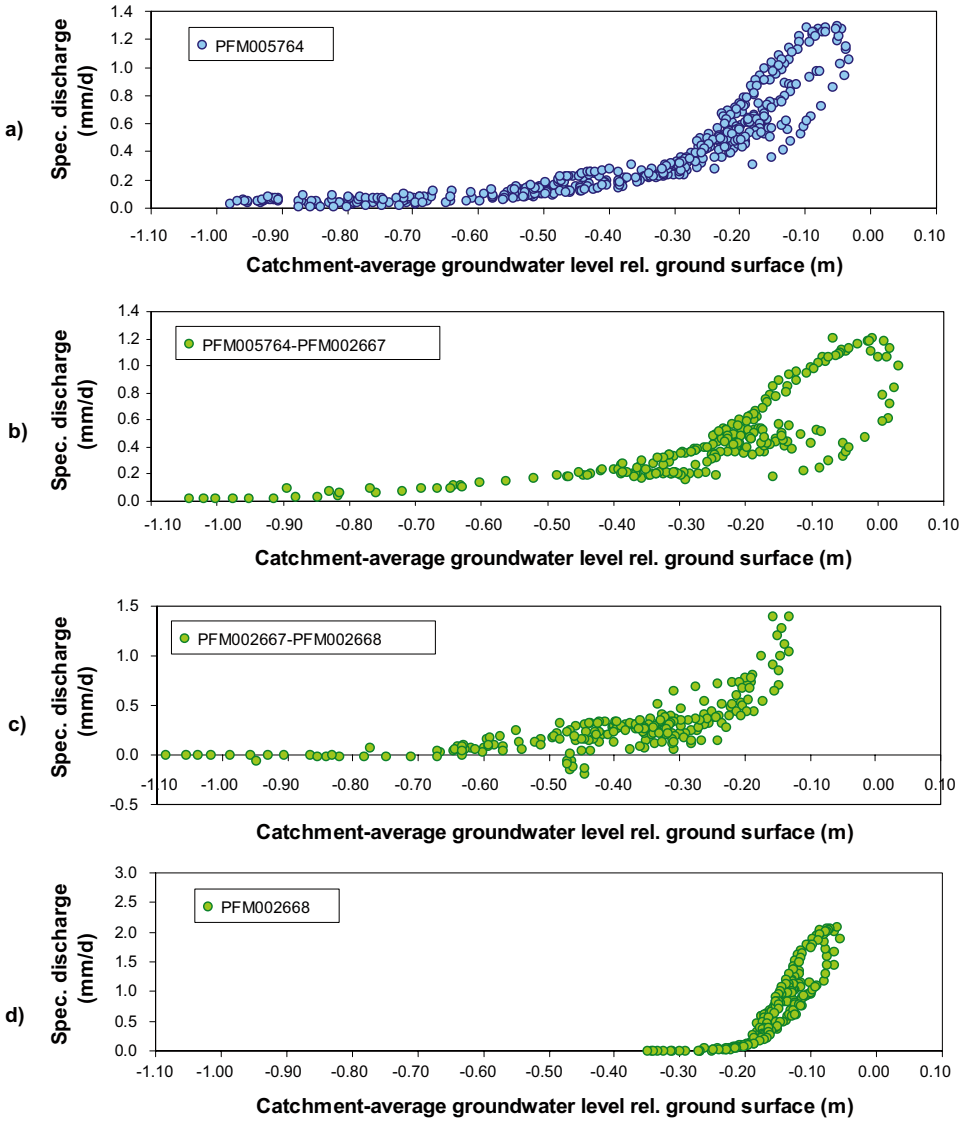

Figure 3-55. *Relationships between specific discharge and groundwater depths below surface in Quaternary deposits for four catchment areas in the site investigation area. Note that the catchment area for PFM005764 (a) is comprised of the sum of the three other sub-catchments (b, c, and d). Note also that the X-axis is similar in all four graphs, but the Y-axes have different scales.*

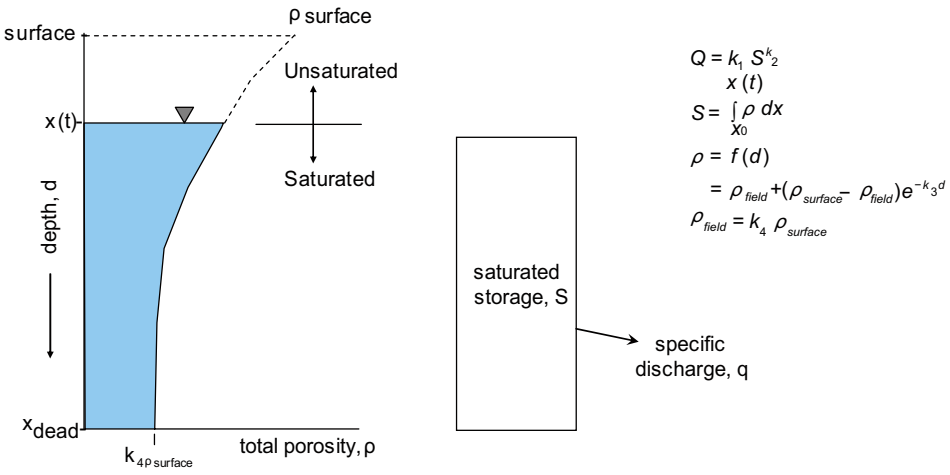

Figure 3-56. *Conceptual model and equations to simulate the relationship between groundwater storage in the Quaternary deposits and surface water discharge.*

Table 3-4 summarises the calibration results and Figure 3-57 shows the simulated and measured time series. The range of values for predicted soil porosities at the ground surface seemed reasonable for the PFM005764, PFM005764-PFM002268, and PFM002667-PFM002668 sub-basins ($p_{surface}$ = 0.33–0.45), and were understandable for the PFM002668 data ($p_{surface}$ =0.60) considering that the modeled response includes the influence of the lake (see discussion above for Figure 3-55). The values for the dead zone depths closely matched values that could be estimated from the depth-discharge plots in Figure 3-55. It is important to note that these parameter values are not unique solutions to model calibration. In practice, there were many parameter sets that provided very similar fit to the data. For instance, equally good solutions were found for the PFM005764 catchment data with surface porosity values in the range of 0.20 to 0.45 (with different k_1 values to compensate), and that was typical for all sub-basins considered. A sensitivity and/or uncertainty study was beyond the scope of this effort. Therefore, the parameter values in Table 3-4 should be thought of as "representative" rather than "optimal".

In general, the time series comparisons in Figure 3-57 were good, with the longer time series (PFM005764) providing the best overall fit. For the PFM005764, PFM005764-PFM002667, and PFM002668 basins, simulated peak discharges tended to lead observed peak discharge by several days. This could be expected since the storage or transport delays that were discussed above in relation to Figure 3-55 were not modeled. However, in general the uniformly good results from this relatively simple model provide a substantial link between three independent data sets: groundwater level time series in Quaternary deposits, surface discharge time series, and soil porosity profiles.

3.10 Hydrological modelling of discharge and groundwater responses in Quaternary deposits

The storage-discharge model of the previous section was expanded to also include simulation of processes in the unsaturated zone. A conceptual one-dimensional hydrological model was developed to explore an integrated understanding of surface hydrology in the site investigation area. The model used precipitation, potential evapotranspiration, and temperature time series as data inputs and simulated groundwater level and surface discharge as model output. The model was calibrated to the same catchment areas that were examined with the groundwater storage-discharge model in the previous section. To the extent that the model was successful, it provided a conceptual integration of four independent data sets included meteorological data, groundwater level time series in Quaternary deposits, surface discharge time series, and soil porosity and soil water retention profiles.

Table 3-4. Summary of calibration parameters and results for the groundwater storage-discharge model.

Parameter	Description	Parameter values			
		PFM005764	PFM005764-PFM002667	PFM002667-PFM002668	PFM002668
$\rho_{surface}$	Soil porosity at the ground surface	0.35	0.35	0.45	0.60
k_1	Scalar in discharge equation	116	41	108	179
k_2	Exponent in discharge equation	3.0	3.0	3.0	3.0
d_{dead}	Groundwater rel. ground that produces no discharge	–0.96	–1.20	–0.79	–0.36
R^2	Coefficient of determination for goodness of fit.	0.88	0.69	0.74	0.73

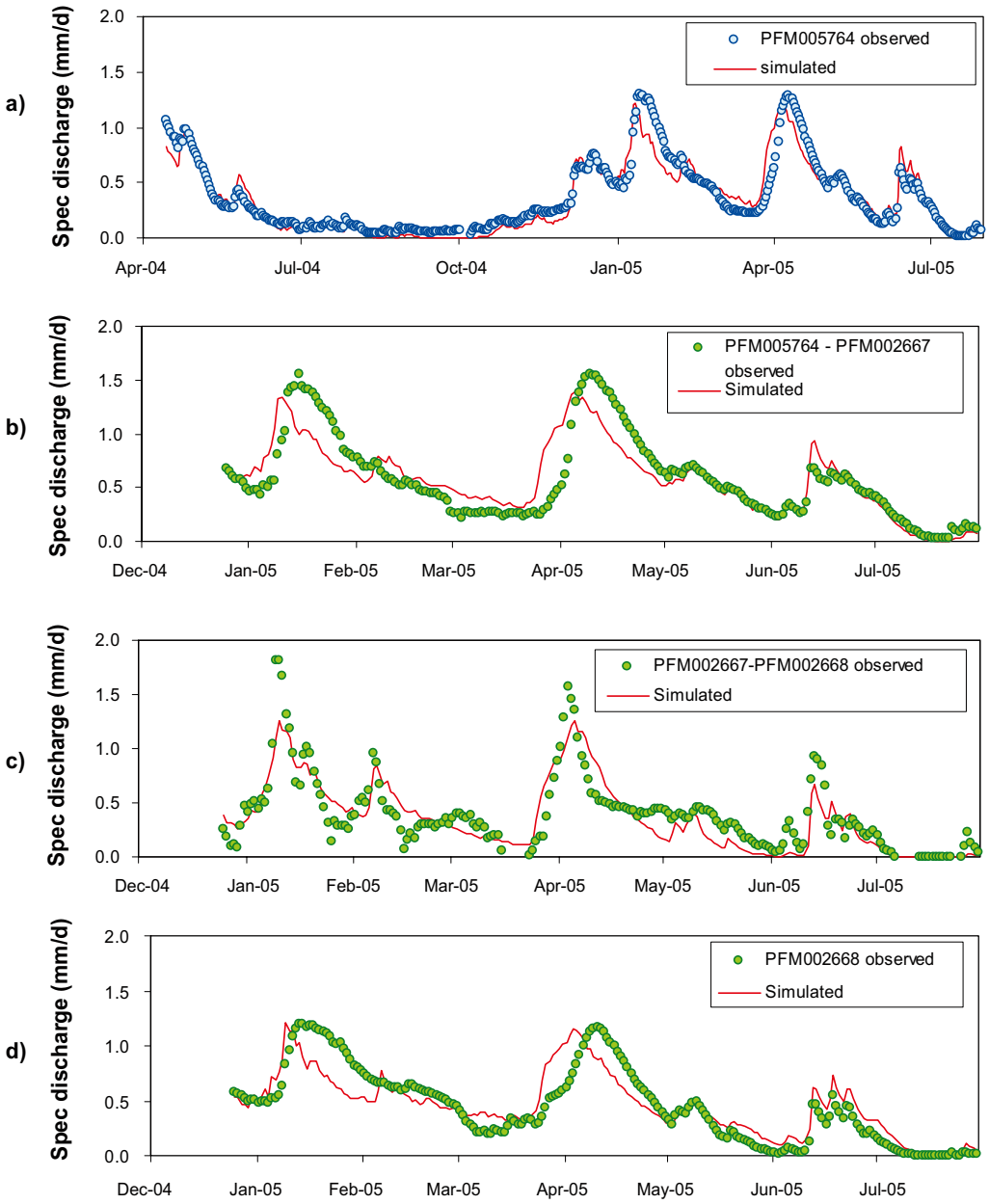

Figure 3-57. *Comparison of measured and simulated surface water discharge from catchment areas for a) PFM005764, b) PFM005746-PFM002667, c) PFM002667-PFM002668, and d) PFM002668. Note the longer time scale in a) compared to b), c), and d).*

3.10.1 Model description

Figure 3-58 shows schematic diagrams of physical and conceptual aspects of the model. The model built upon the groundwater storage-discharge model described in Section 3.9, but included also modeling storage and fluxes in an unsaturated zone. Its overall structure was similar to the SMHI HBV-96 model (Lindström et al. 1997). However, there were several noteworthy deviations from the conventional HBV model structure. In the conventional HBV model formulation, the unsaturated storage is modeled with a fixed maximum storage capacity, and fluxes into and out of that storage (infiltration, capillary rise, evapotranspiration) depend on the current value of that storage relative to its capacity. In the present model for the site investigation area, the capacity of the unsaturated storage was dynamic and was determined by the current value of the groundwater level and an estimate of the soil water retention properties. A dynamic unsaturated storage capacity is more appropriate to the Forsmark field conditions, since groundwater depths vary so closely to the surface (most often in the range of

0 to 1 m depth). An additional difference compared with the conventional HBV formulation was the introduction of a soil moisture deficit function for estimating evapotranspiration based on the water content within a fixed root depth and on residual potential evapotranspiration. Furthermore, the model simulated groundwater levels as a function of the volume of water stored in the saturated storage (Figure 3-58).

An overview of fluxes and storages in the model is provided here, but the reader is referred to Appendix 4 for a more detailed presentation of the model and its equations.

The site average precipitation time series was the sole source of water "input" to the model. The interception storage captured input precipitation up to its holding capacity, and passed precipitation in excess of this capacity. The interception storage was preferentially drained as the first source for fulfilling potential evapotranspiration.

A calibrated snow routine (see Section 3.1) differentiated through-fall precipitation as either snow (stored above ground until temperatures exceeded 0°C) or rainfall (available for direct surface inflow). A fixed fraction of the surface inflow infiltrated directly to the saturated storage, while the residual fraction added to the unsaturated storage. Water added to the unsaturated storage until it was full, after which surface inflow added directly to the saturated storage. The capacity of the unsaturated storage was calculated using the dynamic depth to the groundwater zone and by assuming that field capacity was independent of depth and equal to 15% (see relevant field data in Appendix 3).

Daily evapotranspiration from the unsaturated zone was calculated based on the value of a soil moisture function and on residual potential evapotranspiration after evapotranspiration was taken from the interception storage. The soil moisture function calculated the ratio of actual to potential evapotranspiration based on the water content in a fixed and calibrated root zone depth. The root zone depth included the unsaturated zone and often the upper region of the saturated zone, depending on the dynamic value of groundwater depth.

Discharge from the saturated zone was calculated with the same storage-discharge relationship that was identified in Section 3.9. The model assumed that deep seepage from near-surface groundwater to bedrock groundwater was very small in comparison to other water fluxes, and hence was not modelled. Groundwater depths were calculated from the volume of saturated storage (above the dead zone) using a calibrated equation for the soil porosity profile.

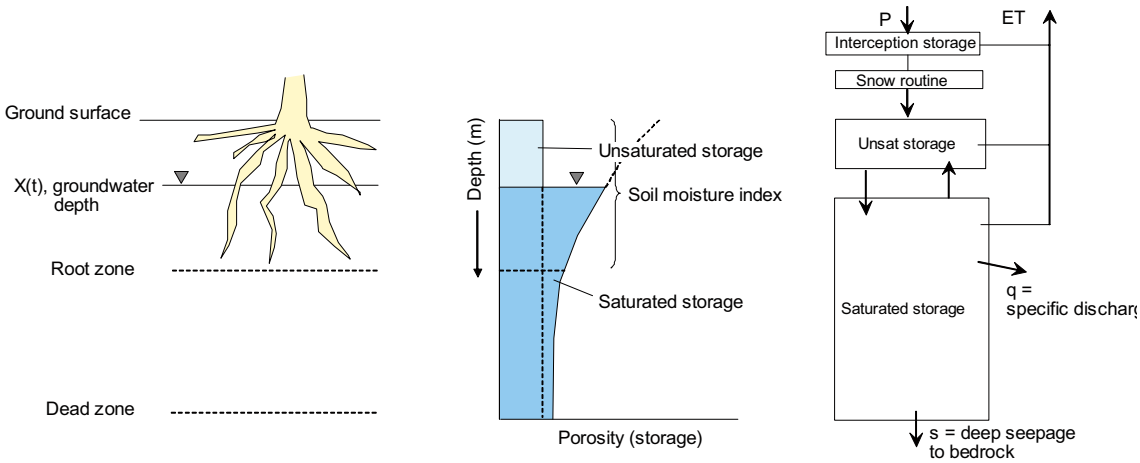

Figur 3-58. *Schematic diagrams describing a 1-D conceptual model of the groundwater hydrology in Quaternary deposits of the site investigation area.*

3.10.2 Calibration procedure

Ten parameters defined flux and storage equations for the model and these are summarised in Table 3-5. Values for the maximum interception storage (INT_{max}), the infiltration flow through fraction ($F_{flow\text{-}through}$), and the exponent in the discharge equation (k_2) were fixed and held constant for all calibrations. Values for the depth to the groundwater dead zone (d_{dead}) were assumed equal to the values identified in the calibration of the storage-discharge model (Table 3-4). The initial calibration approach also attempted to hold the snowmelt constant (K_{snow}) fixed across the four calibration datasets. It was attempted to apply the value of K_{snow} = *1.23 mm/degree* that was derived in earlier efforts as a study site average response (see Section 3.1). However, after observing consistent errors in all four simulations during the winter months of 2005, it was opted to treat K_{snow} as a calibration variable. This approach yielded improved results in all but the PFM002667-PFM002668 sub-basin.

Therefore, six model parameters were estimated for each sub-basin calibration: the snowmelt constant (K_{snow}), the maximum capillary rise (C_{max}), the soil moisture deficit threshold (SM_{thresh}), and the root zone depth (RZ), surface porosity ($\rho_{surface}$), and the scalar multiplier in the discharge equation (k_1). A range of acceptable (minimum and maximum) values for these parameters were identified (Table 3-5) and the resulting parameter space was searched at pre-defined intervals for a parameter set that maximized the objective function. In each case, the objective function was the sum of Nash-Sutcliffe criterion /Nash and Sutcliffe 1970/ for the simulated groundwater depth and discharge time series. However, we applied an additional constraint on the acceptable solutions that the simulated total discharge was within 10% of the available observed data. This last constraint was relaxed for the calibration of PFM002667-PFM002668 because no solutions were obtainable with it in place. Results from the storage-discharge model of the previous section were used for a narrowed range of parameters for $\rho_{surface}$ and k_1.

The start date for all simulations was January 1, 2001. The calibration period for the PFM005764 catchment was 14 months long and began on April 14 2004 (when the discharge measurements initiated). The calibration period for the remaining three catchments was one-year long (July 2004–June 2005), despite discharge data only being available for the last six-months of that interval. The calibration interval ended on June 30, 2005 for all simulations since July precipitation data was estimated and not measured in the site investigation area (see Section 2.2).

Table 3-5. Summary of model parameters for the near-surface hydrological model.

Parameter	Description	Fixed or calibrated	Range of values tested
I_{max}	Interception storage (mm)	fixed	2 mm
K_{snow}	Snowmelt constant (mm/ °C)	calibrated	0.8–1.2 mm/°C
$F_{flow\text{-}through}$	Flow through fraction for surface inflow	fixed	0.5
C_{max}	Maximum capillary rise (mm/d)	calibrated	2–12 mm/d
SM_{thresh}	Water deficit threshold in the soil moisture function for ET limitation (fraction)	calibrated	0.2–0.8
RZ	Root zone depth (m rel. ground surface)	calibrated	–1.2 to –0.1 m
$\rho_{surface}$	Soil porosity at the ground surface	calibrated	informed from storage-discharge model (Table 3-4)
k_1	Scalar in discharge equation	calibrated	informed from storage-discharge model (Table 3-4)
k_2	Exponent in discharge equation	fixed	values from storage-discharge model (Table 3-4)
d_{dead}	Groundwater depth that produces zero discharge	fixed	values from storage-discharge model (Table 3-4)

Initial conditions were set for the three storages in the model (interception, unsaturated zone and saturated zone storages) for the simulation start date. The initial condition for the saturated storage was the most significant of these and it was set to the average observed value for January 1 from the available time series, which was between –0.24 m and –0.10 m for the four simulations. The 40-month (minimum) start-up period for simulations ensured that there was no influence of initial conditions on simulated values during the calibration period.

The model was calibrated separately to each of the four catchment areas considered. In each case, the model was run in batch mode as it marched through various combinations of the three calibration parameters over their specified ranges (Table 3-5). The Nash-Sutcliffe criteria was calculated for each run and the parameter set that maximized this objective function was saved and output along with the best-fit time series simulations.

3.10.3 Model results

Simulation results for the PFM005764, PFM005764-PFM002667, PFM002667-PFM002668, and PFM002668 catchment areas are shown in Figures 3-59 to 3-62. Values of goodness-of-fit parameters for groundwater level and discharge time series for each simulation are summarised in Table 3-6. The calibrated model parameters for each catchment area are presented in Appendix 4. As with the storage-discharge model in the previous section, the simulated responses presented in Figures 3-59 through 3-62 could be very closely replicated with a wide range of alternate parameter values.

Simulation results were good for the PFM005764 and PFM002668 catchment data, and acceptable for the PFM005764-PFM002667 and PFM002667-PFM002668 catchments. In all cases, the groundwater level time series were better simulated than the discharge time series (Table 3-6), as could be expected since the model calculated discharge time series directly from the simulated groundwater depth time series. All sub-basins were simulated with positive errors in specific discharge ranging from +9 to +71% compared to the observed data. Note that the period between January and April 2005 typically provided the largest deviations between measured and simulated responses in the simulations. When more data becomes available, it is believed that this model would benefit from re-examination and possible enhancement to the snowmelt model and groundwater flux assumptions during wintertime.

The PFM005764 sub-basin, which was the largest simulated and had the longest time series for discharge calibration, had the lowest combined errors and highest combined coefficients of determination. For a one-year period of July 2004 through June 2005, total precipitation inflow to the model was 548 mm. During that same interval, the model simulated 137 mm of evaporation from interception storage, 237 mm of transpiration, 152 mm of surface discharge, and 22 mm of net storage changes in the saturated and unsaturated zones. Water balances for the other sub-basins were not estimated because of higher errors in specific discharge.

Table 3-6. Summary of goodness-of-fit parameters for model simulations.

Time series	Goodness-of-fit parameter	PFM005764	PFM005764-PFM002667	PFM002667-PFM002668	PFM002668
Groundwater	Coefficient of determination (Nash-Sutcliffe)	R^2 = 0.90	R^2 = 0.92	R^2 = 0.82	R^2 = 0.83
	Standard Error	0.004 m	0.007 m	0.007 m	0.002 m
	Error in simulated mean	3%	21%	–4%	10%
Specific discharge	Coefficient of determination	R^2 = 0.77	R^2 = 0.61	R^2 = 0.20	R^2 = 0.67
	Standard Error	0.009 m/d	0.018 m/d	0.048 m/d	0.014 m/d
	Error in simulated mean	10%	8%	71%	9%

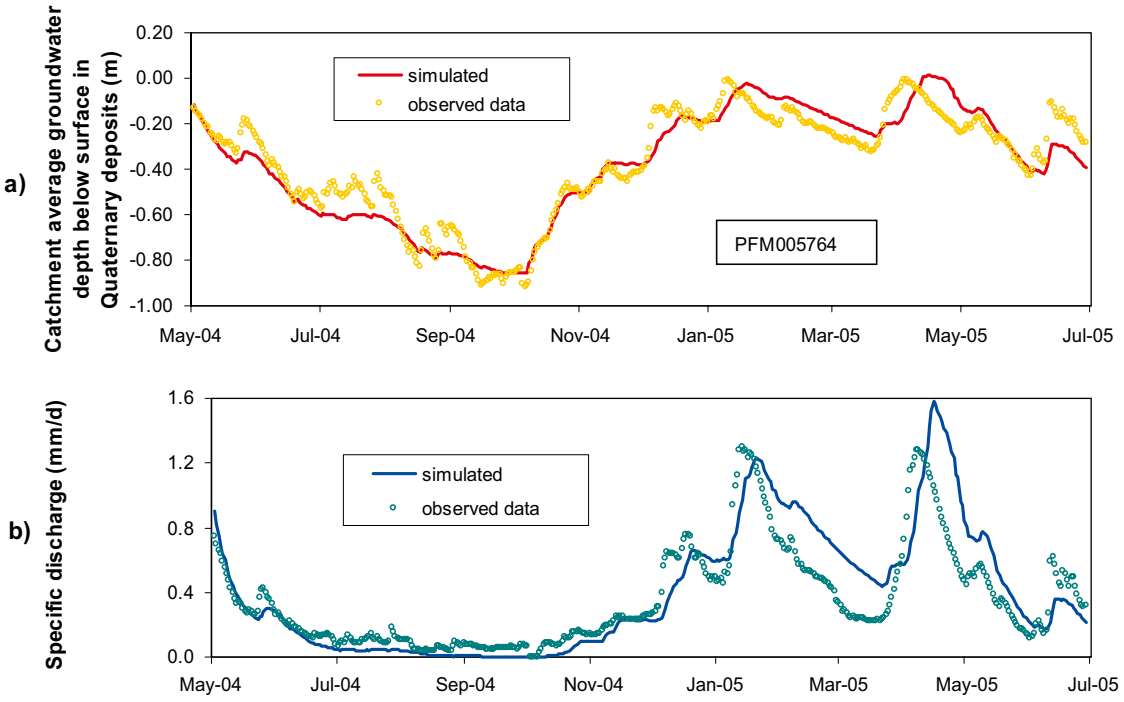

Figure 3-59. *Simulation results from the near-surface hydrological model for the catchment area of PFM005764.*

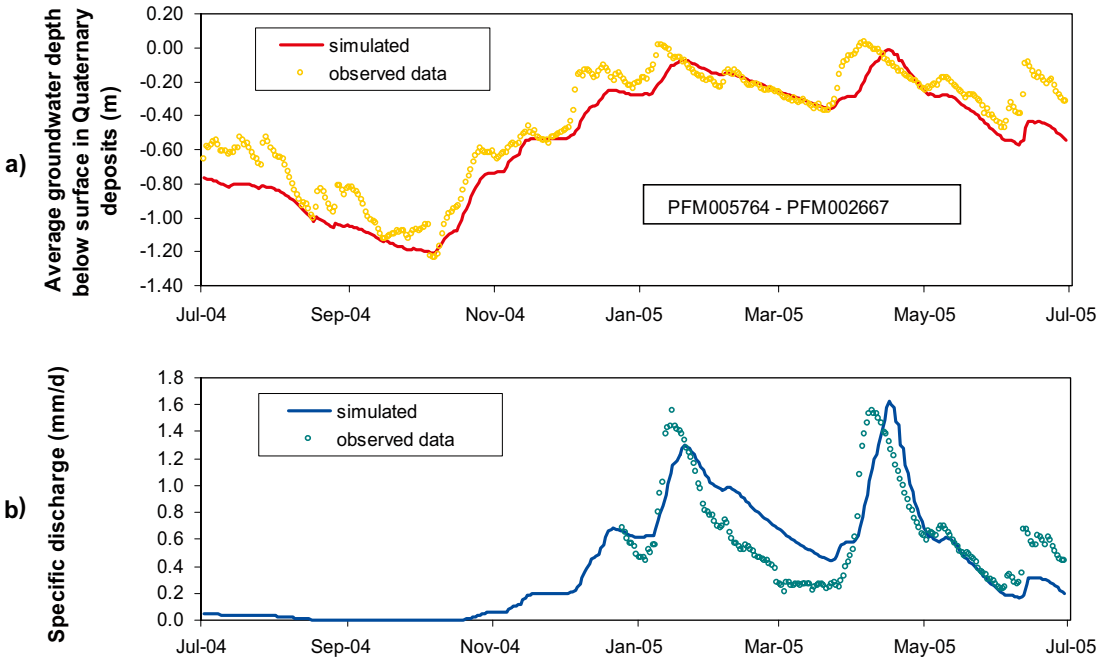

Figure 3-60. *Simulation results from the near-surface hydrological model for the catchment area of PFM005764–PFM002667.*

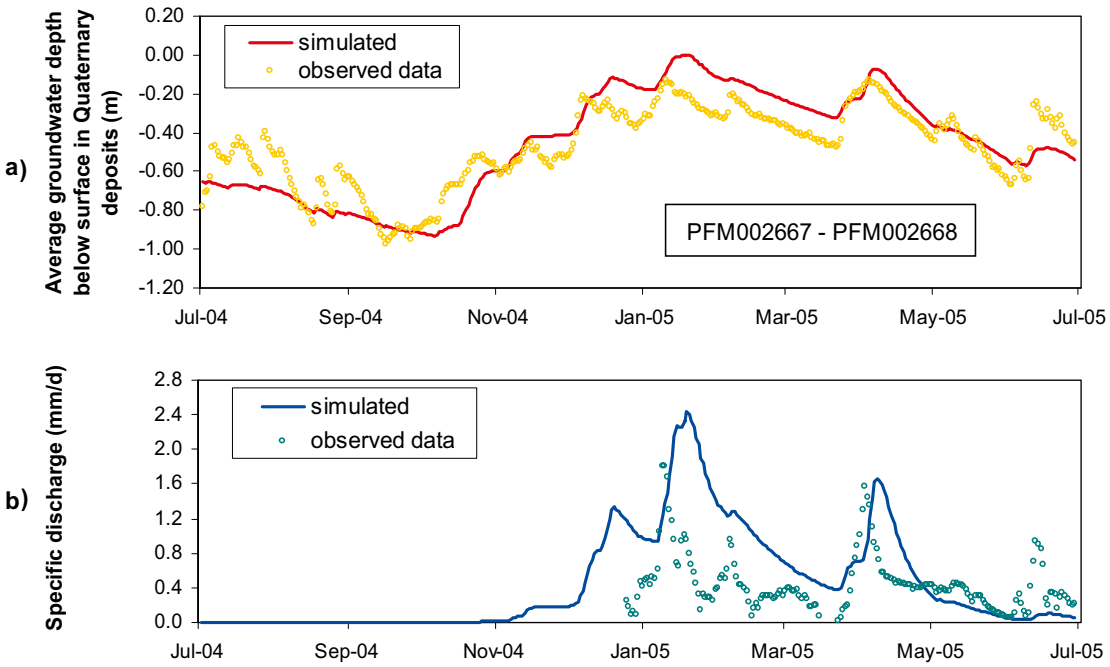

Figure 3-61. *Simulation results from the near-surface hydrological model for the catchment area of PFM002667–PFM002668.*

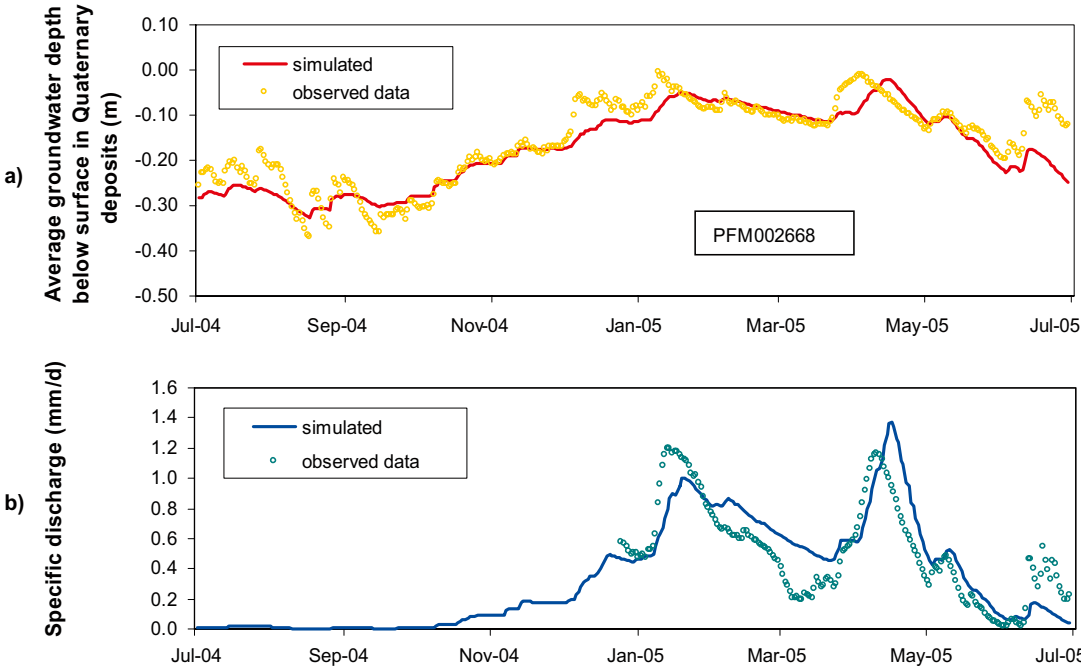

Figure 3-62. *Simulation results from the near-surface hydrological model for the catchment area of PFM002668.*

Figure 3-63 shows a summary of the simulated water balance in the PFM005764 catchment on a monthly time scale. Figure 3-63a shows monthly total precipitation, evaporation from the interception storage, transpiration from the soil zones, and groundwater discharge. Figure 3-63b shows storage changes for surface storage in snow and subsurface storage in saturated and unsaturated zones. Surface storage in snow accumulations are a significant storage during winter months, and, as has been discussed in other sections of this report, snowmelt events act as major inflow events to the subsurface zones. The model predicted that storage changes in the unsaturated zones were largely inversely proportionate to changes in the saturated zone ($R^2 = 0.75$), which could be expected since the maximum storage capacity of the unsaturated zones varies directly and nversely with groundwater depth.

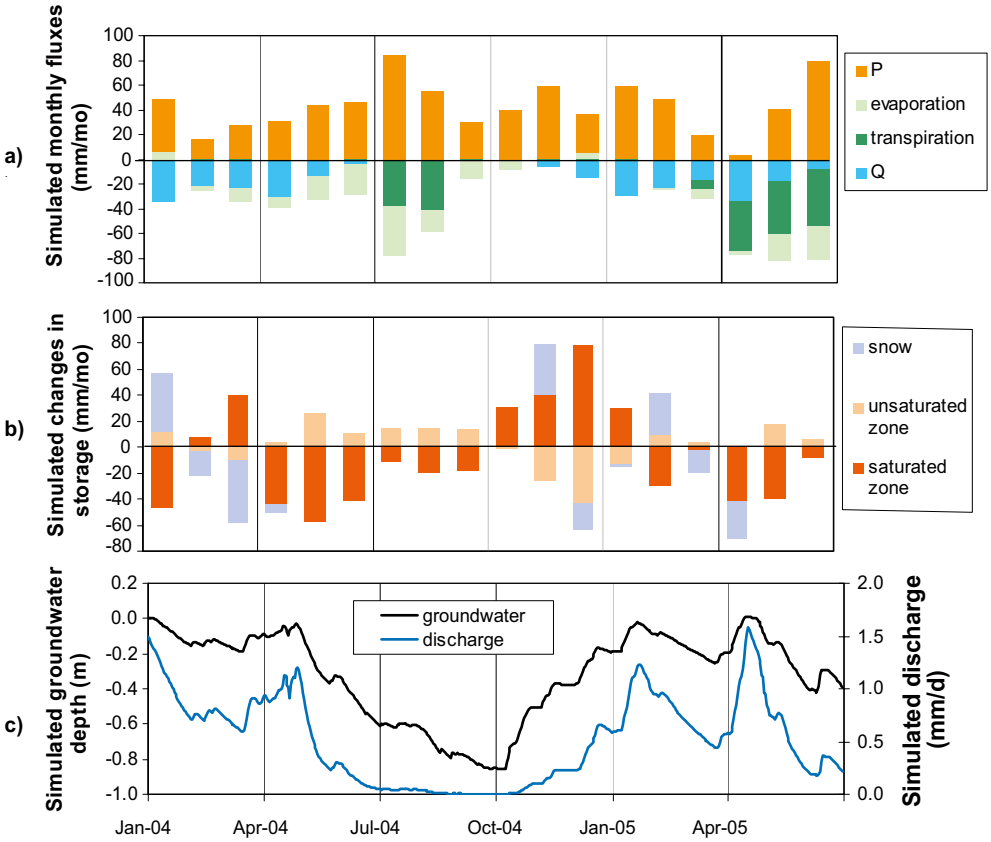

Figure 3-63. *Simulated monthly water fluxes and storage changes in the PFM005764 catchment.*

4 Conclusions and discussion

4.1 Observations in time series data

4.1.1 Meteorological data

- Two meteorological stations were established in the site investigation area in May 2003. The corrected mean annual precipitation of these two stations was 674 and 521 mm for the periods August 2003–July 2004 and August 2004–July 2005, respectively (periods of missing data from one station were filled in by data from the other station and data for July 2005, when data where missing from both stations, were derived from nearby SMHI stations).
- The measurements at the two stations showed good agreement with less than 5% difference in precipitation over the period of available measurements.
- Data indicated that of the nearby SMHI stations, the station at Östhammar had precipitation values most similar to those of the two SKB stations. There is a strong precipitation gradient from east to west, with an annual corrected precipitation at Örskär that is approximately 150 mm lower than at Lövsta.
- Based on data from nearby SMHI stations, SMHI has calculated a 30-year average annual precipitation of 559 mm at Forsmark, meaning that the first year of measurements at Forsmark was considerably wetter than normal while the second year was drier than normal.
- Potential evapotranspiration was calculated from measured data at Högmasten. The calculations was based on the Penman equation applied according to /Eriksson 1981/. For the two one-year periods August 2003–July 2004 and August 2004–July 2005, the potential evapotranspiration was 497 and 507 mm, respectively.
- The collected time series at the meteorological stations in the site investigation area were too short to establish firm correlations with nearby SMHI stations. Establishment of such correlations is important to enable use of SMHI's long-term time series for analysis and modelling.
- The snow depth and snow water content measurements, performed at three sites in the investigation area, proved to be useful for calibration of the snow routine of the hydrological model.

4.1.2 Surface water level data

- Surface water levels were recorded in six lakes and at two locations in the Baltic Sea.
- The highest recorded daily average sea water level was +0.75 and the lowest –0.50 m RHB 70. The single highest 30-minutes value was +0.94 m RHB 70. The highest sea levels were recorded in January 2005 when the storm "Gudrun" hit Sweden.
- At high sea water levels, sea water intruded Norra Bassängen, Bolundsfjärden and Lillfjärden and during the extreme event in January 2005 also Fiskarfjärden. The level of Lillfjärden seemed to be mainly ruled by the sea level, while the levels of Norra Bassängen and Bolundsfjärden, with exception for periods with very high sea levels, were ruled by the lake thresholds and the inflow from inland.
- Salinity profiles from Bolundsfjärden indicated a strong stratification after sea water intrusions when the lake had an ice cover, while a complete mixing appeared when the there was no ice cover. This mixing of the shallow water body (c. 2.5 m as maximum depth) was most probably mainly wind driven.

4.1.3 Groundwater level data in Quaternary deposits

- The measured groundwater levels in Quaternary deposits are actually density-dependent point water heads, but due to short water columns and mostly low salinity, corrections to fresh water heads or environmental water heads were negligible and were not considered.
- Groundwater levels were recorded in 38 wells in Quaternary deposits in the site investigation area. 30 of these wells were located on land, while 8 were placed in till below the bottom of lakes and the Baltic Sea.
- Groundwater levels in Quaternary deposits were in general very shallow. 80% of all recorded groundwater levels in the 30 wells on land were between 0.0 and 1.6 m below ground surface.
- Groundwater levels in Quaternary deposits were strongly coupled to the ground level. However, as anticipated a convex local topography resulted in somewhat deeper average groundwater levels than in areas with concave topography. A classification of the well locations from a recharge-discharge area perspective showed in general very shallow average groundwater levels in discharge areas, while the average depths to groundwater varied substantially in recharge areas.
- In individual wells, the temporal variation in groundwater level was less than 1.5 m in almost all wells and less than 1 m in approximately 50% of the wells.
- Groundwater level time series in many of the wells in Quaternary deposits were highly correlated with correlation coefficients $R^2 > 0.9$ and similar range of variations.

4.1.4 Point water heads in bedrock

- The groundwater in the bedrock is generally brackish and the groundwater levels recorded are therefore regarded as point water heads in the work reported here.
- Point water heads (groundwater levels) from 22 percussion-drilled boreholes in the site investigation area were analysed. No general transformation was made in the report of the actually measured point water heads to fresh water heads or environmental water heads to include the influence of water density effects on horizontal and vertical flow gradients, respectively. However, some preliminary calculations were made to see if changes in flow directions would appear if density effects were considered.
- Due to all ongoing activities in the site investigation area, mainly drilling and pumping, it was difficult to find long enough periods with undisturbed point water heads in the percussion-drilled boreholes for analyses of natural conditions. However, periods of undisturbed conditions of various lengths were identified and used in the analysis.
- Many of the bedrock wells had natural point water heads well above the local bedrock surface.
- In contrary to the wells in Quaternary deposits, there was no evident correlation to the elevation of the local ground surface except for wells with very low transmissivity.
- Bedrock wells in the tectonic lens, constituting the candidate area, had mean natural point water heads between 0.2 and 1.1 m RHB 70. Only two well sections had point water heads outside this range. These two sections had very low transmissivities. The small natural gradients within the tectonic lens indicated high transmissivities in the horizontal and sub-horizontal fracture zones known to exist in the uppermost c. 200 m of the lens.
- The analysis of responses in other bedrock wells on single distinct disturbances of groundwater levels in three bedrock wells indicated good hydraulic contacts over large distances within the tectonic lens. These responses confirmed the high transmissivities in the uppermost c. 200 m indicated by the small natural gradients.

4.1.5 Surface discharge

- Surface discharge was measured at four automatic gauging stations. The upstream catchment areas varied in size from 2.3 to 5.6 km^2. The station for the largest catchment area had been in operation since April 2004 and the other three since December the same year. The time series were too short to draw any strong conclusions on specific discharge and its spatial and temporal variation.
- The discharge from the largest catchment area varied between 1 and 84 L/s during the period of measurements and the specific discharge for the one-year period of August 2004–July 2005 was 136 mm.

4.2 Relationships between datasets

- A model of snow accumulation and snowmelt was calibrated against measured snow water content and used to derive a rainfall/snowmelt time series. Daily values from this time series minus daily potential evapotranspiration (R/S-PET) were used for interpretation of hydrological relationships.
- In an ordinary correlation study, R^2-values for monthly average groundwater levels in Quaternary deposits to average R/S-PET of prior two months were typically 0.6–0.7. In contrary, the correlations between R/S-PET and point water heads in bedrock, according to the ordinary correlations analysis, were weak and inconsistent. Different time periods for averaging and displacement in time were tested. However, a principal component analysis of the bedrock point water heads indicated that approximately 80% of the total variance was coupled to the seasonal variation of R/S-PET. The conclusion was that the annual variation in groundwater levels, both in Quaternary deposits and bedrock is dominated by R/S-PET variations.
- Diurnal variations of groundwater levels in Quaternary deposits, often 2–3 cm, were observed in several wells in areas with shallow groundwater during dry summer conditions. These variations were an indication of direct and/or indirect root water uptake and illustrated the strong connection between transpiration, and water in the unsaturated zone and the groundwater zone.
- The correlation between groundwater levels in Quaternary deposits and the sea level were typically very low with exception of the two well located in a glaciofluvial deposit close to the sea. Different time periods for averaging and displacement in time were tested. Concerning the correlation between the point water heads in bedrock and the sea level, the ordinary correlation study indicated a typically weak and inconsistent correlation. However, studies of short specific events revealed some indications of sea level influence on point water heads. In the independent component analysis, a component coupled to air pressure and/or sea water level could be identified, but still the R/S-PET was totally dominating the annual variation in point water heads. Based on the partial least squares modelling, a preliminary grouping of the percussion-drilled well was made in wells not influenced, possibly influenced and probably influence by sea water level variations. HFM02, HFM15 and HFM20–22 were classified as probably influenced and HFM14 and HFM18 as possibly influenced.
- Where groundwater levels in Quaternary deposits and point water heads in bedrock were observed in wells in close proximity, mostly at Drill sites, the groundwater levels in Quaternary deposits were 1–2 m higher, with Drill site 4 as an exception. Preliminary calculations indicated that the difference in groundwater levels and point water heads could not be explained by water density differences but indicated a downward flow gradient from the Quaternary deposits to the bedrock. However, the lack in response in groundwater levels in Quaternary deposits to pumpings in nearby bedrock wells in most cases indicated a limited contact between groundwater in Quaternary deposits and bedrock, at least in the vicinity of the pumping wells.

At Drill site 4, located outside the tectonic lens, the two monitoring wells in Quaternary deposits with lower groundwater levels than bedrock point water heads were situated in typical groundwater discharge areas for shallow groundwater and with ground elevations 3–4 m lower than at the percussion-drilled boreholes.

It would be desirable to have some additional groundwater monitoring wells in the immediate vicinity of percussion-drilled and core-drilled boreholes to further study vertical flow gradients from the Quaternary deposits to the bedrock. In the interpretation of the data it should also be remembered that the Drill sites, where most of the observations of vertical gradients from Quaternary deposits to bedrock were possible, are located in local topographically elevated areas, constituting typical recharge areas for shallow groundwater.

- A comparison of lake water levels and groundwater levels in Quaternary deposits in the vicinity or below the lakes showed that groundwater levels for most of the time were higher than the lake water levels. This meant that the lakes and their riparian zones acted as discharge areas for shallow groundwater, the actual discharge determined by the hydraulic contact between groundwater and surface water. However, during dry summer conditions the groundwater levels in the riparian zones and for some lakes also below the lake, decreased well below the lake water levels, implying that the lakes constituted potential groundwater recharge sources during these periods. This phenomenon confirmed the important influence of root water uptake on shallow groundwater indicated by the diurnal fluctuations discussed above and was also an indication of a limited hydraulic contact between the lakes and the groundwater.
- Well-defined relationships were found between time series of surface water discharge and averaged groundwater levels of upstream catchments, with some displacement in time during the rising phase. A simple, conceptual groundwater storage – surface water discharge model was developed by which discharge could be simulated from average upstream groundwater level with an R^2 between 0.7 and 0.9 for the three catchments where groundwater levels were available.
- The groundwater storage – surface water discharge model was expanded to a conceptual water balance model by using the precipitation and potential evapotranspiration time series as input, adding on a snow routine, an interception storage, and models of the unsaturated zone and root water uptake. The available time series were too short to allow for both calibration and validation. However, the preliminary results indicated that the model could simulate the measured discharge with good to acceptable accuracy. For the largest catchment, which had the longest available time series, the R^2 (according to Nash and Sutcliffe, 1970) was 0.9 and the error in total discharge 3% over the whole period of available measurements. For the one-year period of July 2004–June 2005, the corrected precipitation input to the model was 548 mm, the evapotranspiration 374 mm, the surface discharge 152 mm and the increase in unsaturated and saturated storage 22 mm.
- A new modelling when extended time series are available would allow for a better establishment of the model including a new calibration and validation. Sensitivity analysis of model parameters could be used to help in the site descriptive modelling of the surface hydrology and the results could be compared with the results from the Mike-SHE model, which has been selected as the main model for simulation of hydrology and surface-near hydrogeology.

4.3 Implications for the hydrogeologic conceptual model

- The variations in groundwater levels in Quaternary deposits and point water heads in bedrock were strongly coupled to variations in rainfall/snow melt and evapotranspiration while sea water levels had no or little influence. Even for the variations in bedrock point water heads, the rainfall/snow melt and evapotranspiration variations could explain about 80% of the annual variations. However, for point water heads in some percussion-drilled boreholes a probable sea water level influence could be identified.

- The available groundwater level time series from the Quaternary deposits confirmed that groundwater levels were very shallow in most parts of the site investigation area, with groundwater levels within one metres below ground during large parts of the year. Furthermore, the groundwater levels were strongly correlated to the ground surface level. The shallow groundwater implied a strong interaction with root water uptake illustrated by diurnal groundwater variations during dry summer periods. Root water uptake also gave rise to groundwater levels in Quaternary deposits well below lake water levels in the riparian zones of the lakes during such periods, changing the lakes from groundwater discharge areas to groundwater recharge areas.
- In contrary to the groundwater levels in Quaternary deposits, there was no strong correlation between the point water heads in bedrock and the ground surface level. Within the tectonic lens, constituting the candidate area, the difference in point water head between most of the bedrock wells was very small, indicating a good hydraulic contact in the horizontal and sub-horizontal fracture zones in the uppermost c. 200 m of the lens. Studies of responses in surrounding percussion-drilled to distinct single pumping events in bedrock wells confirmed good hydraulic contacts over large distances within the lens.
- At locations in the tectonic lens where it was possible to compare groundwater levels in Quaternary deposits and point water heads in bedrock in nearby wells, the groundwater levels in Quaternary deposits were considerably higher. This means that there was a potential for downward flow from the Quaternary deposits to the bedrock, but the large differences in levels indicated a limited hydraulic contact. A probable explanation is that high horizontal transmissivity of the uppermost part of the bedrock meant that the limited quantity of groundwater recharge reaching the bedrock could be conducted at very low gradients. There were no data supporting a discharge of deep groundwater to the surface within the tectonic lens.

4.4 Reliability of results

The installation of the monitoring equipment had been an on-going process from the first installations late in 2002. This meant that the lengths of the times series varied for the observation points and many of the data series were too short to provide a basis for decisive conclusions. The varying lengths of the time series also made comparison between observation points in terms of means and variances more difficult. However, the uncertainty varied between the different data sets as discussed in more detail below:

- A little more than two years of meteorological data were available for the analysis. These time series were too short to establish strong relationships with nearby SMHI stations with much longer time series which is desirable for long-term analysis and modelling.
- The sea and lake level time series are considered to give a good indication of the variations to be expected. Longer time series are not believed to result in changes in the conceptual model but will be important for further analysis of the connections between surface water and groundwater.
- The groundwater level time series from Quaternary deposits are considered to give a good indication of the variations to be expected. However, some additional observations wells are desirable in wetlands, but also in close proximity to bedrock boreholes, to study vertical groundwater flow gradients.
- Due to the extensive drilling and pumping activities in the site investigation area, the available time series of undisturbed point water heads in bedrock were short and meant that the analysis of natural conditions in bedrock was complicated. Therefore, the conclusions involving bedrock point water heads should be considered as preliminary. Especially for studies of correlation to sea water level and vertical flow gradients, extended time series from existing wells as well as additional time series from new wells are considered to be crucial. For studies of correlations between sea water levels and point water heads the

principal component and independent component analyses as well as the partial least squares modelling proved to be powerful tools and should be repeated when longer time series are available. For the recommended studies of vertical groundwater gradients it is important to perform systematic calculations of environmental water heads based on quality assured water density data from the bedrock well sections.

- The available time series of surface discharge are too short to draw any firm conclusions on specific discharge and its spatial and temporal variation. Discharge data are considered very important for the calculation of the water balance of the area and to constrain the terms of the water balance equation in calibrations of the quantitative hydro(geo)logical models. At the last data freeze, March 31 2007, another 1.5 years of data will be available and new analysis and modelling should be performed.

5 References

Alexandersson H, 2003. Korrektion av nederbörd enligt enkel klimatologisk metodik. SMHI, Meteorologi, Nr 111. (In Swedish.)

Brunberg A-K, Carlsson T, Blomqvist P, Brydsten L, Strömgren M, 2004. Identification of catchments, lake-related drainage parameters and lake habitats. SKB P-04-25, Svensk Kärnbränslehantering AB.

Eriksson B, 1981. Den potentiella evapotranspirationen i Sverige. SMHI, Rapport RMK 28. (In Swedish.)

Fredriksson D, 2004. Forsmark site investigation. Peatland investigation Forsmark. SKB P-04-127, Svensk Kärnbränslehantering AB.

Gokall-Norman K, Ludvigson J E, Jönsson S, 2005. Hydraulic interference test in HFM01. Forsmark site investigation. SKB P-05-236, Svensk Kärnbränslehantering AB.

Hedenström A, 2003. Investigation of marine and lacustrine sediments in lakes. SKB P-03-24, Svensk Kärnbränslehantering AB.

Hedenström A, 2004. Investigation of marine and lacustrine sediments in lakes. Stratigraphical and analytical data. SKB P-04-86, Svensk Kärnbränslehantering AB.

Hyvärinen A, Karhunen J, Oja E, 2001. Independent Component Analysis. John Wiley & Sons, New York, 504 pp.

Hyvärinen A, 2006. Matlab algorithm FastICA 2.5 by Aapo Hyvärinen, www.cs.helsinki.fi/u/ahyvarin/whatisica.shtml.

Johansson P O, 2005. Forsmark site investigation. Installation of brook discharge gauging stations. SKB P-05-154, Svensk Kärnbränslehantering AB.

Juston J, Johansson P O, 2005. Forsmark site investigation. Analysis of meteorological data, surface water data, and groundwater level data. SKB P-05-152, Svensk Kärnbränslehantering AB.

Johansson P O, Juston J, 2007. Forsmark site investigation. Monitoring of brook levels, water electical conductivities, temperatures and discharges from April 2003 until March 2007. SKB P-07-135, Svensk Kärnbränslehantering AB.

Johansson P O, Werner K, Bosson E, Juston J, 2005. Description of climate, surface hydrology and near-surface hydrogeology. SKB R-05-06, Svensk Kärnbränselhantering AB.

Larsson-McCann S, Karlsson A, Nord M, Sjögren J, Johansson L, Ivarsson M, Kindell S, 2002. Meteorological, hydrological and oceanographical information and data for the site investigation program in the communities of Östhammar and Tierp in the northern part of Uppland. SKB TR-02-02, Svensk Kärnbränslehantering AB.

Lind B, Lundin L. Saturated hydraulic conductivity of Scandinavian tills. Nordic Hydrology, 21, 107–118.

Lindell S, Ambjörn C, Juhlin B, Larsson-McCann S, Lindqvist K, 2000. Available climatological and oceanographical data for site investigation program. SKB R-99-70, Svensk Kärnbränslehantering AB.

Lindström G, Johansson B, Persson M, Gardelin M, Bergström S, 1997. Development and test of the distributed HBV-96 hydrological model. Journal of Hydrology 201, 272–288.

Lundin L, Stendahl J, Lode E, 2005. Forsmark site investigation. Soils in two large trenches. SKB P-05-166, Svensk Kärnbränslehantering AB.

Lusczynski N J, 1961. Head and flow of ground water of variable density. Journal of Geophysical Reasearch, vol. 66, no. 12, 4247-4256.

Nash J E, Sutcliffe J V, 1970. River flow forecasting through conceptual models, part 1 – a discussion of principles. Journal of Hydrology 10, 282–290.

SKB, 2001. Site investigations. Investigation methods and general execution programme. SKB TR-01-29, Svensk Kärnbränslehantering AB.

SKB, 2004. Preliminary site description. Forsmark area – version 1.1. SKB R-04-15, Svensk Kärnbränslehantering AB.

SKB, 2005. Preliminary site description. Forsmark area – version 1.2. SKB R-05-18, Svensk Kärnbränslehantering AB.

SMHI, 2005. Månadsnederbörd Forsmark och Oskarshamn. SMHI PM for SKB. (In Swedish.)

Sohlenius G, Rudmark L, Hedenström A, 2004. Mapping of unconsolidated Quaternary deposits 2002–2003. Map description. SKB R-04-39, Svensk Kärnbränslehantering AB.

Vikström M, 2005. Modelling of soil depth and lake sediments. An application of the GeoEditor at the Forsmark site. SKB R-05-07, Svensk Kärnbränslehantering AB.

Wern L, Jones J, 2006. Meteorological monitoring at Forsmark, June 2003 until July 2005. SKB P-05-221, Svensk Kärnbränslehantering AB.

Werner K, Johansson P O, Brydsten L, Bosson E, Tröjbom M, Nyman H, 2007. Recharge and discharge of near-surface groundwater in Forsmark. Comparison of classification methods. SKB R-07-08, Svensk Kärnbränslehantering AB.

Werner K, Lundholm L, 2004. Forsmark site investigation. Pumping test in well SFM0074. SKB P-04-142, Svensk Kärnbränslehantering AB.

Appendix 1

The influence of salinity on groundwater levels

Definition of groundwater level, fresh water head and point water head

The illustration in Figure A1-1 shows a groundwater monitoring well, which is open in its lower end. The pressure at the opening is denoted by p_i. The fluid density in the well is constant and has the same value as the density at the point in the aquifer where the opening is. If the groundwater in the aquifer is fresh, the groundwater level (GWL) may be regarded as a fresh water head. If the groundwater in the aquifer is brackish, the groundwater level (GWL) may be regarded as a point water head. As noted in Section 3, groundwater levels in the Quaternary deposits are in general fresh water heads, whereas groundwater levels in the percussion-drilled borehole are in general point water heads.

The fresh water head at any point i in groundwater of variable density is defined as the water level in a well filled with fresh water from i to a level high enough to balance the existing pressure at i, i.e. p_i. From Figure A1-1 we conclude that this pressure is given by $g\,\rho_i\,(H_{ip} - Z_i)$ when point water at i is used in the well. It is given by $g\,\rho_f\,(H_{if} - Z_i)$ when fresh water is used. From this equality, the fresh water head may be expressed in terms of the point water head as:

$$\rho_f\,H_{if} = \rho_i\,H_{ip} - Z_i\,(\rho_i - \rho_f) \qquad \text{(Equation A1-1)}$$

where

ρ_f = density of fresh water,
ρ_i = density of water at i,
H_{if} = fresh water head at i,
H_{ip} = point water head at i,
Z_i = elevation of point i, elevation measured positively upward.

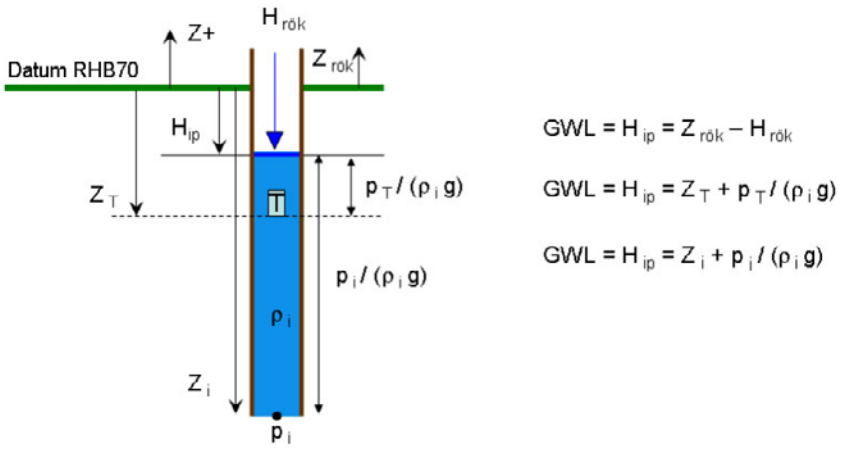

Figure A1-1. *Definition of groundwater level. The pressure at the well opening is denoted by p_i. The fluid density in the well is constant and has the same value as in the in aquifer where the opening is. A pressure transducer (T) is located at elevation Z_T.*

Environmental water head (modified after /Lusczynski 1961/)

If one wants to understand the prevailing directions of flow in a variable-density groundwater flow system based on head measurements it is necessary to transfer point water heads to fresh water heads and environmental water heads, respectively. Fresh water heads are useful for a discussion about the horizontal component of the hydraulic gradients between different points in space, whereas environmental water heads are useful for a discussion about the vertical components of the hydraulic gradients. The relation between fresh water head and point water head is given by Equation A1-1. In Equation A1-2 the relation between environmental water head and fresh water head is expressed. The relation between environmental water head and point water head is expressed in Equation A1-3.

$$\rho_f H_{in} = \rho_f H_{if} - (\rho_f - \rho_a)(Z_i - Z_r) \qquad \text{(Equation A1-2)}$$

$$\rho_f H_{in} = \rho_i H_{ip} - Z_i (\rho_i - \rho_a) - Z_r (\rho_a - \rho_f) \qquad \text{(Equation A1-3)}$$

where

ρ_a average density of water between Z_r and i, as defined by

$$\frac{1}{Z_r - Z_i} \int_{Z_i}^{Z_r} \rho \, dz$$

H_{in} = environmental water head at i,

Z_r = elevation of reference point from which the average density of water to point i is determined and above which water is fresh; elevation measured positively upward.

The hydraulic gradient of Equation A1-2 for any point i in groundwater of variable density is:

$$\rho_f \nabla H_{in} - (Z_i - Z_r)\left[\frac{\partial(\rho_a)}{\partial x}\mathbf{i} + \frac{\partial(\rho_a)}{\partial y}\mathbf{j}\right] = \rho_f \nabla H_{if} + (\rho_i - \rho_f)\,\mathrm{k} \qquad \text{(Equation A1-4)}$$

Along a vertical, the left hand side of Equation A1-4 reduces to $\rho_f (\partial H_{in}/\partial z)$, which is simply a product of fresh water density and a gradient defined by environmental water heads. Along any horizontal, the right hand side of Equation A1-4 reduces to $\rho_f (\partial H_{if}/\partial x)$, which is simply a product of fresh water density and a gradient defined by fresh water heads.

Because environmental water heads define hydraulic gradients along a vertical, they are comparable along a vertical, e.g. a borehole with multiple packer sections.

Example

Figure A1-2 shows the elevations and point water densities associated with the multiple packer system in the percussion-drilled borehole HFM19 together with the elevation and fluid density in the nearby monitoring well in the Quaternary deposits, SFM0058. HFM19 has three monitoring intervals, HFM19:1–3, where HFM19:1 is the deepest.

HFM19:1 has a transmissivity of $2.8 \cdot 10^{-4}$ m^2/s; HFM19:2 has a transmissivity of $2.2 \cdot 10^{-5}$ m^2/s and HFM19:3 has a transmissivity of $4.2 \cdot 10^{-5}$ m^2/s.

Figure A1-3 illustrates measured groundwater levels, i.e. point water heads, gathered in HFM19 and SFM0058. The period of time shown ranges from 2006-01-31 to 2006-06-29 (the data series used in the example belongs to Data Freeze 2.2).

The inset in the upper right shows a schematic illustration of the vertical gradient components if one uses measured point water heads as a reference. Point water heads suggest that HFM19 and SFM0058 are primarily located in a recharge area for most parts of the period except during the dry summer months when evapotranspiration make the groundwater level in the Quaternary deposits drop below the point water head in HFM19:3.

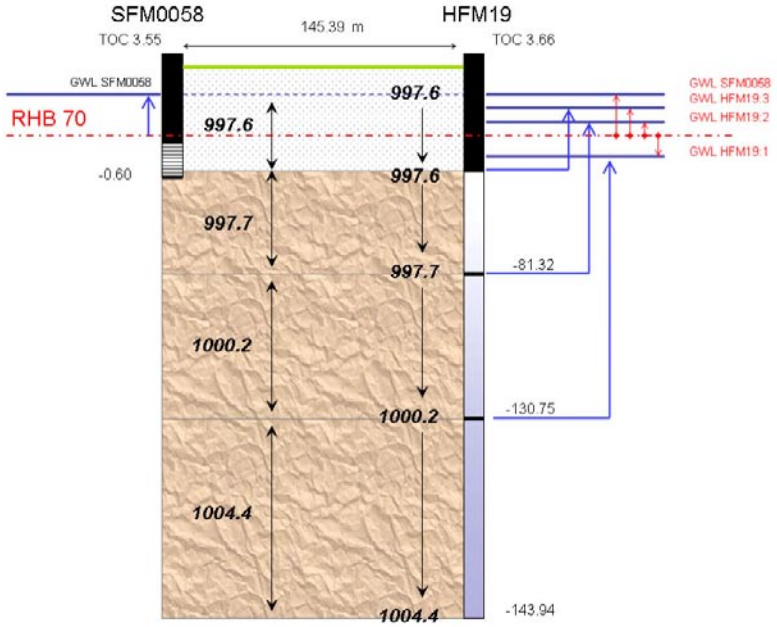

Figur A1-2. *Elevations and point water densities associated with the multiple packer system in the percussion-drilled borehole HFM19 together with the elevation and fluid density in the nearby monitoring well in the Quaternary deposits, SFM0058. Datum is RHB70. TOC = top of casing. Fluid densities between packers are treated in two ways; either uniform (constant) between packers (left) or, alternatively, linearly increasing between packers.*

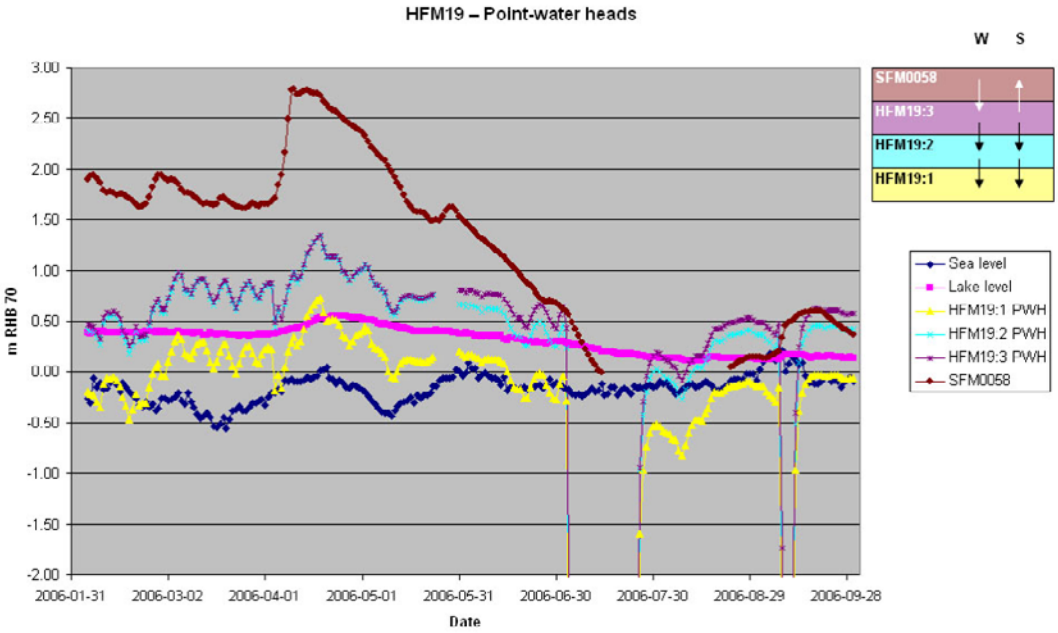

Figure A1-3. *Plot of measured groundwater levels, i.e. point water heads, gathered in HFM19 and SFM0058 from 2006-01-31 to 2006-06-29. The inset in the upper right shows a schematic illustration of the vertical gradient components if one uses point water heads as a reference; W = winter and S = summer.*

Figure A1-4 illustrates the same information as in Figure A1-3 except that the measured groundwater levels have been transformed to point water heads. The inset in the upper right shows a schematic illustration of the vertical gradient components if one uses point water heads as a reference. Point water heads suggest that HFM19:3 is a the main discharge interval for most parts of the period except during the dry summer months when evapotranspiration make the groundwater level in the Quaternary deposits drop below the point water head in HFM19:3.

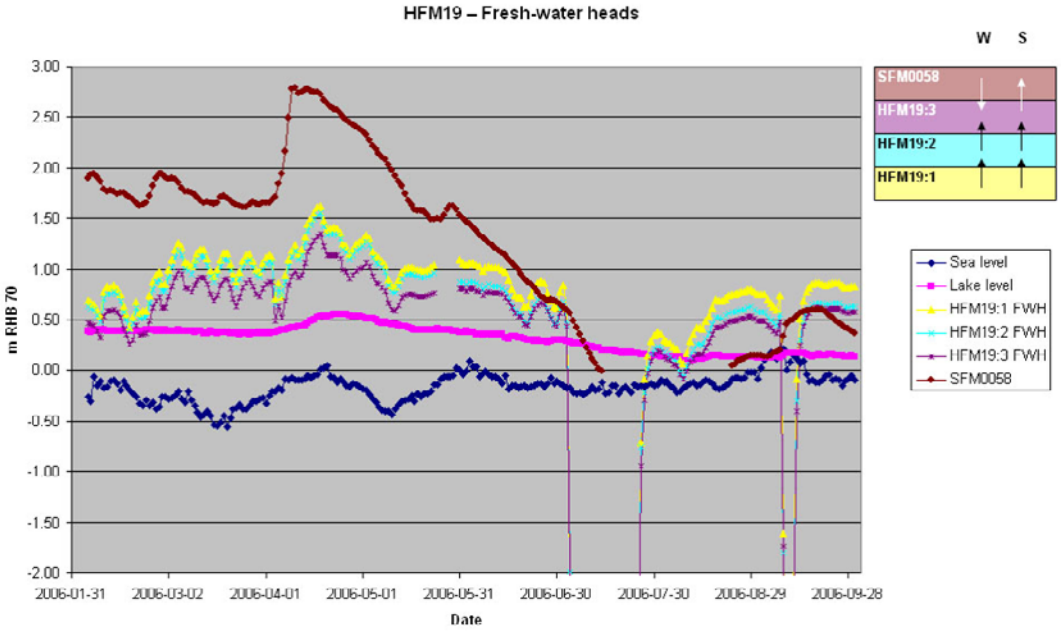

Figure A1-4. *The same information as in Figure A1-3 except that the measured groundwater levels have been transformed to point water heads. The inset in the upper right shows a schematic illustration of the vertical gradient components if one uses point water heads as a reference; W = winter and S = summer.*

Figure A1-5 illustrates the same information as in Figure A1-3 except that the measured groundwater levels have been transformed to environmental-water heads. Figure A1-5 is based on the assumption of a constant fluid density between packers, cf. Figure A1-2. The inset in the upper right shows a schematic illustration of the vertical gradient components if one uses constant-density environmental-water heads as a reference.

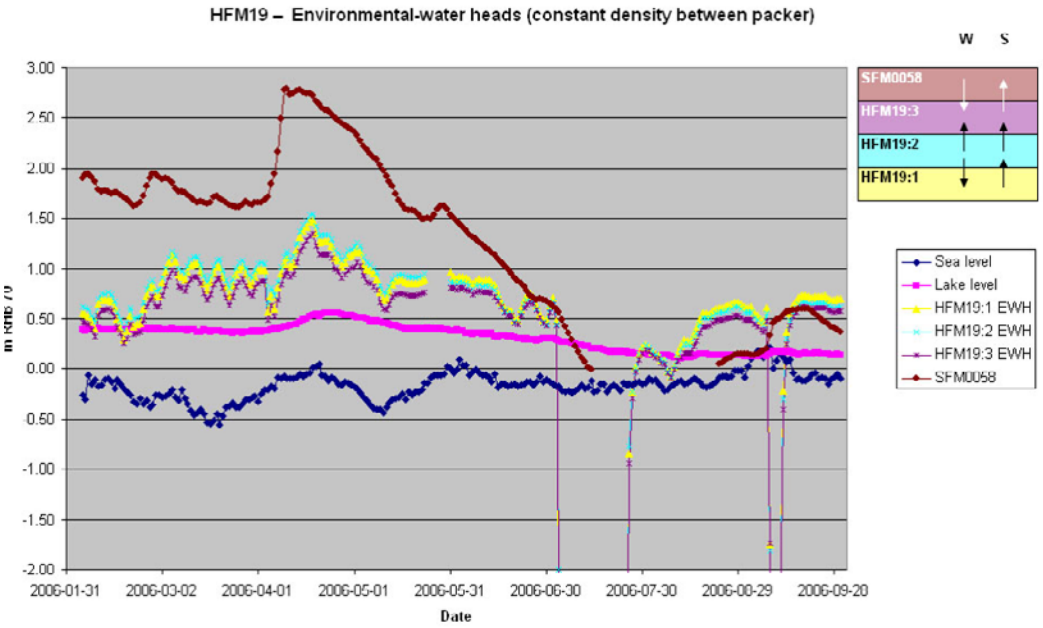

Figure A1-5. *Plot of same information as in Figure A1-3 after that the measured groundwater levels have been transformed to enviromental-water heads. Figure A1-5 is based on the assumption of a constant fluid density between packers, cf. Figure A1-2. The inset in the upper right shows a schematic illustration of the vertical gradient components if one uses environmental-water heads as a reference; W = winter and S = summer.*

Constant-density environmental-water heads suggest a complex gradient pattern between the different "intervals" in the bedrock. During the winter period the environmental-water heads in the middle interval, HFM19:2, are apparently greater than the heads in the bedrock intervals both above and below. The heads in the Quaternary deposits, however, are still the greatest, which suggests that the main "discharge interval" is HFM19:3. During the dry summer period evapotranspiration makes the groundwater level in the Quaternary deposits drop below the point water head in all bedrock intervals.

Figure A1-6 illustrates the same information as in Figure A1-3 except that the measured groundwater levels have been transformed to environmental-water heads. Figure A1-6 is based on the assumption of linearly increasing fluid densities between packers, cf. Figure A1-2. The inset in the upper right shows a schematic illustration of the vertical gradient components if one uses linear-density environmental-water heads as a reference.

Linear-density environmental-water heads suggest a somewhat simpler vertical gradient pattern between the different bedrock "intervals" than do constant-density environmental-water heads. The linear-density environmental-water heads in the middle bedrock interval, HFM19:2, are for most parts greater than the heads in the two bedrock intervals above and below. The heads in the Quaternary deposits are the greatest during the winter period, which means that the main discharge interval is HFM19:3. During the dry summer months evapotranspiration makes the groundwater level in the Quaternary deposits drop below the point water head in all intervals of HFM19.

Figure A1-3 through Figure A1-6 demonstrate that the interpretation of the vertical gradients derived from point water heads or point water heads must be treated with great caution. The two types of environmental-water heads presented in this appendix open up for a discussion about other types of uncertainties. A vital uncertainty is the assumption of the density profile in the bedrock outside the borehole HFM19. The tentative discussion presented here assumes that fractured medium is a continuous porous medium. This uncertainty and others will be treated in greater detail in model version 2.2.

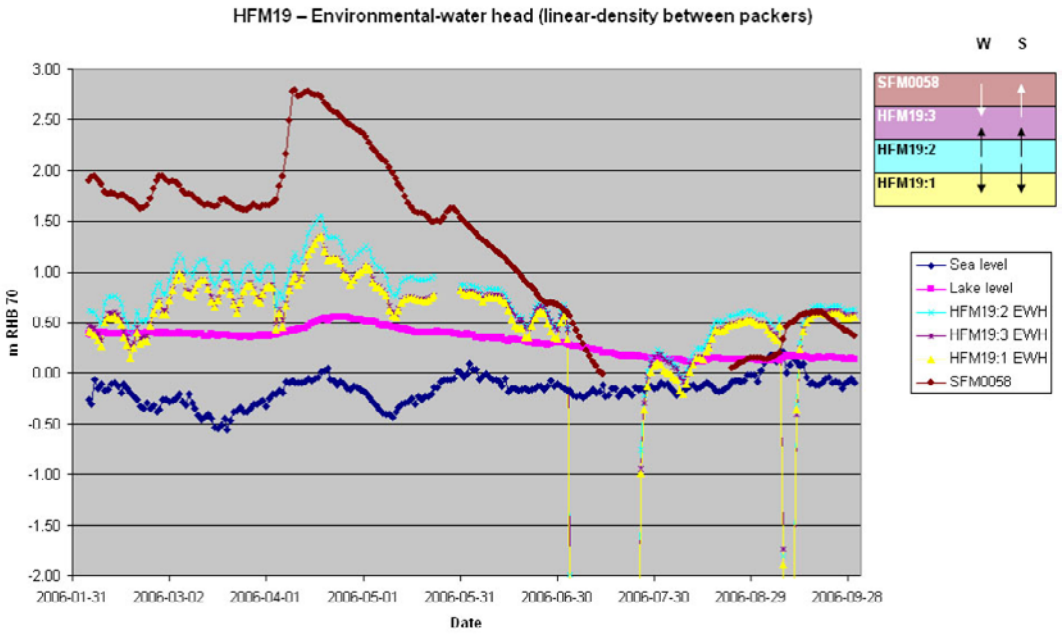

Figure A1-6. *Plot of same information as in Figure A1-3 after that the measured groundwater levels have been transformed to environmental-water heads. Figure A1-6 is based on the assumption of linearly increasing fluid densities between packers, cf. Figure A1-2. The inset in the upper right shows a schematic illustration of the vertical gradient components if one uses environmental-water heads as a reference; W = winter and S = summer.*

Appendix 2

Correlation matrix for groundwater levels in wells in Quaternary deposits

Correlation matrix for the groundwater levels in the wells in Quaternary deposits. r-values ≥ 0.90 marked in red.

	SFM 0001	SFM 0002	SFM 0003	SFM 0004	SFM 0005	SFM 0006	SFM 0008	SFM 0009	SFM 0010	SFM 0011	SFM 0013	SFM 0014	SFM 0016	SFM 0017	SFM 0018	SFM 0019	SFM 0020	SFM 0021	SFM 0026	SFM 0028	SFM 0030	SFM 0033	SFM 0034	SFM 0036	SFM 0049	SFM 0057	SFM 0058	SFM 0059	SFM 0061
SFM 0001	**1.00**	0.97	0.98	0.86	0.85	0.69	0.81	0.79	0.91	0.86	0.91	0.91	0.83	0.86	0.82	0.94	0.92	0.92	0.85	0.93	0.95	0.76	0.96	0.97	0.78	0.95	0.91	0.43	0.30
SFM 0002		**1.00**	0.95	0.81	0.78	0.68	0.71	0.69	0.85	0.79	0.85	0.84	0.73	0.78	0.73	0.91	0.87	0.90	0.72	0.88	0.91	0.73	0.92	0.93	0.67	0.91	0.81	0.43	0.32
SFM 0003			**1.00**	0.85	0.84	0.66	0.75	0.83	0.94	0.89	0.89	0.89	0.84	0.88	0.85	0.94	0.91	0.91	0.84	0.88	0.97	0.74	0.93	0.95	0.82	0.92	0.91	0.30	0.18
SFM 0004				**1.00**	0.88	0.58	0.82	0.82	0.79	0.81	0.88	0.83	0.82	0.80	0.75	0.90	0.91	0.81	0.86	0.87	0.85	0.68	0.85	0.87	0.75	0.83	0.84	0.42	0.36
SFM 0005					**1.00**	0.74	0.79	0.89	0.76	0.81	0.91	0.76	0.83	0.81	0.66	0.88	0.92	0.78	0.82	0.79	0.83	0.56	0.80	0.85	0.79	0.82	0.87	0.28	0.26
SFM 0006						**1.00**	0.66	0.81	0.76	0.74	0.76	0.59	0.66	0.69	0.48	0.73	0.69	0.74	0.78	0.53	0.78	0.19	0.61	0.74	0.69	0.70	0.58	0.03	0.09
SFM 0008							**1.00**	0.74	0.76	0.85	0.90	0.82	0.85	0.80	0.79	0.82	0.85	0.74	0.91	0.89	0.78	0.63	0.85	0.83	0.79	0.88	0.89	0.64	0.55
SFM 0009								**1.00**	0.77	0.92	0.88	0.84	0.93	0.91	0.92	0.84	0.88	0.77	0.89	0.78	0.86	0.60	0.78	0.84	0.95	0.75	0.81	0.10	0.13
SFM 0010									**1.00**	0.86	0.91	0.88	0.85	0.89	0.86	0.91	0.86	0.82	0.86	0.80	0.97	0.65	0.92	0.94	0.82	0.93	0.86	0.33	0.22
SFM 0011										**1.00**	0.93	0.90	0.94	0.93	0.93	0.88	0.90	0.83	0.93	0.86	0.91	0.67	0.87	0.90	0.94	0.88	0.95	0.30	0.24
SFM 0013											**1.00**	0.94	0.93	0.90	0.87	0.93	0.94	0.88	0.92	0.91	0.92	0.75	0.95	0.94	0.87	0.94	0.96	0.44	0.34
SFM 0014												**1.00**	0.95	0.96	0.95	0.94	0.95	0.92	0.93	0.93	0.93	0.77	0.92	0.91	0.85	0.94	0.91	0.46	0.30
SFM 0016												0.95	**1.00**	0.96	0.95	0.88	0.91	0.83	0.95	0.88	0.90	0.71	0.87	0.88	0.93	0.92	0.97	0.36	0.26
SFM 0017														**1.00**	0.98	0.91	0.93	0.88	0.92	0.87	0.93	0.71	0.87	0.89	0.92	0.94	0.95	0.36	0.24
SFM 0018															**1.00**	0.88	0.89	0.89	0.90	0.87	0.90	0.69	0.85	0.84	0.93	0.82	0.90	0.77	0.68
SFM 0019																**1.00**	0.97	0.96	0.89	0.93	0.96	0.77	0.92	0.93	0.80	0.95	0.91	0.43	0.33
SFM 0020																	**1.00**	0.92	0.91	0.93	0.92	0.75	0.92	0.92	0.84	0.93	0.91	0.41	0.31
SFM 0021																		**1.00**	0.83	0.90	0.92	0.75	0.87	0.88	0.74	0.85	0.75	0.44	0.37
SFM 0026																			**1.00**	0.87	0.89	0.65	0.85	0.88	0.90	0.94	0.97	0.39	0.31
SFM 0028																				**1.00**	0.89	0.78	0.95	0.92	0.78	0.86	0.86	0.70	0.57
SFM 0030																					**1.00**	0.75	0.93	0.96	0.87	0.93	0.90	0.33	0.23
SFM 0033																						**1.00**	0.79	0.74	0.60	0.64	0.88	0.41	0.32
SFM 0034																							**1.00**	0.97	0.80	0.92	0.90	0.53	0.38
SFM 0036																								**1.00**	0.85	0.92	0.93	0.39	0.30
SFM 0049																									**1.00**	0.83	0.89	0.24	0.17
SFM 0057																										**1.00**	0.92	0.42	0.26
SFM 0058																											**1.00**	0.46	0.31
SFM 0059																												**1.00**	0.99
SFM 0061																													**1.00**

Appendix 3

Parameterisation of soil pF curves

In /Lundin et al. 2005/, data were presented on soil cores that were collected in two large trenches in the site investigation area and analysed for porosity and water holding capacity. Those data are reproduced in Figure A3-1a and b, showing three profiles for total porosity and water holding capacity at 100 cm suction. Using a standard definition for field capacity, it was assumed that the soil field capacity was equal to the water holding capacity at 100 cm suction. The site data suggested a near constant field capacity of about 15%, independent of both location and depth. Therefore, a constant 15% field capacity was assumed in the unsaturated zone of the models (Sections 3.9 and 3.10).

A simplified means to fit the porosity profiles to a common equation with mostly similar parameters was sought. The equation used was exponential in form and was defined by three parameters:

$$\rho\,(d) = \rho_{depth} + (\rho_{surface} - \rho_{depth})\, e^{-k_3 d}$$

where

$\rho_{surface}$ = soil porosity at the ground surface,

ρ_{depth} = soil porosity at depth,

k_3 = exponent defining the shape of the curve between these porosity endpoints.

In principle, the three parameters in this equation could be uniquely solved to fit the 6–7 data points in each of the three soil profiles. However, this would leave three unknowns that would need to be defined (calibrated) when the equation was used to define soil porosity and water storage properties in our models. Therefore, two further assumptions were introduced that enabled soil profiles to be uniquely defined by a single parameter. We assumed that k_3 was the same at all sites and that the ratio of ρ_{depth} to $\rho_{surface}$ (k_4) was also the same at all sites.

The available soil profile data were used to determine values for these two parameters. The objective function for calibration was to minimize the pooled sum of squared errors in predicting the three soil profiles using the porosity profile equation above. The model had five calibration parameters including three $\rho_{surface}$ variables (one for each profile), one ratio of ρ_{depth} to $\rho_{surface}$ (k_4) common to all profiles, and one exponent term (k_3) also common to all profiles. Before calibration, one data point was eliminated as an outlier (from PFM004460), and this led to a problem setup of 19 unknowns (total available data points) and 5 solution variables.

Figure A3-1c shows a comparison of the results after the terms in the porosity profile equation were calibrated. The parameter values are in the equation were $\rho_{surface}$ = 0.28, 0.30, and 0.45; k_3 = 1.53, and k_4 = 0.52. A cross-plot of modeled versus observed soil porosity (not shown) suggested excellent correlation (R^2 = 0.90, n = 19). The results are good and substantiate the made assumptions.

The equation and assumptions outlined above were used in theconceptual models (Sections 3.9 and 3.10) and allowed for the soil porosity profile equation to be uniquely defined with only one calibration parameter ($\rho_{surface}$).

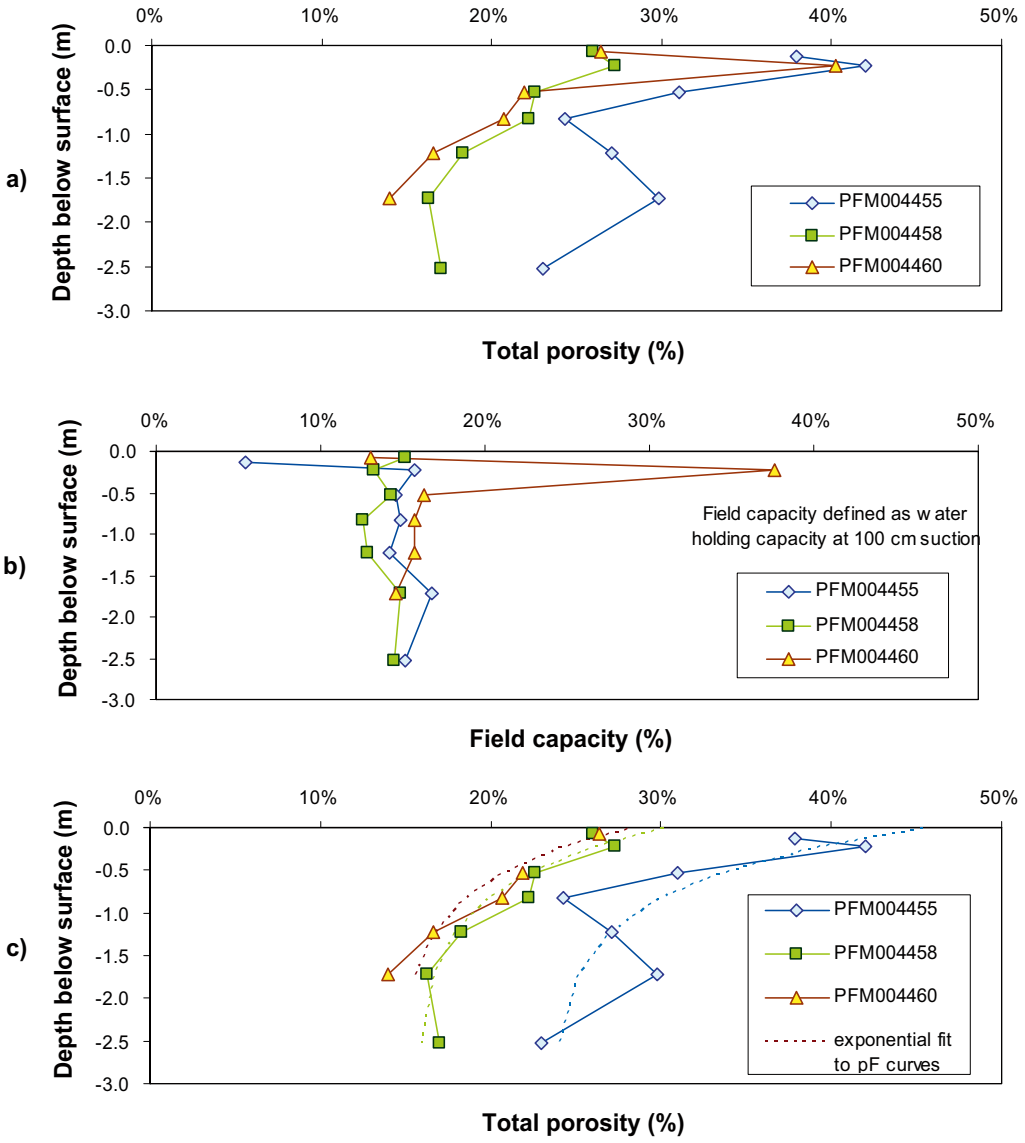

Figure A3-1. *Data from three soil profiles from the site investigation area showing a) total porosity as a function of depth, b) field capacity defined from the water holding capacity at 100 cm suction, and c) porosity profiles fit to a common exponential equation with similar model parameters.*

Appendix 4

Equations for the Forsmark near-surface hydrological model

Figure A4-1 shows schematic diagrams of physical and conceptual aspects of the Forsmark near-surface hydrological model. The model will be described in this Appendix in three steps. First, equations for depth-storage relationships will be developed, followed by a discussion of evapotranspiration calculation using a soil moisture function, and then the model water balance and flux equations will be presented.

Depth-storage relationships

The maximum water holding capacity of the unsaturated zone, US_{max}, was calculated at each time step as:

$$US_{max} = -FC \cdot x(t) \qquad \text{(Equation A4-1)}$$

where

FC = field capacity (fraction),

$x(t)$ = groundwater depth at time t, (m below surface).

Based on data from field samples (see Appendix 3), it was assumed that FC = 0.15 for all simulations.

As was developed in Appendix 3, the soil porosity profile was represented by:

$$\rho(d) = \rho_{depth} + (\rho_{surface} - \rho_{depth})\, e^{-k_3 d} \qquad \text{(Equation A4-2)}$$

where

$\rho(d)$ = porosity at depth, d,

ρ_{depth} = asymptotic soil porosity at depth,

$\rho_{surface}$ = maximum soil porosity at the surface,

k_2 = exponent of porosity shape function.

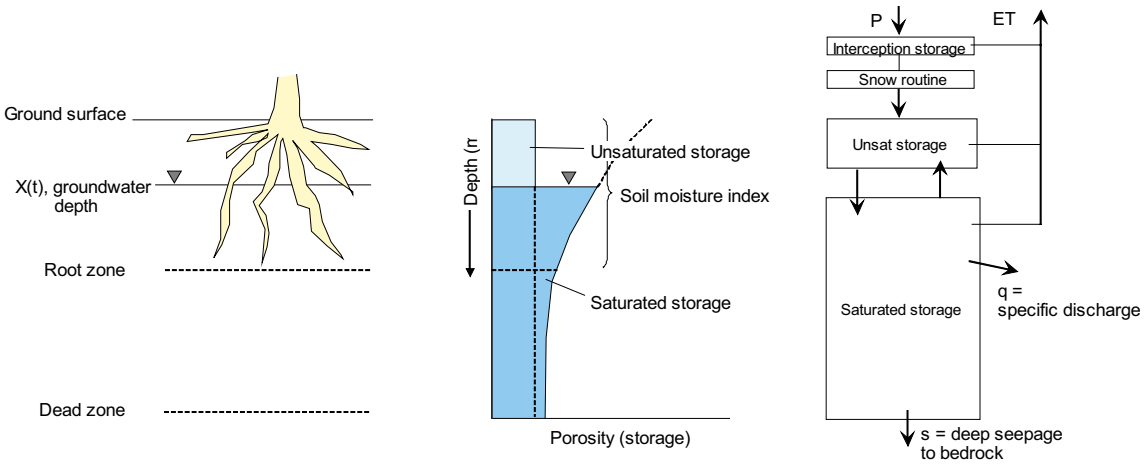

Figure A4-1. *Schematic diagrams of the model for near-surface hydrology.*

As was also developed in Appendix 3, it was assumed that the soil porosity at depth and at the surface were proportionally related as

$$\rho_{depth} = K_4 \rho_{surface} \qquad \text{(Equation A4-3)}$$

A value of $k_4 = 0.52$ was calibrated from field data and used in all simulations.

An "active" storage in the saturated zone was defined as the volume of water above a dead zone, as shown schematically in Figure A4-1. Therefore, the volume of active water stored in the saturated zone was calculated by integrating Equation A4-2 from the depth to dead zone (DZ) to the depth to groundwater ($x(t)$). The resultant equation for the the volume of active saturated storage, *SS*, was given as:

$$SS = \rho_{depth}\left(x(t) - DZ\right) + \frac{(\rho_{surface} - \rho_{depth})}{k_3}\left(e^{-k_3 x(t)} - e^{-k_3 DZ}\right) \qquad \text{(Equation A4-4)}$$

Equation A4-4 was back-solved in the model (by iteration) for daily values of $x(t)$ given updated values for *SS* based on the water balance and flux equations shown below. A new value for the storage capacity of the unsaturated zone, US_{max}, was then calculated using Equation A4-1.

Soil moisture deficit function for ET calculation

A soil moisture index was calculated in the model within the specified root zone depth. The index specifided a fractional soil moisture deficit, *SMD*, as:

$$SMD = 1 - \frac{RZ}{RZ_{\max}} \qquad \text{(Equation A4-5)}$$

where

RZ = daily value for water storage in the root zone,

RZ_{max} = the maximum water storage capacity in the root zone.

The maximum capacity for water storage in the root zone, RZ_{max}, was given by integration of Equation A4-2 from the depth of the root zone to the ground surface (d = 0) as

$$RZ_{\max} = -\rho_{depth} RZ + \frac{(\rho_{surface} - \rho_{depth})}{k_3}\left(1 - e^{-k_3 RZ}\right) \qquad \text{(Equation A4-6)}$$

The daily value for actual water stored in the root zone was the sum of water storage in unsaturated zone and the upper fraction of the saturated zone that was within the root zone

$$RZ = US + RZ_{sat} \qquad \text{(Equation A4-7)}$$

Here again, the saturated water storage in the root zone was calculated by intergrating Equation A4-2 and was given by

$$RZ_{sat} = \rho_{depth}\left(x(t) - RZ\right) + \frac{(\rho_{surface} - \rho_{depth})}{k_3}\left(e^{-k_3 x(t)} - e^{-k_3 RZ}\right) \qquad \text{(Equation A4-8)}$$

The value for SMD from Equation A4-5 was updated on a daily basis in the model. Daily ET was calculated from daily PET values using the SMD-dependent function defined in Figure A4-2. The SMD function limits ET at very wet conditions (SMD < 0.10) and beginning at a threshold defined as SM_{thresh} in the figure. SM_{thresh} was treated as a calibration parameter and typically had values of 0.2 to 0.6 in calibrated solutions. The SMD function defined ET = 0 for values of SMD > 0.95.

This SMD function is a simplified aggregation of complex root zone processes. Overall, evapotranspiration in the model is effectively regulated by two calibration parameters: RZ (root zone depth) and SM_{thresh} (SMD threshold for ET limitation). More detailed sub-models for ET

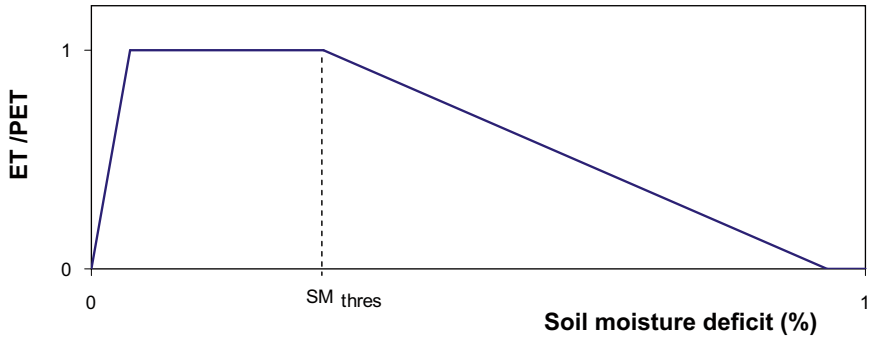

Figure A4-2. *Relationship between actual and potential evapotranspirations (ET and PET), and a soil moisture deficit function calculated within the specified root zone.*

estimation could have been included in the model and possibly increased the accuracy of process representation. However, this simplified representation was chosen to minimize the number of calibration parameters and to keep the near-surface hydrological model as simple as possible.

Model storage and flux equations

The model operates by maintaining daily water balances on the interception, snow, unsaturated, and saturated storages using finite difference equations with daily time steps. Flux equations defined flows to and from each storage, and those flows were also updated on a daily basis.

The finite difference water balance equation for the interception storage was given by:

$$I(t) = I(t–1) + (P(t) – ET_I(t) – TF(t)$$ (Equation A4-9)

where

$I(t)$ = new storage value for day = t, (mm),

$I(t–1)$ = value of interception storage for the prior day = t-1,

$P(t)$ = daily precipitation input time series (mm/d),

$ET_I(t)$ = daily evaporation from interception storage (mm/d),

$TF(t)$ = daily throughfall available for surface inflow (mm/d).

The daily evaporation from the interception storage, $ET_I(t)$, was estimated from the PET time series. If the value of interception storage exceeded the value for daily PET, then all PET was "consumed" at the interception storage, with no residual PET available for transpiration from the soil. If the value of interception storage was less than the value for daily PET, then the interception storage was emptied and a residual PET was available for transpiration from the soil. The interception storage had a maximum capacity, I_{max}, that was defined equal to 2 mm for all simulations. Daily throughfall, $TF(t)$, was calculated by difference and occurred when the maximum storage capacity for the interception storage was exceeded.

The snow routine was outlined in Section 3.1 in the main body of this report and used daily average air temperature, $T(t)$, as an addition input time series. The finite difference water balance equation for the snow storage, $snow(t)$, was given by:

$$snow(t) = snow(t–1) + TF(t)|_{T(t) < 0} – SM(t)|_{T(t) > 0}$$ (Equation A4-10)

where

$SM(t)$ = daily snowmelt time series (mm/d).

Throughfall added to the snow storage when the average daily air temperature was less than 0°C. Snowmelt, $SM(t)$, occurred using a calibrated degree day constant, varying between 0.8 and 1.2 mm/d, when the snow storage was non-zero and average daily air temperatures exceeded 0°C.

A net surface inflow time series was defined as:

$$SI(t) = TF(t)|_{T(t) < 0} + SM(t)|_{T(t) > 0} \quad \text{(Equation A4-11)}$$

In this way, surface inflow to the unsaturated storage, *SI(t)*, was equal to throughfall, *TF(t)*, when the average daily temperature was greater than zero and the snow storage was empty. Surface inflow was equal to throughfall plus snowmelt when the average daily temperature was greater than zero and the snow storage was non-zero.

The finite difference water balance equation for the unsaturated storage, *US(t)*, was given as:

$$US(t) = US(t-1) + SI(t) - Inf(t) - ET_{US}(t) + CR(t) \quad \text{(Equation A4-12)}$$

where

$Inf(t)$ = daily infiltration to the saturated zone (mm/d),

$ET_{US}(t)$ = daily transpiration from unsaturated storage (mm/d),

$CR(t)$ = daily capillary rise from the saturated zone (mm/d).

The unsaturated storage had a maximum capacity, US_{max}, given by Equation A4-1. In this model, it was assumed that daily infiltration, *Inf(t)*, was a fixed fraction of surface inflow, SI(t), equal to 0.5, plus the excess unsaturated storage above capacity after the storage value was updated with Equation A4-12. Several values for the fixed fraction of surface inflow were explored, as well as different formulations for this relationship, but the net effect in all cases was very small on simulation results.

Transpiration from the unsaturated storage, $ET_{US}(t)$, was calculated using the SMD function that was described in the previous section and the residual PET remaining after evaporation was accounted for from the interception storage. If the resulting new value for the unsaturated storage, *US(t)*, in Equation A4-12 was less than zero, then the value for $ET_{US}(t)$ was decreased to exactly drain the unsaturated storage with no negative deficit. This occurred rarely in the simulations, but when it did the residual evapotranspiration was passed onto the saturated storage.

Capillary rise from the saturated storage to unsaturated storage was calculated with a maximum as linearly proportional based on a capacity ratio for the unsaturated storage and was given by

$$CR(t) = CR_{\max}\left(1 - \frac{US(t)}{US_{\max}}\right) \quad \text{(Equation A4-13)}$$

where

CR_{max} = maximum daily value for capillary rise (mm/d).

The maximum daily value for capillary rise, CR_{max}, was a calibration parameter that was limited to a range of 2–12 mm/d in model calibrations.

The finite difference equation for the saturated storage was given by

$$SS(t) = SS(t-1) + INf(t) - ET_{ss}(t) - CR(t) - q(t) - s(t) \quad \text{(Equation A4-14)}$$

where

$ET_{ss}(t)$ = residual evapotranspiration taken from saturated storage,

$q(t)$ = specific discharge from saturated storage (mm/d),

$s(t)$ = deep seepage to bedrock from saturated storage (mm/d).

It was rare in simulations that a residual evapotranspirations was passed to the saturated storage (accounting for at most 1% of total ET in the simulations conducted), and this feature could have been left out of the model with little observable significance.

The specific discharge, $q(t)$, was calculated using the same storage-discharge function that was explored in Section 3.9 of this report and was given by

$$q(t) = {}^{k_1} SS(t)^{k_2} \qquad \text{(Equation A4-15)}$$

With no basis for calibration or estimation, deep seepage, $s(t)$, was assumed to be small and negligible to the near-surface hydrological model. Clearly this is a very important flux within the greater context of the conceptual hydrogeological model. However, it is likely a very small flux relative to precipitation, evapotranspiration and discharge, and hence any estimation of this in the near-surface hydrological model would have been pure conjecture.

Summary of calibration parameters

Tabell A4-1 shows the calibrated parameter values from the four simulations that were conducted with the near-surface hydrological model.

Tabell A4-1. Summary of calibration parameters for the four simulations discussed in Section 3.10.3.

Parameter	Description	Parameter values			
		PFM005764	PFM005764-PFM002667	PFM002667-PFM002668	PFM002668
I_{max}	Interception storage (mm)	2	2	2	2
K_{snow}	Snowmelt constant (mm/ °C)	0.83	0.85	1.1	0.83
$F_{flow-through}$	Flow through fraction for surface inflow	0.50	0.50	0.50	0.50
C_{max}	Maximum capillary rise (mm/d)	10	12	6	12
SM_{thresh}	Water deficit threshold in the soil moisture function for ET limitation (fraction)	0.4	0.4	0.4	0.6
RZ	Root zone depth (m)	–0.3	–0.2	–0.3	–0.3
$\rho_{surface}$	Soil porosity at the ground surface	0.32	0.30	0.30	0.65
k_1	Scalar in discharge equation	105	90	350	200
k_2	Exponent in discharge equation	3.0	3.0	3.0	3.0
d_{dead}	Groundwater depth that produces zero discharge (m)	–0.96	–1.2	–0.79	–0.35